CO2 Chemical Utilization through Dry Reforming of Methane : Development of Non-Noble Metals Catalysts Supported on Natural and Synthetic Clays

Hongrui Liu

SORBONNE UNIVERSITÉ
CRÉATEURS DE FUTURS DEPUIS 1257

∂'Alembert
Institut Jean le Rond d'Alembert

Sorbonne Université

Ecole doctorale SMAER (ED 391)

Sciences Mécaniques Acoustique Electronique Robotique

Programme Doctoral Génie des Procédés

Institut Jean Le Rond d'Alembert / Combustion, Clean Energy and Turbulence

CO_2 Chemical Utilization through Dry Reforming of Methane: Development of Non-Noble Metals Catalysts Supported on Natural and Synthetic Clays

Par M. Hongrui LIU

Thèse de doctorat de Génie Chimique

Dirigée par Prof. Maria Elena GALVEZ et Prof. Patrick DA COSTA

Présentée et soutenue publiquement le 01/10/2018

Devant un jury composé de :

Mme. BATIOT-DUPEYRAT Catherine, Full Professor, Université de Poitiers, Rapporteur
M. MARCEAU Eric, Associate Professor, Université Lille, Rapporteur
M. GARIN François, Full Professor, Université de Strasbourg, Examinateur
M. CAVADIAS Siméon, Full Professor, Sorbonne Université, Examinateur
Mme. GALVEZ Maria Elena, Associate Professor, Sorbonne Université, Directeur de Thèse
M. DA COSTA Patrick, Full Professor, Sorbonne Université, Co-Directeur de Thèse

Dédicace

Remerciements

I sincerely thank China and the China Scholarship Council for my scholarship in the UPMC Sorbonne Universités, France.

First of all, this doctoral dissertation is completed under the careful guidance of Prof. Maria Elena GALVEZ and Prof. Patrick DA COSTA. Prof. Maria Elena GALVEZ and Prof. Patrick DA COSTA have profound knowledge, rigorous experimental attitude and unique insights into the development of the research fields, thus providing ample guarantee for the successful completion of my Ph.D. research. The attitude and spirit of research that I learned from them will surely affect me in my whole life. Here, I would like to express my sincere respect and sincere thanks to Prof. Maria Elena GALVEZ and Prof. Patrick DA COSTA.

I would like to thank my reviewers Prof. Catherine BATIOT-DUPEYRAT and Prof. Eric MARCEAU. Meanwhile, I would like to thank the other members of my jury, Prof. François GARIN, Prof. Siméon CAVADIAS, thank all of you for willing to participate in my defense. The comments and suggestions from my jury allow me to complete my doctoral dissertation better and provide me the directions for further research.

I would like to appreciate the research group that gives me a lot of help both in research and life. Yiquan XIE, Sandrine DUONG, Armando IZQUIERDO, Hailong ZHANG, Maya DAOU, Johnny ABBOUD, Maria MIKHAIL, Mira IBRAHIM, Laureanne PARIZOT and my colleagues from Poland, Dominik Wierzbicki, Radosław DĘBEK, Katarzyna Świrk, Natalia Czuma, I need thank all of you for helping me so that I can successfully complete my doctoral research.

I would like to thank all professors, researchers, administrators, engineers and technicians in Institut Jean le Rond d'Alembert. Prof. Stéphane ZALESKI, Prof. Philippe GUIBERT, Prof. Guillaume LEGROS, Alexis MATYNIA, Evelyne MIGNON, Anne MARCHAL, Renaud JALAIN , Jean-François KRAWCZYNSKI, Jean-Marie CITERNE, Jérôme BONNETY, Hugo DUTILLEUL, Christian OLLIVON, Dominique BUSQUET, Jêrome PÉQUIN, and Frédéric SEGRETAIN. Thank all of you for providing support for my doctoral research.

In the end, I wish to thank my friends for their constant companionship and encouragement, which make my life to be full and warm. Thanks to my father: LIU Cheng and mother: YANG Lingfeng) for giving me the best love I can imagine. Thanks to my father-in-law: CHI Peng and mother-in-law: WANG Yongmei support me and my wife in all aspects. Let me bravely do what I want to do, so that I can concentrate on my scientific research. Thanks to the useful advices and supports for my research from my godfather: HU Kewei. Thanks to my wife CHI Junqing for my companionship and help for the last three years, I love you!

Résumé

Notre stratégie de développement «croissance à tout prix» a causé de nombreux problèmes environnementaux. Ainsi, la dépendance vis-à-vis des combustibles fossiles tels que le pétrole est encore plus élevée. On se doit de réduire cette dépendance. Parmi les stratégies permettant de réduire cette dépense on peut citer la production d'hydrogène, de gaz de synthèse ou d'autres produits utilisant du CO_2 et / ou du CH_4. L'utilisant de ces derniers est l'un des moyens prometteurs de convertir les gaz à effet de serre (CO_2 et CH_4) en produits chimiques est le procédé de reformage à sec du méthane (DRM: CH_4 (g) + CO_2 (g) ⇌ 2CO (g) + $2H_2$ (g), ΔH^0 (298K) = +247kJ·mol^{-1}). En outre, de bonnes performances catalytiques et des prix relativement bas font des catalyseurs à base de nickel des matériaux prometteurs pour le reformage à sec du méthane. Cependant, il existe certains problèmes liés aux conditions de réaction comme par exemple, une température élevée conduisant au frittage des catalyseurs.

Ainsi, cette thèse vise à proposer de nouveaux supports utilisant de différents promoteurs pour améliorer la sélectivité et la stabilité des catalyseurs à base de nickel pour le reformage à sec du méthane ; et à analyser les performances catalytiques des catalyseurs préparés en associant les effets de température (entre 850 et 550 °C) avec des caractérisations physico-chimiques telles que la mesure de surface (BET), la diffraction des rayons X (XRD), la réduction programmée de la température H_2 (H_2-TPR) et la désorption programmée à la température du CO_2 (CO_2-TPD).

Tout d'abord, différents promoteurs (Ce, Zr, La, Al, Mn et Mg) avec du nickel ont été imprégnés sur une argile naturelle ou de l'argile modifiée Fe/Cu de Tunisie. Les choix de différents promoteurs et supports conduisent toujours à des modifications de la surface spécifique, de la taille des cristallites NiO, de la réductibilité et de la basicité du Ni, ce qui peut encore affecter la performance catalytique des catalyseurs préparés. Tous les promoteurs à l'exception du Mn améliorent la performance catalytique puisque les espèces actives de NiO sont partiellement ou totalement couvertes par la formation d'oxydes de Mn et de Fayalite, riches en Mn.

Deuxièmement, les catalyseurs dérivés de l'argile synthétique (Ni-hydrotalcite, Ni-hydrocalumite, Ni-hydro-strontium et Ni-hydro-barium) ont été préparés par une méthode

de co-précipitation pour rechercher les influences de la structure sur le DRM. Les catalyseurs choisis, Ni-hydrotalcite et Ni-hydrocalumite, sont davantage favorisés par différentes teneurs en lanthane pour vérifier la promotion du lanthane. Les catalyseurs dérivés d'argile synthétique présentent généralement une activité plus élevée, en particulier pour le catalyseur dérivé de Ni-hydrotalcite, qui pourrait être attribué à sa plus grande surface spécifique moins l'adsorption de CO_2 sur des sites basiques forts. De plus, la présence de lanthane améliore dans une certaine mesure la performance catalytique.

Enfin, les catalyseurs ayant la même composition que d'excellents catalyseurs dérivés de Ni-hydrotalcite ont été synthétisés mécaniquement par broyage planétaire pour comparer l'effet de la vitesse de rotation et de la préparation à des synthèses classiques. La vitesse de rotation de 600 rpm présente la meilleure promotion basée sur sa taille de cristallite de Ni0 appropriée sur les catalyseurs, même similaire à l'activité catalytique des catalyseurs dérivés de Ni-hydrotalcite.

Mots clés: Reformage à sec du méthane, Gaz de synthèse, Catalyseurs au nickel, Argile naturelle, Argile synthétique

Abstract

The development strategy of "growth-at-any-cost" has not been applied to the current development with the increased attention of various countries to environmental issues. But the dependence on fossil fuels such as petroleum will be still high in a short period of time based on the consideration of economic and social development. Thus, the focus on the production of hydrogen, syngas or other products using CO_2 and/or CH_4 has attracted more attention in recent years. One of the promising ways to convert greenhouse gases (CO_2 and CH_4) into chemical products is the process of dry reforming of methane (DRM: $CH_4(g) + CO_2(g) \rightleftharpoons 2CO(g) + 2H_2(g)$, $\Delta H^0(298K)=+247kJ\bullet mol^{-1}$). Furthermore, good catalytic performance and relatively low prices of supported nickel catalysts make it be a hopeful commercial catalyst for dry reforming of methane. However, there are some problems related to catalysts and reaction conditions inhibit its practical application, for example, it requires high temperature leading to sintering of catalysts.

Thus, this research focuses on proposing new supports loaded with different promoters to enhance the catalytic selectivity and stability of nickel-based catalysts for dry reforming of methane, and analyze the catalytic performance of prepared catalysts by associating temperature effects (between 850 and 550 °C) with multiple characterizations such as Brunauer-Emmett-Teller (BET), X-ray diffraction (XRD), H_2-temperature programmed reduction (H_2-TPR) and CO_2-temperature programmed desorption (CO_2-TPD).

First, different promoters (Ce, Zr, La, Al, Mn and Mg) with nickel are impregnated on natural clay or Fe/Cu-modified clay from Tunisia. The choices of different promoters and supports always lead to changes in the specific surface area, Ni^0 crystallite size, Ni reducibility and basicity, which may further affect the catalytic performance of prepared catalysts. All promoters except Mn improve the catalytic performance since the active NiO species are partially or totally covered through the formation of Mn oxides and Fayalite, Mn-rich.

Second, the synthetic clay derived catalysts (Ni-hydrotalcite, Ni-hydrocalumite, Ni-hydro-strontium and Ni-hydro-barium) are prepared by co-precipitation method to research the influences of structure on the DRM. The selected Ni-hydrotalcite and Ni-hydrocalumite derived catalysts are further promoted by different contents of lanthanum to

check the promotion of lanthanum. Synthetic clay derived catalysts generally present higher activity, especially for the Ni-hydrotalcite derived catalyst, which could be attributed to its larger specific surface area and less CO_2 adsorption on strong basic sites. Moreover, the presence of lanthanum improves the catalytic performance to a certain extent.

In the end, catalysts having the same composition as excellent Ni-hydrotalcite derived catalysts are further synthesized by ball milling to compare the effect of rotational speed and preparation. The 600 rpm rotational speed presents the best promotion based on its suitable Ni^0 crystallite size on prepared catalysts, even similar with the catalytic activity of Ni-hydrotalcite derived catalysts.

Keywords: Dry reforming of methane, Syngas, Nickel catalysts, Natural clay, Synthetic clay

Sommaire

Chapter I
Introduction

1. Introduction

1.1 Overview

With the increased attention of various countries to environmental issues, the development strategy of "growth-at-any-cost" has not been applied to the direction of current development since its pollution to the environment. However, based on the consideration of economic and social development, the dependence on fossil fuels such as petroleum is still high in a short period of time, which also leads to further emission of greenhouse gases such as carbon dioxide (CO_2) and methane (CH_4). Against this background, many studies have focused on the production of hydrogen, syngas or other products using CO_2 and/or CH_4 in recent years. The goal of these researches is to recover more potential and control greenhouse gas emissions.

The process of dry reforming of methane ($CH_4(g)+CO_2(g)\rightarrow 2CO(g)+2H_2(g)$, $\Delta H^0(298K)=+247kJ\bullet mol\text{-}1$) has attracted much attention in recent years because it consumes two main greenhouse gases (CO_2 and CH_4) and convert them into useful chemical building blocks, which also present its great significance on both science and environment. Due to the good catalytic performance and relatively low prices of supported nickel catalysts, it is promising to be a commercial catalyst in the industrialization of dry reforming of methane. But nickel-based catalysts are not selective and prone to sinter, and their efficiency decreases over time. Therefore, it is necessary to enhance the catalytic selectivity and stability of nickel-based catalysts by improving various factors such as catalyst preparation, promoters and supports. Thus, my PhD research focuses on proposing new supports loaded with different promoters to disperse active Ni for dry reforming of methane, and analyze the catalytic performance of prepared catalysts by associating temperature effects with multiple characterizations.

The thesis is divided into 7 chapters. The first three chapters include the general introduction, research background and experiments of catalytic activity and characterizations respectively. The fourth, fifth and sixth chapters introduce the main experimental results, including clay-based catalysts, synthetic clay-based catalysts and

Mg-Al mixed oxides supported Ni-based catalysts prepared by ball milling. The seventh chapter is a summary of the experimental results.

The first chapter is a general introduction to the thesis. The general contents of various chapters, and the research objectives and methods are introduced.

The second chapter is a literature review of the research background. First, under the premise that CO_2 emissions are higher than the alarming rate, the importance of developing CO_2 chemical has become more prominent as global warming becomes more serious. Then CO_2 fixation as the second part is introduced, including three aspects on physical, chemical and biological methods. The third part describes some of the specific industrial processes involved in biological processes and relatively mature chemical processes in CO_2 valorization and resources utilisation. The fourth part is to introduce synthetic fuels that show great developing potential in the CO_2 resources utilisation, including the definition of synthetic fuels, synthetic routes and problems that need to be solved in the development of synthetic fuels. The fifth part leads to the specific research direction of this thesis, which can provide syngas for the preparation of synthetic fuels, that is, dry reforming of methane. After introducing the thermodynamics of dry reforming of methane, the reaction mechanism, the advantages and problems faced in the preparation of synthesis gas, the catalytic performance of some specific catalysts is summarized from the aspects of catalyst synthesis, support selection, promoter addition and catalyst deactivation.

The third chapter mainly introduces the experimental part. The experimental equipment and operating conditions for different characterizations (BET, XRD, H_2-TPR, CO_2-TPD, TGA, TEM, Raman) are described. At the same time, the procedure of activity test based on temperature effects, and the related reactor and equipment are introduced, as well as the calculation equations of both CH_4, CO_2 conversion and H_2/CO ratio that are mainly used to evaluate the catalytic performance.

The discussion of the experimental results in chapter 4 mainly focuses on the comparison of the catalytic performance of natural clay-based catalysts prepared by

impregnation. In the first part, different promoters (Ce, Zr, La, Al and Mn) are introduced on Fe-modified clay supported Ni based catalysts. The specific surface area, Ni^0 crystallite size, Ni reducibility and basicity are analyzed by different characterizations to evaluate the influences on catalytic activity. The second part is the comparison of the activity between natural clay based catalysts and natural clay modified with Fe and Cu based catalysts. Meanwhile, the difference in activity caused by different reduction temperatures (800 and 900 °C) is also discussed. The same physicochemical properties are also tested to evaluate the possible reasons for the differences in catalytic performance. In the third and fourth parts, the selected promoters Ce, Zr (part 3) and Mg (part 4) are respectively loaded on different clay based catalysts (natural clay, Fe and Cu modified clay) to check their catalytic performance. Besides, the effect of Mg loading on Fe-modified clay supported Ni based catalysts catalyst is further studied on catalytic activity. The relationship between the physicochemical properties and the catalytic activity of each catalyst is still presented based on different characterizations.

The experiment in chapter 5 focuses on synthetic clay-based catalysts prepared by the co-precipitation method, i.e. Ni-hydrotalcite Ni-Hydrocalumite, Ni-Hydro-Strotium and Ni-Hydro-Barium-derived catalysts. The first part discusses the difference in activity for the catalysts prepared by Group 2 elements (Mg^{2+}, Ca^{2+}, Sr^{2+} and Ba^{2+}), Ni^{2+} and Al^{3+}, and associates the activities with physicochemical properties of the catalysts characterized by BET, XRD, H_2-TPR, CO_2-TPD and so on. In the second and third parts, the main research is to investigate the effect of different amounts of La on the catalytic activity of catalysts with a layered structure (hydrotalcite and hydrocalumite), i.e. layered double hydroxides, and try to explain the possible reasons of differences in activity based on the specific surface area, Ni^0 crystallite size, Ni reducibility, basicity and carbon deposition.

In chapter 6, the catalysts with the same content of Ni, Mg and Al as the Ni-hydrotalcite-derived catalysts in chapter 5 are prepared by mechanical ball milling, and the effect of rotational speed on catalytic performance is compared. At the same time, the Ni-Mg-Al mixed oxides catalysts prepared by the ball milling are compared with those catalysts prepared by the co-precipitation to investigate the effects of

different preparation methods on the structure and activity of the catalysts. Trying to find out the factors that affect the catalytic performance through the specific surface area, Ni^0 crystallite size, Ni reducibility, basicity and carbon deposition.

The last part is a summary of all experiments and the perspectives for further experiments on dry reforming of methane. The main results of the experimental chapters (chapter 4, chapter 5 and chapter 6) are summarized, which could contribute to the further study of natural clay and synthetic clay based catalysts. In addition, based on the doctoral research, some suggestions are provided for further research on dry reforming of methane.

1.2 Objectives of Ph.D. work

My PhD research focuses on the preparation and characterization of noble-metal free catalysts for Dry Reforming of Methane (DRM), using clay as support. Two main groups of materials have been considered: 1) Natural clays from Tunisia, modified using Fe/Cu and other promoters such as Ce, Zr, La, Al, Mn and Mg, in order to adjust the metallic Ni site size; and 2) Synthetic clays, i.e. Ni-hydrotalcites Ni-hydrocalumite, Ni-hydro-strontium and Ni-hydro-barium. These were prepared according to different synthesis methods and their physico-chemical properties were carefully evaluated by means of different techniques, in order to study the influence of the different textural, structural and chemical parameters on the DRM activity and selectivity. Parasite reactions, such as direct methane decomposition and reverse water gas shift were found to occur to a relatively important extent. Nickel dispersion, together with surface basicity, was found to play a major role in DRM having a strong influence in process selectivity. Provided that these aspects are properly tailored, both natural and synthetic clays stand as very promising materials that can be successfully used in the preparation of active, selective and stable Ni-containing catalysts for DRM.

Chapter II

Literature review on CO_2 valorization

2. Literature review on CO_2 valorization

2.1 CO_2 emission, global warming and industrial development

With the continuous progress of industrialization, the dramatic growth in population which will reach approximately 8.5 billion by 2030 and 1.3% annual growth in global energy demand, the world energy consumption is always increased from 1860 which is only the first statistic date as show in Figure 2-1, and traditional fuels are therefore difficult to fulfill the developmental demand [1-3]. In addition, consumption of fossil resources leads to high CO_2 emissions [4]. Although the annual growth in CO_2 emissions from energy use on 2017 (0.6%) is less than the past 20 years (2.1%), the total CO_2 emissions will increase by 13% until 2035 [2]. It much be higher than alarming rate (400 ppm) even the growth rate is zero, because the CO_2 level in 2017 has exceeded 403 ppm [5]. It means a serious of anthropogenic damages on dynamic equilibrium states of CO_2 formation and consumption, and further causing increased CO_2 concentration in the atmosphere year-by-year, even more than natural limitations. The rising temperature on the earth's surface, i.e. global warming, as a consequence of this unbalanced situation.

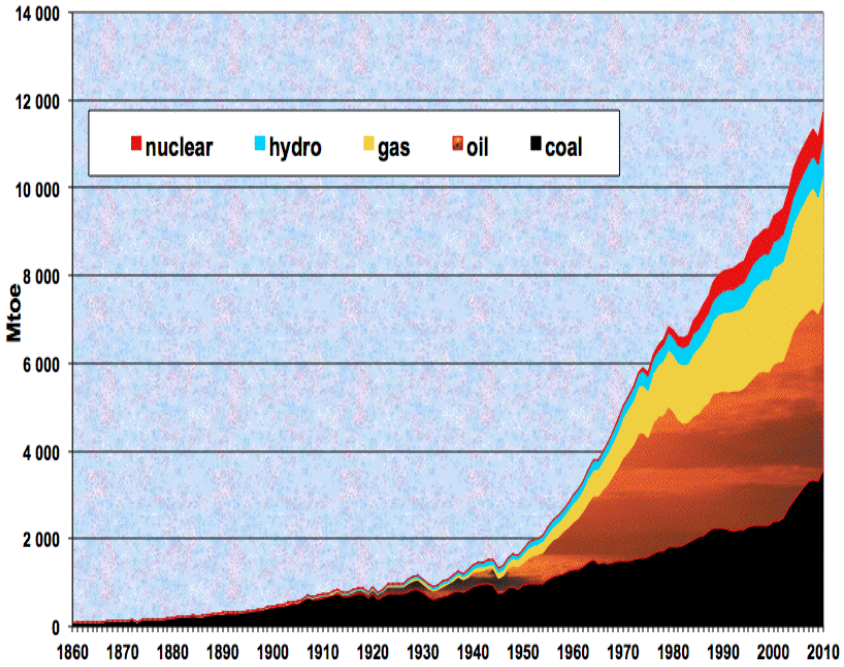

Figure 2-1. Growth trend of word energy consumption from 1860 to 2010 [3].

To mitigate the emissions and global impacts of greenhouse gas, 195 United Nations Framework Convention on Climate Change (UNFCCC) members have signed the "Paris Climate Agreement" [6]. CO_2 as the major greenhouse gas, the control of CO_2 emissions control is the main issue. The main line for reducing CO_2 emissions is controlled from the source, that is, through the structural adjustments of industrial, economic and energy, encouraging the construction of low-emission and low-energy consumption enterprises, the implementation of technological transformation of high-energy consumption enterprises to improve energy efficiency, looking for alternative energy and so on. However, it is difficult to completely adjust the structures of industrial, economic and energy to meet the requirements of environmental protection in a short period. It is also difficult for alternative energy to change the dominance of fossil fuels. Therefore, technologies such as recovery and separation, capture and storage, resource utilization and other technologies for CO_2 that needs to be emitted, are another viable routes for reducing or eliminating carbon emissions [7]. For example, CO_2 capture and storage can reduce 94 gigatonnes (Gt) of CO_2 emissions by 2050, with 56% of the reduction coming from the power industry, especially from coal-fired power generation (80%), 31% from industrial processes and 14% from fuel conversion. Internationally, gaseous CO_2 has a wide range of utilisations in industry, and it has begun to take advantage of the use of CO_2 as a chemical raw materials. Currently, millions of tons of CO_2 are used in industry every year in the world. Enhanced oil recovery (EOR) is the single largest CO_2 utilisation with an average annual consumption of 70 million tons of CO_2, but about 70% CO_2 come from the natural resources. Other industries that use more than one million tons of CO_2 include CO_2 miscible displacement, urea production, filling agents for carbonated beverage, refrigerant and so on [8].

From the perspective of environmental protection and sustainable development, CO_2 industry is more progressively developed into a potential choice since CO_2 is inexhaustible, thus most of the required carbon source for the chemical industry may ultimately come from CO_2.

2.2 CO_2 fixation

From the global perspective on the structure of CO_2 emissions, CO_2 emissions from construction, transportation, industrial, mining and electric power enterprises account for the main part, it can receive considerable economic benefits if this part of CO_2 as a research topic is fixed and utilized as the resources [4]. In the CO_2 fixation and the area of CO_2 capture and storage, it can usually be divided into physical, chemical and biological methods which are already listed in Figure 2-2 [9].

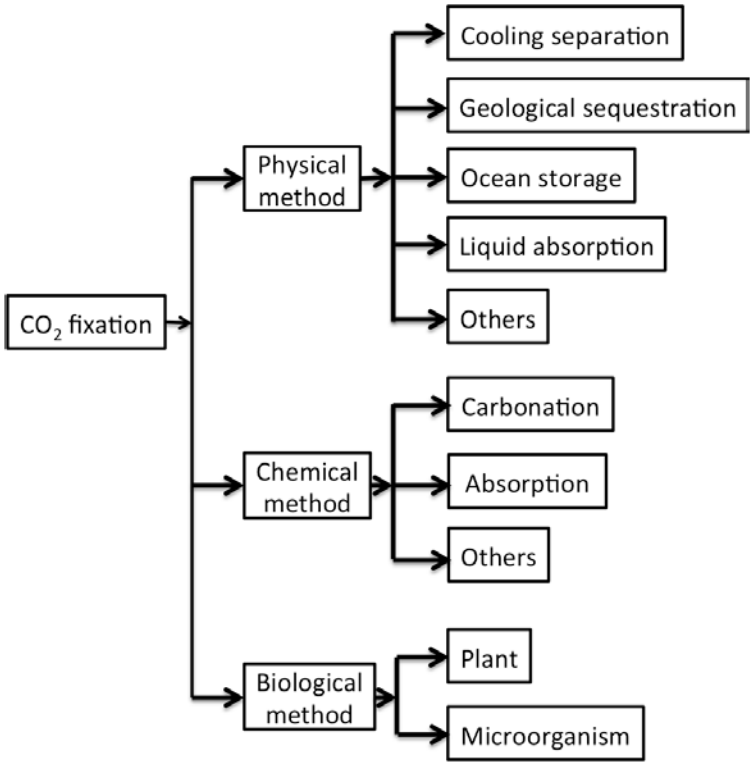

Figure 2-2. Methods of CO_2 fixation.

Physical methods include cooling separation, geological sequestration, ocean storage, liquid absorption and so on [9- 13]. Among them, cooling separation refers to the characteristic of CO_2 liquefaction at 31 °C and 7.38 Mpa, multiple stages of compression and cooling of flue gases allow CO_2 to be separated by liquefaction. Geological sequestration directly injects CO_2 into underground geological structures such as oil fields, natural gas reservoirs, salt bearing strata and non-coal seams are all suitable for CO_2 storage. Another approach associated with geological sequestration is CO_2 reuse. CO_2 is injected into the almost depleted oil field to increase the yield of oil recovery. There are two main options for ocean storage: transporting CO_2 to a storage

site by ship or pipeline and inject it into the sea at a depth of over 1000m to dissolve it naturally or injecting CO_2 into the sea at a depth of more than 3000 m to form solid CO_2 hydrates or liquid CO_2 lakes on the seafloor based on the density of CO_2 is greater than seawater to retard the process of CO_2 decomposition into the environment. Liquid absorption is achieved by changing the pressure and temperature between the CO_2 and absorption liquid to achieve the purpose of absorbing CO_2. The common absorption liquid is acrylic, methanol, ethanol, polyethylene glycol and other high boiling point organic solvents. The absorption capacity depends on the operating temperature and pressure, higher partial pressure of the gas or the lower temperature lead to stronger system's absorption capacity.

Chemical methods include carbonation, absorption and others [9, 14]. The carbonization is the use of the reaction between CO_2 and metal oxides to form the stable carbonates so that the CO_2 could be permanently fixed. Chemical absorption mainly uses alkaline solutions to dissolve and separate CO_2, the CO_2 is then separated by desorption and the solvents are regenerated. Typical solvents of chemical absorption are potassium carbonate (K_2CO_3) water solvent (plus a small amount of amine salts or vanadium and arsenic oxides) and ethanolamines solution (such as Diethanolamine (DEA), Monoethanolamine (MEA), Methyldiethanolamine (MDEA), etc.).

Biological CO_2 fixation mainly depends on the role of plants and microorganisms [9,15,16]. Photosynthesis of green plants is the most common and largest reaction on earth, which also plays a significant role in the synthesis of organic compounds and the stability of the carbon cycle. Plants can be divided into C3 plants, C4 plants, C3-C4 middle plants and others according to the different pathways of carbon assimilation in higher plants. The environmental adaptability and efficiency of carbon sequestration for microorganisms are higher than plants. The principal factors affecting the efficiency of biological carbon sequestration are the pathways of carbon sequestration, activities of key enzymes, as well as the effective supply of required energy for CO_2 fixation.

In terms of the utilization of CO_2, the ideal method is to convert CO_2 into CO or syngas currently, and the syngas can be converted to methanol or others, then further converted them into synthetic fuels [17].

2.3 CO_2 valorization and resources utilisation

Chemical and biological processes, as the most basic contents of CO_2 valorization, are already mentioned partly in CO_2 fixation, such as carbonation in chemical method and photosynthesis in biological method. But CO_2 valorization which gets more extensive research and utilization is more effective in resource utilization than CO_2 fixation. Because it consumes CO_2 and creats high value-added products at the same time, which is more in line with the needs of social and economic development [18,19]. Partial processes of CO_2 valorization are presented in Figure 2-3.

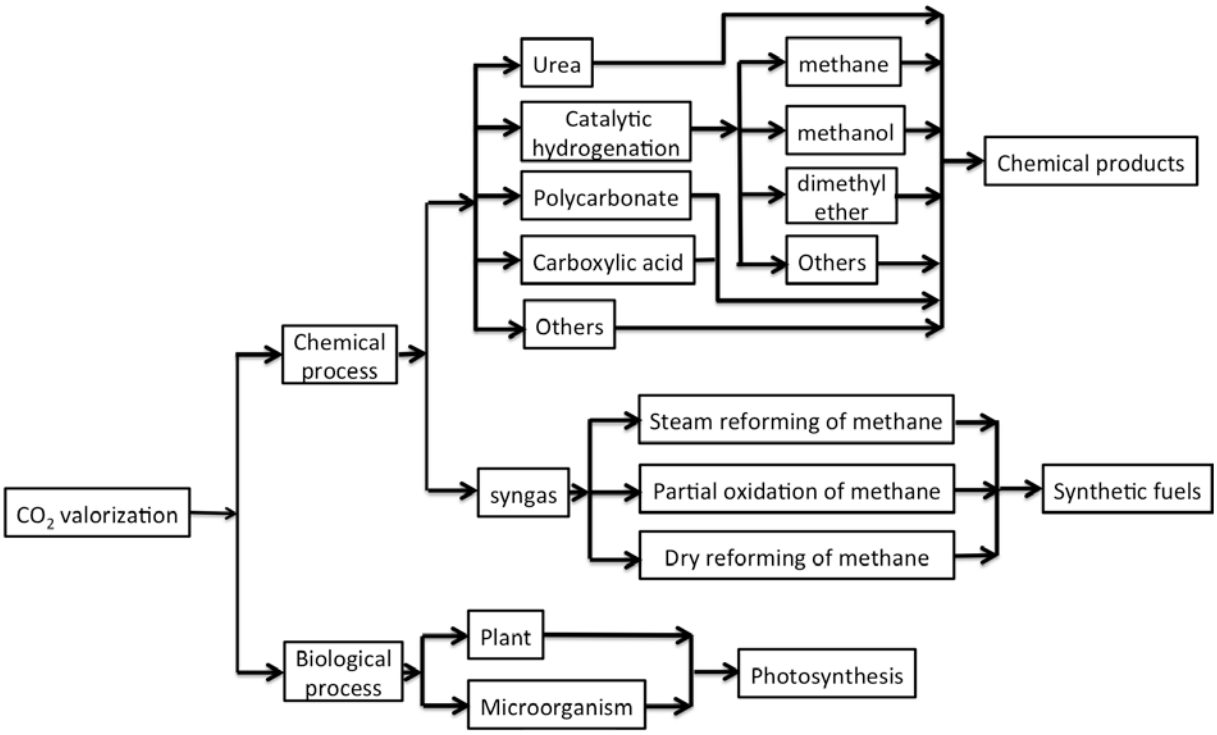

Figure 2-3. Partial processes of CO_2 valorization.

The biological process as one basic method of CO_2 valorization, it mainly relies on the photosynthesis of plants and microorganisms. Because photosynthetic microorganisms are more adaptable and efficient than plants, the resource utilization of CO_2 by culturing photosynthetic microorganisms has been extensively studied, and

it may become an effective way to control carbon dioxide. Microalgae, as a photosynthetic microorganism, can be used to produce biofuels and biological products, such as ethanol by fermentation, biodiesel from bio-oil in microalgae by transesterification, production of agar, carotenoids and other biological products for industrial purposes. However, algae biofuel is still in experimental stage, and there is a distance to large-scale production [18,19].

Compared with the biological process, the research on chemical process in CO_2 valorization has been more mature and complete. The main products of the chemical process can be divided into two categories, chemical products and fuels. The chemical products from chemical CO_2 valorization include synthesis of urea from the mixture of carbon dioxide and ammonia, which is a typical large-scale use of CO_2, and urea-based synthesis of dimethyl carbonate and other chemical raw materials or organic chemical intermediates further extend the utilization of CO_2. In addition, CO_2 can be converted to methane by methanation, methanol and dimethyl ether through catalytic hydrogenation, and as raw materials to produce polycarbonates, carboxylic acid and others [18,19]. However, in terms of chemical CO_2 valorization, the ideal utilization is to produce syngas which can further convert into synthetic fuels currently. In general, syngas is produced through three routes, including steam reforming of methane ($CH_4(g)+ H_2O(g) \rightleftharpoons CO(g) + 3H_2(g)$, ΔH^0 (298K) = +206.3kJ·mol^{-1}), partial oxidation of methane ($CH_4(g)+ 0.5O_2(g) \rightleftharpoons CO(g) + 2H_2(g)$, ΔH^0 (298K) = -35.6kJ·mol^{-1}), and dry reforming of methane ($CH_4(g)+ CO_2(g) \rightleftharpoons 2CO(g) + 2H_2(g)$, ΔH^0 (298K) = +247.3kJ·mol^{-1}). Due to the high hydrogen production of methane steam reforming in products, it is mainly used in the industrial production of hydrogen from natural gas (CH_4). Moreover, in order to control the carbon deposition on the catalyst, it is normally necessary to feed in excess water vapor, which also requires more energy consumption for the strongly endothermic steam reforming of methane itself [20,21]. Compared with steam reforming of methane, the ratio of H_2/CO produced by partial oxidation of methane is lower, which is more conducive to the synthesis of methanol by Fischer-Tropsch (F-T) process. Otherwise, the partial oxidation is an exothermic reaction with a small enthalpy. Its reaction energy consumption is also lower, and it is safer than direct oxidation. However, the partial oxidation of methane reaction needs to pass through oxygen and requires high purity of natural gas, which is not suitable for the case of high CO_2

content in natural gas [20-22]. Compared to steam reforming and partial oxidation of methane, dry reforming of methane consumes both greenhouse gases (CH_4 and CO_2) and produces a H_2/CO ratio closer to 1, making it more favorable to subsequent F-T synthesis and further production of chemical products. In addition, dry reforming of methane is reversible endothermic reaction with a large enthalpy, so it can be used to store energy. Based on these advantages of dry reforming of methane, it attracts more researches in recent years. Since CH_4 and CO_2 are stable molecules, their activation requires the presence of a catalyst. However, the sintering of the active components at high temperature and carbon deposition happen during dry reforming of methane, and the presence of a large number of side reactions limits its industrial application. Although the large-scale test device of dry reforming of methane is developed and operated jointly by Shanghai Advanced Research Institute, Chinese Academy of Sciences, Shanxi Lu'an Environmental Energy and Royal Dutch Shell in August 2017, the research on a more efficient and stable catalyst with lower cost is still emphasis. This is also the main research direction of this thesis [23,24].

In addition, CO_2 is also commonly used in petrochemical, agriculture and even food industry. Some of its specific application technologies are listed in Figure 2-4 and explained as following:

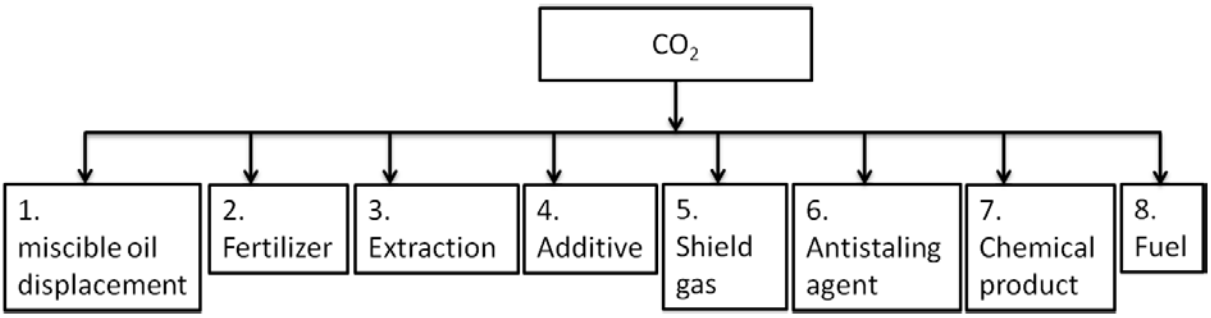

Figure 2-4. Partial resource utilizations of CO_2.

1. CO_2 miscible oil displacement in oilfield

Over the past decade, as crude oil extraction in oilfields becomes ever difficult, CO_2 gradually becomes a super user in the field of oil recovery due to the continuous application of new technologies that increase the recovery factor of crude oil. The CO_2 miscible oil displacement process is considered to be the most promising process currently [17,25].

2. Fertilizer feedstock for plants

Chlorophyll in plants absorbs CO_2 and convert it into plant starch under photosynthesis. This is the natural law of plant production. The gas fertilizer of CO_2 increases the concentration of CO_2 in plant growth space, which can increase the dry matter of plants in order to achieve the purpose of increasing production [17,25].

3. Supercritical fluid extraction-CO_2

When the temperature and pressure are higher than the critical temperature (31°C) and pressure (73.8 atm) of CO_2, the properties of CO_2 will change. The density of CO_2 is close to liquid and its viscosity is close to gas. And the diffusion coefficient is 100 times of liquid, so it has a good dissolving ability. The CO_2 which has been heated and pressurized into the supercritical state as a solvent dissolves a variety of substances, and then extracts the active ingredients. The supercritical fluid extraction has been used in the food industry, cosmetic industry, chemical industry and medical industry currently [17,25].

4. Food additives in beverages

CO_2 can be used for soft drinks, sparkling wine and beverages, and the amount depends on the requirements of normal production. Generally it is produced by the fermentation of sugar and processed by washing, purification, drying, cooling, and then compressed into liquid. CO_2 is primarily used in carbonated drinks, such as carbonation agent, packaging gas, refrigerant, leavening agent, pH regulator and processing aid [17,25].

5. Welding shield gas

CO_2 shielded welding is a recognized welding method of superior efficiency, low cost, time and labor saving. Compared with shielded metal arc welding, the effectiveness of automatic CO_2 shielded welding can be increased by 2 to 5 times and 1 to 2 times for semi-automatic, furthermore the energy consumption decreased by 50 percent. The CO2 shielded welding accounts for a few scales of all welding in China which is much lower than developed countries [12,26].

6. Fruit and vegetable antistaling agents

Common components of fruit and vegetable antistaling agents are ethylene, CO_2 absorbent, oxygen absorber, growth regulator and so on, of which CO_2 absorbent is to adjust the CO_2 content, such as activated carbon, lime, magnesium chloride [12,27].

7. Inorganic and organic chemical products

Inorganic chemical products made of CO_2 and metal or non-metal oxides mainly include light $MgCO_3$, Na_2CO_3, $NaHCO_3$, $CaCO_3$, K_2CO_3, $BaCO_3$, $PbCO_3$, Li_2CO_3 and MgO. Most of them are basic chemical raw materials and widely used in metallurgy, chemical industry, medicine, electro-mechanical and other industries. Organic chemical products mainly produced by CO_2 are dicyandiamide, salicylic acid, formic acid and its derivatives, methanol, methane and organic polymer [17,25].

8. CO_2 to fuel

In January 2010, Carbon Sciences Incorporated Company announced that it has made breakthroughs in the CO_2 recycle. The developed biocatalytic process can convert CO_2 into low-carbon hydrocarbons (C1-C3) and then reform them into gasoline or fuel. In addition, this technology is an industrial process that does not need to wait plant growth compared to biofuels, and it can be completed in a matter of hours. Thus, it can meet the fuel needs on a larger scale [28]. Furthermore, in May 2017, Wei et al. published an article to introduce a novel Na-Fe_3O_4/HZSM-5 catalyst that can directly convert CO_2 to gasoline-range (C5–C11) hydrocarbons. These researches offer more possibilities and methods for solving the shortage of fossil fuels [29].

Utilizing CO_2 in an efficient way is certainly one of the best ways to reduce CO_2 emissions. Therefore, converting CO_2 into more value-added energy or chemical raw material through chemical, biological and other methods has become the focus of scientific work nowdays. With the rapid development of science and technology and the growth of emerged disciplines, it can be said that the solution for solving greenhouse effect will be more and more abundant. At the same time, the scope of resource utilization of CO_2 will also be more widespread. In view of the current shortages of energy and basic chemical raw materials, it is foreseeable that another

huge improvement will be brought to the world if CO_2 fixation and resource-recycling technologies can further break through the limitation.

2.4 Synthetic fuels

As the pressure of population growth on traditional fossil energy demand gradually increases, energy issues continue to be the focus of human concern. With the continuous expansion of the exploitation and utilization of traditional fossil fuels, easily available reserves for fossil energy are not optimistic [30]. In order to positively deal with the energy crisis, all countries in the world are continuously looking for alternative energy sources, and Figure 2-5 describes the synthetic fuel projects in the world based on proven natural gas reserves where GTL, CTL, BTL and OTL represent natural gas into liquids, coal to liquids, biomass to liquids, bitumen from oil sands to liquids (OTL) through Fischer-Tropsch process respectively [31]. The development of synthetic fuels such as coal-based fuels and biofuels has become the focal point for every country since the synthetic fuels have the advantages of being energy-efficient and reducing emissions compared to other traditional fossil fuels in applications [32]. The technologies of synthetic fuels are more mature compared to hydrogen energy, more available energy than wind and solar energy, and lower technical requirements than nuclear energy [30]. In addition, the sources of raw materials for synthetic fuels are more extensive which means it facilitates the better development and utilization of synthetic fuels.

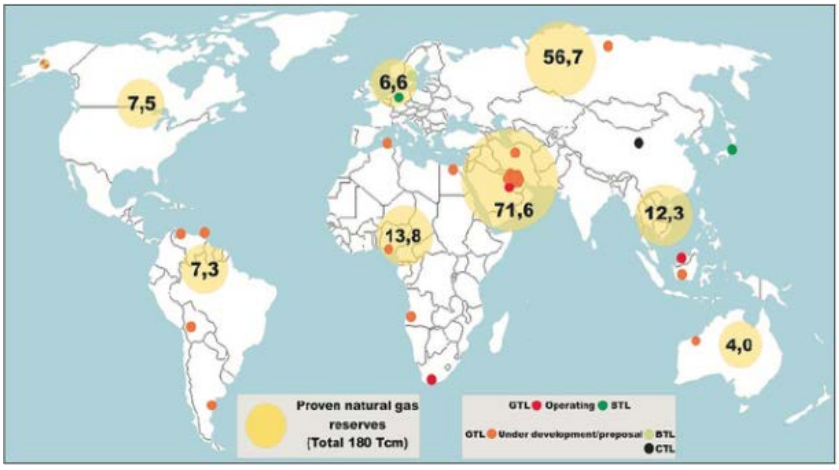

Figure 2-5. The syntheic fuel projects around the world based on proven natural gas researves. GTL: natural gas into liquids, CTL: coal to liquids, BTL: biomass to liquids, OTL: bitumen from oil sands to liquids (OTL) [31].

The synthetic fuels are new fuels that convert one or more coal, natural gas and/or biomass feedstocks into synthetic liquid products through chemical conversion according to the definition of Energy Information Administration [33]. Currently, the common method of preparing synthetic fuels is Fischer-Tropsch (F-T) synthesis, the simplified Fischer-Tropsch process which can form $-CH_2-$ that is basis for longer-chain hydrocarbons and conceptual Fischer-Tropsch plant are showed in Figure 2-6 (a) and (b) respectively [32]. Then the F-T synthesis can further generate new fuels and biofuels from coal or natural gas through carbonation. For example, coal can be directly vaporized to produce water gas (a mixture of CO and H_2), which can be used as a clean fuel. Natural gas is converted into CO and H_2 by steam reforming, and then into methanol by water shift reaction. Futhermore, methanol can be converted to gasoline through Mobil Process. Biological resources can produce ethanol, biodiesel fuel and so on [32,34,35]. And the production of synthetic fuels can not be separated from the important raw syngas. The main components of syngas are CO and H_2, and it is used as a feedstock for chemical raw materials [36]. Ammonia is produced by the pressure reaction of hydrogen in the syngas and nitrogen in the air under the catalytic action. The products that can be processed through ammonia include urea, ammonium salts (such as nitrogen and compound fertilizers), nitric acid, melamine and so on [13]. The syngas not only is pressurized to produce hydrocarbons with an iron catalyst (F-T synthesis), but also can be developed into the gasoline, acetone, alcohol and other low-boiling products [35]. The hydrocarboxylation of linear and branched C2-C17 olefins with syngas produces the oxo synthesis products, which are important raw materials for plasticizers [37].

(a)

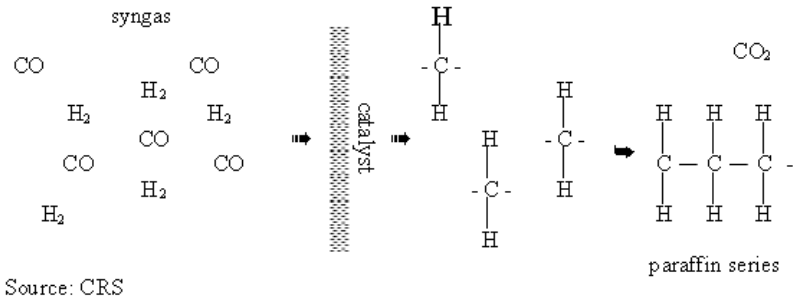

Source: CRS

(b)

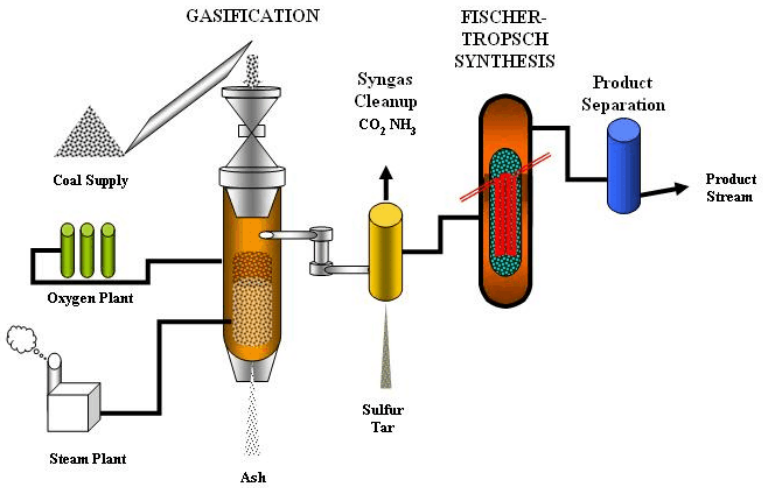

Figure 2-6. The (a) theoretical Fischer-Tropsch synthesis and (b) conceptual Fischer-Tropsch plant [32].

However, there are still some drawbacks of synthetic fuels, such as the sulfur which is generated during coal liquefaction produces sulfur oxides upon contact with oxygen and eventually acid rain from the environmental viewpoint, or the cost of synthetic fuels is relatively high now from the economic viewpoint [30]. However, most of these problems have been properly solved with the innovation and progress of science and technology, and these drawbacks will not really affect the further promotion and development of synthetic fuels. For instance, the sulfur fixation method can solve its impact on the environment [33]. With the progress and improvement of synthetic sciences and technologies, the cost of synthetic fuels will inevitably become lower. For example, the raw materials originally used for bioethanol are crops such as wheat, but it is possible to initially reduce the cost of producing bioethanol by using lignocellulose which could be obtained from agricultural, industrial, forestry and urban wastes currently, and it is also useful to effectively alleviate the problem of high foodstuff price caused by the lack of foodstuff [38].

Therefore, the outlook of synthetic fuels is still optimistic on the whole. The synthetic fuels are also bound to ease the dependence of many countries on traditional fossil fuels and more widely used, or even to replace some traditional fossil fuels.

2.5 Dry reforming of methane (DRM) for chemical CO_2 valorization

2.5.1 Thermodynamic and chemical kinetics aspects

The process of dry reforming of methane (DRM) produces syngas as an effective way to consume two important greenhouse gases (methane and carbon dioxide) and transfer them into high value-added chemical products attracts much more attention [39-40]. The ratio of sygnas (carbon monoxide (CO) and hydrogen (H_2)) is about 1, and it could be used for Fischer–Tropsch (F-T) process. The sygnas is not only the basic feasible material for the F-T process to produce synthetic fuels, but also an effective way to control greenhouse gases [41-42].

Thermodynamic research is usually used to calculate the contents of each component in the phase equilibrium in the range of reaction temperatures, and it can roughly determine the conversion degrees at each temperature stage [43]. From the equation of dry reforming of methane ($CH_4(g)+ CO_2(g) \rightleftharpoons 2CO(g) + 2H_2(g)$, ΔH^0 (298K) = $+247.3 kJ \cdot mol^{-1}$), it can be noticed that the gas volume of forward reaction is increased and it is endothermic reaction. Therefore, increasing reaction temperature and decreasing pressure are beneficial to the reaction. And thermodynamic analysis can effectively determine the range of system operation and reaction conditions exactly [44-46]. Dry reforming of methane also require efficient and selective catalysts to promote the forward reaction, but the catalyst deactivation which in turn affects the overall activity always happens since the large number of parallel side reactions which are listed in Figure 2-7 take place during the range of reaction temperatures, and carbon deposition from sintering and side reactions such as the CO disproportionation at upper limit 973K and CH_4 decomposition above 828 K [43,44,47]. Therefore, gradually improving the operating conditions according to the stage of carbon formation contributes to the catalytic activity and stability activity of

catalysts. With the thermodynamic analysis, the carbon formation is more effectively analyzed in the system.

Reaction number	Reaction	ΔH^0_{298} (kJ/mol)
	Dry reforming	
1	$CH_4 + CO_2 \rightleftharpoons 2CO + 2H_2$	+247
	Reverse Water Gas Shift	
2	$CO_2 + H_2 \rightleftharpoons CO + H_2O$	+41
	Carbon forming reactions	
3	$CH_4 \rightleftharpoons C + 2H_2$	74.9
4	$2CO \rightleftharpoons C + CO_2$	-172.4
5	$CO_2 + 2H_2 \rightleftharpoons C + 2H_2O$	-90
6	$CO + H_2 \rightleftharpoons C + H_2O$	-131.3
	Oxidative coupling of methane	
7	$2CH_4 + CO_2 \rightleftharpoons C_2H_6 + CO + H_2O$	+106
8	$2CH_4 + 2CO_2 \rightleftharpoons C_2H_4 + 2CO + 2H_2O$	+284
	Dehydrogenation	
9	$C_2H_6 \rightleftharpoons C_2H_4 + H_2$	+136
	Hydrogenation of CO and CO_2	
10	$CO + 2H_2 \rightleftharpoons CH_3OH$	-90.6
11	$CO_2 + 3H_2 \rightleftharpoons CH_3OH + H_2O$	-49.1
12	$2CO + 4H_2 \rightleftharpoons CH_3OCH_3 + H_2O$	
13	$CO_2 + H_2 \rightleftharpoons HCOOH$	15
	Reforming	
14	$CH_3OCH_3 + CO_2 \rightleftharpoons 3CO + 3H_2$	+258.4
15	$C_2H_6 + 2H_2O \rightleftharpoons 2CO + 5H_2$	+350
16	$C_2H_6 + 2CO_2 \rightleftharpoons 4CO + 3H_2$	+430
17	$C_2H_4 + 2CO_2 \rightleftharpoons 4CO + 2\ H_2$	+290
18	$C_2H_4 + 2H_2O \rightleftharpoons 2CO + 4H_2$	+210
	Dehydration	
19	$2CH_3OH \rightleftharpoons CH_3OCH_3 + H_2O$	-37
	Hydration	
20	$CH_3OCH_3 + 3H_2O \rightleftharpoons 2CO_2 + 6H_2$	+136
21	$CH_3OCH_3 + H_2O \rightleftharpoons 2CO + 4H_2$	+204.8
	Methanation	
22	$CO_2 + 4H_2 \rightleftharpoons CH_4 + 2H_2O$	-165
23	$CO + 3H_2 \rightleftharpoons CH_4 + H_2O$	-206.2
	In theory possible is also FT synthesis with CO_2 to higher hydrocarbons than methane:	
24	$CO + H_2 \rightleftharpoons -(CH_2)- + H_2O$	
	And MTG and MTO reactions given in genral as:	
25	$CH_3OH \rightleftharpoons$ hydrocarbons $+ H_2O$	

Figure 2-7. Possible parallel reactions during dry reforming of methane [47].

In this research, Gibbs energy minimization method is used to calculate the equilibrium values for each component by means of HSC Chemistry 5.0 software, and carbon formation is also considered in the reaction system.

With the addition of optimized data of dry reforming of methane provided by thermodynamic analysis and the continuous development of microscopic research, the

theoretical research has gradually shifted from thermodynamic to basic reaction mechanism in chemical kinetic. When the optimization of actual experimental process encounters limitations, backing to the research on basic mechanism is usually beneficial to further improving the experiment. The earliest dry reforming of methane was studied on Ni and Co catalysts by F. Fischer and H. Tropsch in 1928 [48]. The widely accepted mechanism of DRM is bi-functional pathway currently, especially for the catalysts with better activity and stronger resistance to carbon deposition. It means CH_4 and CO_2 are activated on metal and support respectively. For inert material supported catalysts, such as SiO_2 and Al_2O_3, the reaction mechanism is more inclined to a mono-functional pathway, which means CH_4 and CO_2 are activated on metal [40]. For example, Mark et al. proposed a simple mechanism based on Ir/Al_2O_3 catalysts for DRM that CH_4 is directly dissociated to produce active carbon (C) and H_2, and then CO is generated from the mixture of C and CO_2 [49].

2.5.2 Development of Catalysts for DRM

2.5.2.1 Introduction

Dry reforming of methane (DRM) has received considerable attention in the last years, as one of the most promising routes for CO_2 valorization [50,51]. It involves consumption of two important greenhouse gases CH_4 and CO_2, resulting in the formation of a syngas (CO + H_2 gas mixture) with a H_2/CO ratio equal to 1, ideal for liquid fuel synthesis through Fischer-Tropsch or for chemical synthesis through hydroformylation [52]. DRM is nevertheless an endothermic reaction (ΔH^0 (298K) = +247kJ·mol^{-1}) that is only thermodynamically favorable at moderate-high temperatures (>750 °C). In addition, carbon dioxide is the highest oxidation state of carbon. It is an inert, linear and centrosymmetric molecule that means its electrical dipole is zero since the opposite direction among three atoms cancel the dipole, which is illustrated in Figure 2-8 (a) and (b) [53,54]. The carbon-oxygen (C-O) bond length of CO_2 is 0.116nm, which is between C-O double bonds (0.122nm) and triple bonds (0.110nm). It means the C-O bond in CO_2 also has some characteristics of triple bonds [55,56]. Besides, the bond energies of C-O double bonds in CO_2 and triple bonds are 803 and 1075 kJ/mol respectively [56]. Both the relatively short bond

length and high bond energy point to the single C-O bond-dissociation in CO_2 is high, so the CO_2 dissociation need high temperature and energy, which means CO_2 molecule has high thermal stability. Futhermore, a relatively high first ionization energy of CO_2 (13.97 eV) indicates that CO_2 molecule is weak electron donor, higher electron affinity energy (38 eV) and lower energy level of empty orbital leads to CO_2 molecule to be strong electron acceptor, thus CO_2 molecule is easy to be reduced [54]. It also indicates the difficulty of ionization of the CO_2 molecule and further reflects the CO_2 stability to a certain extent. Moreover, metastable state of CO_2^- is only approximate 0.5 eV higher in energy than ground state of CO_2 [57]. Therefore, it could be found that the best way for CO_2 activation is inputting electron, i.e. reduction. From the above analyses, it could be concluded that the CO_2 activation is quite difficult. The common activation includes coordinating activation, reductive activation, as well as electric catalytic activation, biological activation and so on. Thus, at these moderate-high temperatures the reaction is still kinetically slow unless in the presence of a catalyst, i.e. mainly Ni-containing catalyst, preferred to non-noble metal-based ones due to lower cost, higher availability and even similar catalytic activity compared to supported noble metals which have showed better catalytic performance on DRM [40].

(a)

(b)

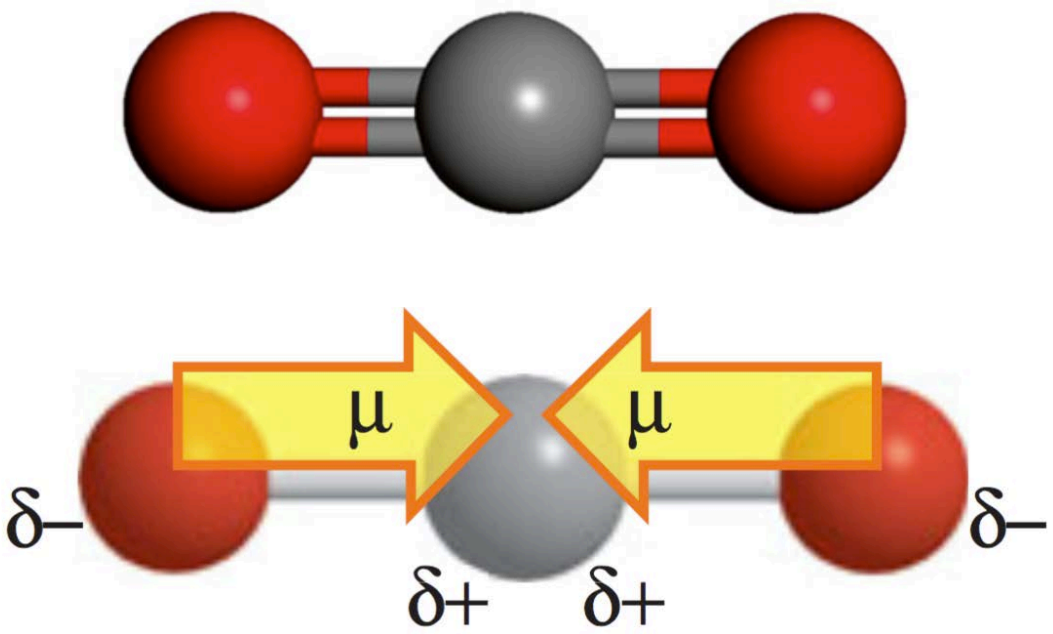

Figure 2-8. Structure of CO_2: (a) molecular model (b) nonpolar modle [53,54]

However, DRM as a strongly endothermic reaction, it requires a lot of energy consumption. Futhermore, with a catalyst, many parallel reactions listed in Figure 2-7 occur during the DRM process, which seriously affect the selectivity of the target products (H_2 and CO) and are prone to carbon deposition further inactivating catalyst and clogging pipelines [23]. Therefore, the exploration on an efficient and stable catalyst for DRM is the key point of industrialization.

Thus, research on improving the catalytic performance of the catalyst with different methods is always the focal point on DRM. Studies on catalyst synthesis [58-62], as well as choice of precursors and supports [63-82], promotion effects [83-92] and mechanism of carbon deposition [40,41,70,71,93-97] are main directions for improving DRM catalysts in recent years (Table 2-1).

2.5.2.2 Catalyst synthesis

Prepared methods have certain effects on catalysts. The catalysts with the same amount and components that are produced by different methods are not the entirely same in composition, crystal size of the active component and dispersion, therefore further affecting its catalytic performance. The common prepared methods for the catalysts of DRM include co-precipitation, impregnation, sol-gel method, ion exchange method and hydrothermal synthesis method [58- 62].

Aghamohammadi et al. [58] studied the catalytic properties of CeO_2 as a promoter in support of Ni/Al_2O_3 catalysts with sequential impregnation and sol-gel methods. This research showed that the catalyst obtained a smaller particle size and evenly dispersed active metal by using sol-gel method which was characterized by XRD and FESEM respectively. Furthermore, the catalysts that were prepared by sol-gel method exhibited higher catalytic activity at different reaction temperatures, gas hourly space velocity and feed compositions, and better stability during 10 h experiments than impregnation synthesis.

Mahboob et al. [59] researched the different pretreatments on the synthesis of $Ni\text{-}Co/Al_2O_3\text{-}ZrO_2$ catalysts through ultrasound-assisted impregnation method,

including irradiation power (30, 60, 90 W) and irradiation time (0, 20, 80 min). The results described that not only did sonochemistry method promote the catalytic properties, such as specific surface area, Ni particle size distribution and dispersed active sites, thus improving carbon deposition and catalytic performance, but also sonochemistry method with higher irradiation power and longer irradiation time showed better catalytic performance by further limiting the amount of the carbon deposition.

Zhu et al. [60] investigated the influences of different calcined atmospheres (Ar, CO_2, O_2 and H_2) for preparing Ni-Ce/SiO_2 catalysts. Although Ni-Ce/SiO_2 catalysts had similar initial activities after calcining in these gases, these calcined gases had an impact on stability. The catalysts which were calcined in Ar have better stability since their better Ni species dispersion and more reactive carbonaceous species, which could inhibit the sintering of Ni and carbon deposition on the catalyst. Otherwise, relatively low stability in H_2 calcination was related to the partial lack of oxygen storage capacity of CeO_2 which could suppress the elimination of filamentous carbon.

Ay et al. [61] investigated the CeO_2 supported Ni and/or Co catalysts that was prepared by incipient wetness impregnation method with different calcined temperature (700 °C and 900 °C). The catalysts Ni/CeO_2 and Ni-Co/CeO_2 had similar and good catalytic activities, both CH_4 and CO_2 conversions were close to 80% at 700 °C. But these catalytic activities were decreased with increasing calcined temperature. The conversions of Ni/CeO_2 and Ni-Co/CeO_2 decreased a little at the beginning 50min, then maintaining relatively high activities for the following time.

Luisetto et al. [62] surveyed different prepared methods on Ni/CeO_2-Al_2O_3 catalysts for DRM. It indicated that the conversions of CH_4 and CO_2 increased with increasing temperature in the sequence: solution excess wet impregnation method ≈ sol-gel method < citric acid method < co-precipitation method. The co-precipitation method had the best catalytic activity, and all of these methods showed excellent stability during 5h since the formation of $CeAlO_3$ which could promote the carbon gasification. Thus, the order of the amount of carbon deposition on the catalyst after DRM was co-precipitation method > solution excess wet impregnation method > sol-gel method >

citric acid method. Compared to other prepared methods, citric acid method had a higher content of $CeAlO_3$ and smaller Ni particle size.

2.5.2.3 Influence of support

In general, support itself is not catalytically active, however it may strongly influence the catalytic performance of the overall catalytic system. Dependent on the type of support used, the interaction active phase-support may be favored, it can also provide acid or basic sites that may promote the adsorption of reaction species, and furthermore, it offers adequate surface area and may improve the mechanical properties of the catalytic system [63]. DRM as an endothermic reaction, the process is usually carried on at high temperatures. So the choice of support should have relatively high thermal stability. The common supports include SiO_2, Al_2O_3, MgO, ZrO_2, TiO_2 and composite oxide supports CaO-SiO_2, MgO-Al2O_3, ZrO_2-CeO_2-Al_2O_3. Otherwise, the conventional macroporous materials, microporous molecular sieves and mesopore molecular sieves have been researched widely in recent years [64-82].

Zhang et al. [64] studied the Ni-based Al-modified/unmodified SBA-15 supported catalysts for DRM. It showed that the Al-modified SBA-15 as the support led to smaller Ni particle size and better hydrothermal stability, which were probably main reasons for its catalytic performance. Otherwise, the synthesis of Al-modified/unmodified SBA-15 by using ethylene glycol as the solvent showed better distribution of Ni particles in mesoporous silica compared to deionized water as the solvent.

Drif et al. [65] used different M_xO_y-Al_2O_3 oxides (M = Zr, Mg, Ni, Ce, La) through sol-gel method to synthesize different supports for rhodium (Rh) based catalyst that was prepared by wet impregnation method. This research proved that only La_2O_3-Al_2O_3 support was amorphous support which was possibly related to its lowest surface area. The Rh/NiO-Al_2O_3 presented the best catalytic performance at 700 °C for DRM due to the formation of $NiAl_2O_4$ spinel phase which could control carbon deposition, fill Al_2O_3 vacancies to maintain stability and inhibit the migration of ionic Rh species to make it reduce completely.

Frontera et al. [66] investigated the Ni-based highly ordered (Silicalite-1)/ highly defective pure silica (MCM-41)/ pure silica delaminated zeolite (ITQ-6) supported catalysts that were prepared by impregnation method. The different catalytic activities at 700 °C for 10h illustrated that the support surface had a closely related to catalytic properties. The ITQ-6 supported catalyst had smaller Ni particle sized and better distribution of Ni particles which could maintain strong interaction with support, inhibit metallic sintering and unlimited from carbon deposition, thus it showed the best catalytic performance.

Wang et al. [67] surveyed the effect of reducible metal oxides (CeO_2, Nb_2O_5, Ta_2O_5, TiO_2, and ZrO_2) and irreducible metal oxides (γ-Al_2O_3, La_2O_3, MgO, SiO_2, and Y_2O_3) as supports for the catalytic properties of Rh based catalysts. The consequences described that γ-Al_2O_3 and MgO as the supports provided higher catalytic performance than others. In comparison, the reducible metal oxides except CeO_2 and ZrO_2 supported Rh catalysts showed relatively low catalytic activities and stabilities.

Otherwise, clays have been widely used as supports for the preparation of diverse catalysts, including Ni-containing catalyst for dry methane reforming. Among them, synthetic clays, i.e. hydrotalcites, have shown to yield high activity, selectivity and catalytic stability in DRM, since they provide adequate surface area, mostly in terms of mesopores and intrinsic surface basicity, resulting in enhanced Ni dispersion and reducibility [68- 71]. Natural clays stand as a most interesting option, since they are naturally available, green and low-cost materials. They have been recently used as supports in several catalytic applications [72- 77], including DRM [77- 82]. Either raw [77] or Al-pillared [78] smectites were used for in the preparation of Ni-based catalysts for DRM. Daza et al. [79], Wang et al. [80], and Barama et al. [81] considered the utilization of raw, LaAl and Al-pillared montmorillonites. Hao et al. [82] employed a Zr-pillared laponites. All these works point out the benefits of using these natural clays as supports in the preparation of DRM catalysts. Moreover Wang et al. reported a direct influence of the mesoporous surface area of LaAl-pillared clays on their activity, in terms of CH_4 conversion [80].

2.5.2.4 Promotion effect

In order to develop a highly efficient and stable catalysts for DRM, it is the most common method to add promoters currently, and the further research on the category and content of different promoters is also concerned. A large number of metals as promoters have been studied on modified research for common Ni-based catalysts, including alkali metals, alkaline earth metals and rare earth metals [40,83]. For example, Mg, La, Ce and Zr have been reported to effectively improve the catalytic performance through inhibiting carbon deposition. In addition, the presence of different promoters can also improve the basicity of catalyst which is related to the ability of adsorption and desorption of carbon dioxide, change the dispersion of active components on the surface and adjust to the interaction between the metal and the support [84-87].

The introduction of alkali metals and alkaline earth metals can improve the basicity of the catalyst, thus leading to enhance its absorption of CO_2 and promote the timely elimination of the carbon deposition on the surface of the catalyst [86,87]. Castro Luna et al. [88] reported the catalysts with alkali metal potassium (K) on Ni-Al_2O_3 for DRM, which had shown better stability in 30h experiments and less carbon deposition on the catalysts. The additional K inhibited the carbon formation and increased the Ni reducibility, but did not affect the Ni particle size and structure. The migration of K from support to the catalyst surface, even on part of active sites, affected a few catalytic activities, less than 4% of CH_4 and CO_2 conversions. Alipour et al. [89] researched the Ni-based catalyst promoted by alkaline earth metals MgO, CaO, and BaO on Al_2O_3. This study indicated that the MgO was beneficial to CH_4 conversion and inhibition of carbon deposition. The introduction of CaO and BaO reduced CH_4 conversion to a certain degree with decreasing carbon formation. Chang et al. [85] studied common influences of the alkali metal K and alkaline earth metal Ca on zeolite supported Ni based catalysts. The dissociations of CO_2 and CH_4 were confirmed as initial steps of DRM to produce CO and H_2 respectively in this catalyst system. The addition of both K and Ca effectively hindered the coke formation through suppressing direct CH_4 decomposition and oxidation of surface carbon with CO_2 or carbonate, so that it had stable activity compared to non-modified catalyst.

Furthermore, the adsorbed carbon (Ni-C(s)) and oxygen (Ni-O(s)) on the catalyst surface also led to regeneration of active Ni species to maintain high stability.

Rare earth metals can significantly enhance the catalytic performance of the catalyst. For example the introduction of Ce, it ascribes to an improved reducibility of Ni species, together with slightly higher Ni crystallite size, that, on the other hand, also catalyze undesired parallel reactions resulting in carbon formation, such as direct methane decomposition. Ce also promotes the presence of weak and medium strength basic sites, which are thought to favor CO_2 adsorption and desorption on the catalyst surface, leading to enhanced catalytic activity [90]. Otherwise, when CeO_2 is incorporated in ZrO_2 for Pt-promoted catalysts, it can promote the formation of oxygen vacancies and increase the oxygen exchange capacity of catalysts based on the strong oxygen storage and interaction between Pt and CeO_2, and further accelerating the gasification of carbon deposition on the catalyst surface to improve the catalytic stability [91,92]. Cao et al. [83] investigated the effects of rare earth metals (Sc, Y, Ce, and Pr) on the catalytic properties of Ni-hydrotalcite-derived catalysts. It proved that all these promoters were beneficial to catalytic performance, especially the catalysts with Ce and Pr, not only did they improve the dispersion of Ni particles, but they inhibited also the migration of active Ni species to achieve relatively stable catalytic performance. In addition, the redox pairs, such as Ce^{3+}/Ce^{4+} or Pr^{3+}/Pr^{4+}, were beneficial to form oxygen vacancies and promote redox properties, thus removing carbon deposition and further improving the catalytic performance.

2.5.2.5 Catalyst deactivation

The deactivation of non-noble catalysts, especially for Ni-based catalysts, in the whole range of reaction temperatures specifically at low-moderate reaction temperatures (< 750 °C) carbon forming reactions are bound to take place among other side reactions, for example CH_4 decomposition ($CH_4 \rightleftharpoons C + 2H_2$) and boudouard reaction ($2CO \rightleftharpoons C + CO_2$), resulting in the formation of carbon deposition on the catalyst surface. Carbon deposition can clogs the pores of catalyst and/or covers the active centers, and/or inhibits the further CH_4 adsorption through preventing the production of carbon which is arose from CH_4, and then leading to the

catalytic deactivation [40]. This problem of catalyst deactivation needs to be assessed in order to increase the stability of the catalytic system in view of its practical utilization. Different approaches, in terms of the utilization of nano-structured supports [93,94], and in terms of increasing the dispersion and controlling the crystal size of the Ni particles deposited on the catalysts surface [70,71], proof the possibility of tailoring the selectivity of the DRM reaction with the final aim of minimizing carbon deposition.

Liu et al. [95] reported the influences of La_2NiO_4/γ-Al_2O_3 synthesized through sol-gel process on carbon deposition and catalytic stability in DRM. The La_2O_3 produced from the reduction of La_2NiO_4 contributed to strong adsorption of CO_2, which was further leading to CO_2 decomposition to form CO and O. Thus, the O would reactive with carbide (CH_x) to inhibit the formation of graphite so that the catalyst obtained higher stability. In our research, lanthanum (La) was also beneficial to reduce carbon formation through the formation of lanthanum oxycarbonates ($La_2O_2CO_3$) which could promote the gasification of amorphous carbon deposits [41].

Schulz et al. [96] described different pathways of carbon formation on Ni and Pt-based catalysts through isotope-labeled reactants. The analysis showed that DRM on both Ni and Pt-based catalysts relied on the CH_4 gradual dissociation, but C* species were prone to be formed on the surface of Ni-based catalysts compared to common formation of CH* and CH_2* species on Pt-based catalysts. Although the initial CO_2 conversions for Ni and Pt-based catalysts presented almost the same level, the activation of CO_2 resulted in CO* and O* on Ni while CO* and OH* on Pt. The main fraction of surface carbon species on Ni-based catalysts was generated from CO* by means of isotope-labeled reactants, so it was produced from CO_2 dissociation. For Pt-based catalysts, surface carbon species were mainly detected from CH_4 decomposition. Furthermore, carbon formation was more facile on Pt-based catalysts since C* species gasified faster.

Theofanidis et al. [97] discussed the carbon species and mechanisms of carbon gasification on Ni-Fe/$MgAl_2O_4$ catalysts. Above all, two kinds of carbon species, amorphous and graphitic, were discovered on the catalysts, and the persistent carbon

species were not adjacent to active sites. Thus, for the process of gasification of carbon species by CO_2, CO_2 dissociation on Ni happened and then the carbon species were gasified by surface oxygen, meanwhile Fe was oxidized by CO_2 to provide lattice oxygen for the oxidation of carbon species that were far away from active sites. For the mechanism of gasification of carbon species through O_2, carbon species on active surface were gasified first, and then the carbon species away from active sites were oxidized by lattice oxygen from nickel and/or iron oxides.

Table 2-1. A brief description and comparative summary for catalysts of dry reforming of methane.

Method	Species/ Approach	Reference
Catalyst synthesis		
	● Sequential impregnation and sol-gel methods for Ni/Al_2O_3-CeO_2	[58]
	● Different pretreatments (irradiation power (30, 60, 90 W) and irradiation time (0, 20, 80 min)) for Ni-Co/Al_2O_3-ZrO_2 catalysts through ultrasound-assisted impregnation method	[59]
	● Different calcined atmospheres (Ar, CO_2, O_2 and H_2) for Ni-Ce/SiO_2 catalysts	[60]
	● Different calcined temperature (700 °C and 900 °C) for Co promoted Ni/CeO_2 catalysts	[61]
	● Different prepared methods (impregnation method, sol-gel method, citric acid method and co-precipitation method) for Ni/CeO_2-Al_2O_3 catalysts	[62]
Support		
	● Ni-based Al-modified/unmodified SBA-15 supported catalysts	[64]
	● M_xO_y-Al_2O_3 oxides (M = Zr, Mg, Ni, Ce, La) supported Rh based catalyst	[65]
	● Ni-based highly ordered (Silicalite-1)/ highly defective pure silica (MCM-41)/ pure silica delaminated zeolite (ITQ-6) supported catalysts	[66]
	● Reducible metal oxides (CeO_2, Nb_2O_5, Ta_2O_5, TiO_2, and ZrO_2) and irreducible metal oxides (γ-Al_2O_3, La_2O_3, MgO, SiO_2, and Y_2O_3) supported Rh based catalysts	[67]
	● Hydrotalcite-derived catalysts	[68-71]
	● Natural clay based catalysts	[72-77]
	● Raw or Al-pillared smectites supported Ni based catalysts	[77,78]
	● Raw, LaAl and Al-pillared montmorillonites	[79-81]
	● Zr-pillared laponites supported Ni based catalysts	[82]
Promoter		
	● Rare earth metals (Sc, Y, Ce, and Pr) on Ni-hydrotalcite-derived catalysts	[83]

Catalyst deactivation	● Alkali metal K and alkaline earth metal Ca on zeolite supported Ni based catalysts	[85]
	● Alkali metal potassium (K) on Ni-Al_2O_3	[88]
	● Alkaline earth metals MgO, CaO, and BaO on Ni-Al_2O_3	[89]
	● Ce modified natural clay based Ni catalysts	[90]
	● Pt on ZrO_2 and CeO_2-ZrO_2 catalysts	[91,92]
	● CeO_2-ZrO_2 promoted Ni/SBA-15 catalysts	[93]
	● Ni-based silicalite-1 type catalysts	[94]
	● Effect of La_2NiO_4/γ-Al_2O_3 synthesized by sol-gel method on carbon deposition	[95]
	● Different pathways of carbon formation on Ni and Pt-based catalysts through isotope-labeled reactants	[96]
	● Different mechanisms of carbon gasification by CO_2 and O_2 on Ni-Fe/$MgAl_2O_4$ catalysts	[97]

Chapter III
Experimental method

3. Experimental method

3.1 Physicochemical characterization

3.1.1 Brunauer–Emmett–Teller (BET)

The textural characterization was performed through N_2 adsorption at -196 °C in a BelSorb-Mini II (BEL-Japan) device. The BET method was used for the calculation of the specific surface area, whereas the BJH method was chosen for the evaluation of mesopore volume.

3.1.2 X-Ray Diffraction (XRD)

The X-ray diffraction (XRD) were acquired in a PANalytical-Empyrean diffractometer, equipped with CuKα (λ = 1.5406 Å) radiation source and 2θ range between 3 and 90°, with a step size of 0.02°/s. The Ni crystallite sizes in the reduced catalysts were calculated using the Scherrer equation.

3.1.3 Temperature-Programmed Reduction (TPR)

The temperature-programmed reduction (H_2-TPR) profiles were obtained using a BELCAT-M (BEL-Japan) apparatus, equipped with a thermal conductivity detector (TCD). The readily calcined materials were outgassed and activated at 100 °C for 2 h, then reduced until 900 °C in 5 vol.% H_2/Ar at a heating rate of 7.5 °C/min.

3.1.4 Temperature-Programmed Desorption (TPD)

The same apparatus (BELCAT-M) was also used for the acquisition of the temperature-programmed desorption (CO_2-TPD) profiles. The catalysts were degassed and activated from room temperature to 500 °C in pure He at a heating rate of 10 °C/min, degased for 2 h and then cooled down to 80 °C. The materials were subsequently exposed to 10 vol.% CO_2/He for 1 h in order to saturate their surface

with CO_2, followed by the desorption of weakly (physically) adsorbed CO_2 under a flow of pure He for 15 min. Then the adsorbed CO_2 was desorbed in pure He at temperatures from 80 °C to 900 °C and at a heating rate of 10 °C/min after .

3.1.5 Thermal Gravimetric Analysis (TGA)

The amount of carbon deposited on the surface of each catalysts upon the DRM reaction was measured by means of its thermogravimetric oxidation in a SDT Q600 apparatus (TA Instruments), under air flow (100 mL/min), heating from ambient temperature to 900 °C at a rate of 10 °C/min.

3.1.6 Transmission Electron Microscope (TEM)

The transmission electron microscopy (TEM）was tested by JEOL JEM100-CXII, accelerating voltage of 100 keV. In the thesis, It was used to examine the fine structure on the catalysts, as well as the distribution of Ni particle size.

3.1.7 Raman Spectroscopy (Raman)

Raman spectroscopy was performed in a Horiba Jobin Yvon HR800 UV device using a green laser source (532 nm). The additional phase that could not be determined by XRD might be presented by Raman.

3.2 Catalytic activity tests

The catalytic activity tests were analysed in dry reforming of methane (DRM) equipment, the design drawing and physical profile were listed in Figure 3-1 (a) and (b) repectively. The activity tests were performed at temperatures from 850 °C to 600 °C (at 50 °C intervals of 30 minutes) at atmospheric pressure, in an “U” type tubular quartz reactor which was described in Figure 3-2. The total reactant gas flow was 100 ml/min, corresponding to a gas hourly space velocity (GHSV) of 20,000 h^{-1}. Because GHSV was widely used in commerical systems and catalysts were used in fixed bed in most cases, thus GHSV could be defined as the ratio of total volume flow

rate of feed gases and catalyst volume [98]. The molar composition of the gas mixture fed to the reactor was $CH_4/CO_2/Ar$ = 1/1/8. The calcined catalysts were reduced in situ at 900 °C for 1 h in the stream of 5 vol.% H_2/Ar prior to each DRM experiment. The composition of gas was continuously analysed with the help of a micro chromatograph (Varian GC4900), equipped with a thermal conductivity detector (TCD). The conversions of CO_2 and CH_4, as well as the molar ratio of H_2 to CO and carbon balance, were calculated using the following equations, where n_i^{in} and n_i^{out} represent the number of moles at, respectively, the inlet and outlet of the reactor for each of the species:

$$X_{CO_2} = \frac{\left(n_{CO_2}^{in} - n_{CO_2}^{out}\right)}{n_{CO_2}^{in}} \times 100\%$$

$$X_{CH_4} = \frac{\left(n_{CH_4}^{in} - n_{CH_4}^{out}\right)}{n_{CH_4}^{in}} \times 100\%$$

$$\frac{H_2}{CO} = \frac{n_{H_2}^{out}}{n_{CO}^{out}}$$

$$\text{Carbon deposion} = [(M_c \times \frac{\overline{V_{CH_4}}}{V_m} + M_c \times \frac{\overline{V_{CO_2}}}{V_m})_{Input} - (M_c \times \frac{\overline{V_{CH_4}}}{V_m} + M_c \times \frac{\overline{V_{CO_2}}}{V_m} + M_c \times \frac{\overline{V_{CO}}}{V_m})_{Output}] \times 300\text{min}$$

In the formula of carbon balance, M_c is the molar mass of carbon, V_m is the molar volume and $\overline{V}$ is the average volumetric flow rate for each components. Otherwise, the isothermal stability is tested on selected catalysts.

(a)

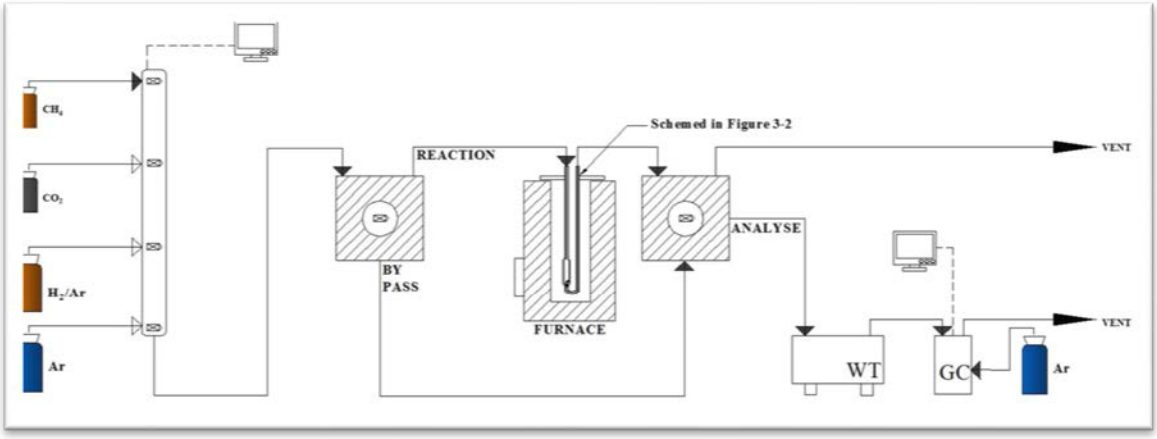

(b)

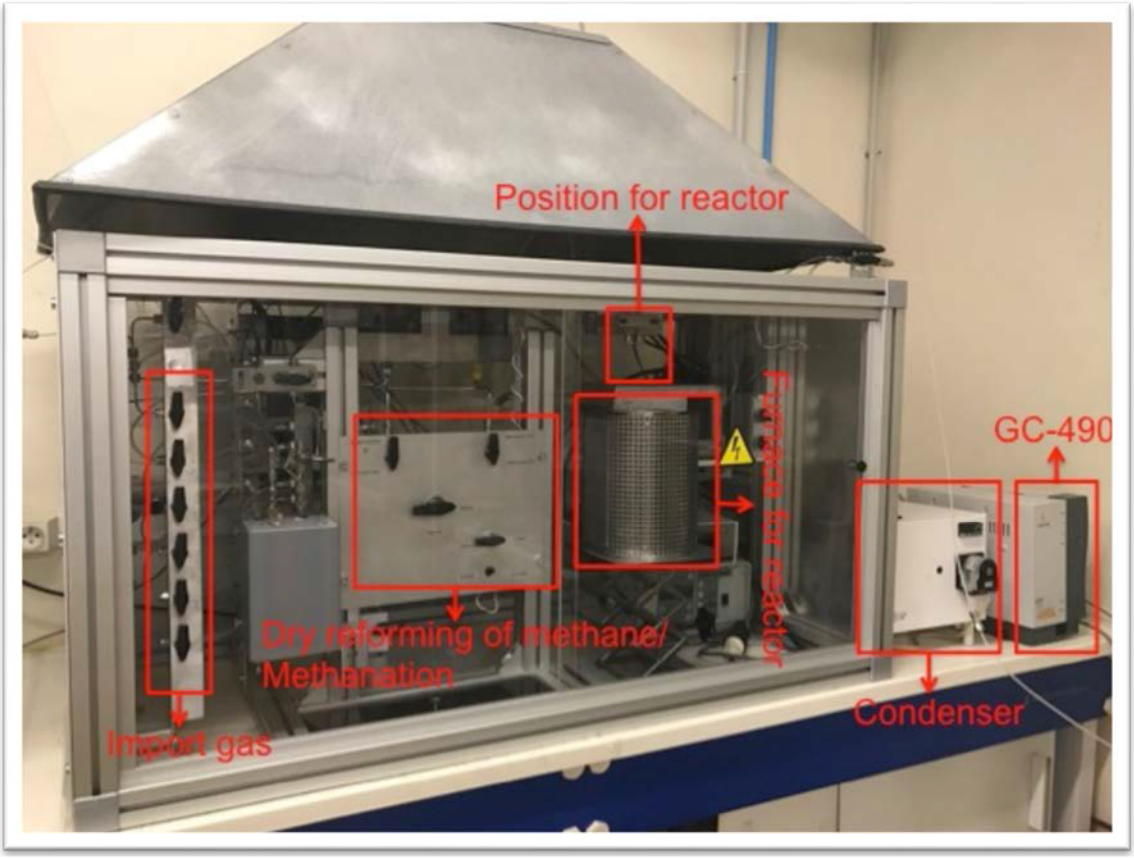

Figure 3-1. The (a) design drawing and (b) physical profile of DRM equapment.
Remarks: GC- Micro Gas Chromatograph.

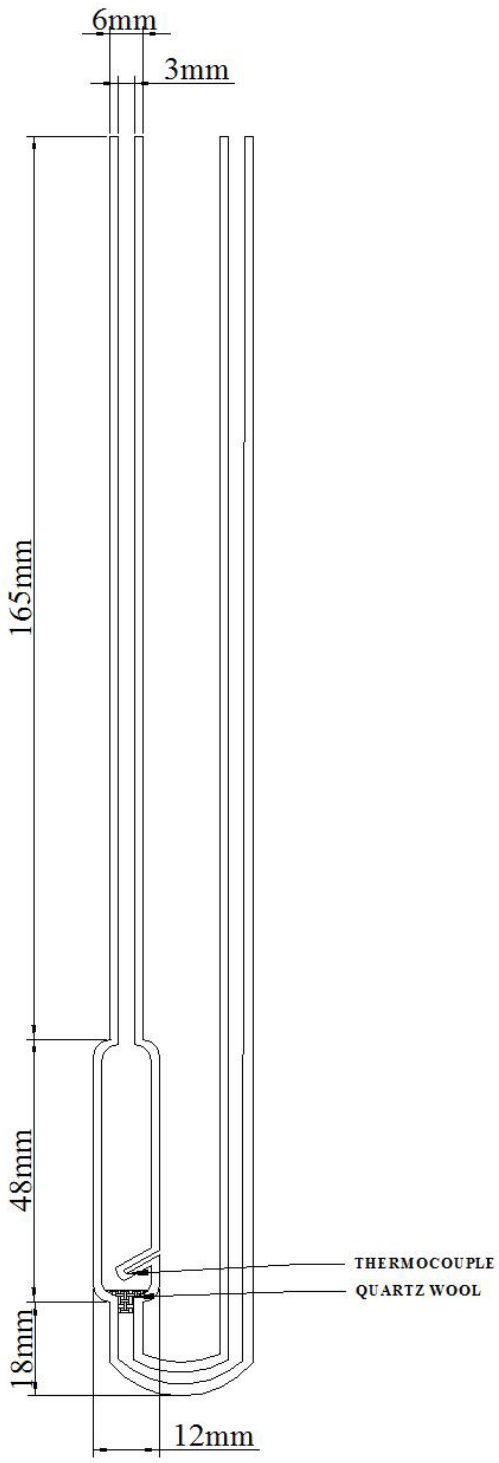

Figure 3-2. Scheme of "U" type tubular quartz reactor.

Chapter IV

Natural clay as support in the preparation of Nickel (Ni)-based catalysts for dry reforming of methane (DRM)

4. Natural clay as support in the preparation of Nickel (Ni)-based catalysts for DRM

4.1 Introduction

With increased consumption of fossil fuels and energy demand, the research of available resources, such as abundant natural gas, has lately become an urgent need in our nowadays society. Natural gas is not only a high quality and relatively clean energy carrier, but also an important chemical intermediate. Methane, the main component of natural gas, can be therefore converted to high value-added products, fuels and/or chemicals, such as syngas and its derived synthetic fuels, via dry reforming of methane (DRM). However, methane is a rough molecule to activate, since it contains four highly stable C-H bonds [99,100]. DRM is only thermodynamically possible at temperatures higher than 650 °C and it is additionally strongly kinetically hindered. Therefore relatively high temperatures and the use of an active and selective catalyst are required. The presence of simultaneous reactions, such as reverse water gas shift (RWGS) and direct carbon decomposition, may occur to a greater extent than the DRM reaction itself. Among them, carbon deposition as a consequence of direct methane decomposition poses a real challenge in terms of catalytic stability. Still, dry reforming of methane yields an equimolar mixture of H_2 and CO, suitable for direct Fischer-Tropsch synthesis [101-103], and consumes methane and CO_2, which are moreover two important greenhouse gases.

Although noble metal based catalysts, such as Pt, Rh and Ru, evidence very high activity and selectivity, and a good resistance towards coking [104-106], they are scarce and very expensive, which limits their utilization. Nickel-based catalysts are thus preferred and have become the most widely used catalysts in DRM, since they exhibit similar activity and have much lower cost. However, the deactivation of Ni-based catalysts due to carbon deposition remains an issue, together with Ni sintering taking place at relatively low temperatures, especially in the presence of CO [107,108]. Thus, the support and promoter play important roles in the preparation of efficient DRM catalysts. The possible influences on textural properties, the dispersion of the active phase, Ni reducibility, basicity and carbon deposition will may eventually have an impact on the catalytic performance.

The use of natural, Fe and/or Cu-pillared clays as supports in the preparation of Ni-based catalysts for DRM have never been described in the existing literature. Thus, Fe and/or Cu modified natural clays are used in the preparation of Ni based catalysts that are further promoted by different promoters including cerium (Ce), zirconium (Zr), lanthanum (La), aluminum (Al), manganese (Mn) and magnesium (Mg) oxides in this chapter. The outline for each section is presented in Figure 4-1. The so-prepared catalysts are tested and characterized from a physicochemical point of view with the aim of assessing the relationship between catalytic activity and important properties such as porosity, Ni distribution and crystal size, as well as basicity.

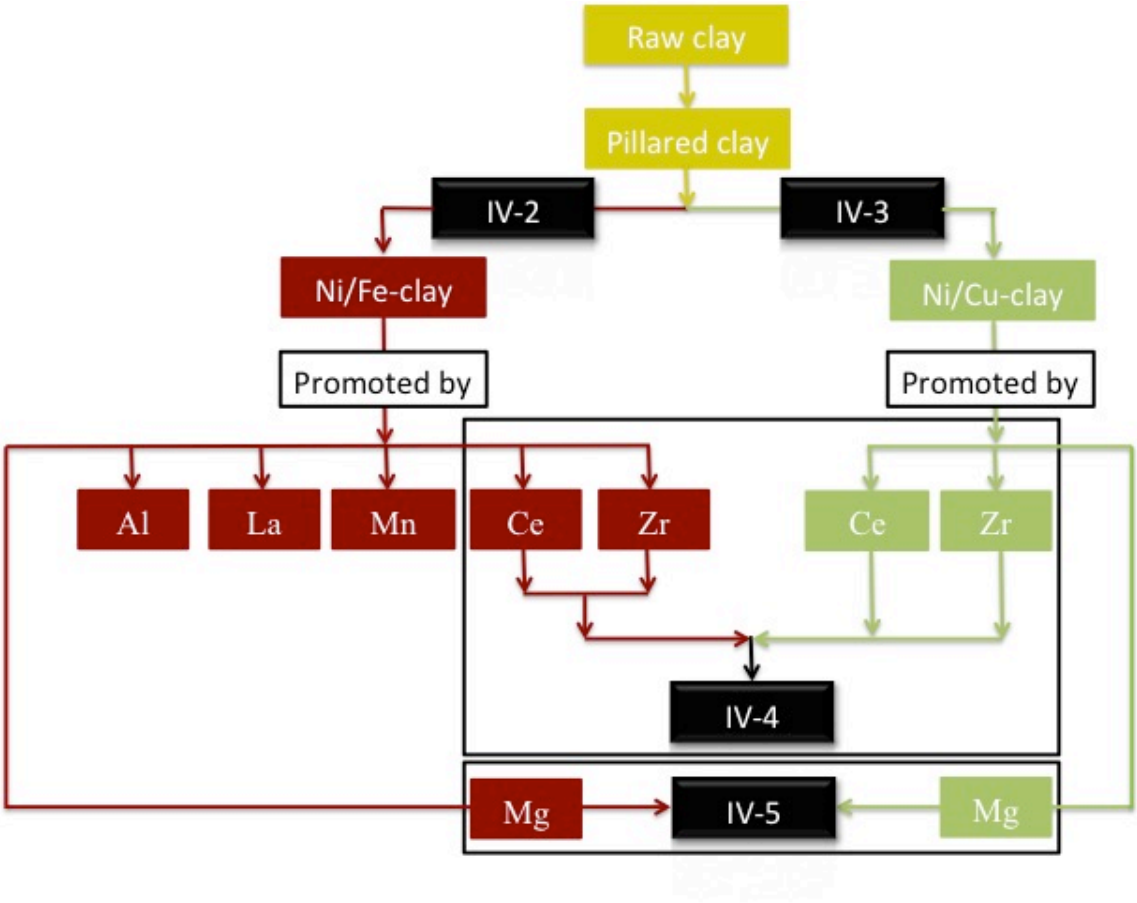

Figure 4-1. Outline for each section.

4.2 Ce, Zr, La, Al and Mn promoted Fe-pillared clay supported Ni-based catalysts

The addition of different promoters has been considered as a way of further improving the catalytic performance. Ce and Zr oxides have been widely used in general for the promotion

of DRM catalysts. Osawa et al. [109] studied the Ce-promotion of illite clay-supported catalysts for DRM. They showed that the presence of Ce enhanced the dispersion of Ni on the clay surface. Daza et al. [110] reported an important beneficial effect of the presence of Ce on the activity and selectivity of mineral clay-supported Ni-catalysts, as well as a diminution in the formation of coke, that however depended on the nominal amount of Ce used. Liu et al. [111] showed that Zr promoted catalytic activity through the enhancement of the structural stability of the prepared materials, the improvement of the dispersion of Ni, and through the partial activation of CO_2. The promoting effect depends however on the clay composition and thus origin.

In this section, La, Al and Mn promoted Fe-clay based nickel catalysts were synthesized by conventional impregnation method and tested in dry reforming of methane (DRM) in the temperature range of 850 °C to 600 °C. Ce and Zr promoter Fe-clay catalysts were also explained for a sake of comparison in this section, but in range of 800 °C to 600 °C. The effect of different promoters on iron (Fe) modified clay based catalysts containing 15 wt.% nickel on physicochemical characterizations and catalytic activity were analyzed based on X-ray diffraction (XRD), Brunauer-Emmett-Teller (BET), temperature-programmed reduction (H_2-TPR) and temperature-programmed desorption (CO_2-TPD) respectively.

4.2.1 Preparation of Fe-clay supported Ni-based catalysts with different promoters

4.2.1.1 Preparation of Fe-pillared Clay Supports

Natural clay from the deposit of Jebal Cherahil (Kairouan, Central−West of Tunisia) was chosen as the raw material. The raw clay was suspended in distilled water to disperse and decant, following by wet sieving (diameter of the sieve mesh is 2 μm). The the selected clay was introduced in 1 M NaCl solution and stirred 12 h at room temperature. This process would be repeated three times to get Na-exchanged clay, and then it was separated and washed by centrifugation and distilled water respectively. The Na-exchanged clay is then recovered and dried at 60 °C in an oven. It is subsequently grinded by hand until to 100-mesh. These procedures used for its purification and Na-ion exchange from its surface have also been described in Reference [112]. For the preparation of the Fe-modified clay, a pillaring

solution was prepared by slow addition of Na_2CO_3 powder (97%, MERCK) into a 0.2 M solution of $Fe(NO_3)_3$ (Fe $(NO_3)_3 \cdot 9H_2O$ 97%, MERCK) while stirring at 100 rpm for 2 h at room temperature until the molar ratio Fe/Na_2CO_3 reached 1:5. The solution was then aged during 4 days at 60 °C. Finally, the resulting oligomeric Fe (III) solution was added into a 2 wt.% aqueous dispersion of the purified Na-exchanged clay, at a ratio of 10^{-3} mol of Fe^{3+} per gram of clay. The dispersion was agitated at 100 rpm for 24 h, then filtered, washed by with deionized water several times, and finally centrifuged at 4000 rpm for 10 min. The resulting solid material was calcined at 300 °C for 24 h, and subsequently ground to 100-mesh. The compositions of raw, Fe-pillared clays are shown in Table 4-1.

Table 4-1. Composition of raw, Fe and Cu-pillared clays (XRF analysis)

Material	Composition [wt.%]							
	SiO_2	Al_2O_3	Fe_2O_3	MgO	K_2O	Na_2O	CaO	CuO
Raw clay	43.4	16.8	7.7	5.5	0.8	2.5	7.9	-
Fe-Clay	38.4	15.4	32.5	1.1	0.6	1.0	1.13	-

4.2.1.2 Preparation of different promoters (cerium (Ce), zirconium (Zr), lanthanum (La), aluminum (Al) and manganese (Mn)) promoted Fe-pillared clay supported Ni-based catalysts

Ce, Zr, La, Al and Mn promoted Fe-clay based Ni catalysts containing constant loading of nickel (15 wt.%) were synthesized by the impregnation method. These clay based catalysts were introduced into mixed solutions of $Ni(NO_3)_2 \cdot 6H_2O$ and/or $Ce(NO_3)_3 \cdot 6H_2O$/ $ZrO(NO_3)_2 \cdot 6H_2O$/ $La(NO_3)_3 \cdot 6H_2O$/ $Al(NO_3)_3 \cdot 9H_2O$/ $Mn(NO_3)_2 \cdot 4H_2O$ with distilled water, and subsequently aged for 2 hours at room temperature. The water in suspension was extracted at 40 °C in a rotary evaporator, and then the solid material was kept at 110 °C in an oven overnight. Finally, all solid materials were calcined in air at 550 °C for 5 h after grinding in order to obtain the corresponding catalysts. The nominal (assumed) concentration of different components in each catalyst and their labels were presented in Table 4-2.

Table 4-2. Promoted Fe-modified clay based Ni catalysts: nominal composition.

Catalyst	Label	Ni [wt.%]	Ce [wt.%]	Zr [wt.%]	La [wt.%]	Al [wt.%]	Mn [wt.%]
Ni-Ce/Fe-Clay	Ni-Ce	15	10	-	-	-	-
Ni-Zr/Fe-Clay	Ni-Zr	15	-	10	-	-	-
Ni-La/Fe-Clay	Ni-La	15	-	-	10	-	-
Ni-Al/Fe-Clay	Ni-Al	15	-	-	-	10	-
Ni-Mn/Fe-Clay	Ni-Mn	15	-	-	-	-	10

4.2.2 Physicochemical properties

4.2.2.1 Textural properties

The results of textural characterizations such as the BET surface area and total pore volume obtained for the calcined catalysts through N_2 adsorption isotherms are listed in Table 4-3. BET surface areas change owing to impregnate different promoters, which are contributed to the partial pore blockage and different pore sizes. Compared to non-promoted catalysts, the presences of different promoters increase BET surface areas to varying degrees in addition to lanthanum. According to literatures, the addition of La oxides decreases the BET surface area to a large extent [113,114]. It can be concluded that lanthanum species enter and occupy the pores [114]. On the contrary, the introduction of Ce, Zr, Mn and Al oxides enhances the surface area, especially the Al-promoted catalysts that own relatively small pore volume (only larger than the La-promoted catalysts). The high specific surface area could be attributed to pure Al_2O_3 formed during the catalyst synthesis [115]. In general, a large specific surface area corresponds to a small pore size [116]. However, the tendency has not been followed by the Ce/Mn-promoted catalysts compared to the non-promoted catalysts in the view of the calculated results in Table 4-3. Because the average pore size is calculated on the basis of total pore volume (General: average pore size=k × total pore volume/specific surface area, $k=4\times10^3$), a deviation in the value could exist. Moreover, non-promoted and Ce/Mn-promoted catalysts have similar average pore sizes, which are 9, 11 and 13 nm respectively. Therefore, relatively accurate pore sizes for the Ce/Mn-promoted catalysts may be less than non-promoted catalysts. The range of average pore sizes for all prepared catalysts, between 7.0 and 28.0 nm, indicates the mesoporous structure of prepared catalysts. Furthermore, type IV adsorption isotherms and H3 adsorption loops could be observed for this catalyst system.

Table 4-3. BET results, Ni^0 crystal size and H_2-consumption for the different promoter loaded Fe-modified clay catalysts.

Catalyst	S_{BET} [m^2/g]	V_p[1] [cm^3/g]	d_p[2] [nm]	V_{BJH}[3] [cm^3/g]	Ni^0 crystal size [nm]		H_2-consumption[5] [mmol H_2/g]
					Reduced	Spent	
Ni/Fe-clay	44	0.11	9	0.11	13.4	-	1.66
Ni-Ce/Fe-clay	52	0.15	11	0.15	12.9	-	1.20 [4]
Ni-Zr/Fe-clay	56	0.11	7	0.11	11.8	-	0.68 [4]
Ni-Mn/Fe-clay	45	0.15	13	0.14	10.6	12.6	1.85 [6]
Ni-La/Fe-clay	13	0.10	28	0.10	9.8	17.3	1.46
Ni-Al/Fe-clay	63	0.11	7	0.08	9.2	13.8	1.20

[1] *total pore volume*
[2] *average pore size*
[3] *BJH desorption cumulative pore volume*
[4] *reduction is completed at 800°C*
[5] *theoretical H_2 consumption for Ni species is 2.5 mmol/g catalyst*
[6] *theoretical H_2 consumption for Mn species is 1.8 mmol/g catalyst*

4.2.2.2 Crystallinity: Ce/Zr/La/Al/ Mn-promotion on Fe-modified clays and Ni^0 crystal size

The XRD patterns of reduced Fe-modified clay based catalysts are shown in Figure 4-2 a) and b) respectively. Two identical reflections, i.e. metallic Ni phase (at around 44.5°, 51.8°, 76.3°) and quartz, could be detected for all prepared catalysts. The presence of Ce, Zr, La, Al and Mn results in the additional phases corresponding to CeO_2, ZrO_2, La_2O_3, $La_2O_2CO_3$, Al_2O_3, Mn_3O_4 and $NiMnO_3$, the other Ni-promoter oxides and/or complex compounds with CO_3 may exist in the corresponding catalysts, but these compounds are not detected since their small particle sizes and/or low contents. Furthermore, the impregnated promoters do not affect the other crystal structure. After reaction, two additional reflections of NiO and Fayalite, Mn-rich are presented on spent Mn-promoted catalysts in Figure 4-2 c), which may influence the Ni reducibility.

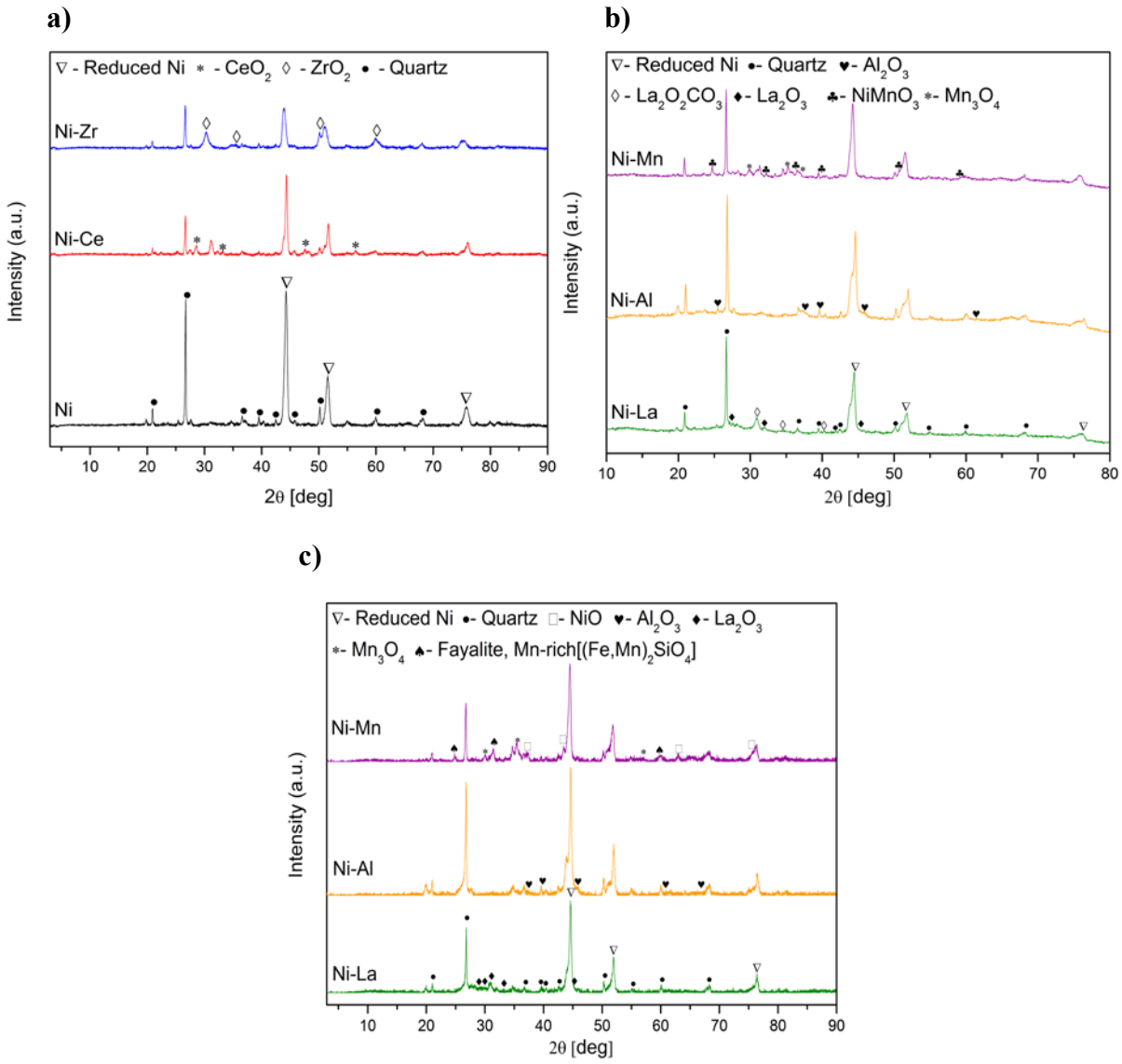

Figure 4-2. XRD profiles for the reduced a) non-promoted and Ce/Zr-promoted, b) La/Al/Mn-promoted Fe modified catalysts and c) spent La/Al/Mn-promoted Fe modified catalysts.

The calculation of Ni^0 crystallite size based on the Scherrer equation for all catalysts is located at around 76.3° to avoid the effects of overlapping peaks and listed in Table 4-3, and the existence of promoters resultes in slightly small Ni^0 crystallite size corresponding to the sequence: Ni-10Al/Fe-clay < Ni-10La/Fe-clay < Ni-10Mn/Fe-clay < Ni-10Zr/Fe-clay < Ni-10Ce/Fe-clay < Ni/Fe-clay. For supported metal catalysts, the particle size is inversely proportional to the dispersion [117]. The formula could be described as d=k/D (where d is paticle size, D is dispersion and k is a constant that is decided by tested metal. Thus, it suggests that the Ce, Zr, La, Al and Mn promote the dispersion of metallic nickel in reduced catalysts. Similar results have been reported in literatures [114,118,119]. However, for Mn-promoted catalysts, the amount of manganese is pivotal, excessive manganese is not

benefical to the Ni dispersion [120]. Otherwise, the formation of NiMnO3 indicates the strong interactions between NiO and promoter that may influence the Ni reducibility. On La-promoted catalysts, Akri [113] also found a higher Ni dispersion on low specific surface area catalysts. It was reported in the literature that the presence of lanthanum oxide could promote the dispersion of metallic crystallites [113, 121]. Otherwise, the formation of lanthanum oxycarbonates ($La_2O_2CO_3$) is benefical to the gasification of amorphous carbon deposits since it provides oxygen that can react with the carbon on the nickel surface [122]. For Al promoted catalysts, since a higher surface area (Table 4-3) is found, the Ni dispersion should be favored, and an enhancement of the catalytic performance should be obtained [123]. Moreover, there is not a big difference for reduced and spent La/Al/Mn-promoted catalysts, it means that there is no sintering during reaction.

4.2.2.3 Reducibility of the Ni-species

H_2-TPR patterns of different promoters on Fe modified clay are presented in Figure 4-3. All prepared catalysts except Mn-promoted catalysts present two main peaks, the first peak below 600 °C is not only ascribed to bulk NiO weakly bonded to Fe-modified clay, but also as a consequence of the reductions of Fe oxides species at about 450-600 °C [113,124-126]. The peak at around 700 °C can be attributed to well dispersed NiO species strongly bonded to the surface of Fe-clay [113]. In addition, the shoulder for La-promoted catalysts corresponds to the reduction of segregated NiO species. For Mn-promoted catalysts, the obvious peak at about 385 °C and small shoulder at about 410 °C for Mn-promoted catalysts can be assigned to the reduction of MnO_2 to Mn_2O_3 and/or segregated NiO species. The second peak before 600 °C comes from the reduction of Mn_2O_3 to Mn_3O_4, Fe oxides species and/or weakly bonded bulk NiO. Tha last peak at about 700 °C can be concluded to the reduction of Mn_3O_4 to Mn^{2+} and/or strong connection between fine NiO species and support. The existence of Mn_3O_4 in reduced and spent catalysts from XRD patterns means the partial reduction of Mn_3O_4. And the presence of NiO in spent Mn-promoted catalysts indicates incomplete reduction of NiO species, it may influence the catalytic performance. Otherwise, comparing to the other prepared catalysts, the obvious wide peaks for Mn-promoted catalysts are assigned to the multistep reduction of Mn oxides ($MnO_2 \rightarrow Mn_2O_3 \rightarrow Mn_3O_4 \rightarrow Mn^{2+}$), which also can explain its highest H_2 uptake (in Table 4-3) calculated through integrating areas [127-129]. Meanwhile, the reduced H_2 consumption for La/Al-promoted catalysts indicates

the presence of La and Al promotes the interactions between Ni species and Fe-modified clay, i.e. more highly dispersed Ni species are formed, in agreement with the results of Ni crystal sizes calculated through XRD patterns (in Table 4-3). Akri et al. already reported similar results on La-promoted catalysts on illite-based materials [113]. The same situation also happens on Ce/Zr-promoted catalysts that will be explained in section 4.4.2.2.

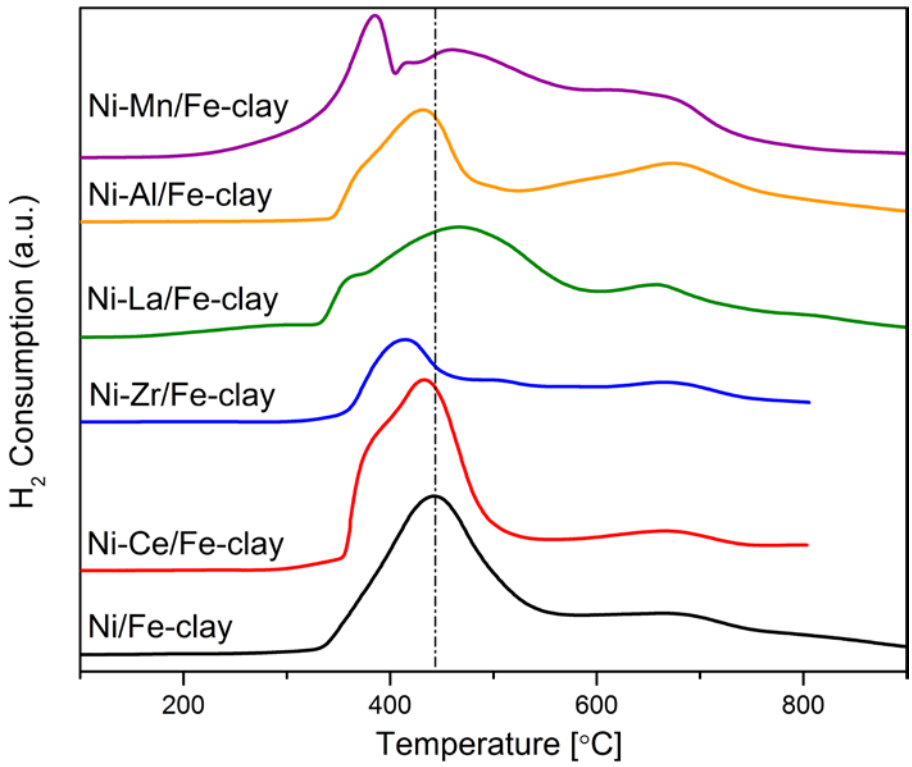

Figure 4-3. H_2-TPR profile for the Ni-X/Fe-clay (X=Non, Ce, Zr, La, Al, Mn) catalysts.

Furthermore, the main peak position shifts to slightly higher temperature for La-promoted catalysts pointing out stronger interaction between Ni species and supports, thus decreasing Ni reducibility. It could be linked to the formation of nickel-lanthanum complex oxide. It also suggests the existence of better Ni dispersion comparring to non-promoted and Ce/Zr-promoted catalysts, which is in agreement with the analysis of XRD. The similar results were also reported by Yu et al. [130]. When compared to Ni/Fe-clay, the Al-promoted catalysts increase the Ni reducibility since the peak at around 450 °C is slightly shifted to lower temperature. On Ni-Al/Fe-clay catalyst, it is observed a decrease of the peak at around 450 °C corresponding to weak interactions between NiO species and Fe-clay and a increase of the second peak (ca. 700 °C) which could be explained by its lower Ni^0 crystallite size (9.2 nm) and higher dispersion. For Mn-promoted catalysts, the assignments of peaks are not

obvious because of the presence of manganese oxides, thus it is hard to determine the Ni reducibility clearly.

4.2.2.4 CO_2 adsorption and basicity

CO_2-TPD profiles are presented in Figure 4-4. All prepared catalysts have three typical CO_2 desorption peaks ranging from 100 to 600 °C. The different peaks correspond to weak Brønsted basic sites such as surface OH groups (low temperature), medium-strength Lewis acid-base sites (intermediate temperature), and low-coordination oxygen anions acting as strong basic sites (high temperature) [124,131].

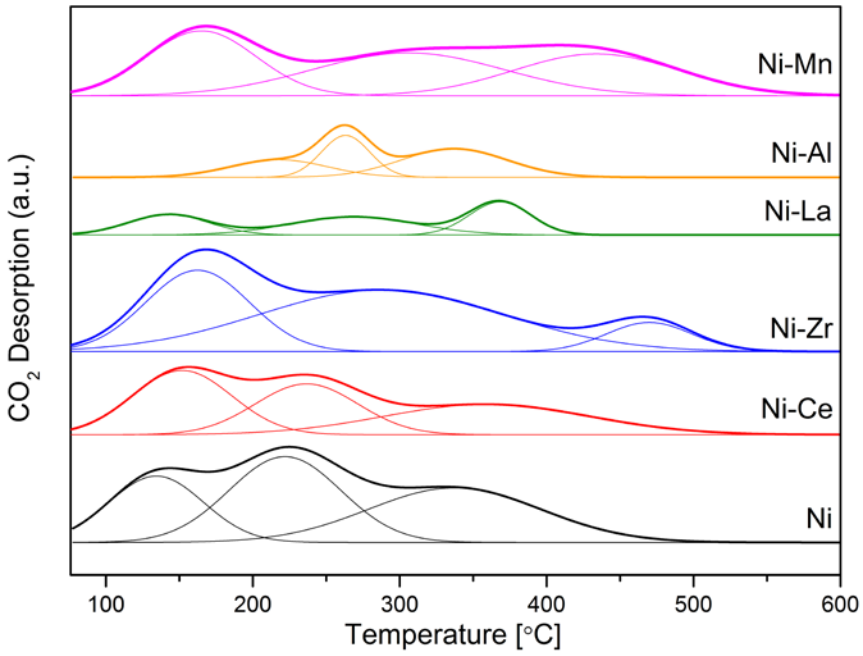

Figure 4-4. CO_2-TPD profile for the different promoters on Fe-clay based catalysts.

For all promoted catalysts, the centers of weak basic sites, medium-strength Lewis acid-base sites and strong basic sites occur at 140-210 °C, 238-305 °C and 337-470 °C respectively, which are listed in Table 4-4. Thus, comparing to the centers of non-promoted catalysts that are located at 135 °C, 222 °C and 335 °C, all basic sites on each promoted catalysts shift to higher temperature. It means the presences of Ce, Zr, La, Al and Mn strengthen CO_2 chemisorption, especially for Zr- and Mn-promoted catalysts, three basic sites appear 26 °C, 62 °C, 134 °C and 30 °C, 83 °C, 100 °C late respectively. The existence of La increases the medium basic sites and strong basic sites by 42 and 32 °C respectively. The addition of Al

mainly shifts the weak basic sites and medium basic sites, the variations are about 80 and 40 °C. Ce-promoted catalyst slightly increases the position of each basic site.

The CO_2 desorption listed in Table 4-4 always changes due to the addition of different promoters. For Fe-modified clay based catalysts, both additions of La and Al not only strongly modify the CO_2 desorption on each basic sites, but change the distribution of basic sites as well, especially on the strong basic sites. Furthermore, the introduction of Mn slightly decreases the CO_2 amount on each basic site while Ce and Zr maily decrease the CO_2 amount on strong basic sites compared to non-promoted catalysts. The influences on strong basic sites may affect the catalytic performance and/or carbon deposition during DRM reaction, because CO_2 on strong basic sites is more difficult to react with CH_4 and then more direct methane decomposition can be carried out [132].

Table 4-4. CO_2-TPD data and carbon deposition for different promoters promoted catalysts.

Catalyst	Peak position [°C]			Basicity [µmol CO_2 desorbed/g]			Total basicity [µmol CO_2/g]	Carbon Deposition[1] [mg]
	1st	2nd	3rd	1st	2nd	3rd		
Ni/Fe-Clay	135	222	335	7.02	6.68	8.88	22.58	92.9
Ni-Ce/Fe-Clay	151	238	359	6.34	3.79	5.63	15.76	241.0[2]
Ni-Zr/Fe-Clay	162	286	470	7.29	12.17	2.20	21.66	212.9[2]
Ni-Mn/Fe-Clay	166	305	434	6.85	5.27	7.32	19.44	15.1
Ni-Al/Fe-Clay	210	262	337	1.44	1.73	2.76	5.95	284.8
Ni-La/Fe-Clay	140	267	368	2.24	1.39	3.14	6.76	239.6

[1] *Carbon deposition is calculated at 750°C during 5h based on the mass of tested catalyst, which is not converted into 1g of catalyst.*
[2] *Carbon deposition is calculated for catalysts that are reduced at 800°C*

4.2.3 Catalytic activity and selectivity of Ce, Zr, La, Al and Mn promoted Fe-pillared clay supported Ni-based catalysts

DRM results are presented in Figure 4-5, including both conversions of CH_4 and CO_2, and H_2/CO molar ratio for non-promoted/promoted Fe-modified clay based catalysts, as a function of reaction temperature. In order to compare the influences of different promoters, non-promoted and Ce/Zr promoted catalysts that will be discussed in section 4.3 and 4.4 respectively are also introduced in the profile [124,131].

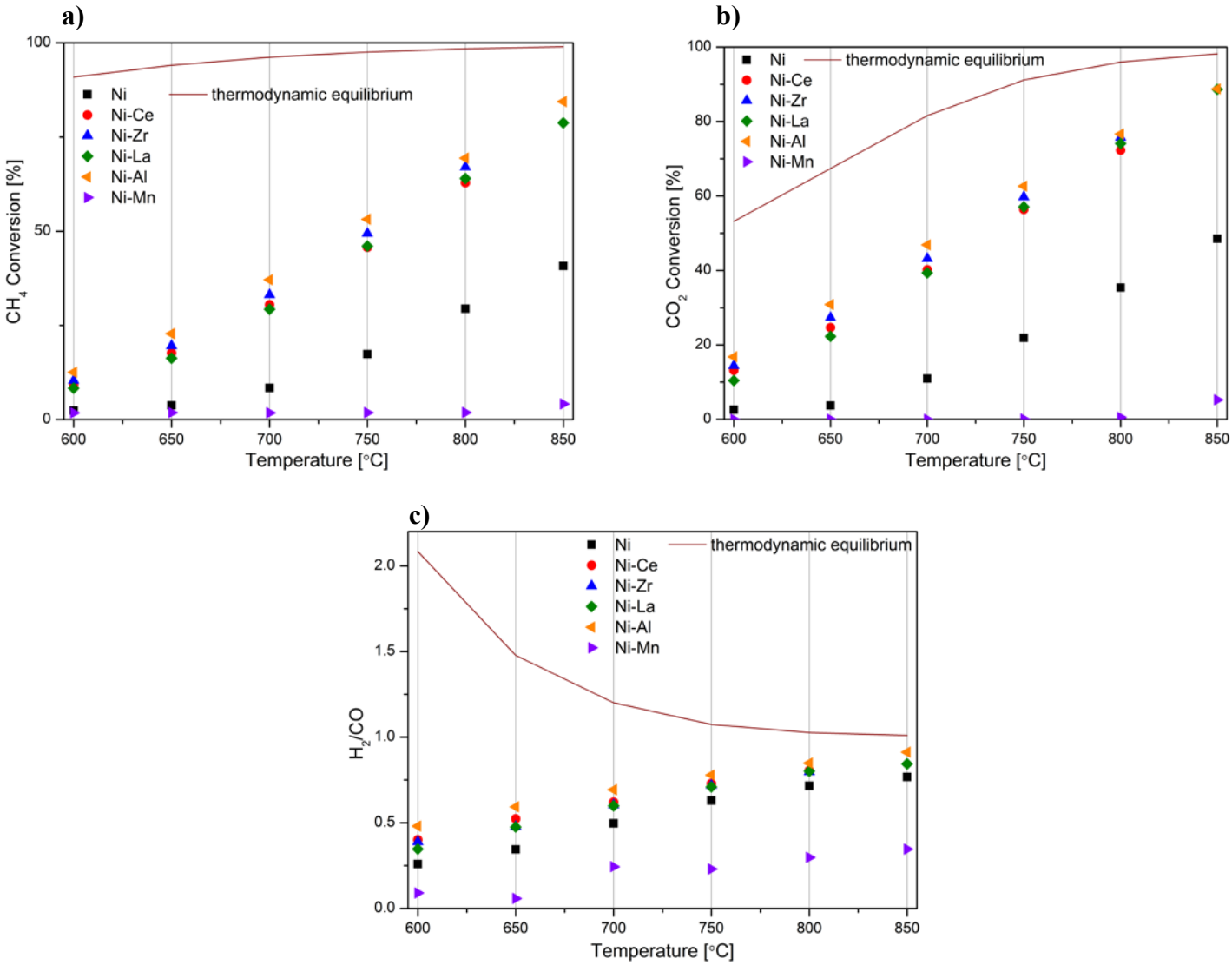

Figure 4-5. DRM Results for the Ni-X/Fe-clay (X=non, Ce, Zr, La, Al, Mn) catalysts, a) CH_4 b) CO_2 c) H_2/CO molar ratio. The points of Non-promoted and Ce/Zr promoted catalysts in section 4.3 and 4.4 are listed in figures to present the influences of different promoters.

CH_4 and CO_2 conversions change with reaction temperatures, together with H_2/CO molar ratio, as expected following the tendencies forecasted by thermodynamics. Both CH_4 and CO_2 conversions on La/Al promoted catalysts are higher than those on Mn-promoted catalysts. The higher activity observed on La promoted catalysts can be attributed to its high Ni dispersion and low strong basic sites (Table 4-3, Table 4-4). Qian et al. [114] reported the pathway of La-promoted Ni/SBA-15 catalysts for DRM. Lanthanum species and Ni formed large interface, CO_2 and CH_4 were adsorbed on the surface of La species and Ni respectively. Then the process of CO_2 dissociation produced oxygen atom that can interact with CH_4 to form promoting intermediates. At last, H_2 and CO was desorbed from the surface of catalysts. The presence of La species mainly enhanced the CO_2 dissociation and further promoted the intermediates. For relatively small Ni patricle sizes in our La-promoted catalysts, the

intermediate could be CH_xO (x = 2-3) species. For Al-promoted catalysts, the low Ni particle sizes and low strong basic sites result in its best catalytic performance. Similar results have also been reported by He et al. [133]. On the contrary, although the good Ni dispersion and medium basicity for Mn-promoted catalysts, lower conversions are observed. This low activity of Mn promoted catalysts can be caused by the presences of Mn oxides and Fayalite, Mn-rich, which may partially or totally cover the active sites on NiO species. The similar results have been reported by Koike et al [120]. However, the real reason cannot be explained based on the characterizations presented in this work, and further characterizations are required. The effect of specific surface area on both CH_4 and CO_2 conversions at 750 °C for DRM reaction is presented in Figure 4-6. High specific surface area corresponds to high conversions for the non-promoted and Ce/Zr/Al-promoted catalysts while the addition of La/Mn leads to the opposite trend. It means that for our catalytic systems the specific surface area is not the major factor involved in the catalytic activity for DRM.

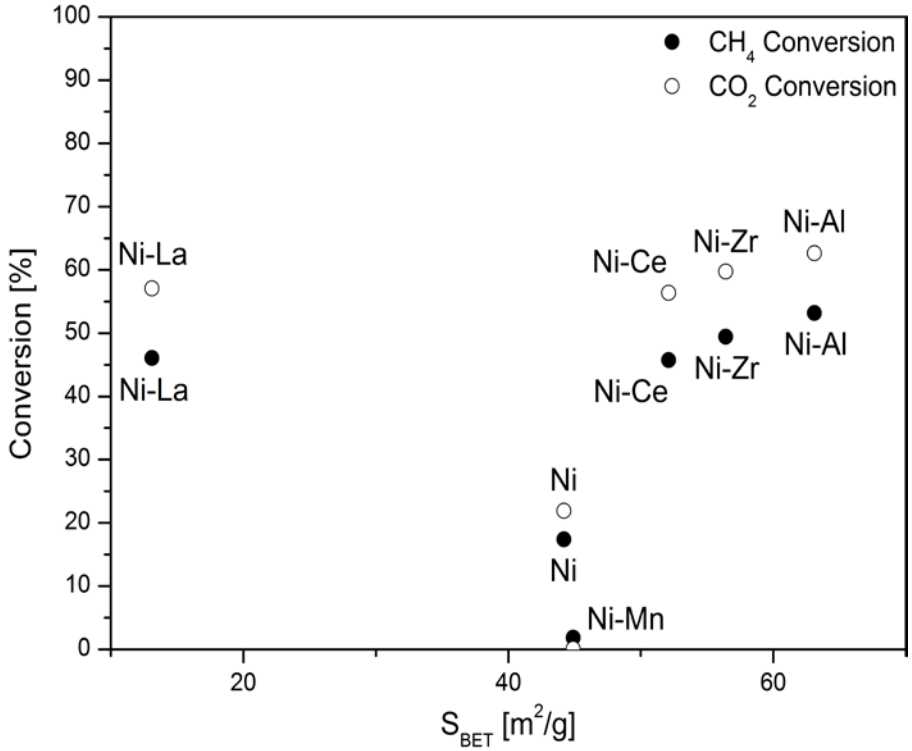

Figure 4-6. CH_4 and CO_2 Conversions (750 °C) vs. S_{BET} for the different promoters catalysts.

For the DRM tests, the conversions of CO_2 are always higher than CH_4 for Ce/Zr/La/Al-promoted catalysts in the range of reaction temperatures, and the values of H_2/CO are almost similar. It indicates the presence and synergy of side reactions during DRM, mainly including the reverse water-gas shift reaction ($CO_2 + H_2 \rightleftharpoons CO + H_2O$), Boudouard

reaction ($2CO \rightleftharpoons CO_2 + C$) and direct methane decomposition ($CH_4 \rightleftharpoons C + 2H_2$), leading to more CO_2 could be consumed [130,134]. Meanwhile, the Boudouard reaction and direct methane decomposition could further lead to non-negligible carbon deposition.

4.2.4 Influence of Ce, Zr, La, Al and Mn promotion on Fe-pillared clay on carbon deposition

The carbon deposition at 750 °C for 5 h for all prepared catalysts is presented in Table 4-4 and calculated through mass balance. The general formula for calculating carbon deposition is carbon deposition=carbon input – carbon output. For our catalytic system, it can be expressed in detail as following by means of the values of micro chromatography:

$$\text{Carbon deposion} = [(M_c \times \frac{\overline{V_{CH_4}}}{V_m} + M_c \times \frac{\overline{V_{CO_2}}}{V_m})_{\text{Input}} - (M_c \times \frac{\overline{V_{CH_4}}}{V_m} + M_c \times \frac{\overline{V_{CO_2}}}{V_m} + M_c \times \frac{\overline{V_{CO}}}{V_m})_{\text{Output}}] \times 300\text{min},$$

in which M_c is the molar mass of carbon, V_m is the molar volume and $\overline{V}$ is the average volumetric flow rate for each components.

It could be found that introduction of Ce, Zr, La and Al oxides promotes the carbon deposition for Fe-modified clay based catalysts, indicating the addition of Ce/Zr/La/Al does not inhibit side reactions. The high carbon deposition for Al-promoted catalyst can be explained by the low interaction between bulk NiO and support, resulting in Ni sintering that is beneficial to the formation of carbon during reaction [135]. The relatively low carbon for La-promoted catalysts comparing to the promotion of Al is also related to the formation of lanthanum oxy-carbonate ($La_2O_2CO_3$) that can gasify the carbon during its deposition [136]. Furthermore, the relatively low carbon of Ce- and Zr-promoted catalysts with relatively high activity compared to La-promoted catalysts may be attributed to form oxygen vacancies and then promote redox properties for Ce-promoted catalysts, and to improve thermal stability of structure and activate CO_2 to oxidize carbon species for Zr-promoted catalysts respectively [111,137]. Finally, the low carbon deposition for Mn-promoted catalysts is ascribed to its lowest activity, even at higher temperature [119,138,139].

4.2.5 Summary

Table 4-5. Summary for the influences of Al, La, Mn, Ce and Zr promotion on Fe-clay.

	Promotion	Ni	Ni-Al	Ni-La	Ni-Mn	Ni-Ce	Ni-Zr
Fe-clay	Specific surface area	0	+	-	+	+	+
	Ni^0 crystallite size[1]	0	-	-	-	-	-
	Ni reducibility	0	+	-	+/-	+	+
	Total basicity	0	-	-	-	-	-
	DRM activity	0	+	+	-	+	+
	Carbon deposition	0	+	+	-	+	+

"0" means the benchmark.
"+" means the strengthened/increased value compared to Ni based Fe-clay catalysts.
"-" means the weakened/decreased value compared to Ni based Fe-clay catalysts.
[1] Ni^0 crystallite size is compared only for reduced catalysts

Table 4-5 presents the different effects of promoters on Fe-modified clay. The addition of Al, La, Mn, Ce and Zr affected the specific surface area and catalyst basicity. All promoters resulted in smaller Ni^0 crystallite size and further promoted Ni dispersion. Al/Ce/Zr-promoted catalysts improved the Ni reducibility compared to La/Mn-promoted catalysts. Al-promoted Fe-clay based catalysts presented the best catalytic performance in DRM. Both CH_4 and CO_2 conversions followed the trend of thermodynamical calculations.

4.3 Cu-pillared clay supported Ni-based catalysts compared with Fe-pillared clay supported Ni-based catalysts

In addition to the influence of promoters, the support also plays an important role in the preparation of efficient DRM catalysts. It influences the dispersion of the active phase, not only providing adequate textural properties, i.e. high specific surface area, but also enhancing the interaction with the metallic phase and the adsorption of the reactants, through the presence of basic surface groups. Among the different possible materials that can be chosen as catalysts, clays as an excellent support is selected for this presented paper due to abundant content and variable physico-chemical properties [140,141]. Gamba et al. [140] used an Al-modified mineral clay as support and reported considerably high DRM activity and low extent of carbon deposition for their Ni-based catalysts promoted with Pr. Wang et al. [142] studied the use of natural clays (montmorillonite and bentonite) in view of their particular pore structure and surface properties. They remarked that these kinds of materials can be promising supports for the preparation of DRM catalysts, however, they also claimed that carbon deposition needs to be further controlled.

In this section, raw, Fe- and Cu-modified clay will be compared in the preparation of Ni-based catalysts for DRM. The presence of Fe and Cu pillars may influence not only the type of porosity of the support, and therefore Ni distribution and catalyst stability, but also the activity and selectivity of these materials, due to the inherent presence of Fe and Cu together with Ni. The present section describes the DRM behavior of Ni-catalysts prepared using raw, Fe-pillared and Cu-pillared natural clay. The so-prepared catalysts are characterized by means of BET, XRD, H_2-TPR and CO_2-TPD to analyze the possible influences of physicochemical properties on catalytic performance, for two different reduction temperatures, i.e. 800 and 900 °C.

4.3.1 Preparation of Fe/Cu-pillared clay supported Ni-based catalysts

The preparation of Fe-modified clay was explained in section 4.2.1.1. For the preparation of the Cu-pillared clay, Cu-Clay, 1 g of Na-exchanged raw clay and 100 mL of 0.02 M copper acetate (Cu $(CH_3COO)_2$ (98%) MERCK) solution were stirred at a pH of 5.2 and 40 °C for 24 h. The resulting suspension was filtered and the precipitate was washed several times with deionized water. The catalyst was then dried at 120 °C for 12 h and subsequently calcined at 400 °C for 5 h. The composition of raw, Fe and Cu-pillared clays are shown in Table 4-6.

Table 4-6. Composition of raw, Fe and Cu-pillared clays (XRF analysis)

Clay	Composition [wt.%]							
	SiO_2	Al_2O_3	Fe_2O_3	MgO	K_2O	Na_2O	CaO	CuO
Raw clay	43.4	16.8	7.7	5.5	0.8	2.5	7.9	-
Fe-Clay	38.4	15.4	32.5	1.1	0.6	1.0	1.13	-
Cu-Clay	37.01	14.32	6.9	1.3	1.1	2.61	0.61	11.1

Nickel was introduced into Fe/Cu-modified clay by means of a conventional impregnation method, using an aqueous solution of nickel nitrate hexahydrate ($Ni(NO_3)_2 \cdot 6H_2O$, Aldrich) as metal precursor. The Ni loading for all catalysts was fixed as 15 wt.%. Upon impregnation, the catalysts were dried overnight at 100 °C and subsequently calcined at 550 °C for 5 h.

4.3.2 Physicochemical properties

4.3.2.1 Textural and structural properties of the natural clay based Ni-catalysts

Table 4-7 contains the results of the textural characterization of the clays and natural clay based Ni-catalysts, performed by means of N_2 adsorption. The adsorption isotherms obtained (not shown) correspond to type IV isotherms, according to IUPAC classification, presenting H3 hysteresis loops, typical of laminar-structured materials containing slit-shaped pores. They all show a strong increase of adsorption at high relative pressured, linked to the presence of macropores. The desorption branch of the isotherms closes at low relative pressures (below 0.4), pointing to impeded diffusion and trapping of N_2 molecules inside the partially collapsed and far too complex laminar structure, maybe as a consequence of an excess of Fe and Cu pillars.

Table 4-7. BET surface area, pore volumes and average pore size for the raw and modified clays, as well as for the natural clay based Ni-catalysts, together with Ni crystal sized calculated from XRD patterns.

Material	S_{BET} [m^2/g]	V_p[1] [cm^3/g]	V_{BJH}[2] [cm^3/g]	V_{micro}[3] [m^3/g]	d_p[4] [cm^3/g]	Ni crystal size [nm]	
						Red 800°C	Red 900°C
Raw clay	73.6	0.148	0.146	0.012	8.1	-	-
Fe-Clay	60.9	0.111	0.112	0.011	6.6	-	-
Cu-Clay	102.8	0.195	0.193	0.016	7.7	-	-
Ni/Clay	55.4	0.112	0.111	0.007	8.9	18.0	13.1
Ni/Fe-Clay	44.3	0.108	0.108	0.006	8.6	13.4	12.4
Ni/Cu-Clay	84.3	0.159	0.156	0.003	8.2	8.1	11.7

[1] *single point desorption total pore volume*
[2] *t-plot micropore volume*
[3] *BJH desorption cumulative pore volume*
[4] *BJH desorption average pore width*

BET surface area decreases upon the addition of Fe and increases through the formation of Cu pillars. Ni loading generally causes a decrease of surface area, due to partial blockage of micropores and narrow mesopores. Average pore sizes around 8-9 nm were found for the three natural clay based Ni-catalysts.

4.3.2.2 Reducibility of the Ni-species

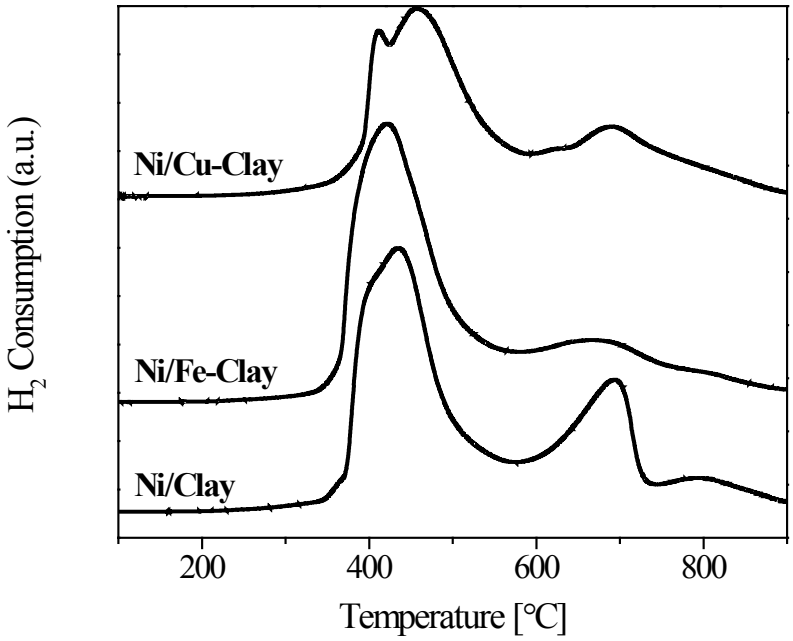

Figure 4-7. Temperature programmed reduction (H_2-TPR) profiles acquired for the natural clay based Ni-catalysts.

The results of the H_2-TPR experiments are plotted in Figure 4-7, for the three natural clay based Ni-catalysts. CuO reduction to Cu^0 should occur at relatively low temperatures, i.e. between 270 and 310 °C [143]. No peaks are clearly observed at these temperatures for the catalyst prepared using the Cu-modified clay. However, the shoulder appearing at about 400 °C can be ascribed to the presence of mixed Cu-Ni oxides [144,145]. In the case of the catalysts, Fe_3O_4 oxidation to Fe_2O_3 is expected to take place at temperatures between 450 and 480 °C, whereas Fe_2O_3 oxidation to metallic Fe^0 occurs at higher temperatures, in a wide range, i.e. from 480 to 600 °C [146]. The reduction of bulk and weakly bonded Ni-oxide species will take place almost simultaneously. However, the presence of a second peak of H_2 consumption at about 650-700 °C points as well to the presence of finely dispersed NiO_x, having a stronger interaction with the clay support, or, in the case of the Fe-Clay based catalysts, even with iron [147-149]. The area of this peak decreases in the catalysts prepared either the Fe or the Cu-modified clay, pointing to the presence of Ni-species of increased reducibility, maybe due to impeded interaction of Ni and the support in the presence of the Fe or Cu-pillars.

4.3.2.3 Crystallinity: Cu/Fe-modified clays and Ni^0 crystallite size

At the sight of the H_2-TPR profiles acquired for this series of catalysts, two reduction temperatures were chosen, 800 and 900 °C, in order to pre-treat the catalysts prior to the DRM catalytic tests. Figure 4-8 a) and b) show the XRD patterns acquired for the catalysts reduced either at 800 °C (Figure 4-8 a) or at 900 °C (Figure 4-8 b), under 5 vol.% H_2/Ar for 1h.

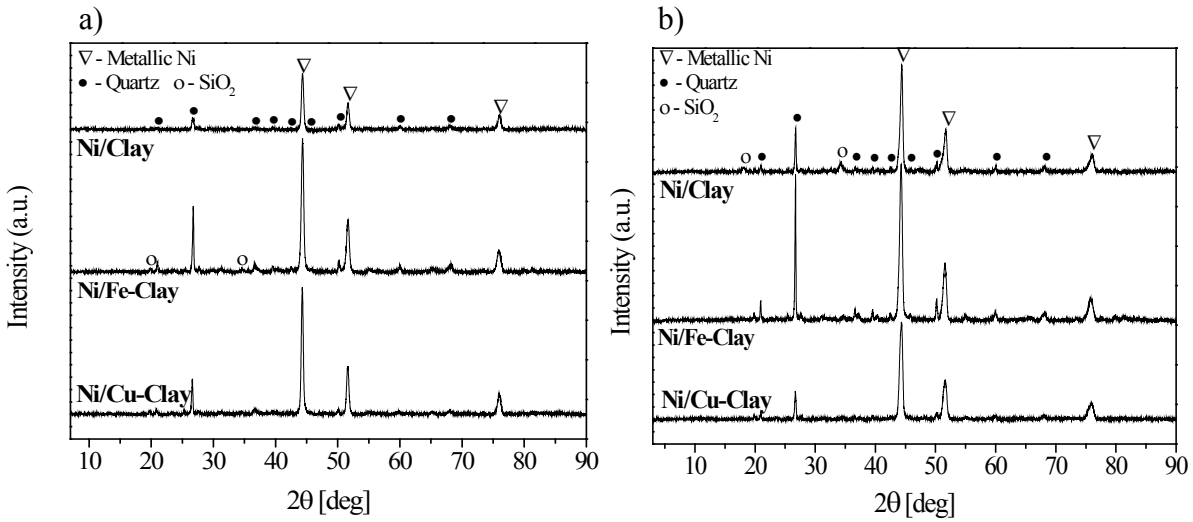

Figure 4-8. XRD patterns acquired for the catalysts reduced at a) 800 °C and b) 900 °C

Independently of the reduction temperature, the XRD patterns for the natural clay based Ni-catalysts evidence the typical reflections from quartz and silica, corresponding to the clay support matrix, together with the diffraction peaks at 2θ = 44.3°, 52.7° and 76.3°, due to the presence of metallic Ni. Ni^0 crystal sizes were calculated applying Scherrer equation to the diffraction peak appearing at 76.3°. The values are shown in Table 4-7, together with the results of the textural characterization. Increasing the reduction temperature from 800 to 900 °C results in a change in Ni crystal size, i.e. values around 11.7-13.1 nm were calculated from the catalysts reduced at 900 °C, vis-à-vis the crystal sizes around 8.1-18.0 nm determined for the catalysts reduced at 800 °C. Ni re-dispersion through the enhancement of the interaction between Ni-species, clay support and maybe Fe or Cu pillars is favored when increasing the temperature of this reduction pre-treatment. In fact, the reduction pretreatment of the catalysts will result in the reduction of Fe and Cu pillaring species. However, the structure of the clay seems to be preserved at the sight of the XRD patterns obtained for the reduced catalysts. Unfortunately, XRD does not provide further information about the

structural changes induced as a consequence of the reduction of Fe and Cu, being very difficult to distinguish segregated Cu^0, FeO or Fe_2O_3 phases in these patterns.

4.3.2.4 CO_2 adsorption and basicity

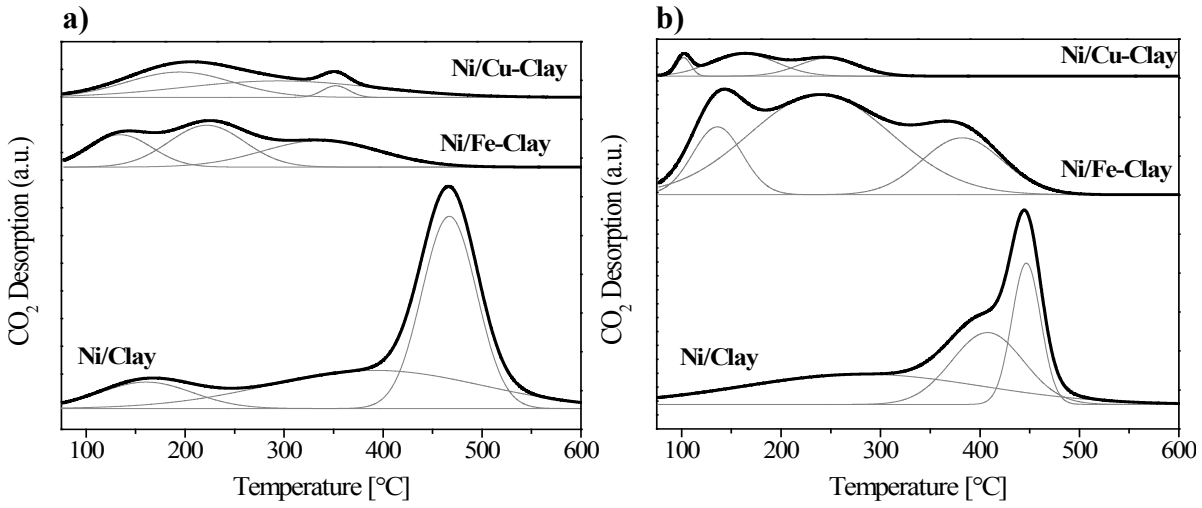

Figure 4-9. CO_2-TPD profiles obtained for the natural clay based Ni-catalysts reduced at a) 800 °C and b) 900 °C.

Figure 4-9 presents the CO_2-TPD profiles acquired for the catalysts reduced either at 800 °C (Figure 4-9 a) or at 900 °C (Figure 4-9 b). Such CO_2 desorption profiles typical exhibit three contributions, corresponding to different types of basic groups: weak Brønsted basic sites such as surface -OH groups (low temperature, 100-250 °C), medium-strength Lewis acid-base sites (intermediate temperature, 250-400 °C), and low-coordination oxygen anions acting as strong basic sites (high temperature, 400-600 °C) [136]. The deconvolution of the TPD profiles was performed taking into account these criteria. The results are shown in Table 4-8. Even at simple sight and independently of the reduction temperature, the peak corresponding to strong basic sites almost disappears for the catalysts prepared using either the Fe or the Cu-modified clays. For these catalysts, basicity is mostly of weak or moderate strength.

Table 4-8. Total basicity and deconvolution of the CO_2-TPD profiles.

Material	Deconvolution [µmol CO_2 /g]			Total basicity [µmol CO_2 /g]	Carbon balance[1] [mg]
	Weak	Medium	Strong		
Raw clay	4.5	11.3	5.5	21.3	-
Fe-Clay	4.7	5.8	2.0	12.5	-
Cu-Clay	0.4	3.7	2.7	6.8	-
Ni/Clay (800 °C)	5.9	19.5	30.8	56.2	241.6
Ni/Fe-Clay (800 °C)	7.0	6.7	8.9	22.6	152.9
Ni/Cu-Clay (800 °C)	9.3	8.4	1.1	18.8	277.1
Ni/Clay (900 °C)	9.9	7.7	6.0	23.6	75.0
Ni/Fe-Clay (900 °C)	4.8	19.6	6.0	30.4	92.9
Ni/Cu-Clay (900 °C)	0.5	2.2	1.4	4.1	161.0

[1]*Carbon deposition is calculated at 750°C for 5 hours*

The results presented in Table 4-8 evidence a decrease in total basicity upon the introduction of Fe and Cu, especially in the case of the Cu-modified clay. This trend is maintained in the Ni-catalysts prepared using these materials. A generally decrease in basicity is however observed after reduction at 900 °C. The lower presence of basic oxides in the modified clays, such as MgO, may explain this general decrease in basicity. Note however that this corresponds to a decrease in strong basic sites, and that this strong basic sites, probably MgO sites, are not the ones preferred in reactions involving CO_2.

4.3.3 Catalytic activity and selectivity of Fe and Cu-pillared clay supported Ni-based catalysts

Figure 4-10 presents the CH_4 and CO_2 conversions, as well as the H_2/CO ratio obtained during the DRM experiments in the presence of the natural clay based Ni-catalysts reduced at 800 °C. Methane and CO_2 conversions increase with increasing reaction temperature. However, and especially in the case of methane conversion, the values reached are quite far from those predicted by the thermodynamic equilibrium calculations. The CO_2 conversion measured is very similar but always a little bit higher than methane conversion. Direct methane decomposition occurs but remains relatively slow, even in the presence of the Ni-containing catalysts. However, the hydrogen generated in this reaction, favored at low temperatures, may react with CO_2 through the reverse water gas shift reaction, which yields CO and water and further explain the low H_2/CO values obtained.

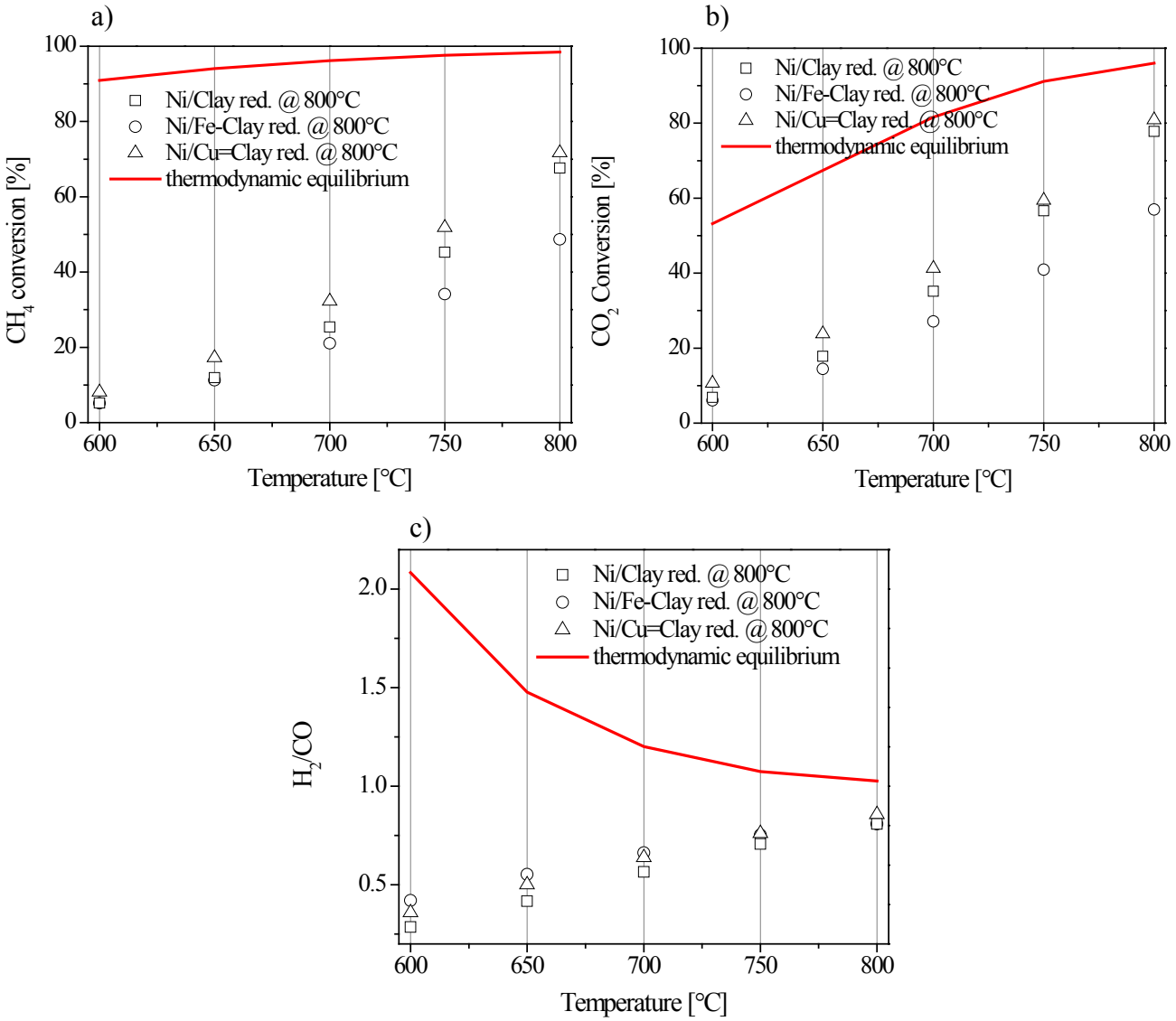

Figure 4-10. Results of the DRM catalytic tests in the presence of the natural clay based Ni-catalysts reduced at 800 °C, a) CH_4 conversion, b) CO_2 conversion, and c) H_2/CO ratio.

As temperature increases, the DRM reaction becomes favorable from a thermodynamic point of view. At 800 °C it may contribute to an important extent to the generation of both H_2 and CO, even though the parallel reactions described, among others, such as Boudouard, steam reforming, etc., will continue taking place. In fact, at 800 °C, the value of the H_2/CO ratio measured approached the thermodynamically forecasted value of 1.

Among the catalysts reduced at 800 °C, the one prepared using the Fe-modified clay shows the lowest activity. Note here that this catalyst shows the relatively low Ni crystal sizes of this series, i.e. 13.4 nm vs. 18.0 nm calculated for Ni/Clay. Moreover, the presence of Cu seems to be positive, yielding increased CH_4 and CO_2 conversions. In fact, Cu-promoted catalysts are well known for its activity in reverse water gas shift and methanol synthesis reactions

involving CO_2 [144,150,151], what may explain its better performance in spite of its lower total basicity.

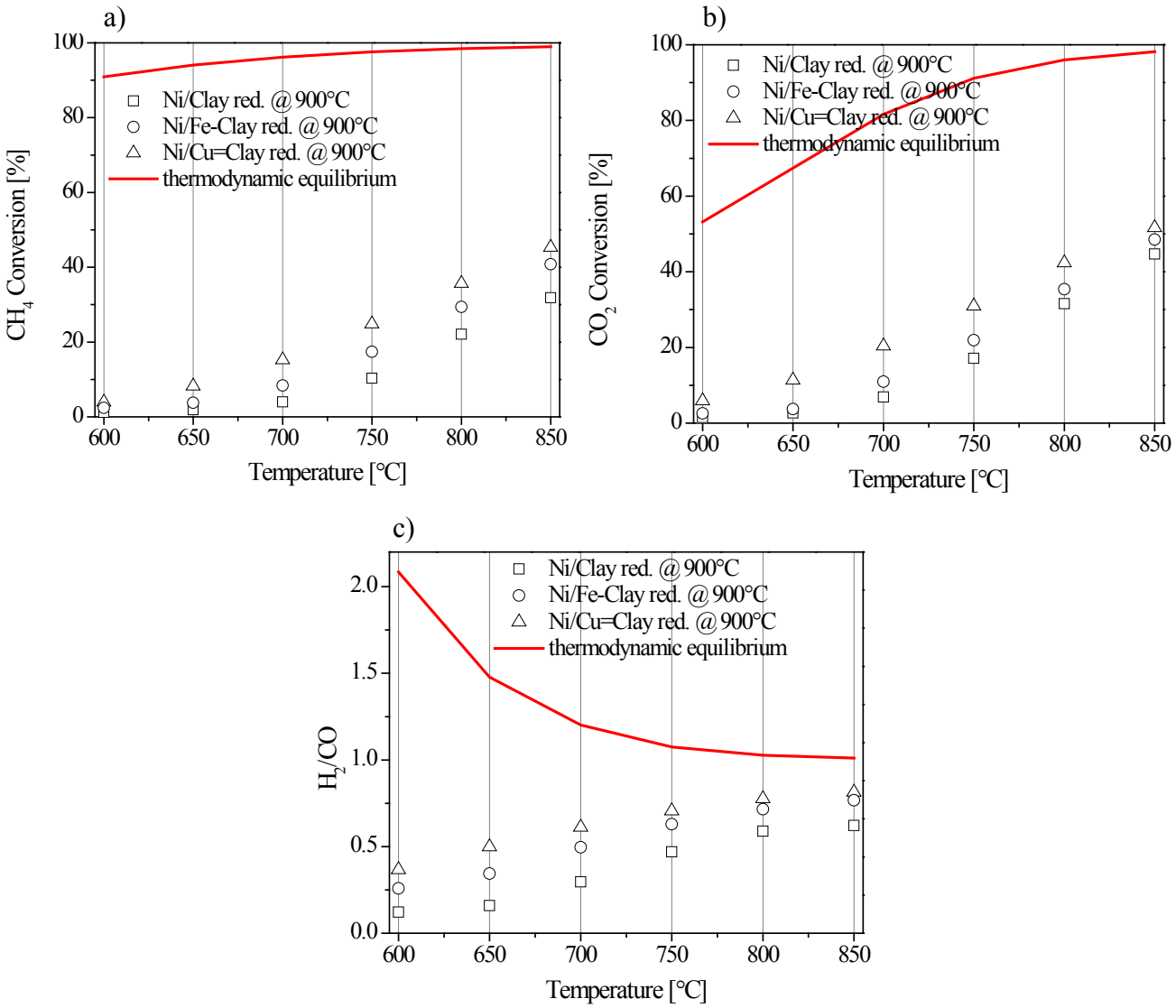

Figure 4-11. Results of the DRM catalytic tests in the presence of the natural clay based Ni-catalysts reduced at 900 °C, a) CH_4 conversion, b) CO_2 conversion, and c) H_2/CO ratio.

Figure 4-11 shows the results obtained in the DRM experiments in the presence of the catalysts reduced at 900 °C. Such catalysts showed generally decreased Ni crystal sizes, probably due to favored support-Ni phase interaction and to a re-dispersion of Ni-species during reduction at higher temperatures. They yield however lower CH_4 and CO_2 conversion than the ones measured in the presence of the catalysts reduced at 800 °C. The general decrease in basicity may explain this fact, together with the lower Ni crystal sizes obtained [152]. Again, the Cu-containing catalyst shows the highest activity.

4.3.4 Influence of Fe and Cu modified clay on carbon deposition

Table 4-8 contains as well the results of the carbon balance performed over 5 hours at 750 °C for each catalyst tested. The extent of carbon deposition is higher for the catalysts reduced at 800 °C, corresponding to higher activity and bigger Ni^0 crystal size, as could be expected. The Ni/Cu-Clay reduced at 800 °C shows the highest total amount of C deposited, corresponding to its higher activity, above all in terms of CO_2 conversion. Since direct methane decomposition results in C formation, together with H_2 production, the H_2 generated can further react with CO_2 by means of the reverse water gas shift reaction, resulting in higher CO_2 conversion. Slightly lower stability can be thus expected when using this Cu-clay based catalyst.

4.3.5 Summary

Table 4-9. Summary for the influences of different Fe/Cu-modified clays.

	Reduction at 800 °C			Reduction at 900 °C		
Support	Ni/Raw-Clay	Ni/Fe-Clay	Ni/Cu-Clay	Ni/Raw-Clay	Ni/Fe-Clay	Ni/Cu-Clay
Specific surface area	0	-	+	0	-	+
Ni^0 crystallite size[1]	0	-	-	0	-	-
Ni reducibility	0	+	+	0	+	+
Total basicity	0	-	-	0	+	-
DRM activity	0	-	+	0	+	+
Carbon deposition	0	-	+	0	+	+

"0" means the benchmark.
"+" means the strengthened/increased value compared to Ni based Raw-clay catalysts.
"-" means the weakened/decreased value compared to Ni based Raw-clay catalysts.
[1]Ni^0 crystallite size is compared only for reduced catalysts

Table 4-9 shows the effects of Fe and Cu on raw clay. Reduction temperature has a determinant influence in Ni crystal size and basicity. The catalysts reduced at 800 °C showed better catalytic performance than those reduced at 900 °C. The catalysts prepared using the Cu-modified clay yielded the highest CO_2 and methane conversions all the time. At 850 °C, 72% CO_2 conversion was measured, corresponding to a H_2/CO ratio near 1, close to the thermodynamically forecasted value.

4.4 Ce/Zr-promoted Fe and Cu-pillared clay supported Ni-based catalysts

Based on the results of different clays (raw, Fe- and Cu-modified clay) in section 4. 3, it could be found the influences of supports. Thus cerium and zirconium are selected as promoters over different clays for experimental comparison because of their relatively high activity and less carbon deposition compared to aluminum and lanthanum (in section 2.4.1).

In this section, Fe and Cu modified natural clays were used in the preparation of Ni catalysts that were further promoted using Ce and Zr oxides. The presence of Fe and Cu pillars may influence not only the type of porosity of the support, and therefore Ni distribution and catalyst stability, but also the activity and selectivity of these materials, due to the inherent presence of Fe and Cu together with Ni. Ceria and zirconia may help controlling coke formation and deposition, improving the catalytic stability.

4.4.1 Preparation of cerium (Ce) and zirconium (Zr) promoted Fe/Cu-pillared clay supported Ni-based catalysts

The preparations of Fe- and Cu-modified clay were introduced in section 4.2.1.1 and 4.3.1 respectively. Nickel, Cerium and Zirconium were introduced into Cu-clay support by means of a conventional impregnation method, using an aqueous solution of nitrate hexahydrate (Ni(NO3)2·6H2O, Ce(NO3)3·6H2O and ZrO(NO3)2·6H2O) as metal precursor. The Ni loading for the prepared catalysts was fixed as 15 wt.%, and the contents of Ce and Zr were controlled at 10 wt.%. Upon 2 h impregnation, suspension dried at 40 °C in rotary evaporator and dried overnight at 110 °C in an oven and subsequently calcined at 550 °C for 5 h.

4.4.2 Physicochemical properties of the natural clay supported Ni-based catalysts

4.4.2.1 Textural properties

The values of BET surface area, pore volume and mean pore size derived from the corresponding N_2 adsorption isotherms acquired for these catalysts are summarized in Table

4-10. BET surface area increases as a consequence of clay structure modification using Fe and Cu, due to the formation of pillars. Upon Ni addition a decrease in both BET surface and pore volume is observed, due to partial pore blockage. The further addition of a Ce and Zr oxide phase slightly increases BET surface area, particularly in the case of the Ce-containing catalysts, where slightly higher pore volumes follow this increase in surface area. Average pore sizes ranging between 6.6 and 10.6 nm confirm the mesoporous texture of these materials. Type IV isotherms, presenting H3 hysteresis loops and typical of laminar-structured materials containing slit-shaped pores, are observed.

Table 4-10. BET surface area, pore volumes and average pore size for the raw, Fe and Cu-modified clays and the different non-promoted, Ce and Zr-promoted catalysts

Material	S_{BET} [m^2/g]	V_p[1] [cm^3/g]	V_{BJH}[2] [cm^3/g]	V_{micro}[3] [cm^3/g]	d_p[4] [cm^3/g]
Raw clay	73.6	0.148	0.146	0.012	8.1
Fe-Clay	60.9	0.111	0.112	0.011	6.6
Ni/Fe-Clay	44.2	0.109	0.108	0.006	8.6
Ni-Ce/Fe-Clay	52.1	0.146	0.146	0.008	10.6
Ni-Zr/Fe-Clay	56.4	0.107	0.106	0.014	7.2
Cu-Clay	102.8	0.195	0.193	0.016	7.7
Ni/Cu-Clay	84.3	0.159	0.156	0.003	8.2
Ni-Ce/Cu-Clay	92.1	0.174	0.173	0.008	8.6
Ni-Zr/Cu-Clay	87.6	0.162	0.161	0.012	8.4

[1] *single point desorption total pore volume*
[2] *t-plot micropore volume*
[3] *BJH desorption cumulative pore volume*
[4] *BJH desorption average pore width*

4.4.2.2 Reducibility of the Ni-species

Figure 4-12 a) and b) shows the H_2-TPR profiles acquired for the non-promoted and promoted Fe-Clay and Cu-Clay based catalysts. A first peak appearing at temperatures from 413 °C to 449 °C correspond to bulk NiO in weak interaction with the clay support, whereas a second peak at about 668 °C can be assigned to the NiO species strongly bonded to the support [110,153]. The introduction of either Ce and Zr shifts this first peak of bulk NiO reduction to lower temperatures, pointing to the weakening of the interaction between the Ni-phase and the clay in the presence of these promoters and to an increased reducibility of Ni-species, in agreement with what was previously reported in the existing literature [110,119]. This shift in reduction temperature may be moreover linked to the catalytic activity of this series of materials. Slightly lower total H_2 consumption (in Table 4-11) is however measured for the Zr-containing catalysts, pointing to the existence of a Ni-phase in far too

strong interaction with Zr or with the clays support that is not fully reduced during the TPR experiments. In fact this is also the main reason for still choosing 900°C as the reduction temperature for the catalyst pre-treatment prior to the catalytic tests in the following sections.

Table 4-11. Main peak position, H_2 consumption and Ni^0 crystal size calculated for the reduced catalysts.

Catalyst	Temperature [°C]	H_2-Consumption	Ni crystal size
	1st peak	[mmol H_2/g]	[nm]
Ni/Fe-Clay	439	1.26	13.4 ± 0.8
Ni-Ce/Fe-Clay	433	1.20	12.9 ± 0.5
Ni-Zr/Fe-Clay	413	0.68	11.8 ± 0.3
Ni/Cu-Clay	449	0.81	8.1 ± 0.9
Ni-Ce/Cu-Clay	419	1.02	15.2 ± 0.2
Ni-Zr/Cu-Clay	431	0.89	10.4 ± 0.3

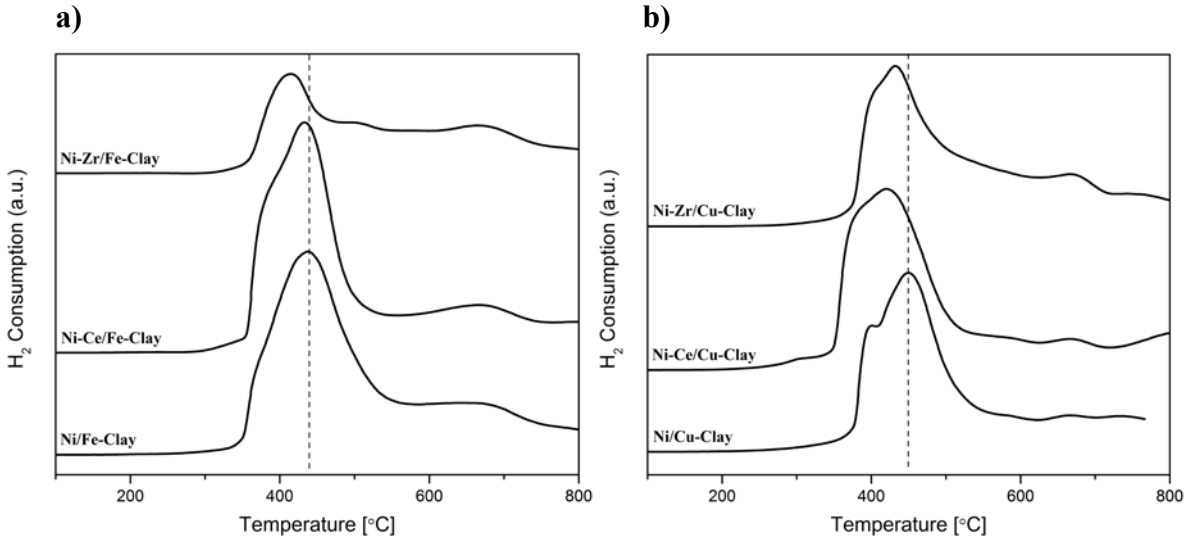

Figure 4-12. H_2-TPR profiles of calcined catalysts: a) Fe-modified clay based catalysts b) Cu-modified clay based catalysts.

4.4.2.3 Crystallinity: Ce/Zr-promotion on Fe/Cu-modified clays and Ni^0 crystallite size

The XRD patterns for the reduced Fe- and Cu-modified clay based catalysts are shown in Figure 4-13 a) and b). There are several reflections for the different components. The profiles evidence the presence of a metallic Ni phase (2θ = 44.3°, 52.7° and 76.3°) in all the catalysts. After introduction of Ce and Zr additional diffraction peaks corresponding to CeO_2 (28.6°, 33.0°, 47.5° and 56.3°) and to ZrO_2 (30.1°, 35.0°, 50.2° and 59.7°) can be as well observed. The crystal size of Ni was calculated using the Scherrer equation considering the peak at 76.3°, the results are listed in Table 4-11. Crystal sizes range from 8.1 to 15.2 nm. In the case

of the catalysts prepared using the Fe-modified clay a slight reduction in Ni^0 crystal size can be observed upon the introduction of Ce and Zr. However, this effect is no longer observed for the Cu-modified clay based catalysts. The values of Ni^0 crystal size calculated from the XRD profiles may be related to the catalytic activity and carbon balance performed for these catalysts.

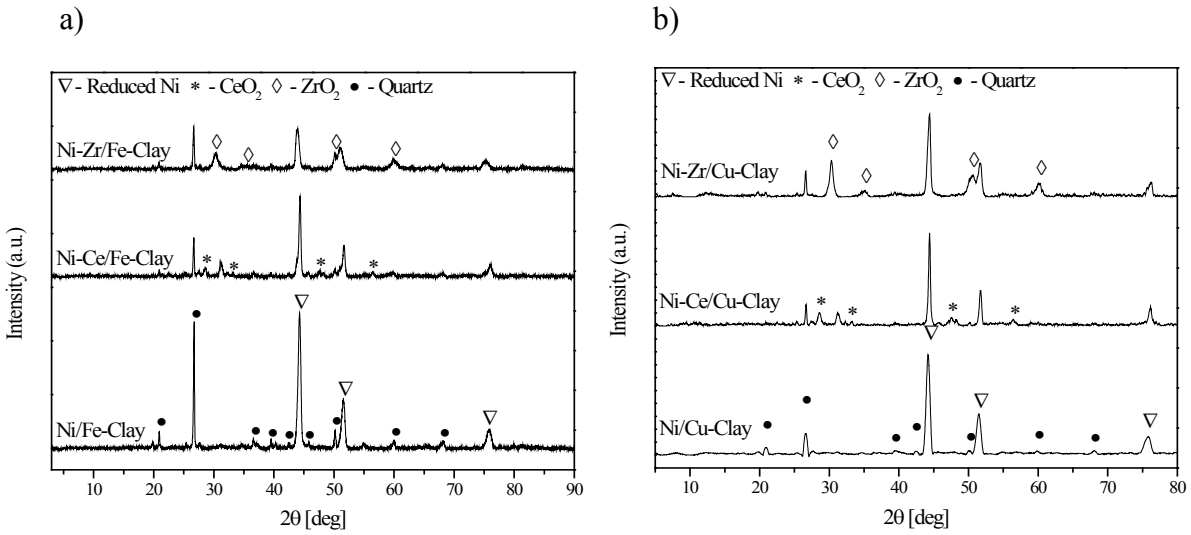

Figure 4-13. XRD profiles for the reduced catalysts: a) Fe-modified clay based catalysts b) Cu-modified clay based catalysts.

4.4.2.4 CO_2 adsorption and basicity

The CO_2-TPD profiles obtained for the different clay-based catalysts are presented in Figure 4-14 a) and b). All of them evidence several CO_2 desorption peaks in the range 100-600 °C, which can be assigned to the presence of different type of basic sites: weak Brønsted basic sites such as surface OH groups (low temperature peak), medium-strength Lewis acid-base sites (intermediate temperature peak), and low-coordination oxygen anions acting as strong basic sites (high temperature peak) [136,154].

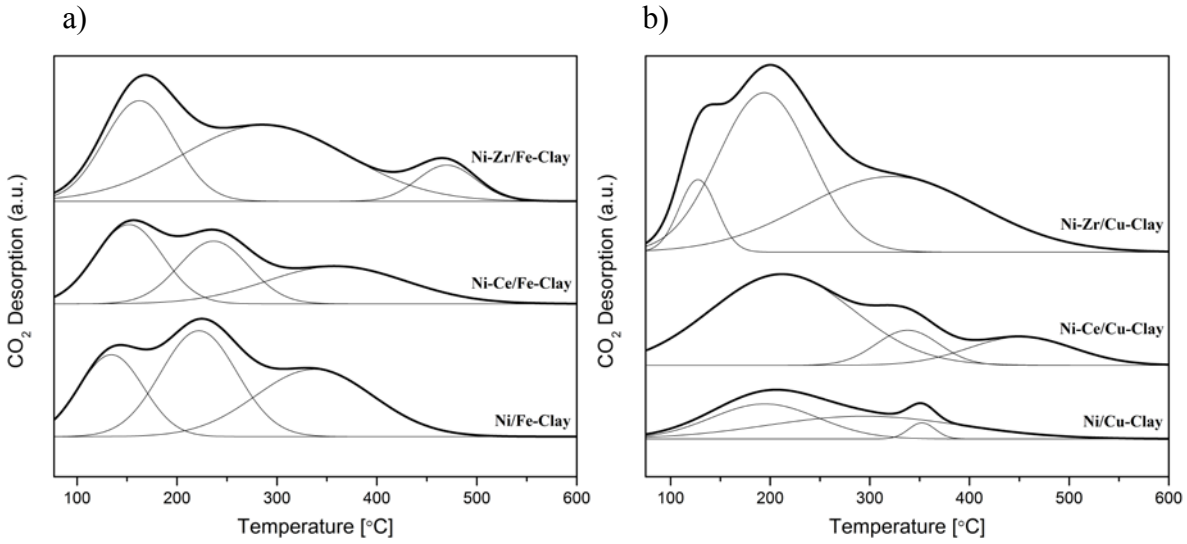

Figure 4-14. CO_2-TPD profiles for the reduced catalysts: a) Fe-modified clay based catalysts b) Cu-modified clay based catalysts.

The deconvolution of these TPD profiles is shown in Table 4-12. The presence of Ce and Zr strongly modifies the total amount of CO_2 desorbed, i.e. total basicity. In the case of the Fe-modified clay based catalysts, the introduction of Ce slightly reduces the total amount of CO_2 desorbed. The distribution of basic sites also changes upon Ce and Zr introduction. In this sense, the amount of strong basic sites is reduced as a consequence of Ce and Zr loading, this fact being probably related to the their activity measured for these two promoted catalysts, as already explained in the existing literature [132]. For the catalysts prepared using the Cu-modified clay, Ce and Zr introduction results in a substantial increase of the total basicity, especially in the case of the Zr-promoted catalyst. No direct influence can be found in this case in terms of the modification of the distribution of basic sites upon Ce and Zr doping. However, the Ni-Ce/Cu-Clay shows a particularly higher contribution of CO_2 adsorbed on weak basic sites, which may contribute to its catalytic activity in DRM since the weakly adsorbed CO_2 is more easily desorbed [134].

Table 4-12. Deconvolution of the CO_2-TPD profiles: peak position and contribution to total basicity.

Catalyst	Temperature [°C]			μmol CO_2 desorbed/g			Total basicity [μmol CO_2/g]
	1st peak	2nd peak	3rd peak	1st peak	2nd peak	3rd peak	
Ni/Fe-Clay	133.5	222.3	339.5	7.02	6.68	8.88	22.58
Ni-Ce/Fe-Clay	151.3	237.7	358.8	6.34	3.79	5.63	15.76
Ni-Zr/Fe-Clay	162.1	285.5	469.9	7.29	12.17	2.20	21.66
Ni/Cu-Clay	195.2	303.7	352.5	9.30	8.40	1.10	18.80
Ni-Ce/Cu-Clay	213.0	339.2	453.2	26.19	3.98	6.05	36.22
Ni-Zr/Cu-Clay	126.3	193.8	323.8	4.92	26.03	21.78	52.73

4.4.3 Catalytic activity and selectivity of Ce and Zr promoted Fe/Cu-pillared clay supported Ni-based catalysts

The conversions of methane and CO_2, together with the H_2/CO molar ratio measured during the DRM experiments in the presence of the Fe-modified clay based catalysts, non-promoted, Ni/Fe-Clay, and promoted either with Ce, Ni-Ce/Fe-Clay, or Zr, Ni-Zr/Fe-Clay, are shown in Figure 4-15 a), b) and c). Both methane and CO_2 conversions increase with increasing temperature, in agreement with the tendency forecasted by thermodynamics. The H_2/CO molar ratio measured in the experiments increase with increasing temperature. At low temperatures, i.e. 600 °C, the H_2/CO ratio measured is much lower than the one forecasted by equilibrium thermodynamics, pointing to the occurrence of H_2 producing reactions, such as direct methane decomposition ($CH_4 \rightleftharpoons C + 2H_2$) to a much lower extent to what could be thermodynamically expected. Additionally, the low H_2/CO ratios indicate that CO-producing parallel reactions, such as reverse water gas shift (RGWS, $CO_2 + H_2 \rightleftharpoons CO + H_2O$) may be taking place simultaneously to an important extent in the presence of these catalysts. In fact, the measured CO_2 conversions are always higher than the CH_4 conversions. The presence of either Ce or Zr enhances the conversions of both CO_2 and CH_4, i.e. 50% CO_2 conversion is measured in the presence of the promoted catalysts, whereas the non-promoted catalyst yielded only 35% CO_2 conversion. The positive effect of Ce and Zr as promoters can be due to the excellent oxygen storage capacity of CeO_2 and to the contribution of gasification of surface hydrocarbons and/or carbon deposits in the presence of ZrO_2 [110,155-157]. The values of H_2/CO ratios are relatively independent of the presence of Ce and Zr. This indicates that the promoting effect may not substantially modify the overall reaction mechanism. In any case, the best catalytic performance is observed for the Zr-promoted Fe-modified clay based catalyst, with methane and CO_2 conversions always slightly higher than those measured in the presence of the Ce-promoted catalyst.

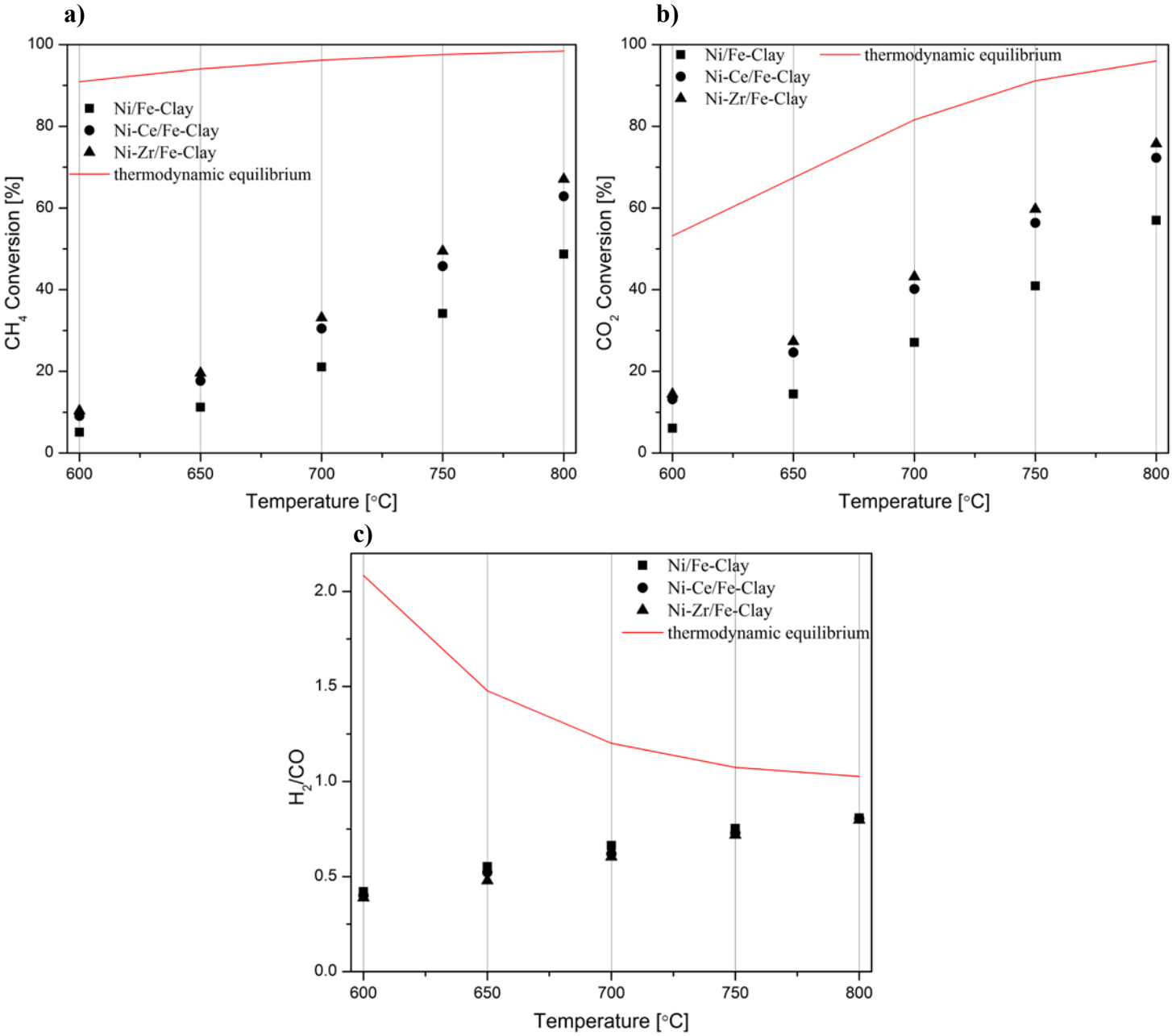

Figure 4-15. Results of the DRM experiments on the Fe-Clay based catalysts: a) CH_4 conversion, b) CO_2 conversion and c) H_2/CO molar ratio, versus reaction temperature.

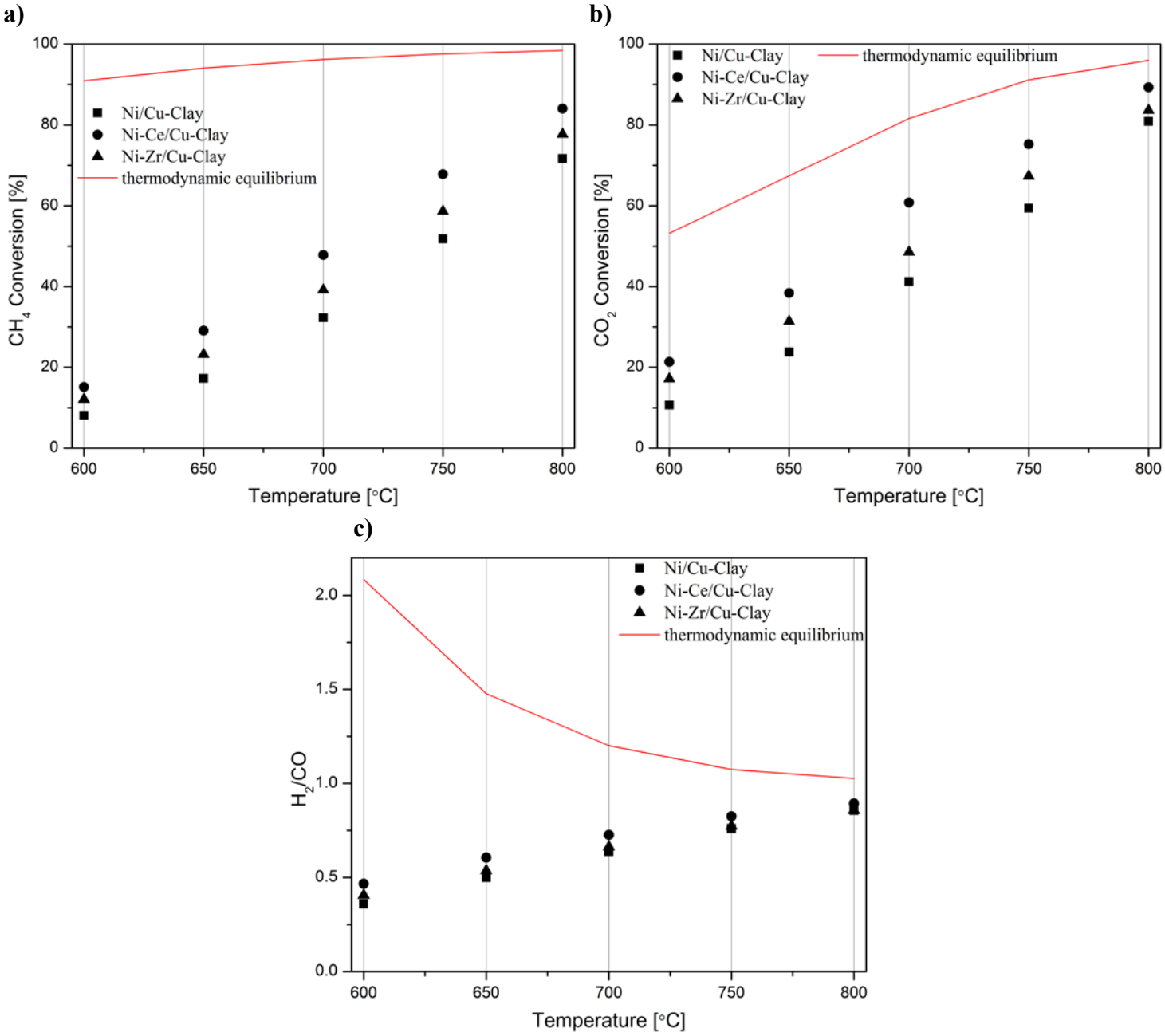

Figure 4-16. Results of the DRM experiments on the Cu-Clay based catalysts: a) CH_4 conversion, b) CO_2 conversion and c) H_2/CO molar ratio, versus reaction temperature.

The results of the DRM experiments performed for the non-promoted and the Ce and Zr promoted catalysts prepared using the Cu-modified clay as support, are shown in Figure 4-16 a), b) and c). The methane and CO_2 conversions obtained in the presence of these catalysts are always higher than those obtained for the ones prepared using the Fe-modified clay, pointing to a positive effect of Cu-pillaring in the catalytic activity. Several studies show that Cu can help improving the catalytic activity through the promotion of the gasification of carbon deposits and may confer the catalysts to improve textural and structural properties at the

macroscopic scale [150,158]. Copper may as well promote some side reactions resulting in an enhanced consumption of CO_2, CO and/or H_2, since it is an excellent catalyst for methanol synthesis and RWGS. The same positive promoting effect of Ce and Zr can be however observed for these Cu-Clay based catalysts, in this case, especially regarding the Ce-promoted catalysts. The methane and CO_2 conversions measured in the presence of the Ce-promoted catalysts are much higher than those recorded for the non-promoted Ni/Cu-Clay catalyst, i.e. at 750 °C: 58% CO_2 conversion vs. only 40% conversion measured for Ni-Ce/Cu-Clay and Ni/Cu-Clay respectively. Slightly higher H_2/CO ratios are also measured all the time for this Ce-promoted catalyst, moreover in the low temperature range.

4.4.4 Influence of Ce and Zr promotion on Fe/Cu-pillared clay on carbon depostion

The amount of carbon deposition in an isothermal 5 h-duration DRM experiment at 750 °C, was calculated closing the carbon balance between feedstock and product gas. The results are presented in Figure 4-17. The introduction of Ce and Zr do not directly result in a lower extent of carbon deposition. On the contrary, higher amounts of deposited carbon were found for the Ce-promoted catalysts either prepared using the Fe or the Cu-modified clays. This points thus to the simultaneous promotion of carbon forming reactions in the presence of Ce and Zr, in agreement to what has been previously reported by other authors [119,132,159]. In fact, the presence of Ce seems to be linked to an increased production of fishbone carbon nanofibers [132]. Moreover, the Cu-Clay series of catalysts shows much higher carbon formation extents than Fe-Clay based ones, indicating that Cu also promotes C-forming side reactions. Otherwise, this may also be related to the sintering of Ni and Cu sites [160], what may inhibit C-gasifying reactions, such as Boudouard ($CO_2 + C \rightleftharpoons 2CO$) [134].

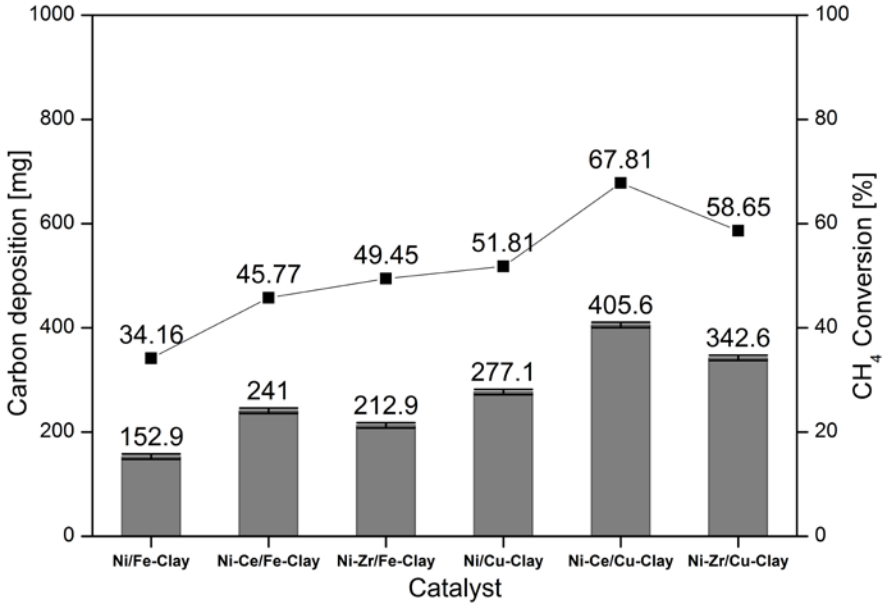

Figure 4-17. Carbon deposition (mg) and methane conversion measured in a 5 h DRM experiment at 750 °C in the presence of the different non-promoted and Ce and Zr promoted Fe-Clay and Cu-Clay based catalysts.

4.4.5 Summary

Table 4-13. Summary for the influences of Ce and Zr promotion on Fe/Cu-clays.

		Promotion	Ni	Ni-Ce	Ni-Zr
Pillared clay	Fe-clay	Specific surface area	0	+	+
		Ni^0 crystallite size[1]	0	-	-
		Ni reducibility	0	+	+
		Total basicity	0	-	-
		DRM activity	0	+	+
		Carbon deposition	0	+	+
	Cu-clay	Promotion	Ni	Ni-Ce	Ni-Zr
		Specific surface area	0	+	+
		Ni^0 crystallite size[1]	0	+	-
		Ni Reducibility	0	+	+
		Total basicity	0	+	+
		DRM activity	0	+	+
		Carbon deposition	0	+	+

"0" means the benchmark.
"+" means the strengthened/increased value compared to Ni based Fe/Cu-clay catalysts respectively.
"-" means the weakened/decreased value compared to Ni based Fe/Cu-clay catalysts respectively.
[1]Ni^0 crystallite size is compared only for reduced catalysts

Table 4-13 presents the effects of Ce and Zr on Fe/Cu-modified clay. Ce and Zr promotion resulted in a considerable increase of the catalytic activity. Both Ce and Zr promotion improved reducibility of Ni species, together with slightly influence on Ni^0 crystal size, that, on the other hand, also catalyze undesired parallel reactions resulting in carbon formation, such as direct methane decomposition. Both Ce and Zr on Cu-modified clay also promoted

the presence of weak or medium strength basic sites, which are thought to favor CO_2 adsorption and desorption on the catalyst surface, leading to enhanced catalytic activity.

4.5 Mg-promoted Fe and Cu-pillared supported Ni-based catalysts

Among the different supports considered, clay materials gather interesting textural and surface properties that can importantly contribute to adequate Ni-dispersion. They are moreover abundant, not expensive and their physicochemical properties can be relatively tailored in order to further improve their catalytic performance in DRM [161,162]. Wang et al. reported important DRM activity for clay-supported Ni-catalysts, together with an important influence of the nature of the clay used, and concretely of its pore structure and surface properties [163]. The presence of mesopores resulted in enhanced catalytic activity. Hao et al. employed zirconia-pillared laponite clays in the preparation of Ni-catalysts for DRM [164]. Through pillaring, the modification of the pore structure and the surface properties resulted in enhanced Ni-dispersion and in minimized pore blockage, finally leading to improved activity and stability.

Further than the clay structure and its physicochemical properties themselves, the use of promoters can highly contribute to boosting catalytic activity and/or avoiding catalyst deactivation. Li and co-workers recently showed that the use of magnesium enhanced the surface basicity of alumina-based catalysts and promoted the gasification of the carbon deposits formed through the undesired C-forming parallel reactions [165]. Singha et al. reported improved catalytic activity and stability for MgO-promoted ZnO-supported Ni-nanoparticles synthesized by hydrothermal method [166]. The authors related this enhanced catalytic performance to the better dispersion of the Ni-phase upon Mg-promotion. Dieuzeide et al. described how the content of Mg affected the catalytic performance of Ni/Al_2O_3 catalysts [167]. Both the improvement of Ni-dispersion and the increase of surface basicity were beneficial to catalytic activity and prevented carbon formation and deposition.

In this section, Fe and Cu-pillared natural clays were promoted with Mg and further used in the preparation of Ni-containing catalysts for DRM. The influence of the presence of Mg, as well as its content, on the important physicochemical properties such as porosity, basicity, Ni-reducibility and dispersion, as well as on the activity, selectivity and stability of the

different natural clay based catalysts, has been carefully analysed. Though there are some evidences in the existing literature on the promoting effect of Mg using different supports, the Mg-promotion of natural clays has not been considered to date. The use of Mg can provide additional basic sites for CO_2 adsorption, resulting in an improved performance of natural clay based catalysts.

4.5.1 Preparation of magnesium (Mg) promoted Fe and Cu-pillared clay supported Ni-based catalysts

The preparations of Fe- and Cu-modified clay were already explained in section 2.1.1 and 3.1 respectively. The Ni-catalysts were prepared using either the non-pillared, the Fe or the Cu-modified clays, at 15 wt.% Ni nominal loading ($Ni(NO_3)_2 \cdot 6H_2O$). The different Mg-promoted catalysts were obtained through excess solution impregnation of each support, at 15 wt.% Ni loading and at either 10, 20 or 30 wt.% Mg loading ($Mg(NO_3)_2 \cdot 6H_2O$). All the suspensions were aged for 2 hours at room temperature, then dried at 40 °C in rotary evaporator. The resulting solid material was kept overnight at 110 °C, calcined in air at 550 °C for 5 h.

4.5.2 Physicochemical properties of the Mg-promoted Fe and Cu-pillared supported Ni-based catalysts

4.5.2.1 Textural properties

Table 4-14 contains the results of the textural characterization for the raw, Fe and Cu-modified clays, as well as for the different Ni and Ni-Mg catalysts. Ni and Ni-Mg loading result all the time in a certain extent of pore blockage, which depends on the clay used as support and on the amount of Mg deposited. The introduction of Cu-pillars in the natural clays leads to increased surface area and pore volume. Consequently, upon Ni and Ni-Mg loading this surface area decreases but to a lower extent than for the catalysts prepared using either the raw clay or the Fe-modified clay as support. In all cases, pore blockage seems to affect mainly the micropore and narrow mesopore fraction of the porosity of the clays.

Table 4-14. BET surface area, pore volumes and average pore size, as well as Ni^0 crystallite size, for the Ni and Ni-Mg loaded raw, Fe and Cu-modified clays.

Catalyst	S_{BET} [m^2/g]	V_p[1] [cm^3/g]	d_p[2] [nm]	V_{BJH}[3] [cm^3/g]	Ni^0 crystal size [nm]
Raw-Clay	73.6	0.148	8.1	0.146	-
Ni/Raw-Clay	55.4	0.112	8.9	0.111	14.7
Ni-10Mg/Raw-Clay	16.9	0.139	32.9	0.136	8.1
Fe-Clay	60.9	0.111	6.6	0.112	-
Ni/Fe-Clay	44.2	0.109	8.6	0.108	15.1
Ni-10Mg/Fe-Clay	16.7	0.073	17.3	0.068	8.4
Ni-20Mg/Fe-Clay	12.0	0.059	19.6	0.057	8.3
Ni-30Mg/Fe-Clay	12.2	0.111	36.4	0.110	7.5
Cu-Clay	102.8	0.195	7.7	0.108	-
Ni/Cu-Clay	84.3	0.159	8.2	0.156	14.1
Ni-10Mg/Cu-Clay	31.8	0.107	13.5	0.100	8.1

[1] *total pore volume*
[2] *average pore size*
[3] *BJH desorption cumulative pore volume*

4.5.2.2 Reducibility of the Ni-species

The analysis of the H_2-TPR profiles yields important information about the reducibility of the different species, including Ni-oxides, contained in the bulk of the catalysts. These profiles are presented in Figure 4-18. Figure 4-18 a) compares the H_2-TPR profiles obtained for the different Ni-Mg catalysts prepared using 10 wt.% Mg. For the sake of comparison, the H_2-TPR profiles corresponding to the non-promoted Ni-containing clay are shown in Figure 4-18 c) and have been described in section 4.3.2.2. All of them present two main areas of interest in which several H_2-consumption peaks can be observed: a first series of peaks appearing at temperatures between 350 and 530 °C, followed by marked H_2-consumption occurring at higher temperatures from 680 to 820 °C.

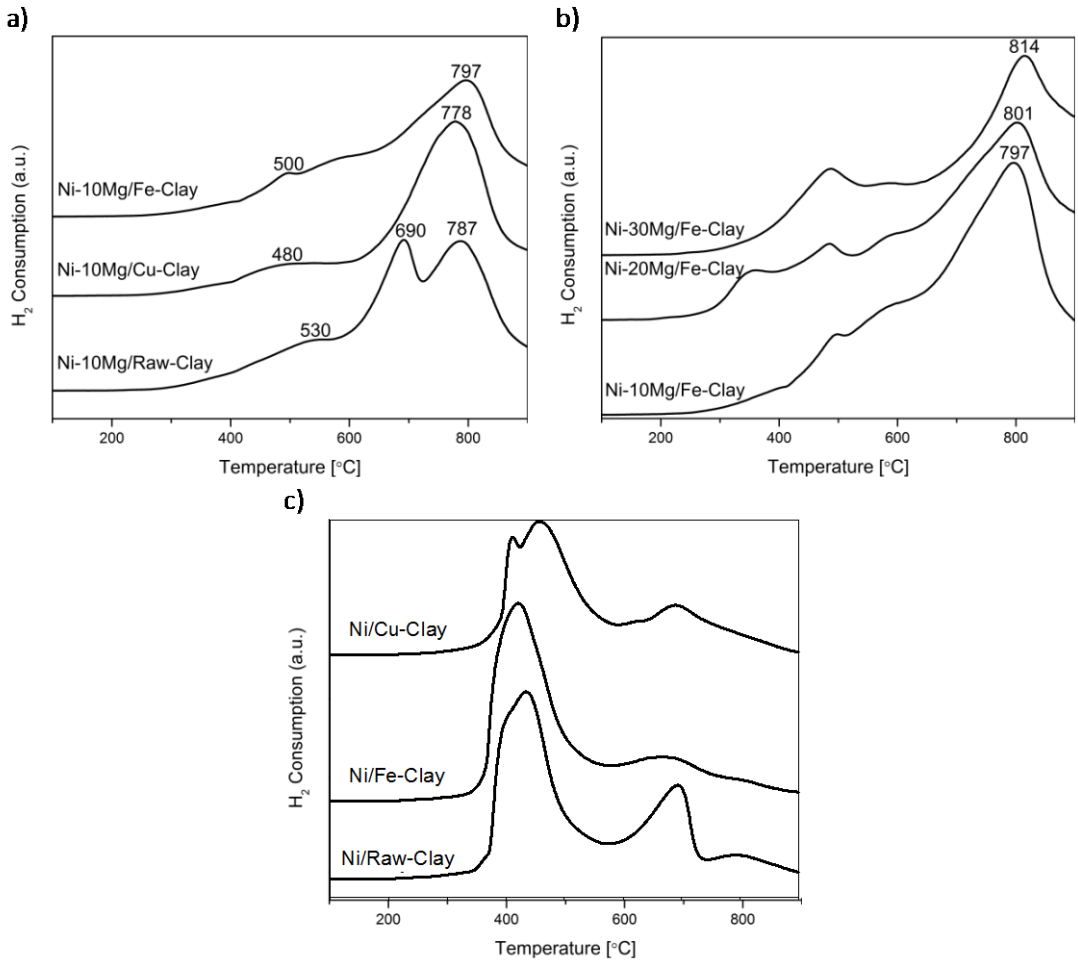

Figure 4-18. H_2-TPR profiles for a) the Ni-Mg (10 wt. %) catalysts, b) the Ni-Mg catalysts prepared at 10, 20 and 30 wt. % Mg-loading, and c) the clay-supported, non-promoted Ni-catalysts.

The three H_2-TPR profiles acquired for the non-promoted Ni-catalysts substantially differ to that obtained for the Mg-promoted catalysts. In the later, H_2-consumption takes place during a wider temperature window, and peaks up a relatively high temperatures, i.e. around 600-700 °C (Figure 4-18 a and b), whereas the non-promoted catalysts (Figure 4-18 c) present a main and almost single peak of H_2-consumption appearing within the low temperature window (420-450 °C), followed by a softer and wider peak at higher reduction temperatures.

Essentially, the H_2-TPR profiles typical of Ni-containing catalysts generally show two main H_2-consumption peaks: the first one occurring at lower-intermediate temperatures, associated to bulk NiO_x species, and a second one at higher temperatures linked to the reduction of finely dispersed NiO_x in tight interaction with the support [152]. The H_2-TPR profiles for natural clay based catalyst can be quite complex, moreover after Fe and Cu pillaring. The reduction of Fe_3O_4 to Fe_2O_3 and subsequently to metallic Fe occurs at about 450-600 °C and may

overlap the H_2-consumption peaks resulting from the reduction of bulk NiO_x species. Similarly, Cu oxides will reduce within the same temperature window [148,149,168,169].

In spite of this, the H_2-consumption peak centred at high reaction temperatures can be clearly assigned to Ni species strongly bonded to the clay, and, more possibly, to a tight interaction between Ni and Mg oxides, as has been previously observed in Ni-containing hydrotalcite-derived catalysts [166,170]. The intensity of this high temperature peak increases with Mg-content in the non-promoted Ni-catalysts, Figure 4-18 c). For the Mg-promoted catalysts it is further shifted to higher reduction temperatures as Mg-loading increases (Figure 4-18 b). The profile acquired for the Ni-10Mg/Raw-Clay catalyst presents indeed two clearly separated peaks appearing in the high temperature window: the first one centred at 690 °C, probably related to Ni in tight interaction with the Mg-species in the pristine structure of the raw clay, and the second one, centred at 787 °C, corresponding to the reduction of Ni species forming a mixed oxide structure with the Mg-species added as promoter. The presence and/or addition of Mg therefore results in the formation of these mixed Ni-Mg species, clearly affecting their reducibility. Moreover, the presence of Fe and Cu may result in other kind of interactions, as previously described in section 4.3.2.2, also resulted in modified reducibility of the Ni-species.

4.5.2.3 Crystallinity: Mg-promotion on Fe/Cu-modified clays and Ni^0 crystallite size

The XRD patterns obtained for the reduced Mg-promoted catalysts are shown in Figure 4-19. Very similar reflections are observed in all catalysts, including metallic nickel (at 44.5°, 51.8°, 76.3°), $MgNiO_2$ and quartz, pointing to neither Fe/Cu nor variable Mg content affecting the crystalline structure of these materials. The presence of $MgNiO_2$ confirms moreover the strong interaction between these species, resulting in a mixed oxide phase. Note here that a pure MgO periclase phase yields normally diffraction peaks appearing always at lower diffraction angles than $MgNiO_2$, i.e. the (200) diffraction peak should appear at 42.97° for MgO whereas for $MgNiO_2$ it appears at 43.1°. However, it is always difficult to distinguish between MgO and $MgNiO_2$ in XRD patterns. In the case of the Ni-10Mg/Fe-Clay catalyst, this (200) pseudo-periclase peak appears centred at even higher diffraction angles, i.e. 43.2°.

The crystallite sizes of metallic nickel calculated using the Scherrer equation (51.8°) are listed in Table 4-14. Ni^0 crystallite sizes are always smaller for the catalysts prepared using the Fe-modified clay, with the only exception of Ni-30Mg/Fe-Clay. Similar results have been previously reported by Dieuzeide et al. [167], who observed better dispersion of Ni at lower Mg content through inhibited diffusion during reduction, as a consequence of the formation of a mixed Ni-Mg oxide phase. The formation of a mixed Ni-Fe phase, such as $NiFe_2O_4$, is not evident from the diffraction patterns, but has been previously described in the literature [171]. Similarly, there are no evidences of the formation of Ni-Cu mixed phases [169]. Note here that Ni cluster sizes estimated using the Scherrer equation might yield quite inaccurate results when trying to evaluate the crystalline state and size of an active phase. As it will be discussed later, and at the sight of the TEM images acquired for this series of catalysts upon DRM reaction, the size of the Ni clusters appears quite inhomogeneous. Indeed, Ni crystallites of few nanometers size co-exist together with much bigger clusters that are formed upon the reduction of bulk NiO_x in weak interaction with either the promoter or the clay's matrix.

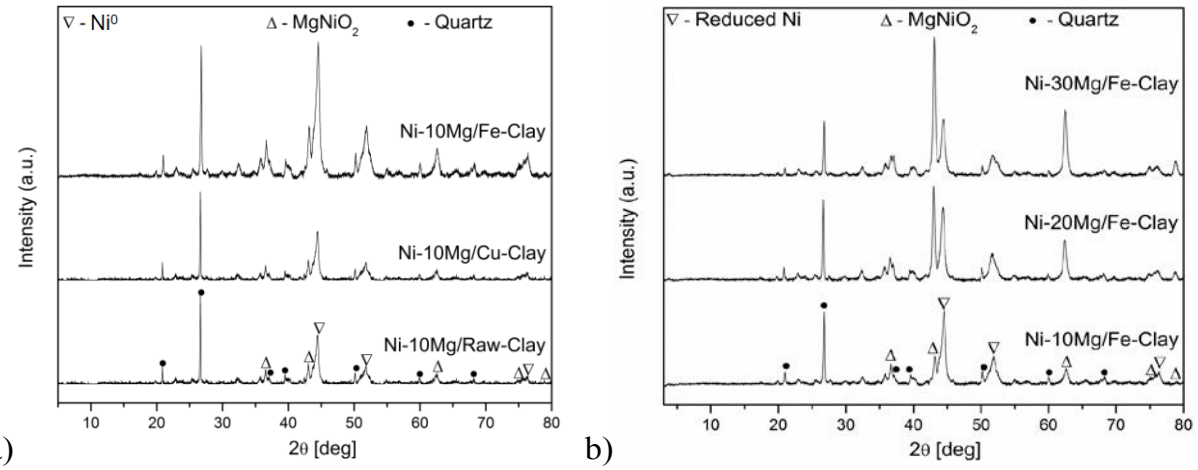

Figure 4-19. XRD patterns for a) the Ni-Mg (10 wt.%) catalysts, and b) the Ni-Mg catalysts prepared at 10, 20 and 30 wt.% Mg-loading.

4.5.2.4 Raman spectra

The Raman spectra acquired for reduced Ni-Mg catalysts are shown in Figure 4-20. The Raman modes typical of an inverse spinel structure, at ca. 710 (s), 660 (sh, m), 589-578 (large, m), 486 (m), 450 (sh, w) and 330 (w) cm^{-1}, are clearly visible in the spectrum registered for the catalyst Ni-10Mg/Fe-Clay, and point to the presence of $NiFe_2O_4$ in this material [171-173]. They can be barely distinguished in the Raman spectrum of Ni-10Mg/Raw-Clay

and they are not visible at all for the Ni-10Mg/Cu-Clay. A part of the iron introduced in the Fe-Clay support is thus able to form this $NiFe_2O_4$ phase. The iron-species naturally present in the Raw-Clay may as well form this kind of spinel, but to a lower extent. However, the formation of $NiFe_2O_4$ does not seem to clearly affect the final Ni^0 size. No remarkable peak shift was moreover observed in any of the Ni^0 reflections present in the XRD patterns.

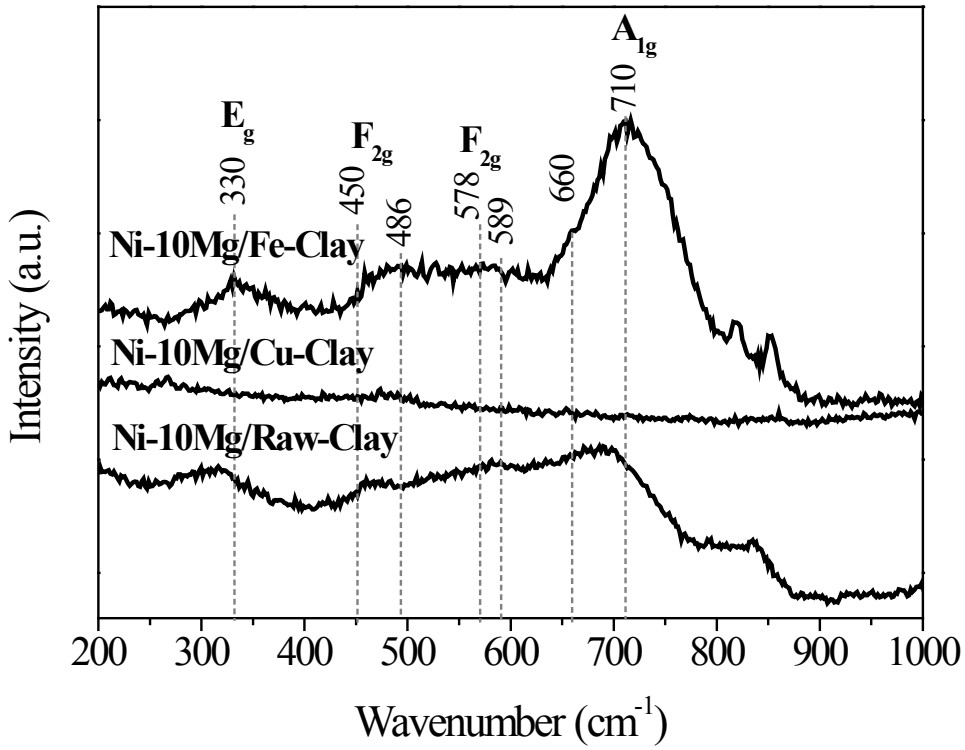

Figure 4-20. Raman spectra obtained from the three the Ni-Mg (10 wt.%) catalysts.

4.5.2.5 CO_2 adsorption and basicity

The CO_2-TPD profiles for the Mg-promoted catalysts are shown in Figure 4-21. These profiles are generally composed by wide CO_2-desorption peaks that can be deconvoluted into three main types of contributions: Low temperature CO_2-desorption (100-250 °C), associated to weak Brønsted basic sites such as surface -OH groups, intermediate temperature CO_2-desorption (250-400 °C), corresponding to medium-strength Lewis base sites, and high temperature CO_2-desorption (400-600 °C), linked to adsorption on low-coordination oxygen anions acting as strong basic sites [132,166]. The results of this deconvolution, as well as the total basicity calculated for this series of catalysts, can be found in Table 4-15. Note here that the results obtained for the non-promoted Ni-containing clay based catalysts have been added

to Table 4-15, for the sake of comparison. The CO_2-TPD profiles, as well as their analysis and discussion, can be found in section 4.3.2.4.

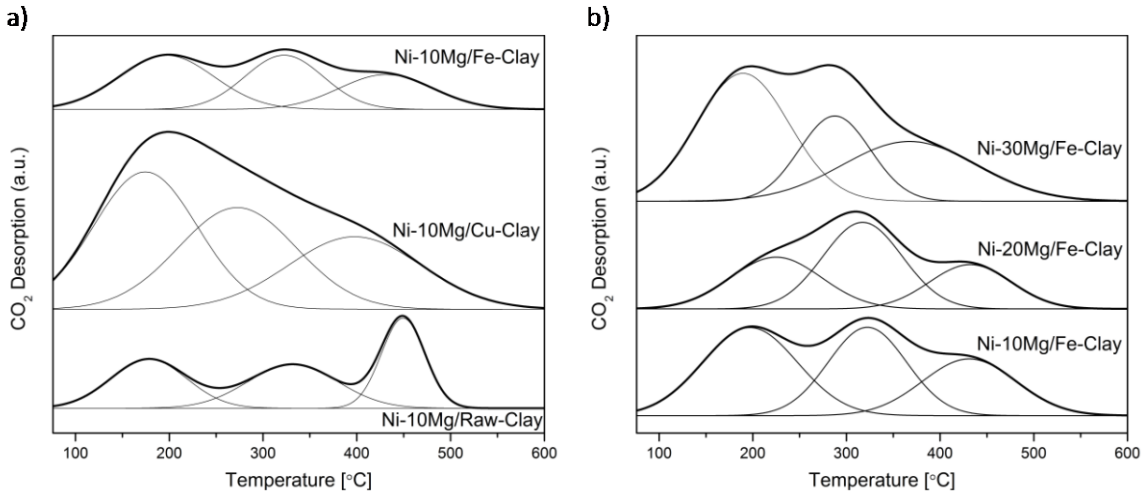

Figure 4-21. CO_2-TPD profiles for a) the Ni-Mg (10 wt.%) catalysts, and b) the Ni-Mg catalysts prepared at 10, 20 and 30 wt.% Mg-loading.

Mg-promotion results in increased total basicity, i.e. higher amounts of CO_2 adsorbed and then desorbed during CO_2-TPD. This CO_2 adsorption ability becomes maximal in the case of the Cu-Clay supported Ni-Mg catalysts, i.e. 99.1 µmol CO_2/g upon Mg-loading vis-à-vis 4.1 µmol CO_2/g measured for the non-promoted catalyst. This Cu-Clay supported Mg-promoted catalyst, which shows the highest participation of strong basic sites, i.e. almost 40% of the total basicity, whereas strong basic sites represent only 28% of the total basic sites in Ni-10Mg/Fe-Clay. Such a favoured presence of such strong basic sites may result in far too tight adsorption of CO_2 and thus to its limited reaction with CH_4 [132].

The amount of CO_2 adsorbed increases with increasing Mg-loading, and especially for the Ni-30Mg/Fe-Clay catalyst. However, in the Fe-Clay supported catalysts, the relative amount of strong basic sites remains relatively moderate, while the concentration of low (Brønsted) and medium-strength basic sites increases. Nevertheless, Ni-cluster size also plays an important role in the final catalytic activity of these materials [174,175], as will be discussed in the following section.

Table 4-15. Deconvolution of the CO_2-TPD profiles and total basicity for the different Mg-promoted and non-promoted natural clay supported catalysts.

Catalyst	Deconvolution [μmol CO_2/g]			Total basicity [μmol CO_2/g]
	Weak	Medium	Strong	
Ni/Raw-Clay	9.9	7.7	6.0	23.6
Ni-10Mg/Raw-Clay	10.2	10.4	11.4	32.0
Ni/Fe-Clay	4.8	19.6	6.0	30.4
Ni-10Mg/Fe-Clay	15.5	11.1	10.4	37.0
Ni-20Mg/Fe-Clay	9.7	13.9	8.6	32.2
Ni-30Mg/Fe-Clay	22.9	11.5	14.9	49.3
Ni/Cu-Clay	0.5	2.2	1.4	4.1
Ni-10Mg/Cu-Clay	35.7	25.7	37.7	99.1

4.5.3 Catalytic activity and selectivity of Mg-promoted Fe and Cu-pillared supported Ni-based catalysts

The results of the DRM catalytic tests performed in the presence of the different materials are shown in Figure 4-22 and Figure 4-23. Figure 4-22 a, b and c show the results obtained in the presence of the Ni-Mg (10 wt.%) catalysts in terms of both methane and CO_2 conversions, and H_2/CO ratio (syngas quality). Both methane and CO_2 conversions increase with increasing temperature, following the trend forecasted by the equilibrium thermodynamics of the CH_4/CO_2/Ar system at 1 bar. The measured H_2/CO ratios also increase with increasing temperature, opposite to the thermodynamically predicted trend. However, both the experimentally determined and the theoretical H_2/CO ratios converge to values close to 1 at the highest reaction temperatures, i.e. 750-850 °C.

The low H_2/CO ratios measured within the low temperature window are indeed a consequence of CO_2 conversions being all the time higher than those of methane. In the low-mild temperature window, methane can be as well consumed through its direct decomposition, resulting in H_2 and C(s). The solid carbon product, C(s), remains on the catalytic surface, covering its active sites, sometimes leading to an important loss of catalytic activity. The resulting H_2 can further react with the CO_2 in the feed gas through the reverse water gas shift (RWGS) reaction, yielding CO and H_2O. If the RWGS reaction occurs to an important extent, both enhanced consumption of H_2 and CO formation result in lower H_2/CO ratios than the ones predicted by the equilibrium thermodynamics. The DRM reaction is indeed just one of the multiple reactions taking place, being thermodynamically feasible at temperatures higher than 700 °C. At mild temperatures, carbon-forming reactions, such as

direct methane decomposition (DMD) and Boudouard reaction ($2CO \rightleftharpoons CO_2 + C$) are favored, together with methanation and CO_2 reduction reactions leading to alcohol and hydrocarbon formation.

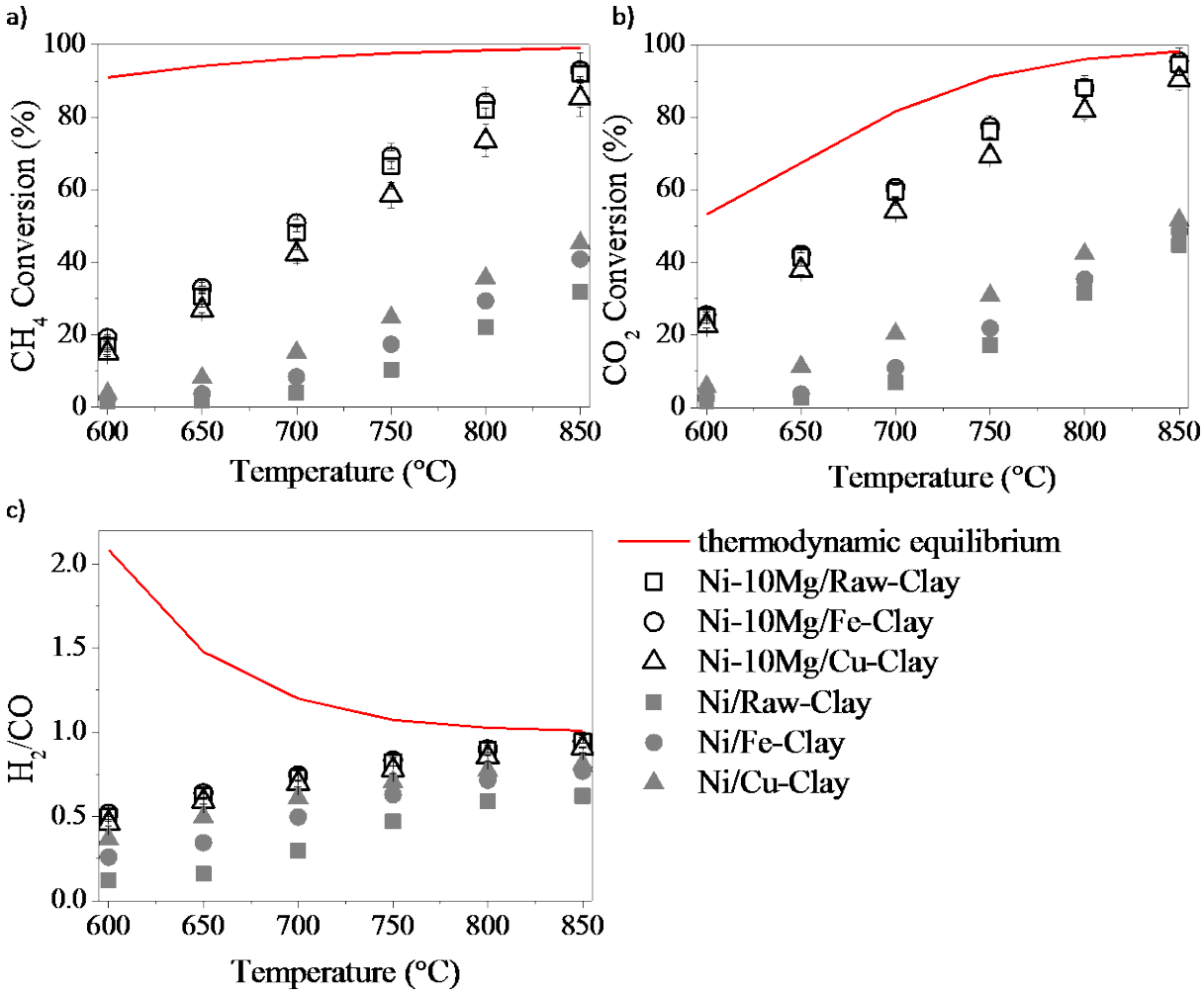

Figure 4-22. DRM activity tests in the presence of the Ni-Mg (10 wt. %) catalysts: methane (a) and CO_2 (b) conversions, and H_2/CO ratio (c). Non-promoted catalysts are showed in the section 3.3.

Though thermodynamically favored, these reactions are as well kinetically hindered. In the presence of a Ni-containing catalyst, DMD may be preferentially catalyzed, among the other carbon forming or hydrogenation reactions. At moderate temperatures RWGS starts taking the lead, until it simultaneously coexist with DRM, which ends up being dominant at temperatures higher than 750-800 °C.

Figure 4-23 shows the results of the DRM experiments performed in the presence of the catalysts prepared using 10, 20 and 30 wt.% Mg. The three catalysts show very similar activity, with similar methane and CO_2 conversions, as well as H_2/CO ratios.

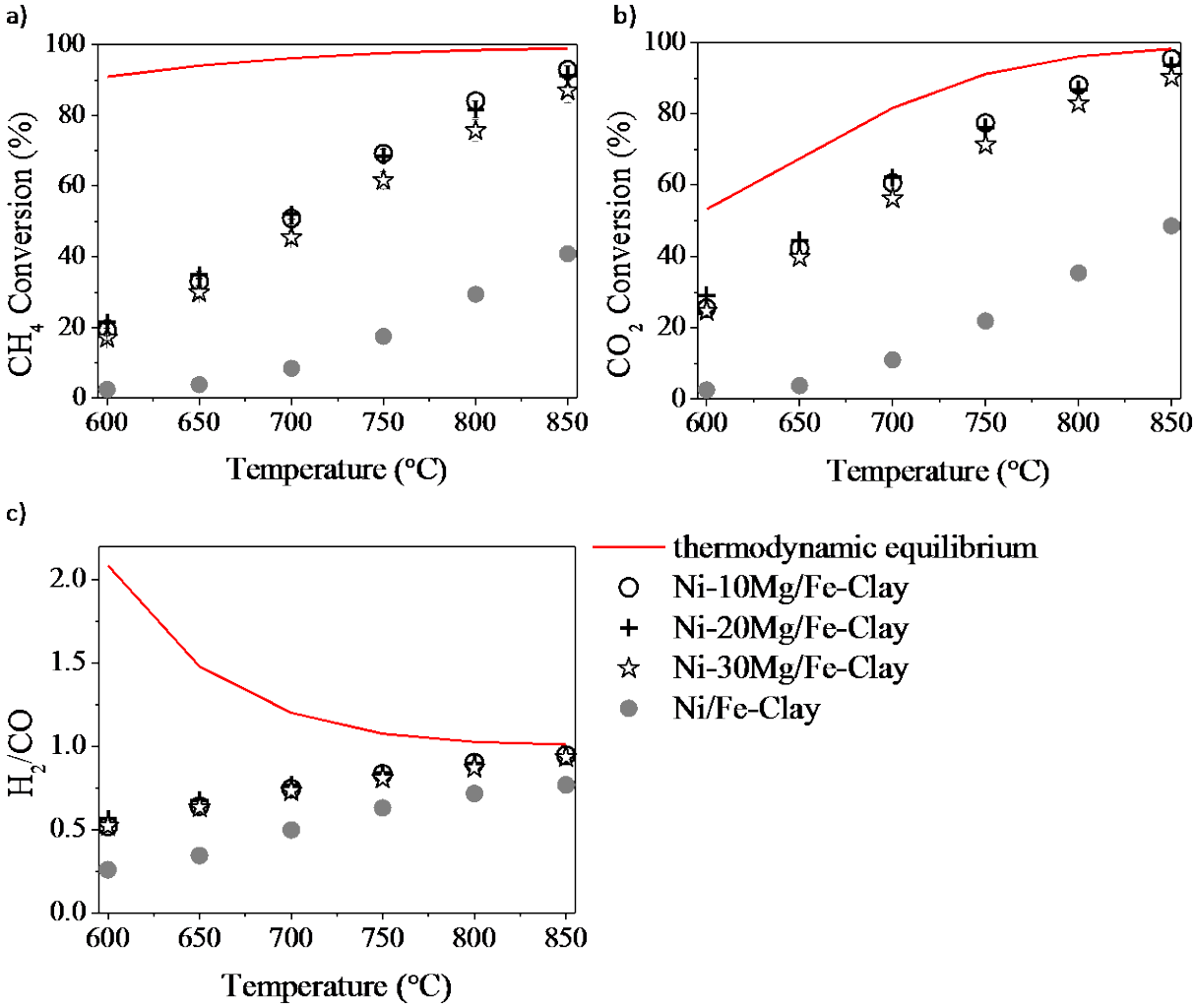

Figure 4-23. DRM activity tests in the presence of the Fe-Clay supported catalysts, containing 10, 20 and 30 wt.%: methane (a) and CO_2 (b) conversions, and H_2/CO ratio (c).

In any case, and in spite of the lower surface areas reported for the Mg-promoted catalysts (Table 4-14), a considerable increase in methane and CO_2 conversions can be observed upon Mg-loading, this being quite independent of the clay used as support (Figure 4-22 a and b). It is clear from the results of the physico-chemical characterization that, in general, Mg-promotion results in highest surface basicity (Table 4-15). The presence of basic sites may enhance CO_2 adsorption, which can result, in turn, in improved DRM activity. As commented before, the favoured presence of strong basic sites may result in far too tight adsorption of CO_2, disabling it for further reaction with CO_2, CH_4, H_2 and/or other species [169]. Indeed, Ni-10Mg/Cu-Clay exhibits the lowest activity of this series while presenting the highest population of strong basic groups.

These differences in basicity do not explain themselves the important increase of the catalytic activity observed upon Mg-promotion. Lightart et al. [174] proved that, in steam methane

reforming, the dispersion of the active metal can be directly related to the type of support used, and further stated that increased metallic dispersion results in increased density of low-coordinated edge and corner metal atoms that favoured methane dissociative adsorption (rate-determining step). Though in DRM CO_2 adsorption plays a very important role, methane activation on the catalytically active sites remains crucial for further reaction leading to H_2 and/or CO formation. Wei and Iglesia [175] performed isotopic experiments in order to elucidate the mechanism of methane reforming both with steam and CO_2. They found that reforming reactions and direct methane decomposition (DMD) follow a common path that is limited by the activation of the C-H bond in CH_4. They showed moreover that the CH_4 turnover rates increase with metal dispersion, for Ni-catalysts but also for noble metal containing catalysts. These turnover rates were apparently independent of the type of support used; i.e. only depended on the metallic dispersion. The authors concluded that correactant activation, such as favoured CO_2 adsorption, may be kinetically irrelevant in reforming reactions and cannot influence the overall reaction rate.

These observations seem to be in agreement with the results obtained in these study. Much higher methane and CO_2 conversions were measured in the presence of the Mg-promoted catalysts. The presence of Mg results in increased basicity. However, only Ni^0 crystallite size explains enhanced methane activation. Mg-loading leads to the formation of a mixed phase $NiMgO_2$ that, upon reduction, results in considerably lower Ni^0 crystallite sizes than in the case of the non-promoted catalysts. Methane activation on such smaller metal clusters leads to its effective participation in all the reactions involved, thus leading to higher methane and CO_2 conversions.

4.5.4 Transmission electron microscope (TEM) analysis

Figure 4-24 contains the TEM micrographs obtained for the Ni-Mg (10 wt.%) catalysts upon the DRM experiments, together with their corresponding histograms. Bulk graphitic carbon formations are observed together with carbon filaments (nanofibres) of very different sizes. Very frequently, these carbon structures appear close to big Ni-agglomerates, pointing to a certain sintering of the metallic phase. However, an important amount of well-dispersed Ni^0 particles is evidenced in any of the TEM images acquired for the Mg-promoted catalysts. The histograms point indeed to mean particle sizes around 7 nm for the Fe and Cu pillared clays

supported catalysts, and around 9 nm for the catalyst prepared using the raw clay. They point also to the presence of Ni^0 particles of bigger size, between 10 and 17 nm that may be generated upon the reduction of bulk NiO_x, as well as big Ni agglomerates (appearing close to C(s) formation) due to the sintering of the metallic phase, as already commented. Let us not here as that no clear evidences of a different behaviour in terms of sintering or Ni cluster size have been observed through the TEM analysis of the Fe-Clay based catalysts, although Raman studies pointed to the presence of an spinel $NiFe_2O_4$ phase in this catalyst.

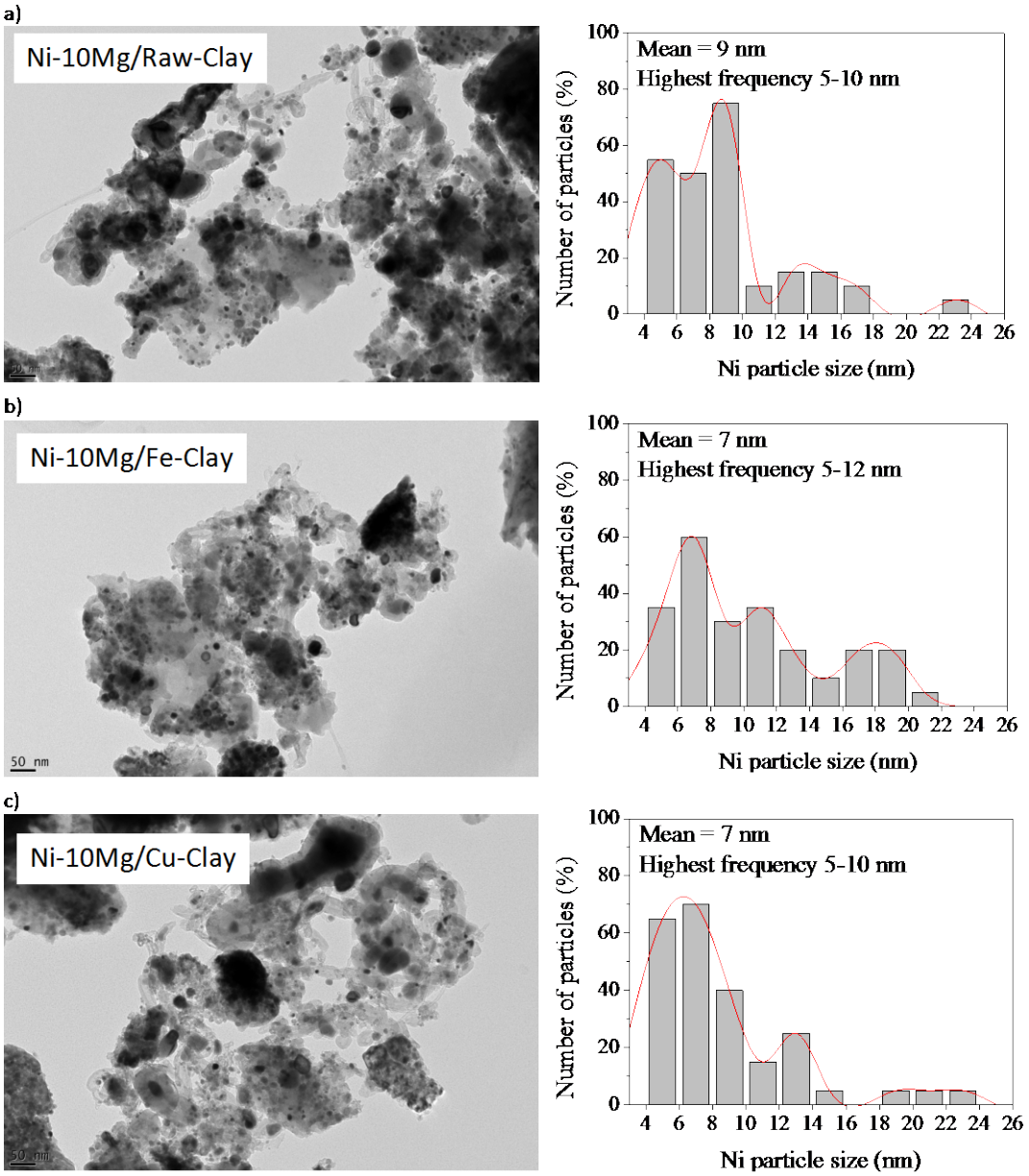

Figure 4-24. TEM micrographs (x25,000) and particle histograms for the spent catalysts (upon DRM experiment): (a) Ni-10Mg/Raw-Clay, (b) Ni-10Mg/Fe-Clay and (c) Ni-10Mg/Cu-Clay.

4.5.5 Infuence of Mg promotion on Fe and Cu-pillared on carbon deposition

Table 4-16 contains the amount of carbon deposited, calculated from the carbon balance C(s) = C in reactants – C in products, for this series of catalysts. Mg-promotion results higher extent of carbon formation and deposition, vis-à-vis the non-promoted catalysts. This can be directly linked to their higher activity, especially in terms of methane activation and conversion, pointing to direct methane decomposition (DMD) occurring to a certain extent. Among the Mg-promoted catalysts, the ones prepared using the Fe-Clay seem to lead to increased carbon formation, in agreement with their enhanced activity. Similarly, the catalyst prepared using 30 wt.% Mg yields relatively lower amounts of solid carbon, corresponding also to its lower activity vis-à-vis the rest of the catalysts in the series. Once again, activity seems to be directly linked to the activation of the C-H bond in methane, which leads also to its direct decomposition, resulting in solid carbon formation. Nevertheless, isothermal runs performed at 750 °C evidenced no sign of activity loss over 5 hours time-on-stream, for any of the Mg-promoted clay-based catalysts.

Table 4-16 Amount of carbon deposited calculated from the carbon balance, applied to the different clay-supported catalysts.

Catalyst	Carbon deposition [mg]
Ni/Raw-Clay	75
Ni-10Mg/Raw-Clay	327
Ni/Fe-Clay	93
Ni-10Mg/Fe-Clay	396
Ni-20Mg/Fe-Clay	409
Ni-30Mg/Fe-Clay	346
Ni/Cu-Clay	161
Ni-10Mg/Cu-Clay	329

4.5.6 Summary

Table 4-17. Summary for the influences of Mg promotion on different clays.

		Promotion	Ni	Ni-Mg
Raw clay		Specific surface area	0	-
		Ni^0 crystallite size[1]	0	-
		Ni reducibility	0	-
		Total basicity	0	+
		DRM activity	0	+
		Carbon deposition	0	+
Pillared clay		Promotion	Ni	Ni-Mg
	Fe-clay	Specific surface area	0	-
		Ni^0 crystallite size[1]	0	-
		Ni reducibility	0	-
		Total basicity	0	+
		DRM activity	0	+
		Carbon deposition	0	+
		Promotion	Ni	Ni-Mg
	Cu-clay	Specific surface area	0	-
		Ni^0 crystallite size[1]	0	-
		Ni Reducibility	0	-
		Total basicity	0	+
		DRM activity	0	+
		Carbon deposition	0	+

"0" means the benchmark.
"+" means the strengthened/increased value compared to Ni based Raw/Fe/Cu-clay catalysts respectively.
"-" means the weakened/decreased value compared to Ni based Raw/Fe/Cu-clay catalysts respectively.
[1]Ni^0 crystallite size is compared only for reduced catalysts

Table 4-17 describes the effects of Mg on all Raw-, Fe- and Cu-modified clays. Mg-promotion of natural clay based Ni-catalysts was considered, as a way of boosting the dry reforming of methane (DRM) activity of these materials. The results of the DRM experiments performed at temperatures from 600 °C to 850 °C evidenced much higher methane and CO_2 conversions for the Mg-promoted catalysts. Mg-promotion leaded of course to a significant increase of CO_2-adsorption ability (basicity). However, the increased catalytic activity of the Mg-promoted materials was rather linked to increased Ni-dispersion and Ni^0 crystallite size. Indeed, the independently of the physicochemical proerties of the support, the presence of Mg led to the formation of a $MgNiO_2$ mixed phase that, upon reduction, resulted in the formation of metallic Ni clusters having sizes around 7-9 nm, considerably smaller than in any of the non-promoted catalysts. Carbon formation was found to take place to a greater extent in the presence of the Mg-promoted catalysts, due to C-H bond activation leading also to favored

direct methane decomposition (DMD). In spite of this, the activity of the Mg-promoted catalysts was well maintained over 5 hours DRM experiments performed at 750 °C.

4.6 Conclusions

Table 4-18. Summary for the influences of different promoters on different clays

	Promotion	Ni	Ni-Al	Ni-La	Ni-Mn	Ni-Ce	Ni-Zr	Ni-Mg
Raw clay	Specific surface area	0	/	/	/	/	/	-
	Ni^0 crystallite size[1]	0	/	/	/	/	/	-
	Ni reducibility	0	/	/	/	/	/	-
	Total basicity	0	/	/	/	/	/	+
	DRM activity	0	/	/	/	/	/	+
	Carbon deposition	0	/	/	/	/	/	+
	Promotion	Ni	Ni-Al	Ni-La	Ni-Mn	Ni-Ce	Ni-Zr	Ni-Mg
Fe-clay	Specific surface area	0	+	-	+	+	+	-
	Ni^0 crystallite size[1]	0	-	-	-	-	-	-
	Ni reducibility	0	+	-	+/-	+	+	-
	Total basicity	0	-	-	-	-	-	+
	DRM activity	0	+	+	-	+	+	+
	Carbon deposition	0	+	+	-	+	+	+
	Promotion	Ni	Ni-Al	Ni-La	Ni-Mn	Ni-Ce	Ni-Zr	Ni-Mg
Cu-clay	Specific surface area	0	/	/	/	+	+	-
	Ni^0 crystallite size[1]	0	/	/	/	+	-	-
	Ni Reducibility	0	/	/	/	+	+	-
	Total basicity	0	/	/	/	+	+	+
	DRM activity	0	/	/	/	+	+	+
	Carbon deposition	0	/	/	/	+	+	+

"0" means the benchmark.
"+" means the strengthened/increased value compared to Ni based Raw/Fe/Cu-clay catalysts respectively.
"-" means the weakened/decreased value compared to Ni based Raw/Fe/Cu-clay catalysts respectively.
"+/-" means it is hard to decide the influence.
"/" means it is not prepared.
[1]Ni^0 crystallite size is compared only for reduced catalysts.

Table 4-18 summarized the influences of different promotions on raw and pillared clays. La, Al and Mn-promoted Ni catalysts supported on Fe-modified Tunisian clays were synthesized by impregnation method and tested in DRM at temperatures between 850 and 600 °C. Based on the DRM results, La/Al-promoted catalysts led to an improvement of the catalytic performance whereas Mn-promoted catalysts inhibited it. Moreover, the addition of Al resulted in the highest catalytic activity. In conclusion, the carbon deposition was brought up with high catalytic activity in this catalyst system. Meanwhile, characterization results based on BET, XRD, H_2-TPR and CO_2-TPR presented the tendencies of texture properties, Ni^0 dispersion, Ni reducibility and CO_2 basicity respectively. The addition of Al and Mn

increased the specific surface area, whereas La decreased it. All promoters led to higher dispersion of Ni. The presence of La shifted the main peak to higher temperature, thus reducing Ni reducibility to a certain extent. On the contrary, the addition of Al slightly moved the main peak to lower temperature and improved the reducibility. The introduction of La, Al or Mn affected the adsorbed CO_2 on each type of basic sites, and almost suppressed the strong basic sites, further leading to higher activity in DRM except for Mn-promoted catalysts. The increase of Ni dispersion and less basicity on strong basic sites for La/Al-promoted catalyst could explain the better catalytic performance for this catalyst, whereas for Mn-promoted catalyst, the presence of Mn oxides and Fayalite, Mn-rich, which may partially or totally cover the active sites on NiO species possibly led to low catalytic performance.

Natural clay based Ni-containing catalysts were prepared using a Tunisian clay that was either modified using Fe or Cu. Their activity was tested in the dry reforming of methane (DRM) at temperatures between 600 and 800 °C. Prior to these catalytic experiments, the catalysts were reduced in 5 vol.% H_2-Ar at two different temperatures: 800 and 900 °C. Reduction temperature had a big influence on Ni crystal size. Generally smaller Ni crystal sizes were found in the catalysts reduced at 900 °C. Basicity, i.e. evaluated by means of CO_2-TPD, was found to be lower in the catalysts prepared using the Cu-pillared clay. Moreover, increasing reduction temperature from 800 to 900 °C resulted in a considerable decrease of basicity. In fact, as a consequence of this generally decreased basicity and smaller Ni crystal size, the catalysts reduced at 900 °C showed lower activity in DRM than those reduced at 800 °C. In spite of their lower basicity, however, the Cu-containing catalysts yielded all the time highest CH_4 and CO_2 conversions. This was maybe linked to the well known activity of Cu-catalysts towards reverse water gas shift reaction, which effectively took place in parallel to reforming reactions in the presence of the natural clay based Ni-containing catalysts.

Ce and Zr promoted Fe and Cu-modified natural clay based Ni-catalysts were prepared. Their activity in dry reforming of methane (DRM) was tested at temperatures from 600 to 800 °C. The presence of the promoters considerable enhanced the activity of the clay-based catalysts, i.e. almost 70% CO_2 conversion was obtained at 750 °C for the Ce-promoted Cu-modified clay based catalyst, in comparison to 56% CO_2 conversion measured for the non-promoted catalyst. Carbon deposition was found to occur, as a consequence of the simultaneous occurrence of carbon-forming reaction, especially in the low temperature range. Ce-promotion resulted in a higher extent of carbon deposition, due to the acceleration of

direct methane decomposition in the presence of these catalysts. The promotion effect could be first of all explained in terms of the highest reducibility of Ni-species, as a consequence of the presence of either Ce or Zr. The resulting Ni^0 crystal sizes varied from 8.1 to 15.2 nm, being higher for the most active catalyst of this series, i.e. Ni-Ce/Cu-Clay, corresponding as well to the highest amount of deposited carbon. The basicity of the catalysts was moreover modified through the addition of Ce and Zr. In the case of the Fe-modified clays based catalyst the presence of the promoters resulted in a decreased presence of strong basic sites. The importance of the presence of either weak or medium-strength basic sites was clearly reflected in the case of the Cu-modified clay supported catalysts, with the highest weak-strength basicity corresponding to the most active catalyst of this series, Ni-Ce/Cu-Clay.

Mg-promoted Ni-containing catalysts were prepared using a Tunisian natural clay as support, modified through the introduction of either Fe or Cu pillars. The physicochemical characterization of these catalysts evidenced surface areas and total pore volume that decrease with increasing Mg loading. Micropores and narrow mesopores were easily blocked upon Mg introduction, leaving the wide mesopores and macropores still available for reaction. Mg-promotion resulted in the formation of a $MgNiO_2$ mixed oxide phase that, upon reduction, led to the formation of Ni metallic clusters around 7-9 nm, considerably smaller than in the non-promoted catalysts. Though Raman observation pointed to the possible formation of an spinel $NiFe_2O_4$, particularly in the case of the Fe-Clay supported catalysts, the presence of this mixed Ni-Fe phase did not seem to influence the final Ni^0 crystallite size in the reduced materials Total basicity, i.e. amount of basic sites able to adsorb CO_2, substantially increased upon Mg-loading. The catalytic activity in DRM within the 650-850 °C was considerably boosted when using Mg as promoter. Methane and CO_2 conversions increased by a factor of two, when DRM was performed in the presence of the Mg-loaded catalysts. H_2/CO ratios also increased with respect to the non-promoted catalysts, approaching values close to 1 at almost any reaction temperature. Still, the CO_2 conversions measured, higher than the corresponding methane conversions, point to the existence of different side reactions, such as reverse water gas shift (RWGS) and direct methane decomposition, taking place simultaneously to DRM, particularly at low-intermediate temperatures. The overall activity seemed to be governed by the Ni0 crystallite size. The enhanced dispersion gained through Mg-promotion lead to a faster activation of the C-H bond resulting in increased activity, both in methane reforming and in direct methane decomposition reactions. TEM observation of the catalysts upon the

DRM experiments evidenced a relatively wide particle size distribution, but confirmed the mean metallic cluster sizes determined from the XRD patterns. Bulk graphitic carbon structures covering sintered Ni-clusters, as well as carbon nanofibres of different sizes were observed. The extent of carbon formation was found to be higher for the Mg-promoted catalysts, corresponding to the improved C-H bond activation. However, the catalytic stability was verified over 5 h duration isothermal DRM experiments performed at 750 °C.

Chapter V

Other natural materials (Hydrotalcite, Hydrocalumite, Hydro-Strotium, and Hydro-Barium) supported catalysts for dry reforming of mehane (DRM)

5. Other natural materials (Hydrotalcite, Hydrocalumite, Hydro-Strotium, and Hydro-Barium) supported catalysts for DRM

5.1 Introduction

Dry reforming of methane (DRM), the reforming of methane with CO_2: $CH_4(g) + CO_2(g) = 2CO(g) + 2H_2(g)$, ΔH^0 (298K)= +247 kJ·mol^{-1}, is nowadays considered as a perspective alternative for the production of syngas, H_2 + CO, involving the valorization of CO_2, coming either from capture or naturally present in the reactant gas, i.e. such in biogas. Furthermore, the H_2/CO molar ratio in DRM-syngas, equal to 1, makes it applicable for Fischer-Tropsch synthesis [176- 179]. There are, however, several important drawbacks that hinder the practical application of DRM, such as its high endothermicity, and different issues related to the selectivity and stability of the DRM catalyst under operation conditions [180,181]. The co-existence of parallel reactions, such as direct methane decomposition and the reverse water gas shift reaction results in low yields and in catalyst deactivation through carbon deposition, especially at low reaction temperatures. Increasing the temperature favors DRM thermodynamics, but Ni particles tend to sinter leading to a dramatic decrease in the catalytic performance.

Different active metals, e.g. Pt, Ir, Rh or Ni, supported on different materials, have been proposed as DRM catalysts [182- 185]. Among them, nickel shows comparable activity to noble metals, being much cheaper and more readily available. Current research focus on finding support materials and promoters that improve the selectivity of the process and that contribute to enhanced catalytic stability. As an example, Verykios et al. [186] showed that the incorporation of Ni onto La_2O_3 support notably improved the catalysts stability in comparison to Ni-Al_2O_3, through the formation of oxy-carbonate species ($La_2O_2CO_3$) that were further able to gasify the already formed carbon deposits.

The layered double hydroxides (LDH) that are generally mixed of two metallic hydroxides materials have the general formula: $[M_{1-x}^{II}M_x^{III}(OH)_2]\left[A_{x/n}^{n-}\right]\cdot mH_2O$, where M^{II} / M^{III} represent divalent and trivalent metal ions and A^{n-} is hydrated anion, such as hydrotalcites.

The composition of LDH can be modified through the substitution of different divalent and trivalent cations in the layers. Cavani et al. showed that monovalent and tetravalent cations such as Li^{+}, Zr^{4+}, Ti^{4+} and Sn^{4+} could be as well introduced into these LDH-layers [187]. Therefore, the acid-base and redox properties of LDH can be properly tailored to fit some particular catalytic applications [188, 189]. For example, the materials obtained after calcinations of the hydrotalcite matrix offer other interesting properties, such as adequate porosity, and a random and homogeneous distribution of the different cations on the resulting mixed-oxide structure. As a consequence, Ni-containing hydrotacite-derived materials have been recently considered as promising catalysts for DRM.

Thus, the present work considers the Ni-based hydrocalumite, hydrotalcite, hydro-strontium and hydro-barium-derived catalysts and the addition of lanthanum (1, 2 and 4 wt.%) to 15 wt.% Ni-containing hydrotalcite or hydrocalumite-derived catalysts for dry reforming of methane in this chapter. Special attention has been paid to the influence of the Ni-hydrotalcite, Ni-hydrocalumite, Ni-hydro-strontium and Ni-hydro-barium-derived catalysts on the physicochemical properties of nickel based catalysts, as well as the La-promotion on the physicochemical properties of the Ni-hydrocalumite and Ni-hydrotalcite-derived catalysts, as studied by means of BET, XRD, H_2-TPR and CO_2-TPD, and its consequences in terms of activity, selectivity and stability in the DRM reaction.

5.2 Nickel based hydrotalcite, hydrocalumite, hydro-strotium and hydro-barium-derived catalysts

In this section, the bivalent metal elements of group 2 (Mg^{2+}, Ca^{2+}, Sr^{2+} and Ba^{2+}) and trivalent metal aluminum (Al^{3+}) were tried to prepare the Ni-containing catalysts and tested in dry methane reforming at low-moderate temperatures. The characterizations including BET, XRD, H_2-TPR and CO_2-TPD were used to analyze the possible influences of different elements of Mg, Ca, Sr and Ba on catalytic performance.

5.2.1 Synthesis of hydrotalcite, hydrocalumite, hydro-strotium and hydro-barium-derived catalysts

Hydrotalcites/hydrocalumite/hydro-strotium/hydro-barium derived catalysts containing trivalent (M^{3+}) and divalent (M^{2+}) metals (Al^{3+}, Mg^{2+}/Ca^{2+}/Sr^{2+}/Ba^{2+}, Ni^{2+}) with M^{3+}/M^{2+} molar ratio of 0.33, were prepared by a co-precipitation method. Two aqueous solutions, one containing the mixed nitrates of divalent and trivalent metals, and the other one containing sodium hydroxide (1 M), were added dropwise into a flask containing an aqueous solution of sodium carbonate, and subsequently kept under vigorous stirring at 65 ± 3 °C and constant pH (from 9.5 to 10). This mixture aged for 1h and then filtered, carefully washed with deionized water and finally dried overnight at 80 °C in the oven. In order to obtain the corresponding catalysts, each sample was calcined under air at 550 °C for 5 hours. The nominal (assumed) concentration of the different components in each catalyst, as well as their labeling, is listed in Table 5-1.

Table 5-1. Ni-containing hydrotalcites, hydrocalumite, hydro-strotium and hydro-barium derived catalysts: nominal concentration of the different cations.

Catalyst	Label	Metal content [wt.%]						$\frac{M^{3+}}{M^{3+}+M^{2+}}$
		Ni	Al	Mg	Ca	Sr	Ba	
NiAlMg	HT	15	8.1	15.8	0	0	0	0.25
NiAlCa	HCa	15	7.4	0	22.5	0	0	0.25
NiAlSr	HSr	15	5.9	0	0	34.9	0	0.25
NiAlBa	HBa	15	5.0	0	0	0	42.1	0.25

5.2.2 Physicochemical properties of the hydrotalcite, hydrocalumite, hydro-strotium and hydro-barium-derived catalysts

5.2.2.1 Crystallinity and textural properties

The X-ray diffractograms of fresh and reduced catalysts are showed in Figure 5-1 a) and b) respectively. From the XRD patterns of fresh Ni-hydrotalcite, Ni-hydrocalumite, Ni-hydro-strontium and Ni-hydro-barium derived catalysts (Figure 5-1 a), It could be found that Ni-hydrotalcite and Ni-hydrocalumite derived catalysts present the reflections of layered double hydroxides. The Ni-hydro-strontium and Ni-hydro-barium derived catalysts cannot obtain the layered structures since their large ionic radius, which is also discussed by Yan et al. [190,191]. One point should be noted that the ionic radius is not the only factor that affects

the synthesis of layered double hydroxides, because Ca^{2+} with large ionic radius has formed layered double hydroxides with Al^{3+}. And the layered double hydroxides in hydrocalumite derived catalysts were also confirmed by Yan et al. [190]. In the fresh Ni-hydro-strontium and Ni-hydro-barium derived catalysts, it seems that nickel aluminum carbonate hydroxides are formed. Moreover, the prensences of Ca^{2+}, Sr^{2+} and Ba^{2+} in respective catalysts form the corresponding carbonate signals, i.e. $CaCO_3$, $SrCO_3$, and $BaCO_3$.

The obtained XRD results of reduced Ni-hydrotalcite, Ni-hydrocalumite, Ni-hydro-strontium and Ni-hydro-barium derived catalysts are presented in Figure 5-1 b). After the reduction at 900 °C, the periclase-like structure of mixed oxides (43.0° and 62.4°) from thermal decomposition of hydrotalcite materials and the katoite-like structure from the decomposition of hydrocalumite are presented. The new phase $BaAl_2O_4$ and strontium aluminum hydroxide observed in reduced catalysts come from $SrCO_3$ and $BaCO_3$ respectively. Moreover, the additional phase metallic nickel is also observed at about 44.6°, 51.9° and 76.5°. The Ni^0 crystallite size for Ni-hydrotalcite, Ni-hydrocalumite, Ni-hydro-strontium and Ni-hydro-barium derived catalysts listed in Table 5-2 is calculated by Scherrer equation using the Full width at half maximum (FWHM) at 51.9° to avoid the effects of overlapping reflections. The Ni-hydrotalcite detived catalysts provide a relatively small particle size corresponding to improved Ni dispersion, it may further influence the catalytic performance [117].

a)

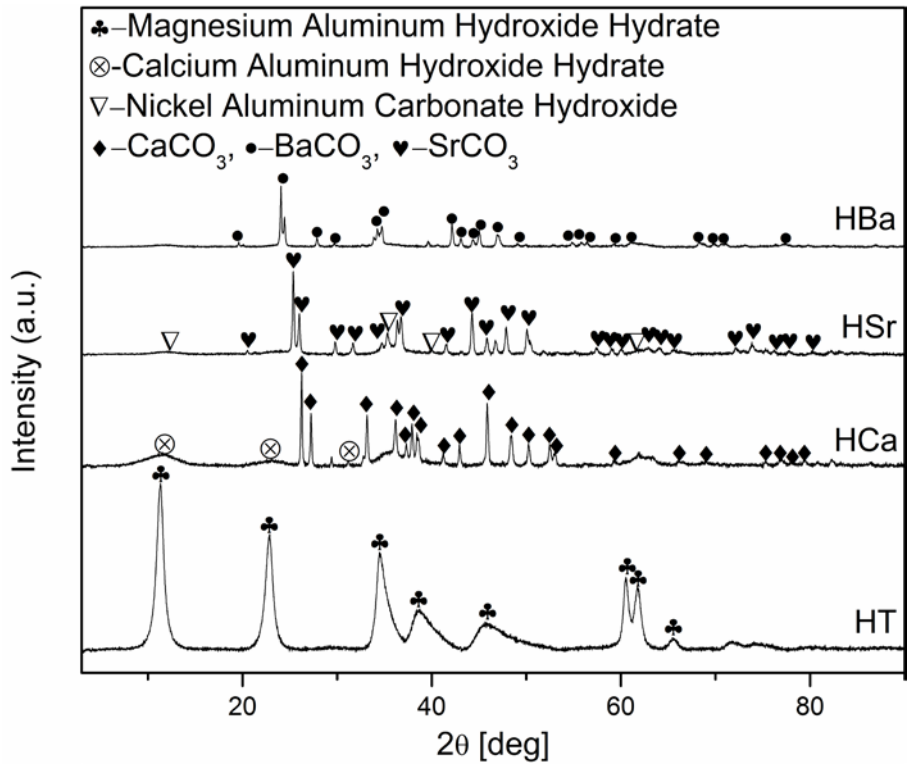

b)

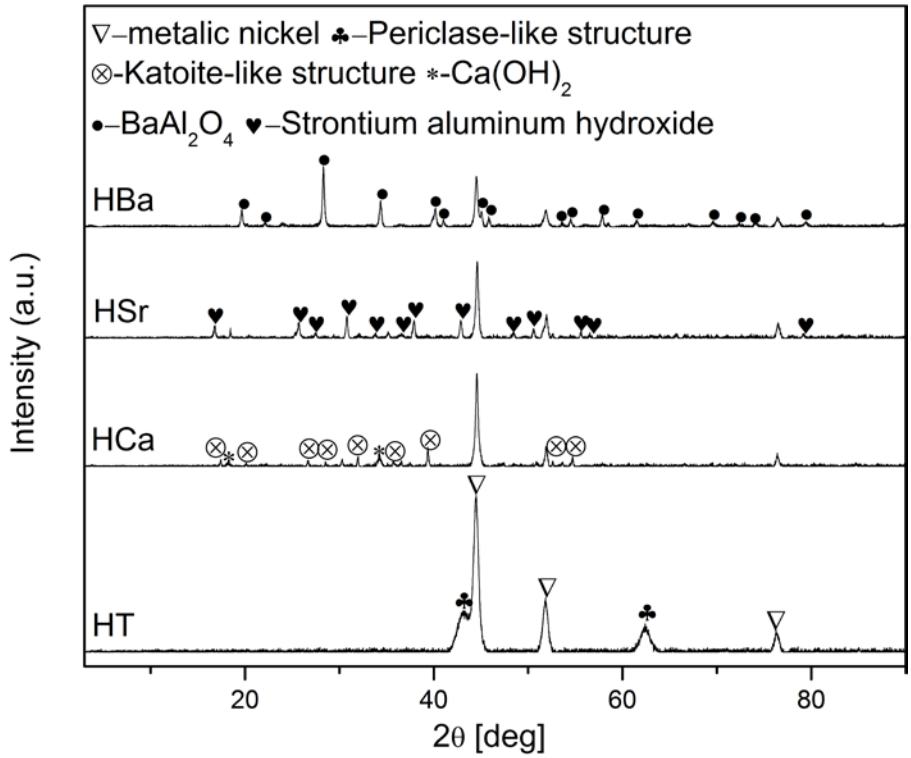

Figure 5-1. X-ray diffractograms acquired for a) the fresh samples, and b) the reduced samples.

Table 5-2 lists the data of texture characterizations for the calcined catalysts based on the N_2 adsorption isotherms, such as their specific surface area, total pore volume and average pore

size. The specific surface area is always changed through impregnating different divalent (M^{2+}) metals (Mg^{2+}, Ca^{2+}, Sr^{2+} or Ba^{2+}), which could be attributed to the formation of different structures, partial pore blockage and/or different pore sizes. The presence of magnesium species presents high specific surface area owing to the formation of layered double hydroxides for fresh catalysts, which is already evidenced by many researchers [192-194]. But the addition of calcium species shows the lowest specific surface area in the catalytic system, it means that calcium species partially blocks the pore system on catalyst although the calcium can form layered structure with aluminum [195]. The introduction of strontium and barium species have higher surface areas than the Ni-hydrocalumite derived catalysts while the layered structures are missed in Ni-hydro-strotium and Ni-hydro-barium-derived catalysts since their large ionic radius, which also contribute to their high specific surface area [190,191]. The high specific surface area probably affect the distribution of Ni species through providing more positions of active sites, which may further affects the catalytic activity and selectivity. In general, higher specific surface area is followed with lower pore size [196]. But the prepared catalysts do not comply with this tendency, also pointing to the influences of layered strucuture and metallic properties for textural properties. The average pore sizes are located at between 5.4 and 11.6 nm, which mean the mesoporous structure of prepared catalysts.

Table 5-2. BET results, Ni^0 crystal size for the Ni-containing hydrotalcites, hydrocalumite, hydro-strotium and hydro-barium derived catalysts.

Catalysts	S_{BET} [m^2/g]	V_p[1] [cm^3/g]	d_p[2] [nm]	V_{BJH}[3] [cm^3/g]	Ni^0 crystal size [nm]
HT	233.5	0.676	11.6	0.667	16.0
HCa	74.4	0.106	5.7	0.104	35.9
HSr	124.4	0.193	6.2	0.180	26.7
HBa	116.6	0.158	5.4	0.151	22.3

[1] *total pore volume*
[2] *average pore size*
[3] *BJH desorption cumulative pore volume*

5.2.2.2 Reducibility of Ni-species

The results of the H_2-TPR experiments are presented in Figure 5-2, for the Ni-hydrotalcite, Ni-hydrocalumite, Ni-hydro-strontium and Ni-hydro-barium derived catalysts. All prepared catalysts show one main asymmetric peak appearing between 638 and 850 °C, which are attributed to the reduction of Ni-oxide species to Ni° that are strongly bonded to support.

Especially for Ni-hydrotalcite derived catalysts, the possible reason for such a high reduction temperature (850 °C) is that Ni-oxide species are probably inserted into the Al-Mg mixed oxide matrix causing from the calcination of the hydrotalcite brucite layers, then forming a solid solution of high thermal stability [197,198]. Meanwhile, the higher position of the main peak for Ni-hydrotalcite derived catalysts indicates stronger interaction between Ni-oxide species and support, pointing to the lower reducibility of Ni-oxide species. Moreover, the further reduction peaks of Ni-oxide species at about 890 °C for Ni-hydro-strontium and Ni-hydro-barium derived catalysts, illustrate the presence of more tight interaction of Ni-oxide species and the support. Additionally, the shoulder appearing at 488, 426 and 435 °C for Ni-hydrocalumite, Ni-hydro-strontium and Ni-hydro-barium derived catalysts respectively, and one wide peak at 351 °C for hydrocalumite derived catalysts can be assigned to the reduction of bulk and weakly bonded Ni-oxide species [199]. Moreover, the main reduction peak moving towards low temperatures in the presence of Ca^{2+}, Sr^{2+} and Ba^{2+} compared to Ni-hydrotalcite derived catalysts illustrates their enhanced Ni reducibility. Thus, the presence of Mg^{2+} may be beneficial to the dispersion of Ni species, since higher reduction temperature points to smaller crystal sizes that correspond to higher Ni dispersion [117,200].

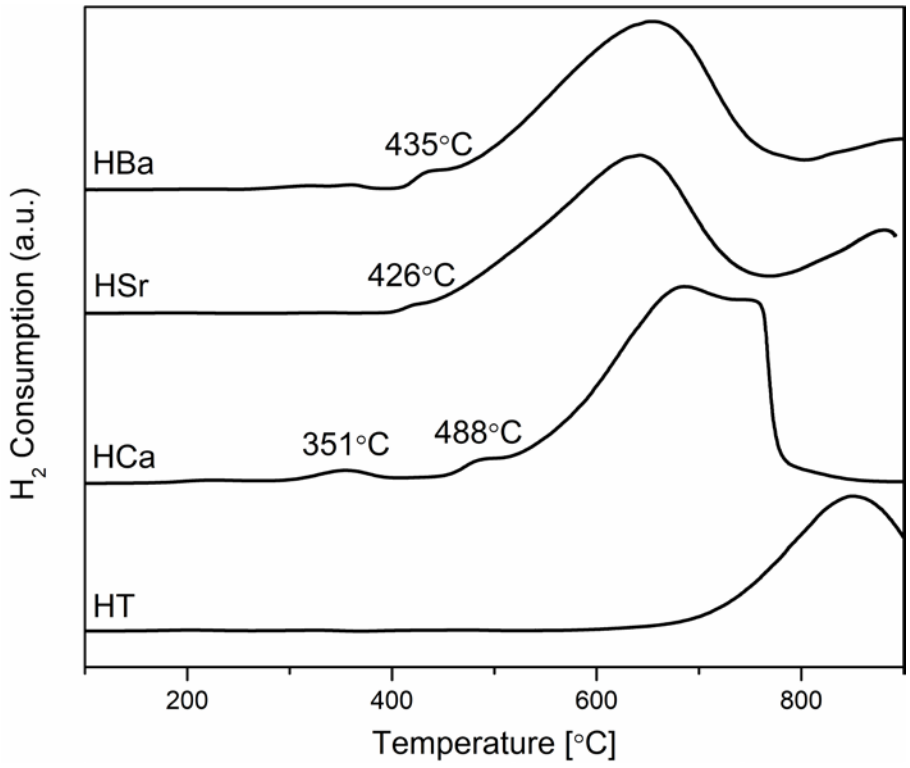

Figure 5-2. H_2-TPR profiles of Ni-hydrotalcite, Ni-hydrocalumite, Ni-hydro-strontium and Ni-hydro-barium derived catalysts.

5.2.2.3 Influence of divalent metals (Mg^{2+}, Ca^{2+}, Sr^{2+} or Ba^{2+}) on catalyst basicity

The basicity of the Ni-hydrotalcite, Ni-hydrocalumite, Ni-hydro-strontium and Ni-hydro-barium derived catalysts evaluated by CO_2-TPD is presented in Figure 5-3. Three typical CO_2 desorption peaks of prepared catalysts appearing between 100 °C and 700 °C from low to high temperatures correspond to three different strength: surface OH groups (weak Brønsted basic sites), Lewis acid-base pairings (medium-strength basic sites) and low-coordination oxygen anions (strong basic sites) [201, 202]. Furthermore, the peak positions and areas always change depending on the addition of different divalent metals (Mg^{2+}, Ca^{2+}, Sr^{2+} and Ba^{2+}), which is listed in Table 5-3.

Comparing with hydrotalcite derived catalysts that the centers of the CO_2 desorption are located at 147 °C, 250 °C and 389 °C, each of the three CO_2 desorption peaks for Ni-hydro-strontium and Ni-hydro-barium derived catalysts shifts to lower temperature, appearing at 119-122 °C, 189-198 °C and 314-325 °C respectively. It means the presence of Sr and Ba lead to weaker CO_2 chemisorption. Meanwhile, the weak Brønsted basic sites for hydrocalumite derived catalysts also shift to lower temperature at 122 °C while the medium-strength basic sites and strong basic sites move to higher temperature at 298 °C and 565 °C respectively, which means Ca mainly strengthens CO_2 chemisorption. This is particularly obvious for strong basic sites appearing 176 °C later than Ni-hydrotalcite derived catalysts, and Ni-hydrocalumite derived catalysts also present the highest basicity on strong basic sites showed in Table 5-3. Thus, the higher basicity and position of strong basic sites may affect the catalytic performance of HCa, because CO_2 on strong basic sites is more difficult to react with CH_4 [203]. In comparison, the addition of Mg and Sr mainly act on weak Brønsted basic sites and medium-strength basic sites, while Ni-hydro-barium derived catalysts with the lowest total basicity primarily affect weak Brønsted basic sites and strong basic sites.

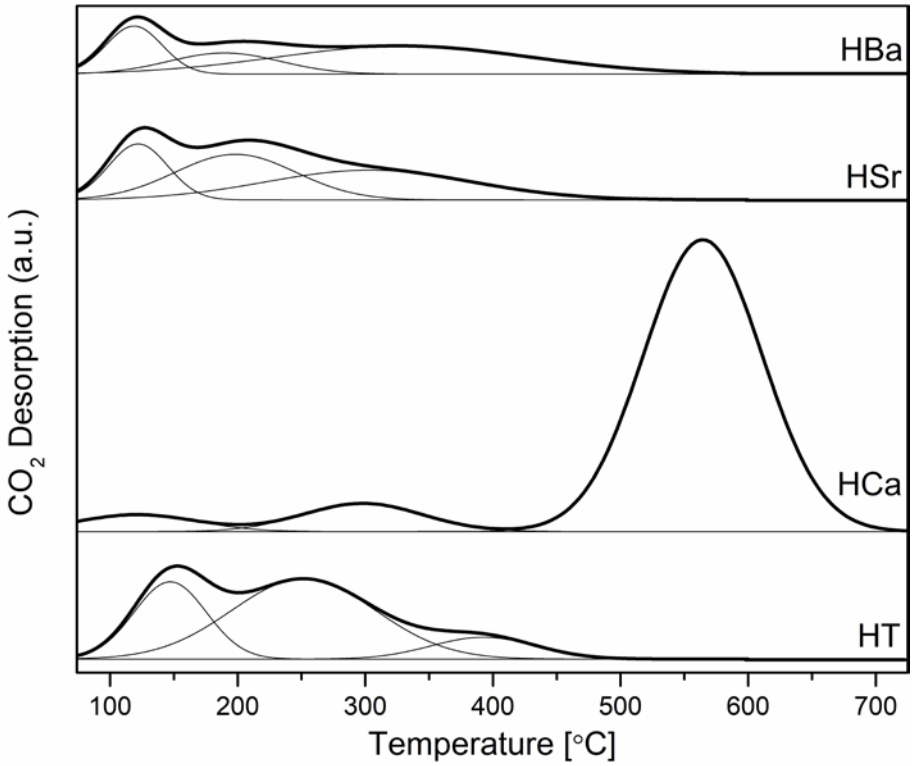

Figure 5-3. CO_2-TPD profiles of Ni-hydrotalcite, Ni-hydrocalumite, Ni-hydro-strontium and Ni-hydro-barium derived catalysts.

Table 5-3. Peak position, CO_2 desorpotion of the CO_2-TPD profiles and carbon depostion obtained for the Ni-hydrotalcite, Ni-hydrocalumite, Ni-hydro-strontium and Ni-hydro-barium derived catalysts.

Catalyst	Temperature [°C]			μmol CO_2 desorbed/g			Total basicity [μmol CO_2/g]	Carbon deposition [mg]
	1st peak	2nd peak	3rd peak	1st peak	2nd peak	3rd peak		
HT	147	250	389	24	35	8	67	636.1
HCa	122	298	565	14	16	173	203	425.9
HSr	122	198	314	31	29	17	77	531.9
HBa	119	189	325	18	8	24	50	562.7

5.2.3 Dry reforming of methane (DRM) experiments

Both carbon dioxide and methane conversions, and H_2/CO molar ratio of Ni-hydrotalcite, Ni-hydrocalumite, Ni-hydro-strontium and Ni-hydro-barium derived catalysts at reaction temperatures between 850 and 550 °C are presented in Figure 5-4 a), b) and c) respectively, the conversions of CO_2 and CH_4, and H_2/CO increase with increasing reaction temperature as expected, which is consistent with the tendency simulated by thermodynamics. One point should be noted that the simulated CO_2 conversion is lower than CH_4 while measured CO_2 conversion is higher than CH_4. The possible reason is side reactions that favor the CH_4 conversion are not fully activated, meanwhile other reactions such as reverse water gas shift

reaction ($CO_2 + H_2 \rightleftharpoons CO + H_2O$) contributing to enhanced CO_2 conversion are carried out. And the presence of Ni is also benefical to reverse water gas shift reaction [204,205]. Moreover, the side reactions is consequently reflected in the measured H_2/CO ratio that should be equal to 1.

During the reaction temperatures, the presence of Mg^{2+}, Ca^{2+}, Sr^{2+} and Ba^{2+} obviously influences the catalytic performance. The Ni-hydrotalcite derived catalyst presents the highest feed gases (CO_2 and CH_4) conversions and H_2/CO ratio all the time, which means its good catalytic activity and selectivity. It may be assigned to its high specific surface area, small Ni^0 crystallite size and less CO_2 adsorption on strong basic sites. In contrary, the Ni-hydrocalumite derived catalyst with the smallest specific surface area, the largest Ni^0 crystallite size and more CO_2 adsorption on strong basic sites in this catalytic system shows the lowest catalytic activity and selectivity. In addition, the levels of specific surface area and CO_2 adsorption on strong basic sites of Ni-hydro-strontium and Ni-hydro-barium derived catalyst are also consistent with their level of catalytic performace. Thus, the textural properties and basicity on strong basic sites pointed out by their physicochemical characterizations may illustrate the differences on catalytic performance, since a large specific surface area contributes to dispersion of the active components and less CO_2 adsorption on strong basic sites makes CO_2 easier to react with CH_4 [203].

Otherwise, it could be noted that both CO_2 and CH_4 conversions as a consequence of the presence of synthetic clay supported catalysts are generally higher than natural clay supported catalysts that were discussed in chapter IV, and H_2/CO ratio is also closer to 1.

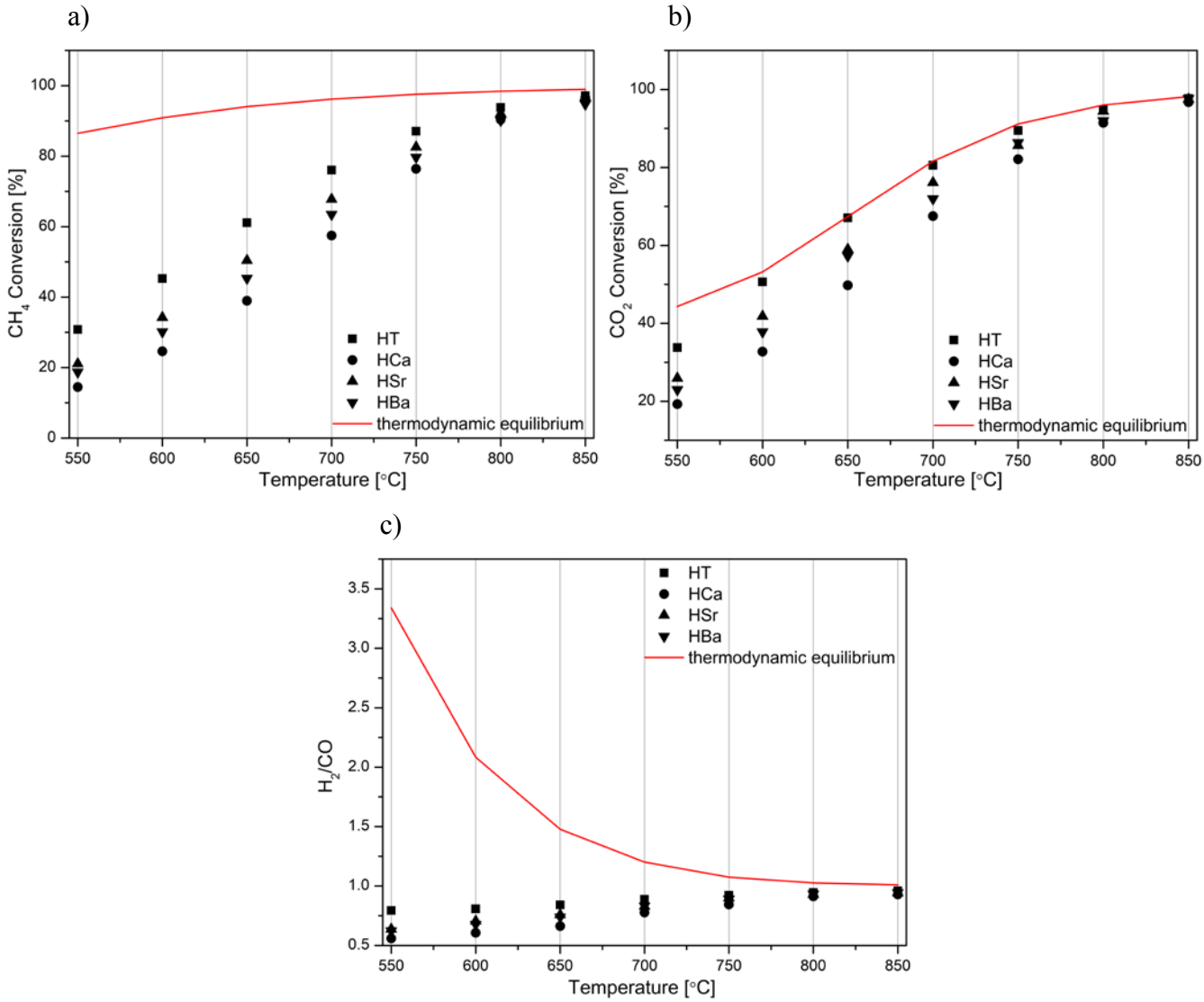

Figure 5-4. DRM experiments: a) CH_4 and b) CO_2 conversions and c) H_2/CO as function of reaction temperature. Red line: thermodynamic equilibrium conversions.

5.2.4 Carbon formation

The carbon deposition at 750 °C for 5 h for all prepared catalysts is calculated by means of mass balance and listed in Table 5-3. The general equation of mass balance is described as carbon deposition = carbon input - carbon output. From the comparison of prepared catalysts, higher catalytic activity generally corresponds to higher carbon deposition except the Ni-hydro-strontium derived catalysts. Compared with the Ni-hydro-barium derived catalysts, the addition of Sr presents relatively high catalytic activity while forms low carbon deposition, it means the presence of Sr inhibit side reactions to a certain extent.

5.2.5 Summary

Table 5-4. Summary for the nickel based hydrotalcite, hydrocalumite, hydro-strotium and hydro-barium-derived catalysts

Physicochemical properties	Catalyst			
	HCa	HT	HSr	HBa
Specific surface area	0	+	+	+
Ni^0 crystallite size[1]	0	-	-	-
Ni reducibility	0	-	+	+
Total basicity	0	-	-	-
DRM activity	0	+	+	+
Carbon deposition	0	+	+	+

"0" means the benchmark.
"+" means the strengthened/increased value compared to HCa.
"-" means the weakened/decreased value compared to HCa.
[1] Ni^0 crystallite size is compared only for reduced catalysts

Table 5-4 presents the different effects of catalysts that is synthesized by different bivalent metal of group 2 (Mg^{2+}, Ca^{2+}, Sr^{2+} and Ba^{2+}) with Ni^{2+} and Al^{3+}. Compared to the HCa catalysts that have the lowest activity in this catalyst system, the addition of Mg^{2+}, Sr^{2+} and Ba^{2+} obtained higher specific surface area and smaller Ni^0 crystallite size that may further increasing the catalytic ativity, and also higher carbon deposition that is proportional to the activity. However, the total basicity, especially on strong basic sites, is reduced. Moreover, the presence of both Sr^{2+} and Ba^{2+} in catalysts enhanced the Ni reducibility compared to HCa catalysts. Both CH_4 and CO_2 conversions followed the trend of thermodynamical calculations.

5.3 La-promoted Ni-hydrocalumite derived catalysts for dry reforming of methane

Through the comparison of different bivalent metal elements of group 2 (Mg^{2+}, Ca^{2+}, Sr^{2+} and Ba^{2+}), it could be found that Mg^{2+} and Ca^{2+} form the layered double hydroxides with trivalent metal Al^{3+}. Thus, Ni-containing hydrocalumite derived catalysts will be discussed. Moreover, the selection of promoter is likewise a crucial link for the catalyst of DRM in addition to the support. The relational results have demonstrated that Lanthanum (La) is one kind of effective promoter [206,207]. Akri et al. [208] also reported the positive influences of lanthanum (La) on activity and stability by inhibiting the formation of $FeNi_3$ alloy.

Therefore, different contents of La (1 wt.%, 2 wt.% and 4 wt.%) on Ni-based hydrocalumite derived catalysts at reaction temperatures between 850 and 600 °C was compared in this section. And the characterizations such as BET, H_2-TPR and CO_2-TPD for prepared catalysts were followed to try to find out the possible reasons for the differences in catalytic activity. Through the study on the influence of different contents of La on the structure and properties of catalysts, more basic experimental data could be obtained to go further research on catalysts of dry reforming of methane (DRM).

5.3.1 Synthesis of La-promoted Ni-hydrocalumite derived catalysts

La promoted hydrocalumite derived catalysts containing trivalent (Al^{3+}) and divalent (Ca^{2+}, Ni^{2+} and La^{2+}) metals with M^{3+}/M^{2+} molar ratio of 0.33, were prepared by a co-precipitation method. Two aqueous solutions, one containing all mixed nitrates of divalent and trivalent metals, and the other one containing sodium hydroxide (1M), were added dropwise into a flask containing an aqueous solution of sodium carbonate at the same time, and subsequently kept with vigorous stirring at 65 ± 3 °C and constant pH (from 9.5 to 10). The suspensions were aged for 1h and then filtered, carefully washed with 1L deionized water and finally dried overnight at 80 °C in oven. All samples were calcined in air at 550 °C for 5 hours to obtain corresponding catalysts. The nominal (assumed) concentration of the different components in each catalyst, as well as their labeling, is listed in Table 5-5.

Table 5-5. Ni containing hydrocalumite derived catalysts: nominal concentration of the different cations.

Catalyst	Label	Metal content [wt.%]				$\frac{M^{3+}}{M^{3+}+M^{2+}}$
		Ni	Al	Ca	La	
NiAlCa	HCa	15	7.4	22.5	0	0.25
NiAlCa+1%La	HCa+1%La	15	7.3	22.2	1	0.25
NiAlCa+2%La	HCa+2%La	15	6.8	22.0	2	0.25
NiAlCa+4%La	HCa+4%La	15	6.3	21.4	4	0.25

5.3.2 Physicochemical properties of the La-promoted hydrocalumite derived catalysts

5.3.2.1 Textural properties

The textural characterizations for prepared catalysts, including specific surface area, total pore volume, average pore size and BJH desorption cumulative pore volume are contained in Table 5-6 based on N_2 adsorption isotherms. It could be found that both BET surface area and total pore volume decrease with increasing La contents, which is attributed to the partial pore blockage. Similar results are also reported by Akri et al. [208]. Thus, it is obvious that lanthanum species enter and occupy the pores in Ni-hydrocalumite derived catalysts. For 4 wt.% La promoted Ni-hydrocalumite derived catalyst, the relatively large average pore size in this catalytic system (16 nm) may also lead to its small specific surface area, because a small pore size corresponds to a large specific surface area in general [196]. The ranging between 5.4 and 16.0 nm for average pore sizes indicate the mesoporous structure of prepared materials.

Table 5-6. BET results for the La promoted Ni-hydrocalumite derived catalysts.

Catalysts	S_{BET} [m^2/g]	V_p[1] [cm^3/g]	d_p[2] [nm]	V_{BJH}[3] [cm^3/g]
HCa	74.4	0.106	5.7	0.104
HCa+1%La	54.2	0.073	5.4	0.064
HCa+2%La	51.5	0.075	5.9	0.068
HCa+4%La	11.6	0.046	16.0	0.047

[1] *total pore volume*
[2] *average pore size*
[3] *BJH desorption cumulative pore volume*

5.3.2.2 Reducibility of Ni-species

The TPR results of La promoted Ni-hydrocalumite derived catalysts are presented in Figure 5-5. The main reduction peaks appearing at 682 °C (non-promoted), 735 °C (1 wt.% La), 735 °C (2 wt.% La) and 672 °C (4 wt.% La) for each prepared catalysts correspond to the reduction of fine NiO species that have strong interaction with support. In addition, the reduction peak below 600 °C for 4 wt.% La promoted catalysts is assigned to the reduction of weakly bonded Ni-oxide species [209,210], which could also be used to explain the two small

peaks at 351 and 488 °C for non promoted catalysts. Meanwhile, one small negative peak is observed at 423 °C on 4 wt.% La promoted catalysts, which is probably due to adsorption of a small amount of hydrogen at low temperatures. The shoulder at 638 and 631 °C for 1 wt.% and 2 wt.% La promoted catalysts point to the presence of segregated NiO species. The presence of lanthanum modifies the reducibility of Ni-species in these HCa-derived catalysts. Compared to the main reduction peak appeared at 682 °C for non-promoted catalysts, both 1 wt.% and 2 wt.% La promoted catalysts shift their main reduction peaks to higher temperature, migrating to 735 °C. It indicates that the addition of 1 wt.% and 2 wt.% lanthanum decrease the reducibility of NiO species. However, increasing the content of lanthanum to 4 wt.% in Ni-hydrocalumite derived catalysts lead to lower reduction temperature and increased area at low temperature, which means weaker interaction between the NiO species and support, thus increasing the Ni reducibility. Furthermore, the presence of lanthanum could promote the dispersion of Ni species based on the situation that low temperature peaks are shifted to slightly higher reduction temperatures, pointing to small Ni^0 crystallite sizes with increasing La-loading [117,211].

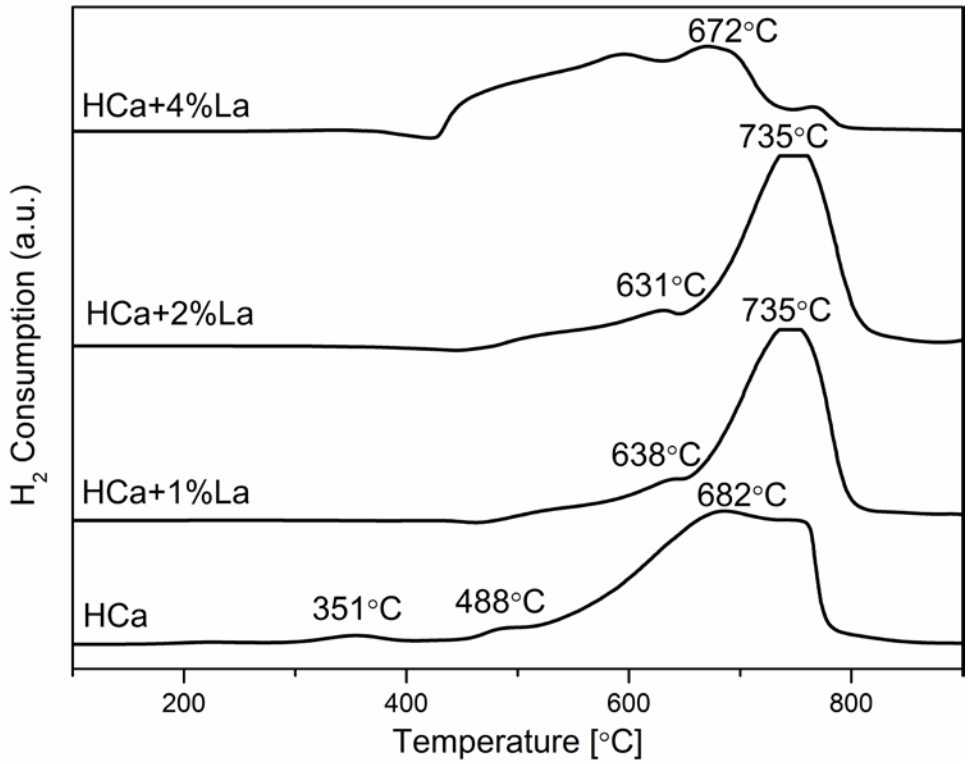

Figure 5-5. H_2-TPR profiles of La promoted Ni-hydrocalumite derived catalysts.

5.3.2.3 Influence of La-promotion on catalyst basicity

The CO_2-TPD characterization of the La promoted Ni-hydrocalumite derived catalysts including CO_2 desorption and basicity is presented in Figure 5-6 and Table 5-7. All prepared catalysts exhibit three CO_2 desorption peaks between 100 to 800 °C, corresponding to surface OH groups (weak Brønsted basic sites), Lewis acid-base pairings (medium-strength basic sites) and low-coordination oxygen anions (strong basic sites) deponding on the strength from weak to strong and temperature from low to high [201,202]. The peak positions and CO_2 desorption always change with increasing the content of lanthanum. Three CO_2 desorption peaks for La promoted catalysts appear respectively at 142-179 °C, 243-460 °C and 515-532 °C, while the centers of the peaks occur at 122 °C, 298 °C and 565 °C respectively for non-promoted catalysts. The presence of low content (1 wt.% and 2 wt.%) of lanthanum shift the weak Brønsted basic sites and medium-strength basic sites toward higher temperature, especially for the first and second peaks of 1 wt.% La promoted catalysts, appearing 57 and 162 °C later than non-promoted catalysts, also pointing to stronger CO_2 chemisorption on weak and medium-strength basic sites. When the La content increases to 4 wt.%, only the position of weak Brønsted basic sites is increased, the medium-strength basic sites is moved to lower temperature. On the other hand, the position of strong basic sites for all promoted catalysts shifts to lower temperature.

The addition of lanthanum improve the medium-strength basic sites. However, all promoted catalysts present less total basicity listed in Table 5-7. And the main factor for reducing the total basicity is reflected in the strong basic sites, especially for the 1 wt.% La promoted catalysts, it presents 125 μmol CO_2 desorbed/g less than non-promoted catalysts. Moreover, in case of 4 wt.% La-loading, the Brønsted basic sites is also inhibited.

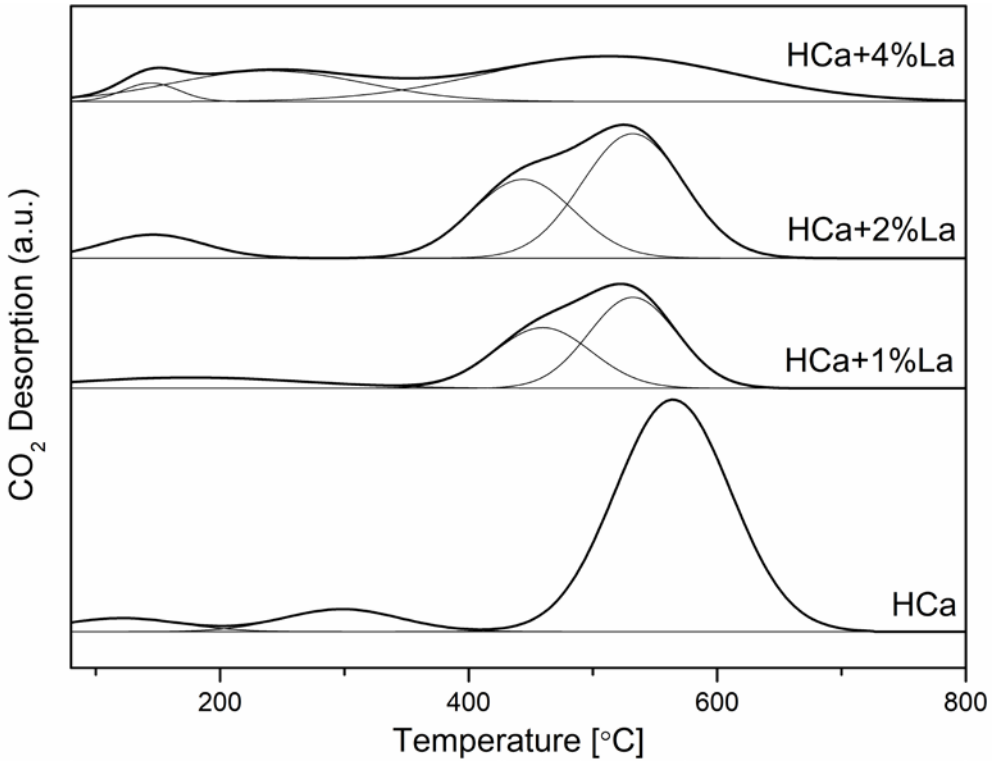

Figure 5-6. CO_2-TPD profiles of La promoted Ni-hydrocalumite derived catalysts.

Table 5-7. Peak position, CO_2 desorpotion of the CO_2-TPD profiles and carbon depostion obtained for La promoted Ni-hydrocalumite derived catalysts.

Catalyst	Temperature [°C]			μmol CO_2 desorbed/g			Total basicity [μmol CO_2/g]	Carbon deposition [mg]
	1st peak	2nd peak	3rd peak	1st peak	2nd peak	3rd peak		
HCa	122	298	565	14	16	173	203	425.9
HCa+1%La	179	460	532	13	28	48	89	501.4
HCa+2%La	145	442	530	14	46	74	134	492.6
HCa+4%La	142	243	515	5	27	58	90	498.5

5.3.3 Dry reforming of methane (DRM) experiments

The CH_4 and CO_2 conversions, and H_2/CO molar ratio for La promoted Ni-hydrocalumite derived catalysts as a function of reaction temperatures are arranged in Figure 5-7 a), b) and c) respectively. Both CH_4 and CO_2 conversions increase with increasing reaction temperatures for all prepared catalysts, which is consistent with the tendency of thermodynamical evaluation. At high temperatures between 850 and 700 °C, the influence of lanthanum on catalytic activity and selectivity is not particularly obvious. While the DRM comes to low reaction temperatures (650 to 550 °C), it could be clearly found that 4 wt.% and 2 wt.% La promoted catalysts always show the highest and lowest catalytic activity respectively. The

better activity from 4 wt.% La promoted catalysts may be attributed to its high reducibility of Ni species. Meanwhile, the opposite trend for the catalysts containing 2 wt.% La can explain the low catalytic performance. Otherwise, the presence of side reactions reflected in the measured H_2/CO molar ratio also contribute to the CH_4 and CO_2 conversions.

By comparing the conversions of carbon dioxide and methane, it could be found that the CO_2 conversion is always slightly higher than CH_4 at reaction temperatures, which indicates the presence of side reactions that can consume more CO_2 in equilibrium during dry reforming of methane, such as boudouard reaction ($2CO \rightleftharpoons CO_2 + C$) and mainly side reaction for DRM - reverse water gas shift reaction ($CO_2 + H_2 \rightleftharpoons CO + H_2O$). Furthermore, these side reactions also affect the consistency between experimental data and thermodynamical calculations. The CH_4 conversion should higher than CO_2 based on thermodynamical evaluation by means of HSC Chemistry 5.0. However, the side reactions, such as direct methane decomposition ($CH_4 \rightleftharpoons C + 2H_2$), favored by thermodynamical evaluation do not seem to be completely activated, resulting in slightly higher CO_2 conversion than CH_4.

a)

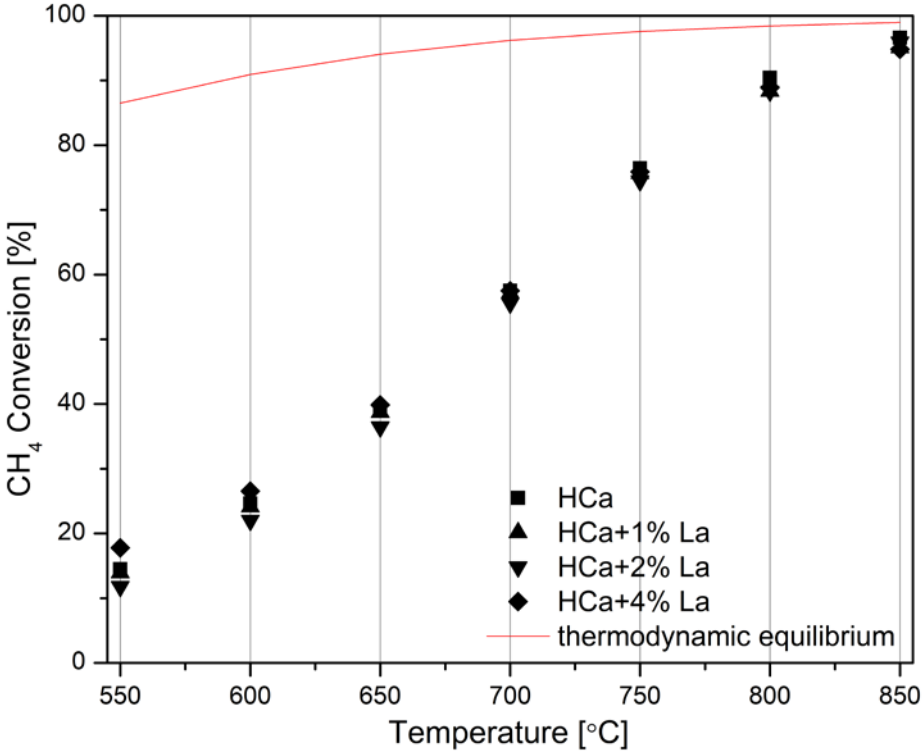

b)

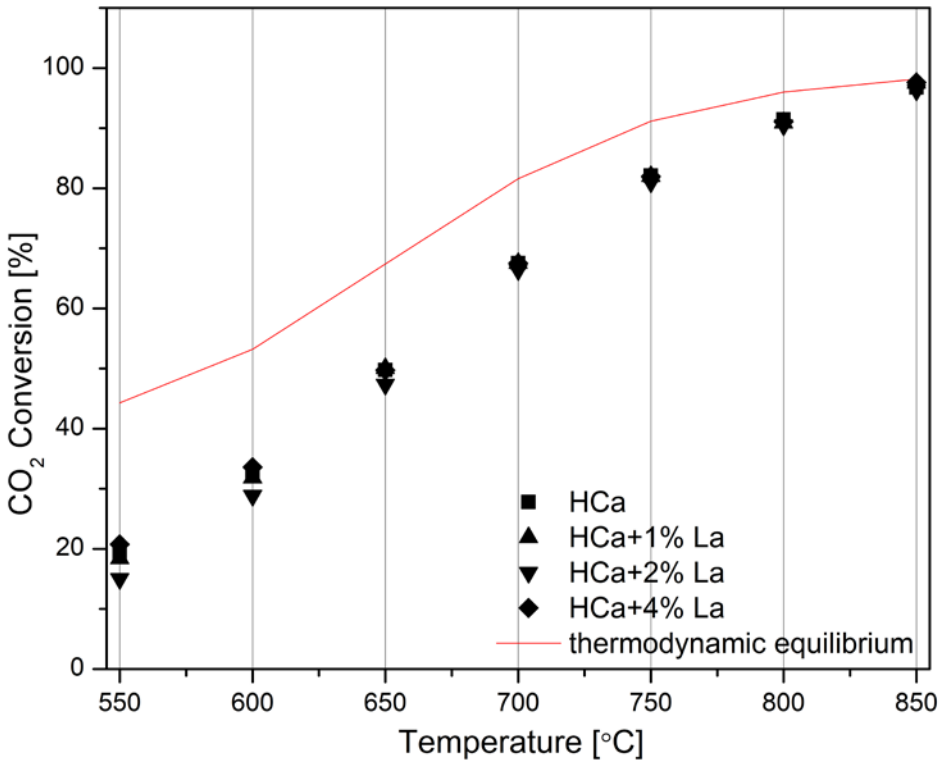

c)

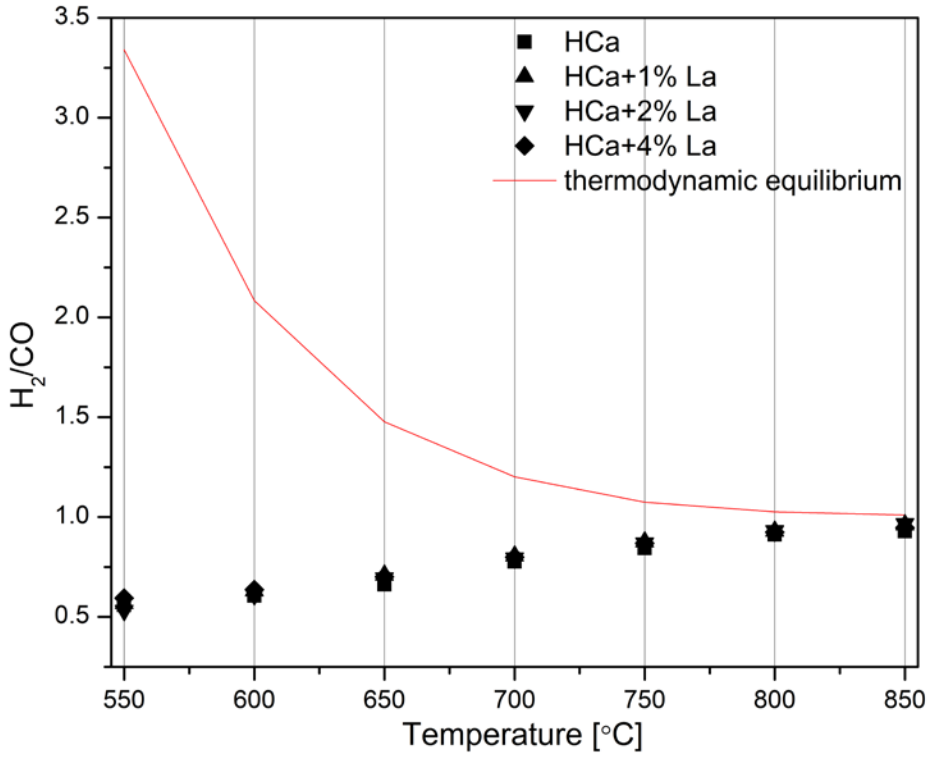

Figure 5-7. DRM experiments: a) CH_4 and b) CO_2 conversions and c) H_2/CO as function of reaction temperature. Red line: thermodynamic equilibrium conversions.

5.3.4 Carbon formation

The carbon depositon for all prepared catalysts is presented in Table 5-7. It is calculated by mass balance based on the difference between carbon inlet and outlet. It could be found that the addition of lanthanum for Ni-hydrocalumite derived catalysts lead to higher carbon deposition, which means the promotion of lanthanum is also used to side reactions that cause carbon deposition to a certain extent, such as direct methane decomposition and boudouard reaction.

5.3.5 Summary

Table 5-8. Summary for the La promoted nickel based hydrocalumite derived catalysts

Physicochemical properties	Catalyst			
	HCa	HCa+1%La	HCa+2%La	HCa+4%La
Specific surface area	0	-	-	-
Ni reducibility	0	-	-	+
Total basicity	0	-	-	-
DRM activity	0	≈	-	+
Carbon deposition	0	+	+	+

"0" means the benchmark.
"+" means the strengthened/increased value compared to HCa.
"-" means the weakened/decreased value compared to HCa.
"≈"means the similar value with HCa.
[1]Ni^0 crystallite size is compared only for reduced catalysts.

Table 5-8 shows the effects of La-loading on Ni-hydrocalumite derived catalysts. The addition of lanthanum resulted in the lower specific surface area and total basicity compared to non-promoted HCa catalysts. The presence of lanthanum also promoted side reactions leading to more carbon deposition, while only 4 wt.% La promoted catalysts obviously presented higher catalytic performance. Meanwhile, the introduction of 4 wt.% La improved the Ni reducibility. Both CH_4 and CO_2 conversion increased with increasing temperatures, corresponding to the tendency calculated by thermodynamics. Furthermore, the H_2/CO is close to 1 at high temperature.

5.4 La-promoted Ni-hydrotalcite derived catalysts for dry reforming of methane

The addition of promoters can positively influence activity, selectivity and/or stability of Ni-hydrotalcite-derived catalysts. Among them, the incorporation of rare earth oxides can help controlling DRM selectivity, through the inhibition of carbon formation reactions, or strengthened CO_2 adsorption on the support [185,203,212]. Dębek et al. [198,203] found that incorporation of Ce into Ni-containing hydrotalcite-derived catalysts resulted in an increased reducibility of nickel species, and led to the formation of new strong basic sites, which improved the long-term stability of these catalysts in DRM reaction. However, CO_2 and CH_4 conversion became somewhat lower. Lanthanum has also been considered as a promoter of Ni-containing hydrotalcite-derived catalysts for DRM. Previous published papers just evidence the promotion effect of La, or its promoting effect in combination with noble metals or other promoters [213-215]. Serrano-Lotina et al. [214] studied the influence of calcination temperature on the activity of a Ni (2.3 wt.%) catalyst containing La (1.3 wt.%). Lucredio et al. [215] prepared several hydrotalcite-derived catalysts containing 10 wt.% of Ni and 10 wt.% of La and/or 1 wt.% of Rh. La-promotion did not lead to improvement of activity but increased the stability in the DRM reaction. It should be taken into account that the activity of Ni-containing hydrotalcite-derived catalysts strongly depends on the amount of Ni-cations introduced in the pristine hydrotalcite structure [216]. The best performance was observed for the catalysts containing ca. 20 wt.% of Ni (i.e. 25 % of exchanged Mg in the catalysts). There is still no clear understanding of the effect of lanthanum incorporated to hydrotalcites containing a constant amount of nickel. Moreover, so far and to the best of our knowledge, only the work of Yu and co-workers takes into consideration the incorporation of different amounts of La, however, La-loadings employed (3-10 wt.%) were much higher than the ones used in the preparation of the catalysts presented herein.

5.4.1 Synthesis of the La-promoted hydrotalcite-derived catalysts

Hydrotalcites containing M(III) trivalent and M(II) divalent metals (Al^{3+}, La^{2+}, Mg^{2+}, Ni^{2+}) with M(III)/M(II) molar ratio of 0.33, were prepared by a co-precipitation method at constant pH (from 9.5 to 10). Two aqueous solutions, one containing the mixed nitrates of divalent and trivalent metals, and a second one containing sodium hydroxide (1M), were added dropwise

into a flask containing an aqueous solution of sodium carbonate, and subsequently kept under vigorous stirring at 65 °C and constant pH. This mixture aged for 24 h and then filtered, carefully washed with deionized water and finally dried overnight at 80 °C. The nominal (assumed) concentration of the different components in each hydrotacite prepared (un-promoted and La-promoted), as well as their labeling, is listed in Table 5-9. In order to obtain the corresponding hydrotalcite-derived catalysts, each hydrotalcite was calcined under air at 550 °C for 4hours.

Table 5-9. Ni-containing La-promoted hydrotalcites and derived catalysts: nominal concentration of the different cations.

Catalyst	Label	Metal content [wt.%]				$\frac{M^{3+}}{M^{3+}+M^{2+}}$
		Ni	La	Mg	Al	
NiAlMg+1%La	HN1	15	1	15.6	7.9	0.25
NiAlMg+2%La	HN2	15	2	15.4	7.6	0.25
NiAlMg+4%La	HN3	15	4	15.0	7.1	0.25
NiAlMg	HN4	15	0	15.8	8.1	0.25

5.4.2 Physicochemical properties of the La-promoted Ni-hydrotalcite-derived catalysts

5.4.2.1 Reducibility of Ni-species

Figure 5-8 a) shows the H_2-TPR profiles for the Ni- hydrotalcite derived catalysts after calcination. All prepared catalysts exhibit one wide asymmetric peak (820-850 °C) arising from the reduction of Ni-oxide species to Ni^0. Such Ni-oxide species are most probably inserted into the Al-Mg mixed oxide matrix resulting from the calcination of the hydrotalcite brucite layers, forming a solid solution of high thermal stability [197,198]. The presence of lanthanum modifies the reducibility of the Ni-species in these Ni-hydrotalcite derived catalysts. The main reduction peak shifts to lower temperatures with increasing La-content, i.e. from 850 °C for HN4, non-promoted, to 830 °C and 820 °C for the La-promoted catalysts. Additionally, a shoulder can be observed at ca. 690 °C for the La-promoted catalysts HN2 and HN3 (2 and 4 wt.% of La, respectively), which can be assigned to segregated NiO species, pointing to weaker Ni-support interaction as a consequence of the incorporation of lanthanum [213-215,217]. In the case of HN2, two wide additional peaks can be clearly observed at about 400 and 450 °C, pointing to the presence of bulk weakly-bonded NiO. Moreover, Yu and co-workers concluded that the presence of lanthanum positively influenced the dispersion

of these NiO species, since such low temperature peaks were shifted to slightly higher reduction temperatures, pointing to smaller crystal sizes upon an increase in the La-content [200].

a)

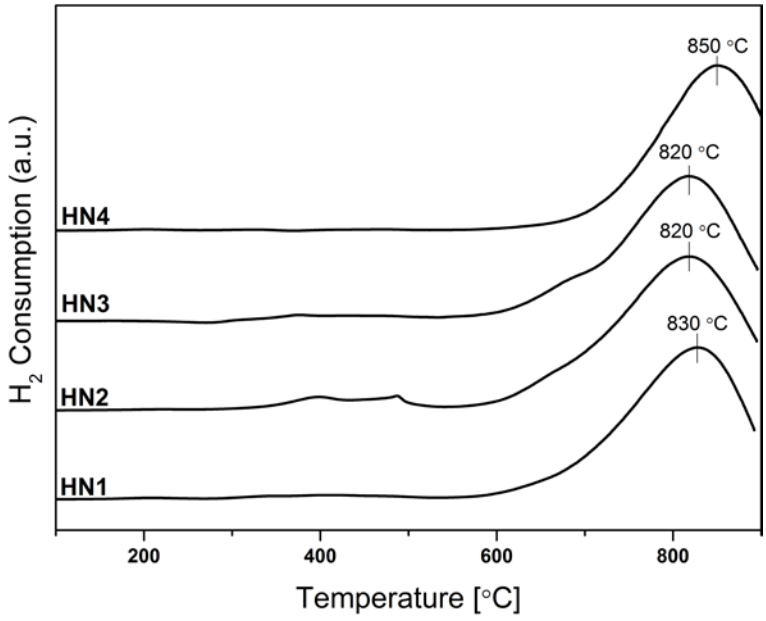

b)

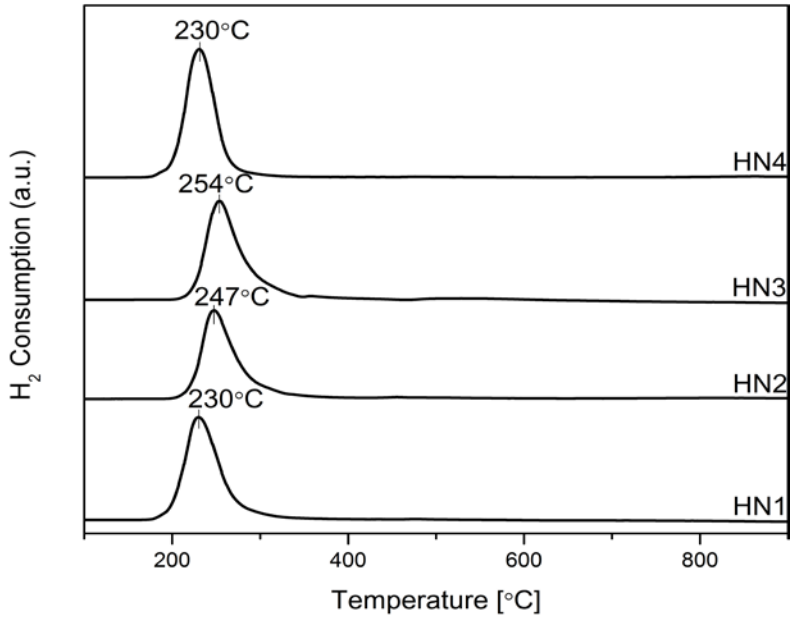

Figure 5-8. H_2-TPR profiles of a) calcined b) reduced Ni-hydrotalcite derived catalysts.

The segregation of Ni-species during reduction, as well as the reducibility of the segregated NiO species were further confirmed by H_2-TPR experiments performed on the Ni-hydrotalcite derived catalysts reduced at 900 °C for 1 h under 5 vol.% H_2/Ar. The results of

these experiments are shown in Figure 5-8 b). A single reduction peak appears now at much lower temperatures, i.e. at 230 °C for HN1 and HN4 (low La-content and non-promoted catalyst), at 247 °C for HN2 (2 wt.% La) and at 254 °C for HN3 (4 wt.% La), pointing to Ni or NiO segregation from the Mg-Al mixed oxide structure during this reduction treatment [192], and corresponding to the reduction temperatures typically reported for bulk NiO [192,218]. The exposure to ambient air of the readily reduced catalysts may have caused the reoxidation of a part of this segregated Ni-species. The integration of each peak allows the quantification of the presence of such bulk NiO species on each catalyst. The results are presented in Table 5-10. Hydrogen consumption during the TPR experiments performed on the reduced catalysts is higher for both the non-promoted catalysts, HN4, and the catalyst containing the highest amount of La, HN3, i.e. 0.529 mmol H_2/g and 0.602 mmol H_2/g, respectively. This points to an increased presence of reluctant NiO species upon the reduction treatment for HN4 and HN3. On the contrary, lower La content leads to a decrease in H_2 consumption, that becomes minimal in the case of the Ni-hydrotalcite derived catalyst promoted with 2 wt.% of La, HN2, i.e. 0.438 mmol H_2/g. Lower H_2 consumption points to a reduced presence of remaining NiO species and, thus, to a higher availability of reduced Ni^0 sites, moreover indicating that there is an optimal La-loading in terms of reducibility of Ni-species.

Table 5-10. H_2 consumption for the reduced catalysts, a and b unit cell parameters and Ni crystal size calculated for the Ni-hydrotalcite derived catalysts (before and after DMR test).

Catalyst	H_2 consumption-reduced catalysts [mmol H_2/g]	a(Å)	c(Å)	Ni^0 crystal size [nm]
				Reduced
HN1	0.471	3.06	23.43	10.3
HN2	0.438	3.06	23.49	12.2
HN3	0.602	3.06	23.52	11.6
HN4	0.529	3.06	23.46	16.0

5.4.2.2 Crystallinity: La-segregation and Ni crystal size

The X-ray diffractograms for the fresh hydrotalcites, the Ni-hydrotalcite derived catalysts before and after reduction are shown in Figure 5-9 a), b) and c). The diffraction patterns acquired for the fresh hydrotalcites, Figure 5-9 a), evidence the typical reflections and a layered hydrotalcite phase at 2θ = 11.0°, 24.0° and 35.0°, respectively corresponding to (003), (006) and (009) planes, confirming the existence of a multilayer structure [192]. The hydrotalcite containing the highest amount of La (HN3) showed the presence of additional

$La_2(CO_3)_2(OH)_2$ and $La_2O_2CO_3$ phases, as seen in Figure 5-9 a). The absence of other phases in these patterns, points to the successful incorporation of nickel into the hydrotalcite structure.

The unit cell parameters were calculated using the method proposed by Rives [218] and are summarized in Table 5-10. The parameter *c* was calculated from the positions of the three first reflections $c = d_{(003)} + 2d_{(006)} + 3d_{(009)}$. This parameter is thus indicative of the distance between brucite layers in the hydrotalcite structure, which strongly depends on the type and orientation of the interlayer anions [219]. The parameter *a* of the unit cell, which describes the average distance between cation-cation in brucite layers, was calculated from the position of the first reflection at $2\theta = 60°$. Parameter *a* remains unchanged upon La-loading, suggesting that La was not incorporated into the interlayer space of the hydrotalcite structure. On the contrary, a large increase in this *a* unit cell distance would have been observed due to the larger ionic radius of La in comparison with Mg and Al ions [200].

After calcination, Figure 5-9 b), XRD patterns evidence two reflections at $2\theta = 43.0°$ and 62.4° characteristic of the periclase-like structure of mixed oxides generated upon the thermal decomposition of hydrotalcite materials. In the case of the La-containing Ni-hydrotalcite derived catalysts, some reflections corresponding to a segregated La_2O_3 phase can be observed, together with some residual La carbonates that might be formed upon exposition of the calcined materials to ambient air conditions.

The XRD patterns recorded for the reduced catalysts, Figure 5-9 c), conserve the characteristic of the mixed oxide periclase structure. Moreover, additional phases can be observed corresponding to metallic nickel, i.e. $2\theta = 44.6°$, 51.9° and 76.5°, and segregated La_2O_3. Crystal sizes calculated (based on the reflections at 51.9°) for the metallic Ni phase range from 10.3 and 16.0 nm. The improvement of La on crystal size can be observed.

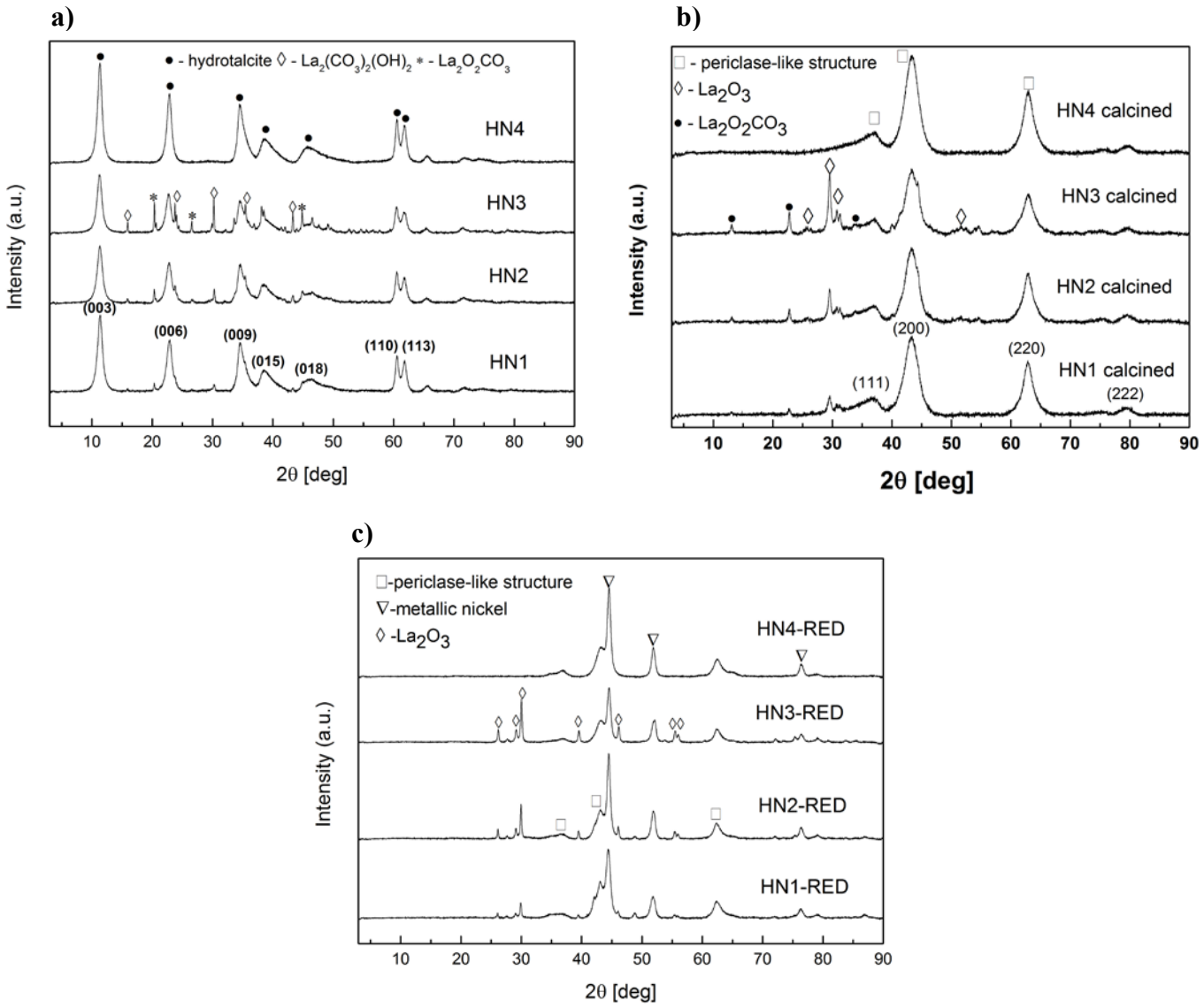

Figure 5-9. X-ray diffractograms acquired for a) the fresh hydrotalcites, and the Ni-hydrotalcite derived catalysts b) before and c) after reduction.

5.4.2.3 Influence of La-promotion on catalyst basicity

The TPD profiles registered for the according to literature [201,202], there are three typical CO_2 desorption peaks normally appearing in CO_2-TPD profiles for Ni-hydrotalcite derived materials, appearing between 100 and 500 °C. These peaks are representative of the presence of basic sites having different strength: weak Brønsted basic sites such as surface -OH groups (low temperature), medium-strength Lewis acid-base sites (intermediate temperature), and low-coordination oxygen anions acting as strong basic sites (high temperature). In fact, these three contributions are clearly visible in the CO_2-TPD profiles acquired for the different

Ni-hydrotalcite derived catalysts, shown in Figure 5-10. However, mean peak positions and its areas change as a consequence of the presence of La and with La-loading.

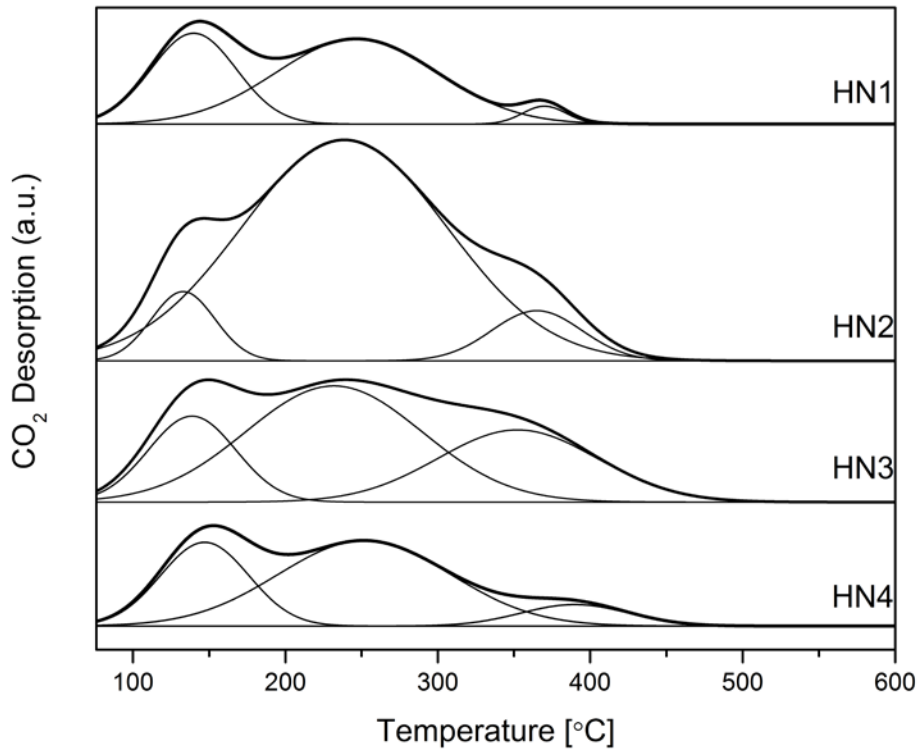

Figure 5-10. CO_2-TPD profiles for the Ni-hydrotalcite derived reduced catalysts.

Table 5-11 contains a listing of the temperatures corresponding to each peak's maximal intensity, as well as the results of its deconvolution and integration (area = μmol CO_2 desorbed per gram of catalyst). In general, the three CO_2 desorption peaks for La-promoted catalysts occur respectively at 133-139 °C, 232-246 °C and 353-385 °C, while in the case of the non-promoted catalyst they appear centered at 147 °C, 250 °C and 389 °C, i.e. at much higher temperatures, pointing to weaker CO_2 chemisorption as a consequence of the presence of La. This is particularly true for HN2, i.e. the HT-derived catalysts containing 2 wt.% La, since the first and the second peak, corresponding to weak and medium-strength basicity, appear 14 and 11 °C earlier than for the non-promoted catalyst, HN4.

Total basicity, i.e. the total area under the three peaks, increases for the La-promoted Ni-hydrotalcite derived catalysts. The maximal amount of CO_2 desorbed corresponds however to HN2, pointing to 2 wt.% La as the optimal La-loading in terms of catalyst basicity. Moreover, upon the introduction of 2 wt.% La, the presence of medium-strenght basic sites

(Lewis pairs) seems to be exceptionally boosted. Upon 4 wt.% La-loading, HN3, weak basic sites seems to be as well promoted.

Table 5-11. Peak position and deconvolution of the CO_2-TPD profiles obtained for the different Ni-hydrotalcite derived catalysts.

Catalyst	Temperature [°C]			μmol CO_2 desorbed/g			Total basicity [μmol CO2/g]
	1st peak	2nd peak	3rd peak	1st peak	2nd peak	3rd peak	
HN1	139	246	370	10	35	18	63
HN2	133	239	365	12	110	12	134
HN3	138	232	353	29	66	28	123
HN4	147	250	389	24	35	8	67

5.4.3 Dry reforming of methane (DRM) experiments

5.4.3.1 Catalytic activity

Figure 5-11 a) and b) shows the CH_4 and CO_2 conversions measured during the DRM experiments in the presence of the different Ni-hydrotalcite derived catalysts, as a function of reaction temperature. The results obtained within the low temperature window, i.e. 550 and 600 °C, are shown in detail in the inset contained in each figure.

a)

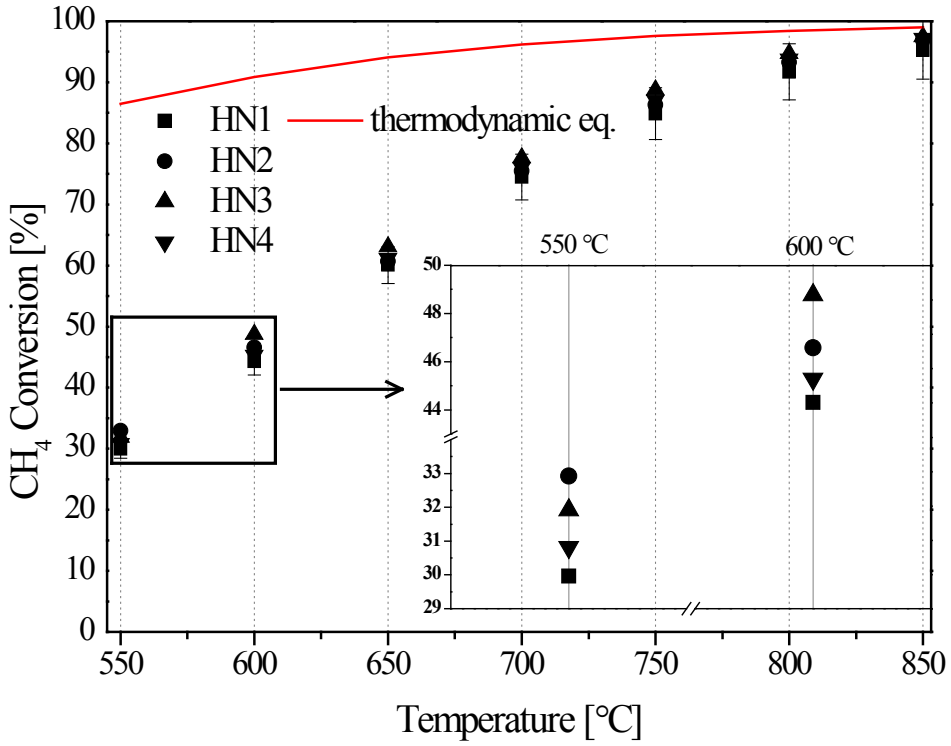

b)

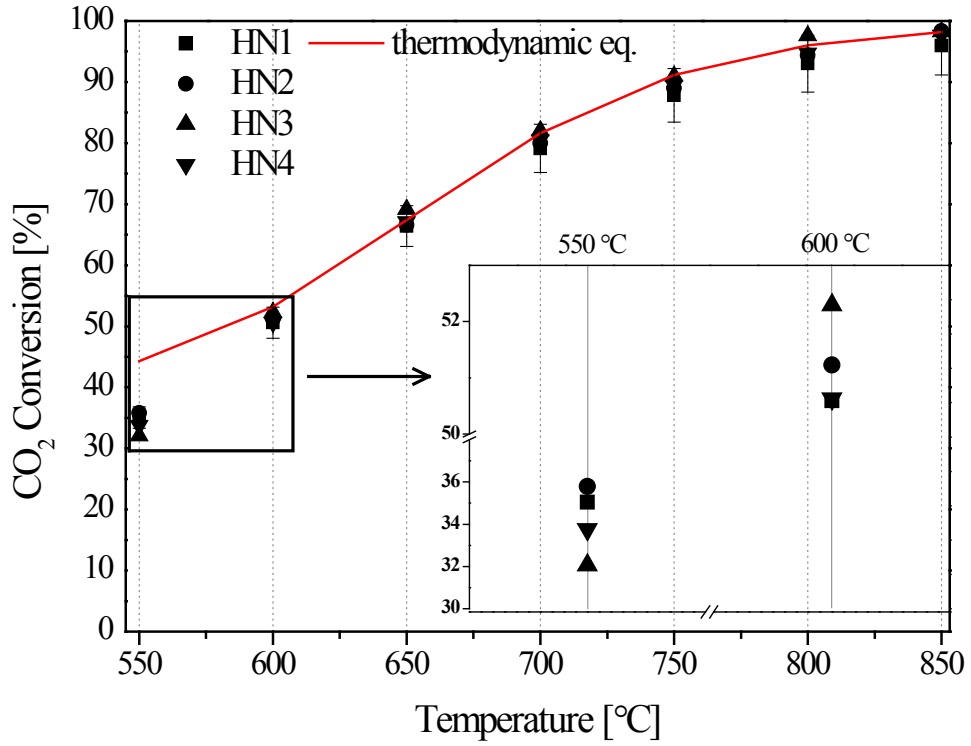

Figure 5-11. DRM experiments: a) CH_4 and b) CO_2 conversions as function of reaction temperature. Inset: zoom of the results obtained at 550 and 600 °C. Solid line: thermodynamic equilibrium conversions.

As expected, both CH_4 and CO_2 conversions increase with increasing temperature for any of the catalysts tested and independently of the La-content, in agreement with the trend forecasted by thermodynamics. However, especially at low temperatures, some differences can be observed that are worth to be remarked. First of all, at 550 and 600 °C, CO_2 conversions measured are all the times slightly higher than CH_4 conversions, whereas the opposite trend is predicted by thermodynamics, i.e. at 550 °C, for HN2 - 36% CH_4 and 33% CO_2 conversion is measured while the thermodynamically predicted conversions are 87% and 42% for CH_4 and CO_2, respectively. Direct methane decomposition reaction, as well as the Bouduard reactions - among other carbon forming reactions - are generally thermodynamically favored reaction at such low temperatures, but they do not seem to be completely activated in the presence of this series of catalysts. Other reactions, such as the water gas shift reaction may contribute to enhanced CO_2 conversion. As a consequence, the H_2/CO ratios experimentally measured, shown in Figure 5-12, considerably apart from the high values 3.5-2 predicted by the thermodynamics in the low temperature window, 550-600 °C. And it is precisely within this range of temperatures that very clear differences are observed among the non-promoted and the La-promoted catalysts.

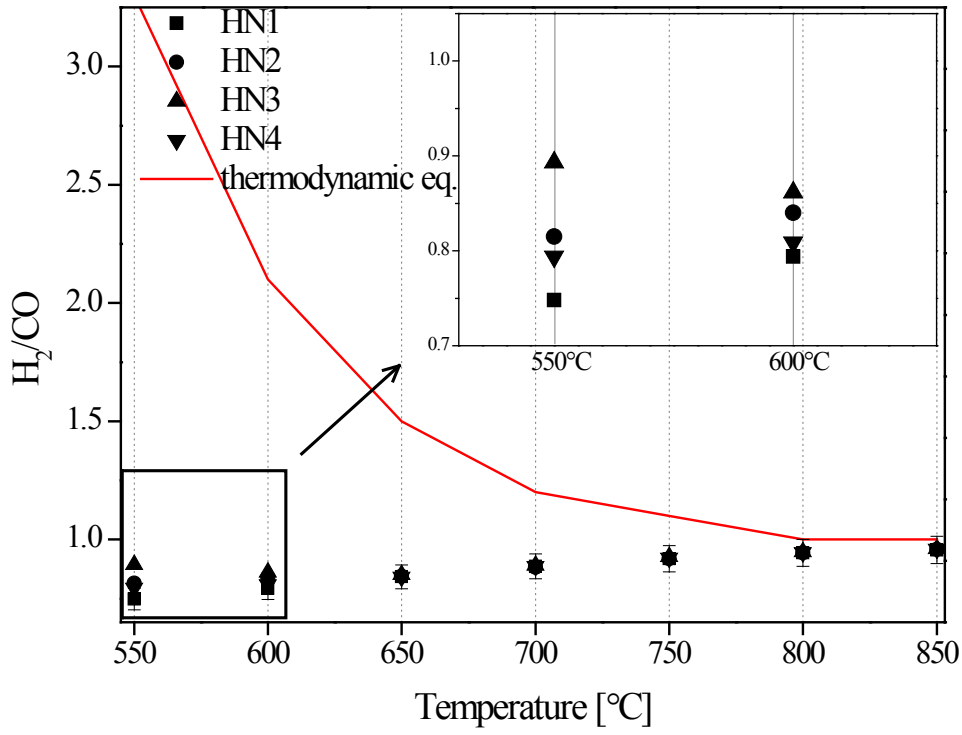

Figure 5-12. H_2/CO molar ratio versus reaction temperature for the different Ni-hydrotalcite derived catalysts. Solid line: thermodynamic equilibrium H_2/CO ratio.

Moreover, La-content influences the activity and selectivity of these Ni-hydrotalcite derived catalysts. The lowest methane conversions are all the time measured for the non-promoted catalyst, which, at the same time, does not seem to be very active towards CO_2 conversion. The presence of La boosts the activity of the catalyst. As a consequence, HN2, containing 2 wt.% La, shows the highest activities of this series at 550 °C in terms of both CH_4 and CO_2 conversion, whereas HN3, containing 4 wt.% La, is the most active catalyst at 600 °C. However, at low temperatures, the thermodynamic prevalence of methane decomposition with respect to the reverse water gas shift reaction leads to a stronger promotion of the former vis-à-vis the later, above all in the presence of a Ni-containing catalyst [220,221]. Moreover, the increased presence of available Ni^0 sites in HN2 and HN3, pointed out by their physico-chemical characterization, may explain such higher activities, since it is well know that, kinetically, the limiting step for both reforming and methane decomposition reaction is the activation of the C-H bond, taking place on metallic Ni sites [222]. At the lowest reaction temperature, i.e. 550 °C, the promotion of direct methane decomposition is consequently reflected in the values of the H_2/CO molar ratio obtained, Figure 5-12, which increase with increasing catalytic activity for the La-promoted Ni-hydrotalcite derived catalysts. The decreasing H_2/CO values measured for HN3 at temperatures from 550 to 650 °C may point to increased selectivity towards the dry reforming of methane (DRM) and/or the reverse water-gas shift (RWGS) reactions at 650 °C for this La-promoted catalysts, as has been previously reported in literature [223]. The increased presence of weak basic sites in this catalyst containing 4 wt.% La, may result in a weak-type of interaction between CO_2 and the support, leading to the promotion of DRM and RWGS, once the temperature is sufficiently high to overcome their thermodynamic barriers.

Other authors have previously studied the behavior of Ni-containing hydrotalcite-derived catalysts in DRM [198,211,214,215]. Dębek et al. [198] evaluated the promoting effect of Ce and Zr in the low temperature DRM behavior of Ni-containing Mg/Al or Al hydrotalcites, under the same experimental conditions used in our present work. The presence of either Ce or Zr resulted in increased stability of the catalysts. Ce was found to partially avoid methane decomposition and enhance the oxidation of the carbon deposits, whereas Zr strongly modified the selectivity of the DRM reaction set. Concerning the influence of La as promoter, the comparison of our results to previously published studies is not straight forward, since the experimental conditions are not quite similar, both for the pretreatment of the catalysts (calcination and reduction temperatures) and DRM activity tests. This is a crucial issue, since

the calcination and reduction temperature plays an important role in the final catalytic activity, as shown by Serrano et al. [214]. However, it can be generally stated that La addition results in an improved stability. Serrano et al. [214] confirmed this fact during DRM experiments performed at 700 °C on Ni (2.3 wt.%) Mg/Al hydrotalcite-derived catalysts promoted with 1.3 wt.% La. Yu et al. [211] also studied the activity of Ni-containing hydrotalcite-derived catalysts promoted with different La contents (3-10 wt.%) at 600-800 °C. The addition of lanthanum increased the CO_2 adsorption ability, the amount of surface Ni and significantly improved the stability of these catalysts.

5.4.3.2 Catalytic stability: carbon formation and evolution of Ni crystal sizes

The Ni-hydrotalcite derived catalysts after DRM testing were analyzed by means of X-ray diffraction. The obtained patterns are shown in Figure 5-13. Some additional phases are now present in the spent catalysts that were not observed in the diffractograms shown previously in Figure 5-9, i.e. representative of the presence of graphite and of the formation of the alloy $MgNi_3$. The formation of this $MgNi_3$ implies the reduction of Mg^{2+} cations. This may be however possible at relatively high temperatures and under carbothermal reduction conditions, i.e. in the presence of methane and C [224]. Graphite formation is due to carbon formation reactions, mainly direct methane decomposition.

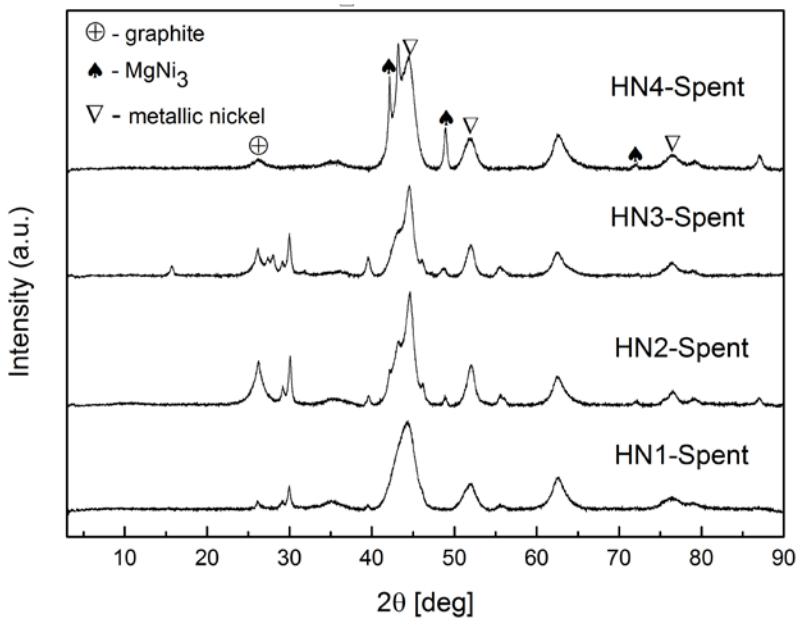

Figure 5-13. X-ray diffractograms for the Ni-hydrotalcite derived catalysts after the DRM activity test.

Isothermal DRM experiments were conducted at 550 °C on HN4 and HN3 catalysts, i.e. the non-promoted and 4 wt.% La-promoted Ni-hydrotalcite derived catalysts. Figure 5-14 shows the CH_4 and CO_2 conversions, as well as the H_2/CO ratio, measured over more than 8 hours time-on-stream (TOS). An estimation of the rate of C formation, in μg/min – estimated from the carbon balance, is plotted together with CH_4 conversion in Figure 5-14 a). The activity and selectivity of both HN4 and HN3 change with time on stream. This means that the evolution of the catalytic system continues even after 8 hours TOS, and that further longer-duration experiments need to be performed in order to further conclude on catalytic stability. In any case, either La-promoted or not, the values of H_2/CO ratio increases as the isothermal experiment progresses. This can be assigned to the direct methane decomposition yielding C(s) and H_2, which is thermodynamically favored at such low temperatures. In agreement with the enhanced reducibility of Ni-species, this fact becomes especially true for the La-promoted catalyst, HN3. In consequence carbon formation rate is as well higher all the time for HN3 than for the non-promoted catalyst, HN4.

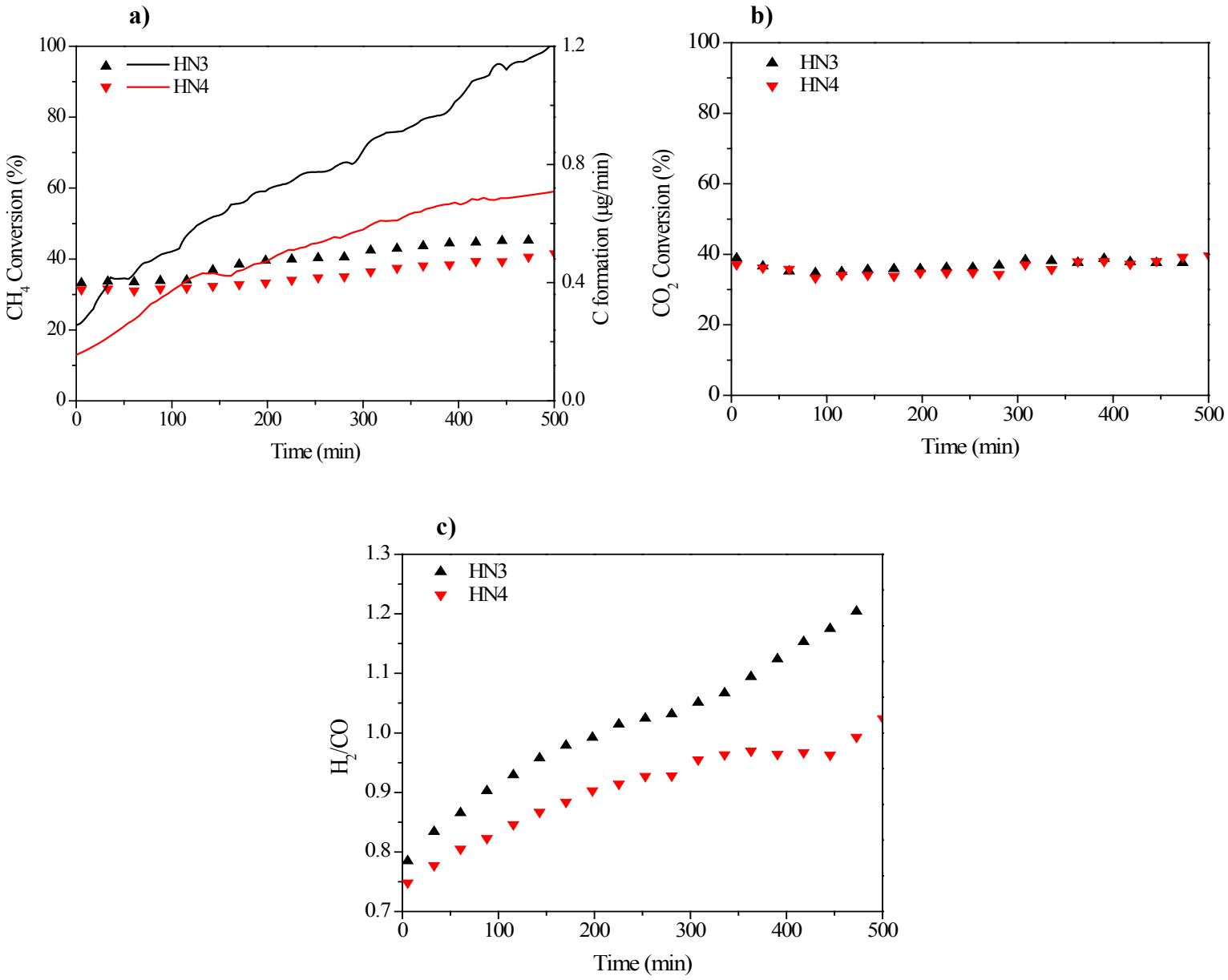

Figure 5-14. Isothermal DRM experiments at 550 °C: a) CH_4 conversion and C formation calculated from carbon balance, b) CO_2 conversion, and c) H_2/CO ratio, vs. time on stream, for HN3 and HN4.

5.4.4 Carbon formation

The extent of carbon formation was evaluated by means of thermogravimetric oxidation of HN4 and HN3 after the isothermal DRM experiments. Figure 5-15 a) and b) shows the thermogravimetric curves – weight loss and its derivative as a function of temperature – obtained for these two catalysts. Slightly higher amount of carbon is formed during DRM at 550 °C in the presence of the non-promoted catalyst, HN4. The presence of La may favor the formation of lanthanum oxycarbonates, able to gasify the carbon deposits, and above all the

non-crystalline amorphous carbon formed during reaction [225]. In fact, the derivative, dTGA, is substantially different for HN3 (La-promoted), than for HN4 (unpromoted), pointing to the presence of different relative amounts of amorphous and graphitic carbon. The d_{TGA} peak can be deconvoluted into two contributions: a first peak, appearing at temperatures higher than 450 °C, due to the oxidation of "coating" or amorphous carbon, and a second one, centered at about 600-650 °C, corresponding to the oxidation of filamentous carbon formed through methane direct decomposition on Ni-sites [226]. The low-temperature peak assigned to the presence of amorphous carbon has a lower contribution to the oxidation profile and appears shifted to higher reaction temperatures. The gasification of such amorphous carbon deposits in the presence of lanthanum oxycarbonate species may have contributed to this fact. Moreover, the high-temperature peak corresponding to carbon filaments and fibers grown on Ni-sites is clearly marked in the La-promoted catalyst, HN3, in agreement with the increased presence of Ni^0 species and its evolution with time-on-stream leading to the enhancement of direct methane decomposition reaction.

a)

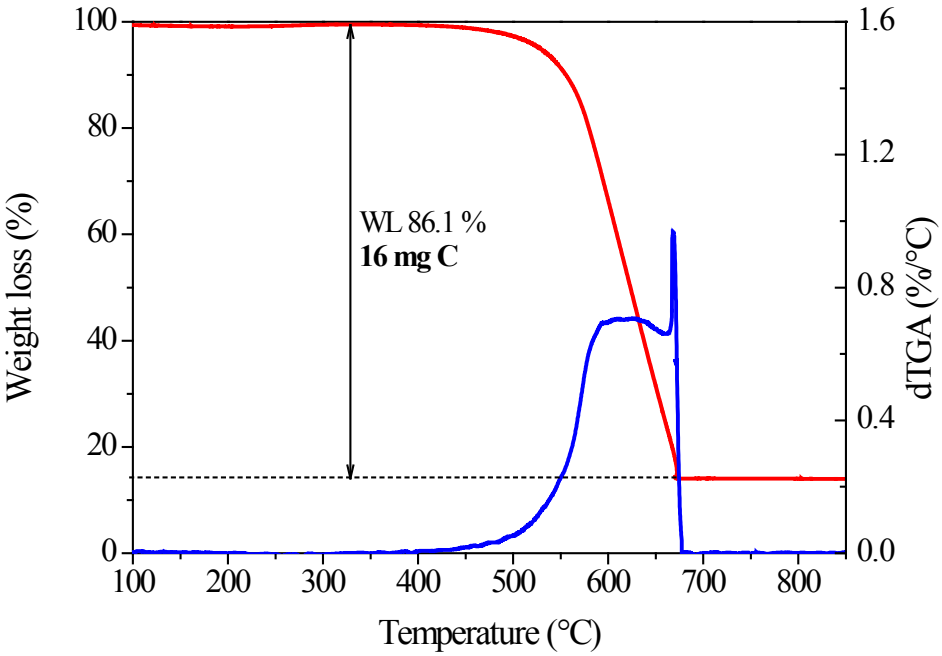

b)

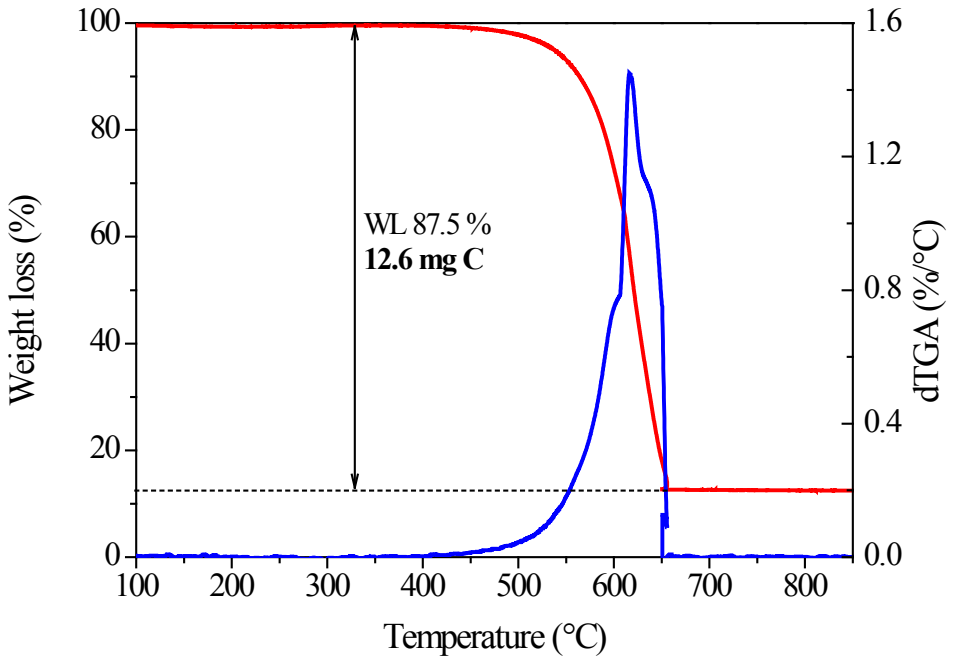

Figure 5-15. Thermogravimetric oxidation of carbon deposits, weight loss and its derivative for a) HN4 and b) HN3 after DRM.

5.4.5 Summary

Table 5-12. Summary for the La promoted nickel based hydrocalumite derived catalysts

Physicochemical properties	Catalyst			
	HT	HT+1%La	HT+2%La	HT+4%La
Ni^0 crystallite size[1]	0	-	-	-
Ni reducibility	0	+	+	+
Total basicity	0	-	+	+
DRM activity	0	≈	+	+

"0" means the benchmark.
"+" means the strengthened/increased value compared to HT.
"-" means the weakened/decreased value compared to HT.
[1]Ni^0 crystallite size is compared only for reduced catalysts.

Table 5-12 presents the influences of La-loading on Ni-hydrotalcite derived catalysts. The presence of lanthanum mainly improved the Ni reducibility, which may further effected the catalytic performance. All La promoted catalysts presented slightly smaller Ni^0 crystallite size. The addition of 2 wt.% and 4 wt.% La promoted resulted in increased total basicity, but adding La always decreased the CO_2 adsorption on strong basic sites.

5.5 Conclusions

Table 5-13. Summary for the La promoted nickel based hydrocalumite derived catalysts

Physicochemical properties	Catalyst						
	HCa	HT	HSr	HBa	HCa+1%La	HCa+2%La	HCa+4%La
Specific surface area	0	+	+	+	-	-	-
Ni reducibility	0	-	+	+	-	-	+
Total basicity	0	-	-	-	-	-	-
DRM activity	0	+	+	+	≈	-	+
Carbon deposition	0	+	+	+	+	+	+
Physicochemical properties	Catalyst						
	HT				HT+1%La	HT+2%La	HT+4%La
Ni^0 crystallite size[1]	0				-	-	-
Ni reducibility	0				+	+	+
Total basicity	0				-	+	+
DRM activity	0				≈	+	+

"0" means the benchmark.
"+" means the strengthened/increased value compared to HCa or HT respectively.
"-" means the weakened/decreased value compared to HCa or HT respectively.
"≈"means the similar value with HCa or HT respectively.
[1]Ni^0 crystallite size is compared only for reduced catalysts.

The Ni-based hydrocalumite, hydrotalcite, hydro-strontium and hydro-barium-derived catalysts and the addition of lanthanum (1, 2 and 4 wt.%) to 15 wt.% Ni-containing hydrotalcite or hydrocalumite-derived catalysts were prepared and tested for dry reforming of methane at temperatures from 550 °C to 850 °C in this chapter.

The catalysts containing Ni^{2+}, Al^{3+} and different bivalent metal elements of group 2 (Mg^{2+}/Ca^{2+}/Sr^{2+}/Ba^{2+}) presented obvious differences on catalytic performance deponding on the specific surface area and the CO_2 adsorption on strong basic sites. For the La-promoted Ni-containing hydrocalumite derived catalysts, the addition of La resulted in less specific surface area and total basicity. The increased activity for 4 wt.% La promoted Ni-hydrocalumite derived catalysts was attributed to its improved Ni reducibility. For the La-promoted Ni-containing hydrotalcite derived catalysts, the physico-chemical characterizations evidenced bulk NiO segregation and enhanced Ni-reducibility for the La-promoted catalysts. The presence of lanthanum also improved the Ni^0 crystallite size. Medium strength and weak basicity were boosted in such La-containing catalyst, depending on La-loading. Mostly as a consequence of the increased presence of reduced Ni^0 sites, the activity of the La-promoted catalysts was found to be higher than for the non-promoted Ni-hydrotalcite derived catalyst. However, the presence of La for both Ni-hydrocalumite and Ni-hydrotalcite derived catalysts resulted as well in the promotion of undesirable side

reactions, such as direct methane decomposition, thermodynamically favorable at low temperatures. In spite of this, La contributed to the gasification of amorphous carbon deposits, through the formation of oxycarbonate species, thus resulting in overall lower carbon formation during long-duration isothermal experiments performed at 550 °C for La promoted Ni-hydrotalcite derived catalysts.

Chapter VI

Effect of Mg-Al mixed oxides supported Ni-based catalysts prepared by ball milling techniques for dry reforming of methane (DRM)

6. Effect of Mg-Al mixed oxides supported Ni-based catalysts prepared by ball milling techniques for dry reforming of methane

6.1 Mechanical synthesis of the catalyst

With the advancement of science and technology and the enhancement of people's awareness on environmental protection around the world, the issues of environmental pollution and global warming have been given more attention [227]. However, the industrial structure of most countries in the world still relies mainly on the consumption of fossil fuels, which means that the environmental situation is still serious. The trend of environmental pollution has not been fundamentally transformed, and the resources and environment are increasingly becoming the constraints of social and economic development. In the face of more and more serious contradictions among economic development, resources and environment, governments in each country are seeking comprehensive ways of environmental protection and optimizing economic development [228]. Therefore, dry reforming of methane (DRM: $CH_4(g) + CO_2(g) \rightleftharpoons 2CO(g) + 2H_2(g)$, ΔH^0 (298K) = +247.3kJ·mol^{-1}) that converts important carbonic resources, carbon dioxide (CO_2) and methane (CH_4), into syngas (CO and H_2) while mitigating the pressure of greenhouse gas emissions, has received widespread attention. In addition, the syngas can be further converted into high value-added chemical products through Fischer-Tropsch (F-T) process. Nevertheless, the process of dry reforming requires an active and stable catalyst. Also, a material without a proper selectivity may contribute to many parallel reactions during the DRM process, such as CH_4 decomposition and Boudouard reaction. The main drawback during DRM is carbon formation that will cover active sites on catalysts and further decrease catalytic activity [229,230]. Therefore, the exploration on a suitable catalyst for DRM is the key point of industrialization.

Noble metals using as the main active components of the catalyst, show high activity and stability in DRM process. However, their high cost limits the possible practical application [231]. In contrast to noble metals, nickel was found to be a promising alternative material for DRM because of its availability, low cost and good catalytic performance. But Ni-based catalysts are prone to carbon deposition and sintering during reaction, which leads to suppress stability of the catalyst [231,232]. This puts the research on a more efficient and stable catalyst with a lower cost at the centre of attention.

Generally, the common approach is a selection of appropriate additives and/or supports, or synthesis in order to improve the catalytic performance of Ni-based catalysts. Therefore, based on the good catalytic performance of the Ni-based hydrocalumite derived catalysts that were discussed in Chapter V for DRM, a mechanochemical synthesis method called ball milling is used to prepare the catalysts with the same components and cononts as Ni-based hydrocalumite derived catalysts (Al^{3+}, Mg^{2+}, Ni^{2+}). Trovarelli et al. [233] reported a method of preparing CeO_2-ZrO_2 catalysts by mechanical milling. The results showed that mechanical ball milling can synthesize CeO_2-ZrO_2 solid solution in a wide range of composition at room temperature, that is, ZrO_2 can enter the CeO_2 lattice to form fluorite-structured. Meanwhile, CeO_2-ZrO_2 catalysts prepared by mechanical milling presented similar redox behaviors with the solid solution synthesized by conventional methods. Xu et al. [234] studied one kind of Ni-Fe bimetal catalysts for catalytic hydrodechlorination of 4-Chlorophenol by means of mechanical ball milling. It showed higher activity and stability than the catalysts prepared by chemical solution deposition since Ni crystallite was evenly distributed in Fe phase. Moreover, the prepared catalysts can be reused without passivation if pH is lower than 6.0. Meloni et al. [235] researched the potassium (K) salts modified hydrotalcites prepared by coprecipitation catalysts through conventional impregnation and mechanical milling for soybean oil transesterification. Both of these two methods obtained corresponded catalysts with high K dispersion on the surface, whereas the milling method is more beneficial to improve basicity. In addition, the leaching of K-species prepared by milling process from catalysts to solution is less compared to impregnation method in the transesterification reaction. Barroso Quiroga et al. [236] also successfully prepared Fe-Mn-O catalysts by ball milling, and predicted the presence of catalytic applications based on the results of chemical and physical transformations.

Thus, the influences of different synthetic methods, co-precipitation and ball milling, are being investigated for DRM in this Chapter. Catalytic performance and physicochemical characterizations including BET, XRD, H_2-TPR and CO_2-TPD, are subsequently tested to compare the effects on activity, stability, textural properties, crystallite size, Ni reducibility and basicity, respectively.

6.2 Preparation of Mg-Al mixed oxides supported Ni-based catalysts prepared by ball milling method

The catalysts containing the 15 wt.% of nickel, 15.8 wt.% of magnesium and 8.1 wt.% of aluminium were synthesized by ball milling (FRITSCH, Planetary Micro Mill, PULVERISETTE 7, premium line) using nickel oxide, magnesium oxide and aluminium oxide with 2 h grinding. The rotational speed of the main disk was controlled at 300, 600 and 900 rpm. Then the materials were calcined at 550 °C for 5 h. Finally, all corresponding catalysts were obtained and listed in Table 6-1. Otherwise, for sake of comparison, the catalysts with the same contents of Ni, Mg and Al that were already described in Chapter V were also presented.

Table 6-1. Nominal composition for the catalysts prepared by co-precipitation and ball milling.

Catalyst	Rotational speed [rpm]	Label	Metal content [wt.%]		
			Ni	Al	Mg
NiMgAl	0	NiMgAl-HT	15	8.1	15.8
NiMgAl	300	NiMgAl-BM300	15	8.1	15.8
NiMgAl	600	NiMgAl-BM600	15	8.1	15.8
NiMgAl	900	NiMgAl-BM900	15	8.1	15.8

6.3 Physicochemical properties of Mg-Al mixed oxides supported Ni-based catalysts prepared by ball milling

6.3.1 Crystallinity: Ni^0 crystallite size

Figure 6-1 a) and b) show XRD patterns of fresh and reduced catalysts. Two identical reflections, i.e. $MgNiO_2$ and/or MgO and $NiAl_2O_4$ spinel, could be detected for all fresh catalysts. Compared with the fresh catalysts prepared by co-precipitation in Chapter 5, the disappeared reflections at 11° in the fresh catalysts prepared by ball milling in Figure 6-1 a) indicate the layered structure is not formed. The remaining unmarked reflections at about may be assigned to the presence of Al_2O_3, but it is difficult to make accurate judgments and requires further characterizations. In addition, metallic Ni phase (at around 44.6°, 51.8°, 76.3°) is observed for all reduced catalysts in Figure 6-1 b). One point should be noted that $NiAl_2O_4$ does not appear in the fresh NiMgAl-BM600 catalyst but in the reduced catalyst, which means that Ni enters the Al_2O_3 lattice during the reduction. The Ni^0 crystallite size on reduced

catalysts is calculated by Scherrer equation and presented in Table 6-2. The calculation is based on the reflections of metallic nickel at ca. 2θ = 76.3° to avoid the influences of overlapping peaks. The Ni^0 crystallite sizes decrease with increasing rotational speed for the catalysts prepared by ball milling, which means higher rotational speed results in more full grinding. Thus, the total sequence is NiMgAl-HT ≈ NiMgAl-BM900 ≈ NiMgAl-BM600 < NiMgAl-BM300 (Table 6-2). For supported metal catalysts, the particle size is inversely proportional to the dispersion [237]. Therefore, NiMgAl-BM600, NiMgAl-BM900 and NiMgAl-HT present better dispersion of metallic nickel. Moreover, the intensities of the $NiAl_2O_4$ reflections on reduced NiMgAl-BM600 and NiMgAl-BM900 may affect the Ni reducibility.

Table 6-2. BET results, Ni^0 crystal size and H_2-consumption for the Mg-Al mixed oxides supported Ni-based catalysts prepared by co-precipitation and ball milling respectively.

Catalyst	S_{BET} [m^2/g]	V_p[1] [cm^3/g]	d_p[2] [nm]	V_{BJH}[3] [cm^3/g]	Ni^0 crystal size [nm] Reuced	H_2-consumption[4] [mmol H_2/g]
NiMgAl-HT	233.5	0.676	11.6	0.668	13.0	1.42
NiMgAl-BM300	8.4	0.065	31.0	0.065	19.0	1.60
NiMgAl-BM600	31.4	0.146	18.5	0.141	14.1	1.40
NiMgAl-BM900	16.8	0.084	20.0	0.083	14.0	0.95

[1] *total pore volume*
[2] *average pore size*
[3] *BJH desorption cumulative pore volume*
[4] *Theoretical H_2 consumption for Ni species is 2.5 mmol/g catalyst.*

a)

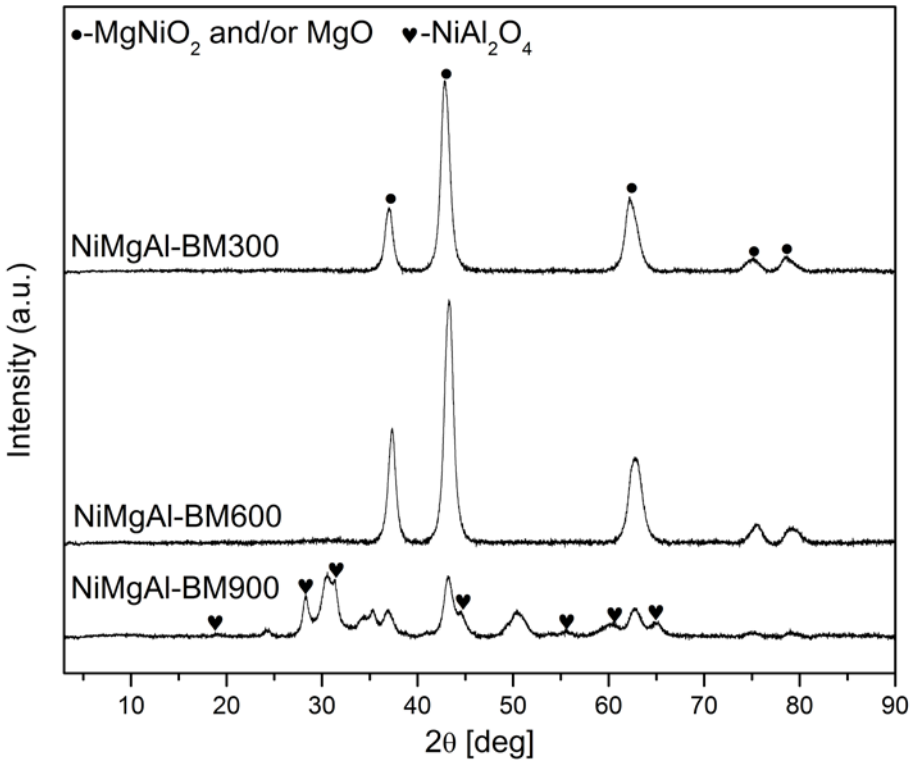

b)

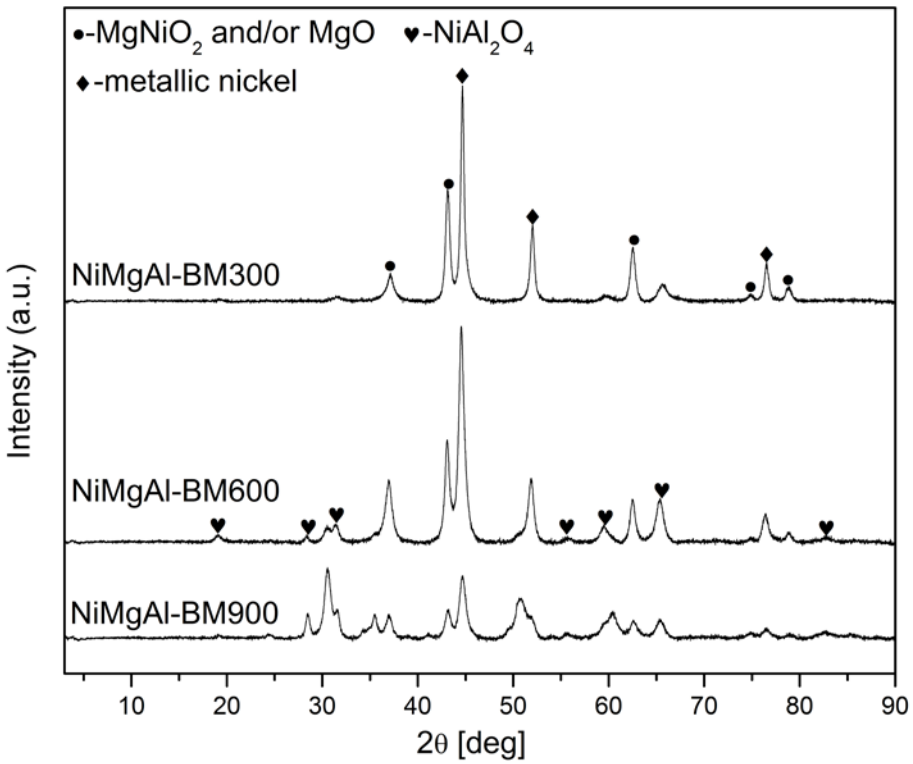

Figure 6-1. XRD patterns for a) the fresh catalyst and b) the reduced catalysts.

6.3.2 Textural properties

Table 6-2 presents textural properties of prepared catalysts, where specific surface areas are 233.5, 8.4, 31.4 and 16.8 m^2/g for NiMgAl-HT, NiMgAl-BM300, NiMgAl-BM600 and NiMgAl-BM900, respectively. The lack of layered structures in the catalysts prepared by ball milling that is already described in XRD patterns lead to their small specific surface area. The average pore sizes are evaluated in the range of 2 to 50 nm, it means the mesoporous structure for all prepared catalysts. Furthermore, the higher specific surface area corresponds to lower pore size in this catalyst system, which is general rule also reported by Ikenyiri et al. [238]. Otherwise, type IV adsorption isotherms and H3 adsorption loops could also be obtained.

6.3.3 Reducibility of the Ni-species

Figure 6-2 presents H_2-TPR profiles of all calcined catalysts. The main reduction peaks for the catalysts prepared by 600 rpm, 900 rpm ball milling and co-precipitation between 790 and 840 °C are attributed to Ni-oxide species strongly bonded to the support, also including the low peak at 710 °C on the catalysts prepared by 300 rpm ball milling. The high reduction temperature is still related to the formation of stable $NiAl_2O_4$ showed in Figure 6-1 b) for NiMgAl-BM600 and NiMgAl-BM900, and the formation of a solid solution with high thermal stability by Ni-oxide species maybe entering into the Mg-Al mixed oxide matrix. The high reduction temperature means better Ni dispersion, in agreement with the analysis of XRD. Meanwhile, the reduction peaks below 500 °C are assigned to the weak interaction between Ni-oxide species and support, especially for NiMgAl-BM300 with the main reduction temperature at 372 °C. Thus, the ball milling method improves the Ni reducibility.

The H_2 consumption for prepared catalysts is listed in Table 6-2. More NiO species are reduced in NiMgAl-BM300 because of their bulk weakly-bonded while less in others. Moreover, the H_2 consumption is also associated with the $NiAl_2O_4$ reflections in NiMgAl-BM600 and NiMgAl-BM900, especially for NiMgAl-BM900, the strong intensities of $NiAl_2O_4$ that need to be reduced at high temperature on NiMgAl-BM900 lead to less Ni being reduced, and it may further affect its catalytic performance.

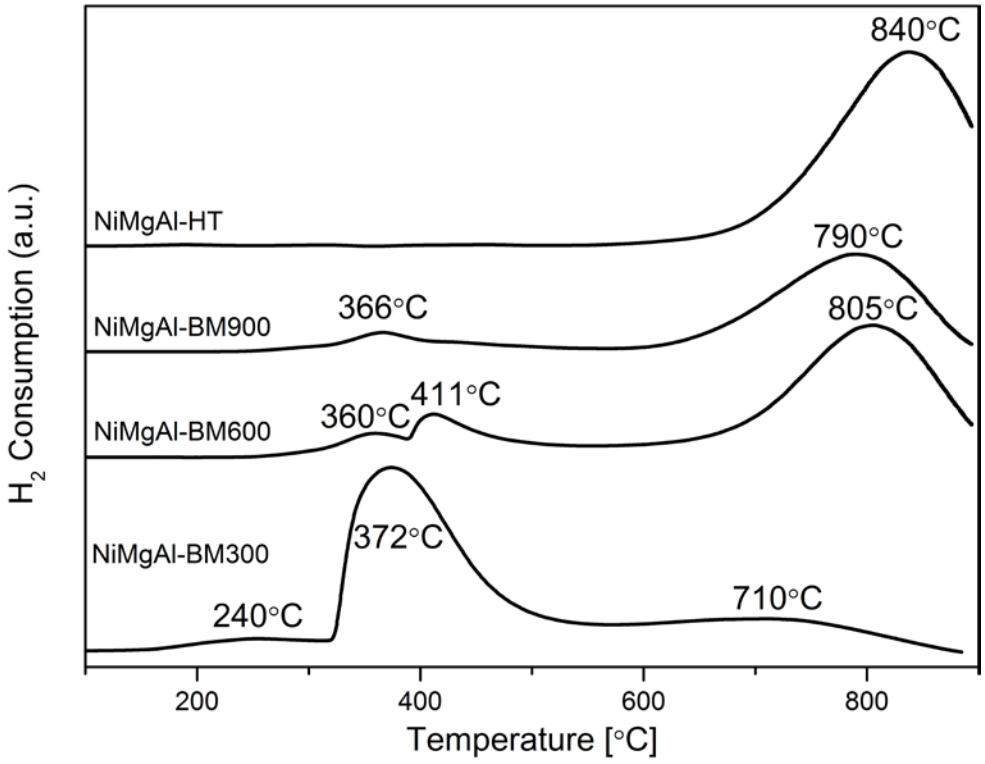

Figure 6-2. H_2-TPR profile for the calcined Mg-Al mixed oxides supported Ni-based catalysts prepared by co-precipitation and ball milling respectively.

6.3.4 CO_2 adsorption and basicity

Generally, the activity in DRM may be correlated with the basicity of the catalysts [239]. Figure 6-3 presents CO_2 desorption profiles for reduced catalysts, where similar desorption peaks appared in the range of 100-600 °C and different values of total basicity were observed (between 33.4 and 67.8 μmol CO_2/g catalyst). Three CO_2 desorption peaks with different strength were registered, corresponding to weak Brønsted basic sites (low temperature), medium-strength Lewis acid-base sites (intermediate temperature), and strong basic sites (high temperature), respecively [240]. In addition, peak position and CO_2 desorption on each peak always change according to the preparation conditions, which is listed in Table 6-3.

Comparing with the centers of weak basic sites, medium-strength Lewis acid-base sites and strong basic sites for the catalysts prepared by co-precipitation that are located at 147 °C, 250 °C and 389 °C, the centers of the catalysts prepared by ball milling occur at 162-173 °C, 290-308 °C and 406-470 °C respectively (Table 6-3). Thus, all basic sites shift to higher temperature, which means the ball milling method strengthen CO_2 chemisorption, especially for NiMgAl-BM600, appearing 26 °C, 51 °C, 81 °C late respectively. Meanwhile, the

mechanochemical synthesis method also result in lower total basicity, and it decreases with increasing rotational speed. Therefore, NiMgAl-BM900 holds the lowest total basicity. However, CO_2 desorption on strong basic sites is slightly increased for all catalysts prepared by ball milling, it may related to the presence of $NiAl_2O_4$ that could lead to a lower acidity [241].

Table 6-3. Peak position, CO_2 desorpotion of the CO_2-TPD profiles and carbon depostion obtained for the Mg-Al mixed oxides supported Ni-based catalysts prepared by co-precipitation and ball milling respectively.

Catalyst	Temperature [°C]			μmol CO_2 desorbed/g			Total basicity [μmol CO_2/g]	Carbon deposition [mg]
	1st peak	2nd peak	3rd peak	1st peak	2nd peak	3rd peak		
NiMgAl-HT	147	250	389	24.5	35.4	7.9	67.8	636.1
NiMgAl-BM300	173	301	470	18.6	35.9	10.3	64.8	617.8
NiMgAl-BM600	162	308	410	16.2	22.4	10.6	49.2	690.0
NiMgAl-BM900	169	290	406	10.4	13.6	9.4	33.4	527.7

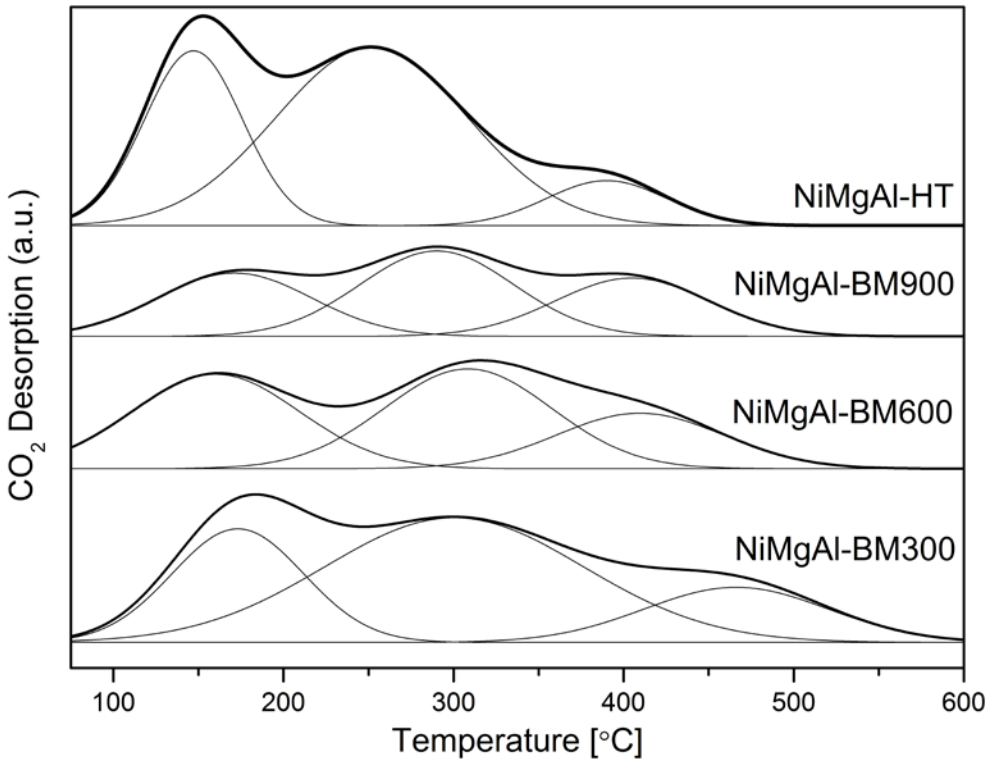

Figure 6-3. CO_2-TPD profile for the reduced Mg-Al mixed oxides supported Ni-based catalysts prepared by co-precipitation and ball milling respectively.

6.4 Catalytic performance and carbon deposition

Figure 6-4 presents the catalytic activity in DRM, including conversions of CH_4 and CO_2 and H_2/CO molar ratio, as function of the temperature. Both CH_4 and CO_2 conversions show the

same trend for all prepared catalysts, presenting an increase in the function of temperatures that is consistent with the thermodynamics simulated by means of HSC Chemistry 5.0. In addition, the situation where measured CO_2 conversion is always higher than CH_4 conversion, which should have opposite trend based on the thermodynamic simulation, is attributed to the fact that the side reactions promoting the CH_4 conversion are not fully activated. It is also consequently reflected in the measured H_2/CO ratio. The H_2/CO ratio refers to the selectivity of the catalysts. The value different than the tendency of thermodynamics still suggests some side reactions are inhibited and/or promoted. Accordingly, the catalysts prepared by both co-precipitation and ball milling may lead to the presence of reverse water gas shift reaction at low temperature, and the process of carbon gasification, which resulted in excess of CO. The latter may be promoted through the surface oxygen from the dissociation of CO_2.

Moreover, at the range of 600 to 750 °C, the following sequence for both CO_2 and CH_4 conversions could be observed: NiMgAl-HT ≈ NiMgAl-BM600 > NiMgAl-BM300 > NiMgAl-BM900, while NiMgAl-BM300 is close to NiMgAl-BM900 at high temperature, especially at 850 °C. The best activity and selectivity for NiMgAl-HT is probably related to its suitable Ni^0 crystallite size, the similar results have also been reported by Seo et al. and Christensen et al. [242,243]. In addition, the large specific surface area that can load more active components and less CO_2 desorption on strong basic sites may also contribute to its excellent catalytic activity. The similar Ni^0 crystallite size makes NiMgAl-BM600 obtain similarly excellent activity as well. However, the lowest catalytic activity of NiMgAl-BM900 in this catalyst system that also has similar Ni^0 crystallite size with NiMgAl-HT may be assigned to its less reduction of NiO_x species (Table 6-2). Besides, NiMgAl-BM600 always receives the highest H_2/CO ratio, which probably means more promotion of CH_4 decomposition and/or boudouard reaction. The decreasing H_2/CO ratio for NiMgAl-BM600 between 600 and 650 °C points to the selectivity towards to DRM and/or reverse water gas shift reaction. The less H_2/CO ratio at low temperature point to the presence of carbon formation in all prepared catalysts.

a)

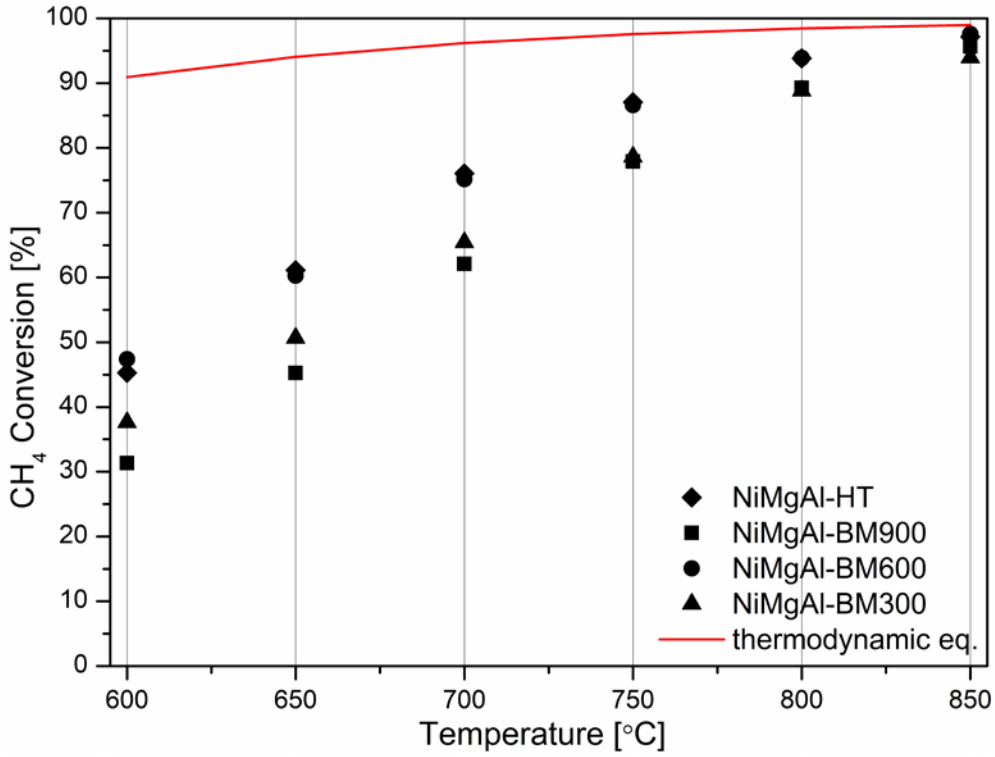
CH4 Conversion [%]
Temperature [°C]
NiMgAl-HT
NiMgAl-BM900
NiMgAl-BM600
NiMgAl-BM300
thermodynamic eq.

b)

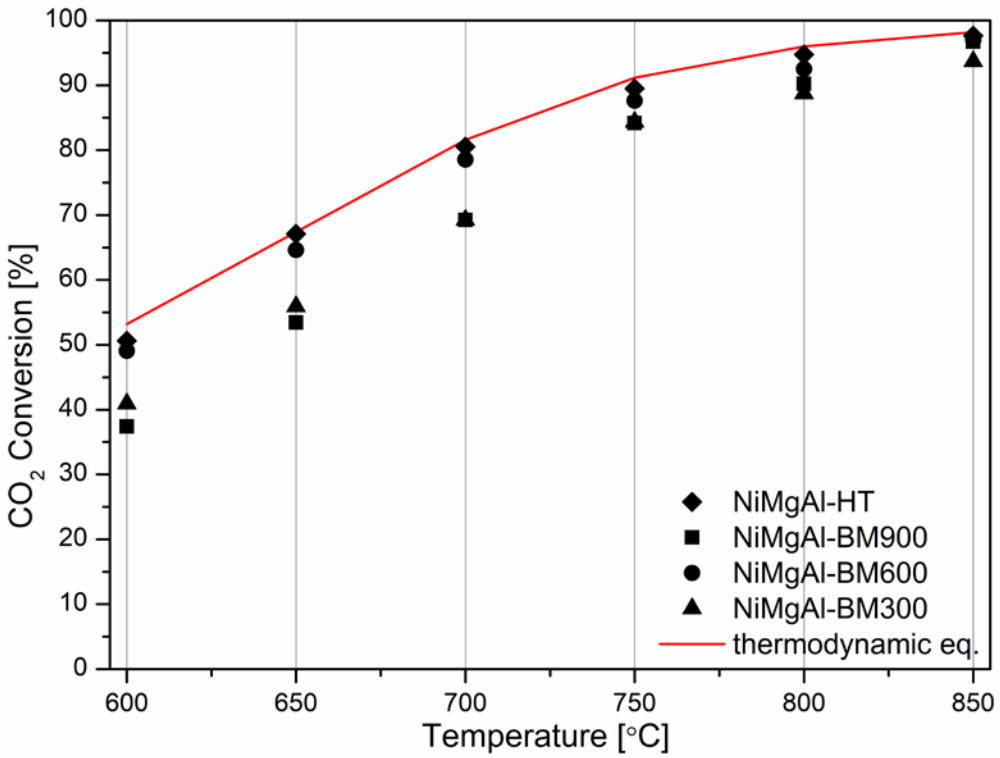
CO2 Conversion [%]
Temperature [°C]
NiMgAl-HT
NiMgAl-BM900
NiMgAl-BM600
NiMgAl-BM300
thermodynamic eq.

c)

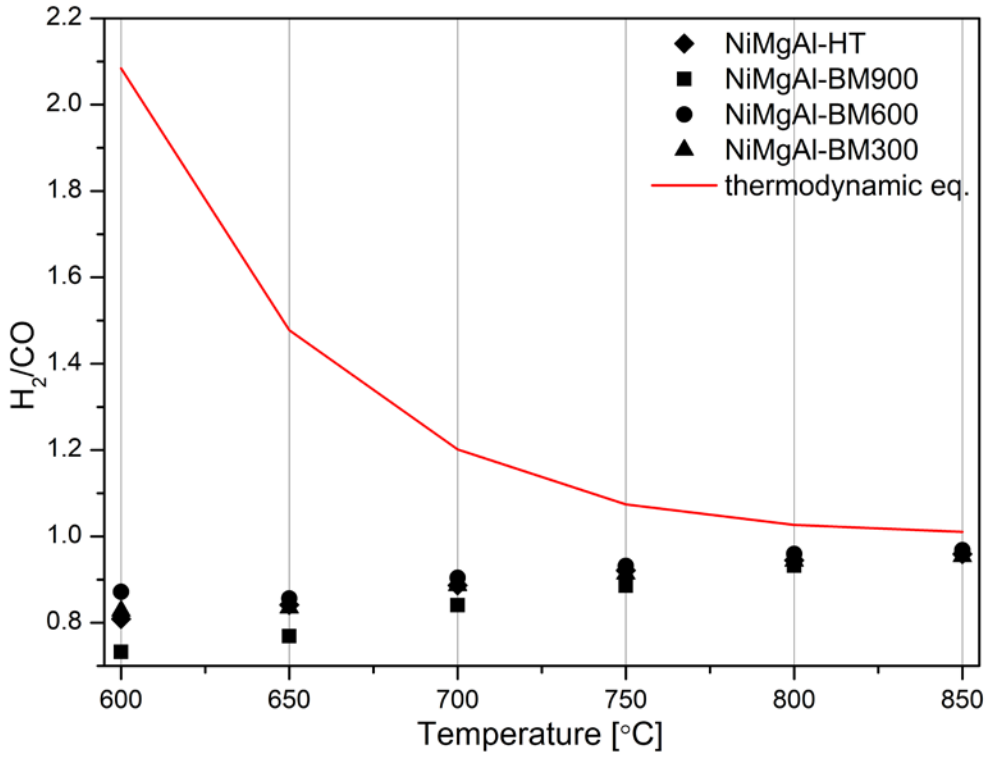

Figure 6-4. DRM activity tests in the presence of the reduced Mg-Al mixed oxides supported Ni-based catalysts prepared by co-precipitation and ball milling: a) CH_4 and b) CO_2 conversions, and c) H_2/CO ratio.

After 5 hours tests at 750 °C, the carbon depostion is calculated based on the mass balance by means of gas chromatography and listed in Table 6-3. The relatively low carbon deposition on NiMgAl-HT compared to NiMgAl-BM600 is observed, which means CH_4 decomposition and/or boudouard reaction is inhibited to a certain extent. The less CO_2 desorption on strong basic sites listed in Table 6-3 may also contribute to its low carbon formation since CO_2 on strong basic sites is hard to be desorbed to react with CH_4 leading to more CH_4 decomposition. For the catalysts only prepared by ball milling, higher catalytic activity corresponds to higher carbon deposition, and it is more obvious at low reaction temperature. This situation indicates that this kind of catalysts simultaneously promote the DRM and side reactions that can form carbon. Meanwhile, higher CO_2 desorption on strong basic sites is probably associated with their much carbon formation (Table 6-3).

6.5 Conclusions

Table 6-4. Summary for Mg-Al mixed oxides supported Ni-based catalysts prepared by ball milling

	Physicochemical properties	NiMgAl-Catalyst		
		BM300	BM600	BM900
Rotational speed	Specific surface area	0	+	+
	Ni^0 crystallite size[1]	0	-	-
	Ni reducibility	0	-	-
	Total basicity	0	-	-
	DRM activity	0	+	-
	Carbon deposition	0	+	-

	Physicochemical properties	NiMgAl-Catalyst			
		HT	BM300	BM600	BM900
Preparation method	Specific surface area	0	-	-	-
	Ni^0 crystallite size[1]	0	+	+	+
	Ni reducibility	0	+	+	+
	Total basicity	0	-	-	-
	DRM activity	0	-	≈	-
	Carbon deposition	0	-	+	-

"0" means the benchmark.
"+" means the strengthened/increased value compared to NiMgAl-BM300 or NiMgAl-HT.
"-" means the weakened/decreased value compared to NiMgAl-BM300 or NiMgAl-HT.
"≈"means the similar value with HCa.
[1]Ni^0 crystallite size is compared only for reduced catalysts.

Table 6-4 presented the influences of rotational speed and preparation method on Mg-Al mixed oxides supported Ni-based catalysts in this chapter. The prepared catalysts were characterized by BET, XRD, H_2-TPR and CO_2-TPD, and tested in dry reforming of methane for syngas production. Higher catalytic activity was found in the catalysts prepared by co-precipitation and ball milling with 600 rpm rotational speed (NiMgAl-HT and NiMgAl-BM600), which may be ascribed to their suitable Ni^0 crystallite size. The less reduction of NiO_x species on NiMgAl-BM900 that obtains similar Ni^0 crystallite size with NiMgAl-HT may limit its activity. Comparing to NiMgAl-BM600 having similar activity, the catalysts prepared by co-precipitation can inhibit carbon formation to a certain extent probably related to its less CO_2 desorption on strong basic sites. However, especially at low temperatures, less H_2/CO ratio was observed, which means carbon forming reaction is presented in all prepared catalysts.

Chapter VII
Conclusion and perspectives

7. Conclusion and perspectives

7.1 Conclusion

In the first part of the experimental results, non-noble metal Ni was used as the main active component, natural clay and/or Fe/Cu modified clay was first used as the support, and promoters such as Ce, Zr, La, Al, Mn, and Mg were introduced to compare the catalytic performance of these catalysts. Then the influences of the catalysts with different prtomoters and supports on textural properties, Ni^0 crystallite size, Ni reducibility, basicity and carbon deposition during dry reforming of methane were investigated based on various characterizations, such as BET, XRD, H_2-TPR, CO_2-TPD and TGA. The effects of physicochemical properties on catalytic performance were further analyzed.

The experiments on the catalytic activity of different promoters (Ce, Zr, La, Al, Mn and Mg) on Fe-modified clay Ni-based catalysts showed that, in addition to the Mn, the addition of other promoters contributed to the improvement of the catalytic activity. The addition of Ce increased the specific surface area of the catalyst and the Ni reducibility, and improved the Ni^0 crystallite size and the CO_2 adsorption on strong basic sites in basicity at the same time. These factors were related to its improvement of the catalytic activity. Compared with Ce, the addition of Zr further improved the specific surface area, the Ni reducibility, the Ni^0 crystallite size and the adsorption of CO_2 on strong basic sites. This fact also maked it presents a better catalytic activity. The higher improvement also led to the higher catalytic activity for the Al promoted catalysts compared to Zr. The addition of La, which showed relatively low level of catalytic performance in the catalyst system, mainly improved catalytic activity by improving the Ni^0 crystallite size and the CO_2 adsorption on strong basic sites. In all of the prepared promoters, the best catalytic activity from the introduction of Mg, almost 80% CO_2 conversion was obtained at 750 °C, was mainly attributed to the suitable Ni^0 crystallite size that promoted the Ni dispersion. Meanwhile, more Mg contents did not have a significant effect on catalytic activity compared to the addition of 10 wt.% Mg. Besides, the introduction of Mn resulted in promoting the specific surface area, the Ni^0 crystallite size and the CO_2 adsorption on strong basic sites, but the presence of Mn oxides and Fayalite, Mn-rich, which may partially or totally cover the NiO species. In addition, the addition of Ce, Zr, La, Al and Mg also promoted the side reactions during dry reforming of methane such as methane

decomposition, so that the carbon deposition is also hgh while the catalytic activity is increased.

For different supports, when the reduction temperature was 900 °C, the Fe and Cu modified clay supported Ni based catalysts with smaller Ni^0 crystallite size showed higher catalytic activity than the natural clay supported Ni based catalysts. When the reduction temperature was reduced to 800 °C, all prepared catalysts show higher activity than those reduced at 900 °C, the imrpovement was mainly attributed to the increased basicity as the positive side, the fact that larger Ni^0 crystallite size tended to promote side reactions also led to higher conversions of both CH_4 and CO_2 as the negative side. Besides, the Cu modified clay Ni based catalysts exhibited the highest activity at all reduction temperatures of 800 °C and 900 °C, which was attributed to the low CO_2 desorption on strong basic sites and also the tendency of Cu favored the reverse water gas shift reaction. After the promoters (Ce, Zr and Mg) were introduced on natural clay and Fe/Cu modified clay supported Ni based catalysts, it was found that the addition of Ce, Zr, and Mg contributed to the improvement of catalytic activity. When the reduction temperature was 800 °C, the addition of Ce and Zr on Fe modified clay improved the Ni reducibility and the CO_2 desorption on strong basic sites, meanwhile the the introduction of Ce and Zr on Cu modified clay increased the Ni reducibility and the CO_2 desorption on weak basic sites and medium basic sites. When the reduction temperature was 900 °C, the presence of Mg resulted in smaller Ni^0 crystallite size through the formation of $MgNiO_2$, which meant the higher Ni dispersion and further obtained better catalytic activity. However, the highly active catalysts promoteed the activation of the C-H bond, which also promoted the CH_4 decompostion, resulting in the higher carbon deposition.

The second part of the experiment attempted to synthesize layered double hydroxides-derived catalysts using Ni^{2+}, Al^{3+} and Group 2 elements (Mg^{2+}, Ca^{2+}, Sr^{2+} and Ba^{2+}). Meanwhile, La as promoter was also introduced in the catalysts to compare the influences of layered structure and La on catalytic performance. Based on the results of the activity tests, the BET, XRD, H_2-TPR, CO_2-TPD and TGA characterizations were also used to analyze the possible influences of textural properties, the Ni^0 crystallite size, the Ni reducibility, the basicity and the carbon deposition on catalytic activity.

In the catalysts prepared by using elements of Ni^{2+}, Al^{3+}, and Group 2 elements (Mg^{2+}, Ca^{2+},

Sr^{2+} and Ba^{2+}), the addition of Mg^{2+} and Ca^{2+} could form a layered structure in catalysts. The presence of Sr^{2+} and Ba^{2+} could not form a layered structure because of their excessive ionic radius. However, all prepared catalysts prepared presented relatively high catalytic activity. Among them, the Ni-hydrotalcite-derived catalysts (Ni^{2+}, Mg^{2+} and Al^{3+}) exhibited the best catalytic activity in this catalyst system due to their larger specific surface area and less CO_2 adsorption on strong basic sites. The catalytic performance of Ni-hydrocalumite-derived (Ni^{2+}, Mg^{2+} and Al^{3+}) with less specific surface area and much CO_2 adsorption on strong basic sites catalysts was relatively poor. Besides, the carbon deposition for all prepared catalysts at 750 °C was proportional to their catalytic activity, which also indicated the promotion of side reactions on the prepared catalyst. After introducing the La to the Ni-hydrocalumite-derived catalyst having a layered structure, the presence of 4 wt.% La showed the best catalytic activity by increasing the Ni reducibility, while the addition of 2 wt.% La presented lower activity. By testing the stability at 750 °C for 5 hours, it was found that the La did not effectively inhibit the side reactions. The presence of different amounts (1 wt.%, 2 wt.%, and 4 wt.%) of La on Ni-hydrotalcite-derived catalysts contributed to the higher catalytic activity, which is mainly assigned to the improved Ni reducibility. At the same time, the results of the stability test at 550 °C showed that the addition of 4 wt.% La produced less carbon deposition by the formation of lanthanum oxycarbonates ($La_2O_2CO_3$) that can vaporize carbon compared to non-promoted Ni-hydrotalcite-derived catalysts.

The third experimental part focused on the different catalytic performance of Mg-Al mixed oxides supported Ni-based catalysts prepared by ball milling, and also compared to Ni-hydrotalcite derived catalyst having good catalytic activity. In addition to the catalytic activity tests, BET, XRD, H_2-TPR and CO_2-TPD were also used to analyze the possible reasons of differences in activity. The XRD characterization showed that the Ni^0 crystallite size decreased with increasing rotational speed in the catalysts prepared by ball milling. By associating characterization results with activity results, it could be found that the catalysts with 600 rpm rotational speed had comparable activity to the Ni-hydrotalcite-derived catalysts prepared by co-precipitation, which is possibly dued to their suitable Ni^0 crystallite size. While the rotational speed was 900 rpm, although the Ni^0 crystallite size is similar with the Ni-hydrotalcite-derived catalyst, the NiO species were not sufficiently reduced, resulting in a lower catalytic activity. For the catalysts prepared by ball milling, the carbon formation increased with the increase of catalytic activity. The lower carbon deposition on the Ni-hydrotalcite-derived catalysts compared to the catalysts prepared by 600 rpm rotational

speed might be attributed to the lower CO_2 adsorption on strong basic sites, thus more CO_2 would react with CH_4, and CH_4 decomposition was reduced to a certain extent.

7.2 Perspectives

With the signing of the "Paris Agreement" and the growing attention of countries to greenhouse effect and environmental pollution, the utilisation of two greenhouse gases (CO_2 and CH_4) producing useful chemical building blocks, i.e. dry reforming of methane, shows its potential on industrial development and research, and attracts more attention. Nickel is used as the main active component for dry reforming of methane because of its superior catalytic activity and cheap price. The catalytic selectivity and stability of nickel-based catalysts are affected by many factors such as nickel loading, promoters, supports, catalyst preparation and experimental conditions. These factors are also the direction in which researchers currently want to increase the dispersion of active metals on catalysts, and further improve the catalytic activity and stability. Although Ni-hydrotalcite-derived catalysts in this thesis and some highly efficient catalyst have been reported, the high temperature required for the reaction and the stability of the catalyst all affect the commercialization of dry reforming of methane. The Shanghai Advanced Research Institute (Chinese Academy of Sciences), Shanxi Lu'an Environmental Energy and the Royal Dutch Shell had tested the carbon dioxide autothermal reforming device in 2017, but the carbon deposition and sintering of active metals still need to be further solved in actual operation.

With the gradual deepening of the research on dry reforming of methane, as well as the continuous improvement of testing and characterization, the related research has been rapidly developed. Combined with the problems that still need to be solved in the process of industrialization, relevant research can be carried out from both the catalyst and the reactor:

1. For catalyst

First, about the Ni^0 crystallite size. The Ni^0 crystallite size has an important effect on the catalytic performance in dry reforming of methane. From this aspect, it is possible to try to prepare the singl-atom catalysis. Second, about the promoter. Trying to find "noble-metal-like" compounds. The addition of noble metals enhances the stability and the

ability to inhibit carbon deposition, so the introduction of "noble-metal-like" compounds as promoter will have positive effects on catalysts, such as tungsten carbide (WC) that has similar properties with Pt [244]. Third, about the choice of reaction temperature. Designing and developing catalyst with high activity at lower reaction temperatures not only conforms to the economic benefits of commercialization but also helps to inhibit the deactivation of active components on the catalyst by sintering at high temperatures. The plasma technology can be used to better develop low-temperature catalysts. Fourth, about the support. In combination with the requirements of low temperature catalysts, metal organic frameworks (MOFs) as one kind of support can be used. The metal-organic frameworks has high specific surface area and excellent performance in CO_2 capture, but high temperatures may break its structure, so it can be considered as one direction of low-temperature catalysts.

2. For the reactor

At present, although the knowledge of the basic reaction processes for dry reforming of methane and the promotions of promoters and supports have been gradually agreed, there are still some objections to the reaction mechanism. The study of the reaction mechanism plays an important guiding role in the development and optimization of the catalyst for dry reforming of methane. Thus, it is significant to evaluate the possible reaction mechanisms of different catalysts by more in situ characterizations, such as diffuse reflectance infrared fourier transform spectroscopy (DRIFTS) that can evaluate the state of adsorbed species, and soft X-ray absorption spectroscopy (sXAS) that is sensitive to changes in valence and electronic characteristics. Meanwhile, the isotopic labeling is also a helpful method for mechanism research.

In addition, changing the composition of the feed gas at the beginning of the reaction is also expected to have a positive effect on the dry reforming of methane. That is, by coupling the dry reforming of methane with other reactions, such as partial oxidation of methane, to achieve the purpose of improving the catalytic efficiency, the introduced oxygen is also expected to eliminate carbon deposition to a certain extent.

Both the development of high-efficiency catalysts and the optimization of reactors and reaction conditions, the main objective is to meet the economical requirements for the commercialization of dry reforming of methane. Meanwhile, the development of different

value-added industries through the utilisation of CO_2 and CH_4 by dry reforming of methane, such as biomass conversion research that can produce CO_2 and CH_4, it can also reflect its significance in terms of resource utilization.

Reference

[1] Population Division (2017), Department of Economic and Social Affairs, United Nations. World population prospects: The 2017 revision, key findings and advance tables [online]. United Nations.

Available on: <https://esa.un.org/unpd/wpp/Publications/Files/WPP2017_KeyFindings.pdf>

(accessed on 09.11.2017)

[2] BP Global. BP energy outlook 2017: Country and regional insights - Global [online]. BP Global.

Available on:

<https://www.bp.com/content/dam/bp/pdf/energy-economics/energy-outlook-2017/bp-energy-outlook-2017-global-insights.pdf>

(accessed on 09.11.2017)

[3] Jean-Marc Jancovici. Energy and choice of life. Revue du Palais de la Découverte [online]. 2010; 11.

Available on:

<https://jancovici.com/en/publications-and-co/newspaper-articles-en/energy-and-choice-of-life/>

(accessed on 20.01.2017)

[4] International Energy Agency. CO_2 emissions from fuel combustion 2017. International Energy Agency.

Available on:

<http://www.iea.org/publications/freepublications/publication/CO2EmissionsfromFuelCombustionHighlights2017.pdf>

(accessed on 10.11.2017)

[5] Global Monitoring Division, Earth System Research Laboratory, National Oceanic and Atmospheric Administration. Trends in atmospheric carbon dioxide [online].

Available on: <https://www.esrl.noaa.gov/gmd/ccgg/trends/index.html>

(accessed on 09.11.2017)

[6] United Nations Treaty Collection. Paris agreement [online].

Available on:

<https://treaties.un.org/pages/ViewDetails.aspx?src=TREATY&mtdsg_no=XXVII-7-d&chapter=27&clang=_en>

(accessed on 09.11.2017)

[7] Kuang S. To develop new technical system for carbon dioxide mitigation. Modern Chemical Industry. 2008; 28(2): 3-15.
[8] International Energy Agency. 20 years of carbon capture and storage - Accelerating future deployment [online]. International Energy Agency.
Available on:
<https://www.iea.org/publications/freepublications/publication/20YearsofCarbonCaptureandStorage_WEB.pdf>
(accessed on 10.11.2017)
[9] Mikkelsen M, Jørgensen M, Krebs FC. The teraton challenge. A review of fixation and transformation of carbon dioxide. Energy Environ Sci. 2010; 3: 43-81.
[10] IEA Greenhouse Gas R&D Programme (IEAGHG). Rotating equipment for carbon dioxide capture and storage [online]. Global CCS Institute.
Available on:
<http://www.globalccsinstitute.com/publications/rotating-equipment-carbon-dioxide-capture-and-storage>
(accessed on 20.11.2017)
[11] White CM, Strazisar BR, Granite EJ, Hoffman JS, Pennline HW. Separation and capture of CO_2 from large stationary sources and sequestration in geological formations - Coalbeds and deep saline aquifers. Journal of the Air & Waste Management Association. 2012; 53: 645-715.
[12] Metz B, Davidson O, Coninck H, Loos M, Meyer L. Carbon dioxide capture and storage [online]. Working Group III of the Intergovernmental Panel on Climate Change. Cambridge University Press, Cambridge, United Kingdom and New York, NY, USA.
Available on: <https://www.ipcc.ch/report/srccs/>
(accessed on 20.11.2017)
[13] Catherine E. Housecroft, Alan G. Sharpe. Inorganic Chemistry, Fourth Edition [online]. Pearson Education Limited.
Available on: <http://31.210.87.4/ebook/pdf/Inorganic_Chemistry_4th_Edition.pdf>
(accessed on 17.11.2017)
[14] Han S-J, Wee J-H. Carbon dioxide fixation by combined method of physical absorption and carbonation in NaOH-dissolved methanol. Energy & Fuels. 2017; 31: 1747-55.
[15] Chery D, Lair V, Cassir M. Overview on CO_2 valorization: Challenge of molten carbonates. Frontiers in Energy Research. 2015; 3.

[16] Appel AM, Bercaw JE, Bocarsly AB, Dobbek H, DuBois DL, Dupuis M, et al. Frontiers, opportunities, and challenges in biochemical and chemical catalysis of CO_2 fixation. Chemical Reviews. 2013; 113: 6621-58.

[17] Aresta M, Dibenedetto A, Angelini A. Catalysis for the valorization of exhaust carbon: from CO_2 to chemicals, materials, and fuels. Technological use of CO_2. Chemical Reviews. 2014; 114: 1709-42.

[18] Aresta M, Dibenedetto A, Angelini A. Catalysis for the valorization of exhaust carbon: from CO2 to chemicals, materials, and fuels. technological use of CO_2. Chemical reviews. 2014;114:1709-42.

[19] Olajire AA. Valorization of greenhouse carbon dioxide emissions into value-added products by catalytic processes. Journal of CO_2 Utilization. 2013;3-4:74-92.

[20] Wang W, Wang F, Shen X, Sun D. Progress on preparation of synthetic gas by catalytic partial oxidating methane. Advances in Fine Petrochemicals. 2006;7(7)：27-31.

[21] Liu K, Song C, Subramani V. Hydrogen and syngas production and purification technologies. John Wiley & Sons, Inc., Hoboken, New Jersey.
Available on:
<http://197.14.51.10:81/pmb/CHIMIE/Hydrogen%20and%20Syngas%20Production%20and%20Purification%20Technologies.pdf>
(accessed on 22.01.2017)

[22] Bharadwaj S, Schmidt L. Catalytic partial oxidation of natural gas to syngas. Fuel Processing Technology. 1995; 42(2-3):109-27.

[23] Usman M, Wan Daud WMA, Abbas HF. Dry reforming of methane: Influence of process parameters-A review. Renewable and Sustainable Energy Reviews. 2015;45:710-44.

[24] Wang Y, Yao L, Wang S, Mao D, Hu C. Low-temperature catalytic CO_2 dry reforming of methane on Ni-based catalysts: A review. Fuel Processing Technology. 2018;169:199-206.

[25] Claudia do Rosario Vaz Morgado, Victor Paulo Pecanha Esteves. CO_2 sequestration and valorization [online]. AvE4EvA MuViMix Record.
Available on: <https://www.intechopen.com/books/co2-sequestration-and-valorization>
(accessed on 22.11.2017)

[26] Abbott DH, Albright CE. CO_2 shielding gas effects in laser welding mild steel. Journal of Laser Applications. 1994; 6: 69-80.

[27] Guo D. Applied Research on fruit and vegetable antistaling agent [in Chinese]. Chinese Agricultural Science Bulletin 2001; 17(3): 62-63.

[28] Carbon Sciences. Carbon Sciences Announces Major Breakthrough to Recycle CO2 into Gasoline [online]. Carbon Sciences.
Available on: <http://www.carbonsciences.com/view_news.php?id=67>
(accessed on 22.11.2017)
[29] Wei J, Ge Q, Yao R, Wen Z, Fang C, Guo L, et al. Directly converting CO_2 into a gasoline fuel. Nature communications. 2017; 8: 15174.
[30] National Research Council. What you need to know about energy (2008) [online]. The National Academic Press.
Available on: <https://doi.org/10.17226/12204>
(accessed on 15.11.2017)
[31] Kurevija T, Kukulj N, Rajković D. Global prospects of synthetic diesel fuel produced from hydrocarbon resources in oil&gas exporting countries. Rudarsko-geološko-naftni Zbornik. 2007; 19: 79-86.
[32] Anthony Andrews, Jeffrey Logan. Fischer-Tropsch fuels from coal, natural gas, and biomass: Background and policy [online]. Library of Congress. Congressional Research Service.
Available on: <https://digital.library.unt.edu/ark:/67531/metadc821070/>
(accessed on 15.11.2017)
[33] Office of Technology Assessment, Congress, United States. Increased automobile fuel efficiency and synthetic fuels: Alternatives for reducing oil imports [online]. Office of Technology Assessment, Congress, United States.
Available on: <https://digital.library.unt.edu/ark:/67531/metadc39481/>
(accessed on 16.11.2017)
[34] Liederman D, Yurchak S, Kuo JCW, Lee W. Mobil methanol-to-gasoline process. Journal of Energy. 1982; 6(5): 340-41.
[35] Mark Crocker. Thermochemical conversion of biomass to liquid fuels and chemicals [online]. Royal Society of Chemistry (RSC) Publishing.
Available on: <http://pubs.rsc.org/en/Content/eBook/978-1-84973-035-8>
(accessed on 16.11.2017)
[36] Schulz H. Short history and present trends of Fischer-Tropsch synthesis. Applied Catalysis A: General. 1999; 186: 3-12.
[37] Harold H. Gunardson. Industrial Gases in Petrochemical Processing: Chemical Industries [online]. Marcel Dekker, Inc.
Available on:

<https://books.google.fr/books?id=opm8gy-0PtsC&pg=PA225&lpg=PA225&dq=syngas+plasticizer&source=bl&ots=xrJ-VqdcpO&sig=7UulkPkiake1tynqcsoAxtetsUM&hl=zh-CN&sa=X&ved=0ahUKEwjphv_JrInYAhUBtBoKHadfA-IQ6AEIOzAD#v=onepage&q=syngas%20plasticizer&f=false>
(accessed on 17.11.2017)

[38] Zabed H, Sahu JN, Boyce AN, Faruq G. Fuel ethanol production from lignocellulosic biomass: An overview on feedstocks and technological approaches. Renewable and Sustainable Energy Reviews. 2016; 66: 751-74.

[39] Arora S, Prasad R. An overview on dry reforming of methane: strategies to reduce carbonaceous deactivation of catalysts. RSC Advances. 2016; 6: 108668-88.

[40] Pakhare D, Spivey J. A review of dry (CO_2) reforming of methane over noble metal catalysts. Chemical Society reviews. 2014; 43: 7813-37.

[41] Liu H, Wierzbicki D, Debek R, Motak M, Grzybek T, Da Costa P, et al. La-promoted Ni-hydrotalcite-derived catalysts for dry reforming of methane at low temperatures. Fuel. 2016; 182: 8-16.

[42] Usman M, Wan Daud WMA, Abbas HF. Dry reforming of methane: Influence of process parameters—A review. Renewable and Sustainable Energy Reviews. 2015; 45: 710-44.

[43] Jafarbegloo M, Tarlani A, Mesbah AW, Sahebdelfar S. Thermodynamic analysis of carbon dioxide reforming of methane and its practical relevance. International Journal of Hydrogen Energy. 2015; 40: 2445-51.

[44] Nikoo MK, Amin NAS. Thermodynamic analysis of carbon dioxide reforming of methane in view of solid carbon formation. Fuel Processing Technology. 2011; 92: 678-91.

[45] Nematollahi B, Rezaei M, Lay EN, Khajenoori M. Thermodynamic analysis of combined reforming process using Gibbs energy minimization method: In view of solid carbon formation. Journal of Natural Gas Chemistry. 2012; 21: 694-702.

[46] Chein RY, Chen YC, Yu CT, Chung JN. Thermodynamic analysis of dry reforming of CH 4 with CO 2 at high pressures. Journal of Natural Gas Science and Engineering. 2015; 26: 617-29.

[47] Nikoo MK, Amin NAS. Thermodynamic analysis of carbon dioxide reforming of methane in view of solid carbon formation. Fuel Processing Technology. 2011;92:678-91.

[48] Fischer F, Tropsch H. Conversion of methane into hydrogen and carbon monoxide. Brennst. Chem.. 1928; 3(9): 39-46.

[49] Mark MF, Mark F, Maier WF. Reaction kinetics of the CO_2 reforming of methane. Chemical Engineering & Technology. 1997; 20: 361-70.

[50] Mondal K, Sasmal S, Badgandi S, Chowdhury DR, Nair V. Dry reforming of methane to syngas: a potential alternative process for value added chemicals-a techno-economic perspective. Environmental science and pollution research international. 2016; 23: 22267-73.

[51] Centi G, Perathoner S. Opportunities and prospects in the chemical recycling of carbon dioxide to fuels. Catalysis Today. 2009; 148: 191-205.

[52] Edwards JH, Maitra AM. The chemistry of methane reforming with carbon dioxide and its current and potential applications. Fuel Process Technol. 1995; 42: 269-89.

[53] Peter Atkins, Julio De Paula. Elements of Physical Chemistry, Fifth Edition [online]. Great Britain by Oxford University Press.
Available on: <http://www.kinetics.nsc.ru/chichinin/books/Chem_Phys/Atkins09.pdf >
(accessed on 13.11.2017)

[54] Eric Lichtfouse, Jan Schwarzbauer, Didier Robert. Hydrogen production and remediation of carbon and pollutants [online]. Springer International Publishing AG.
Available on: <https://link.springer.com/content/pdf/10.1007%2F978-3-319-19375-5.pdf>
(accessed on 14.11.2017)

[55] N. N. GREENWOOD and A. EARNSHAW. Chemistry of the elements, Second Edition [online]. Reed Educational & Professional Publishing Limited.
Available on:
<https://zh.scribd.com/doc/258200651/Chemistry-of-Elements-2nd-Ed-N-N-Greenwood-a-Earnshaw>
(accessed on 13.11.2017)

[56] John C. Kotz, Paul M. Treichel, Gabriela C. Weaver. Chemistry and chemical reactivity, Third Edition [online]. Brooks/Cole Cengage Learning.
Available on: <http://projects.cbe.ab.ca/diefenbaker/chemistry/TEXTBOOK.pdf>
(accessed on 14.11.2017)

[57] Cooper C. Metastable anions of CO_2. Chemical Physics Letters. 1972; 14: 29-32.

[58] Aghamohammadi S, Haghighi M, Maleki M, Rahemi N. Sequential impregnation vs. sol-gel synthesized Ni/Al_2O_3-CeO_2 nanocatalyst for dry reforming of methane: Effect of synthesis method and support promotion. Molecular Catalysis. 2017; 431: 39-48.

[59] Mahboob S, Haghighi M, Rahmani F. Sonochemically preparation and characterization of bimetallic Ni-Co/Al_2O_3-ZrO_2 nanocatalyst: Effects of ultrasound irradiation time and power on catalytic properties and activity in dry reforming of CH_4. Ultrasonics Sonochemistry. 2017; 38: 38-49.

[60] Zhu J, Peng X, Yao L, Deng X, Dong H, Tong D, et al. Synthesis gas production from CO_2 reforming of methane over Ni–Ce/SiO_2 catalyst: The effect of calcination ambience. International Journal of Hydrogen Energy. 2013; 38: 117-26.
[61] Ay H, Üner D. Dry reforming of methane over CeO_2 supported Ni, Co and Ni-Co catalysts. Applied Catalysis B: Environmental. 2015; 179: 128-38.
[62] Luisetto I, Tuti S, Battocchio C, Lo Mastro S, Sodo A. Ni/CeO_2-Al_2O_3 catalysts for the dry reforming of methane: The effect of $CeAlO_3$ content and nickel crystallite size on catalytic activity and coke resistance. Applied Catalysis A: General. 2015; 500: 12-22.
[63] Liu H, Yao L, Hadj Taief HB, Benzina M, Da Costa P, Gálvez ME. Natural clay-based Ni-catalysts for dry reforming of methane at moderate temperatures. Catalysis Today. 2016.
[64] Zhang X, Zhang L, Peng H, You X, Peng C, Xu X , Liu W, Fang X, Wang Z, Zhang N, Wang X. Nickel nanoparticles embedded in mesopores of AlSBA-15 with a perfect peasecod-like structure: A catalyst with superior sintering resistance and hydrothermal stability for methane dry reforming. Applied Catalysis B: Environmental. 2018; 224: 488-99.
[65] Drif A, Bion N, Brahmi R, Ojala S, Pirault-Roy L, Turpeinen E, et al. Study of the dry reforming of methane and ethanol using Rh catalysts supported on doped alumina. Applied Catalysis A: General. 2015; 504: 576-84.
[66] Frontera P, Macario A, Aloise A, Antonucci PL, Giordano G, Nagy JB. Effect of support surface on methane dry-reforming catalyst preparation. Catalysis Today. 2013; 218-219: 18-29.
[67] Wang H, Ruckenstein E. Carbon dioxide reforming of methane to synthesis gas over supported rhodium catalysts: The effect of support. Applied Catalysis A: General. 2000; 204: 143-152.
[68] Daza CE, Gallego J, Mondragón F, Moreno S, Molina R. High stability of Ce-promoted Ni/Mg-Al catalysts derived from hydrotalcites in dry reforming of methane. Fuel. 2010; 89: 592-603.
[69] González AR, Asencios YJO, Assaf EM, Assaf JM. Dry reforming of methane on Ni–Mg–Al nano-spheroid oxide catalysts prepared by the sol–gel method from hydrotalcite-like precursors. Applied Surface Science. 2013; 280: 876-87.
[70] Dębek R, Radlik M, Motak M, Galvez ME, Turek W, Da Costa P, et al. Ni-containing Ce-promoted hydrotalcite derived materials as catalysts for methane reforming with carbon dioxide at low temperature - On the effect of basicity. Catalysis Today. 2015; 257: 59-65.
[71] Dębek R, Motak M, Duraczyska D, Launay F, Galvez ME, Grzybek T, et al. Methane dry reforming over hydrotalcite-derived Ni-Mg-Al mixed oxides: the influence of Ni content

on catalytic activity, selectivity and stability. Catalysis Science & Technology. 2016; 6: 6705-15.
[72] Ramirez JH, Costa CA, Madeira LM, Mata G, Vicente MA, Rojas-Cervantes ML, et al. Fenton-like oxidation of Orange II solutions using heterogeneous catalysts based on saponite clay. Applied Catalysis B: Environmental. 2007; 71: 44-56.
[73] Gil A, Korili SA, Vicente MA. Recent Advances in the Control and Characterization of the Porous Structure of Pillared Clay Catalysts. Catalysis Reviews. 2008; 50: 153-221.
[74] Zhou CH. An overview on strategies towards clay-based designer catalysts for green and sustainable catalysis. Applied Clay Science. 2011; 53: 87-96.
[75] Cao J-L, Shao G-S, Wang Y, Liu Y, Yuan Z-Y. CuO catalysts supported on attapulgite clay for low-temperature CO oxidation. Catalysis Communications. 2008; 9: 2555-9.
[76] Bel Hadjltaief H, Da Costa P, Beaunier P, Gálvez ME, Ben Zina M. Fe-clay-plate as a heterogeneous catalyst in photo-Fenton oxidation of phenol as probe molecule for water treatment. Applied Clay Science. 2014; 91-92: 46-54.
[77] Iwasa N, Takizawa M, Arai M. Preparation and application of nickel-containing smectite-type clay materials for methane reforming with carbon dioxide. Applied Catalysis A: General. 2006; 314: 32-9.
[78] Gamba O, Moreno S, Molina R. Catalytic performance of Ni-Pr supported on delaminated clay in the dry reforming of methane. International Journal of Hydrogen Energy. 2011; 36: 1540-50.
[79] Daza CE, Kiennemann A, Moreno S, Molina R. Dry reforming of methane using Ni-Ce catalysts supported on a modified mineral clay. Applied Catalysis A: General. 2009; 364: 65-74.
[80] Wang S, Zhu HY, Lu GQ. Preparation, characterization, and catalytic properties of clay-based nickel catalysts for methane reforming. Journal of Colloid and Interface Science. 1998; 204: 128-34.
[81] Barama S, Dupeyrat-Batiot C, Capron M, Bordes-Richard E, Bakhti-Mohammedi O. Catalytic properties of Rh, Ni, Pd and Ce supported on Al-pillared montmorillonites in dry reforming of methane. Catalysis Today. 2009; 141: 385-92.
[82] Hao Z, Zhu HY, Lu GQ. Zr-Laponite pillared clay-based nickel catalysts for methane reforming with carbon dioxide. Applied Catalysis A: General. 2003; 242: 275-86.
[83] Cao Y, Li H, Zhang J, Shi L, Zhang D. Promotional effects of rare earth elements (Sc, Y, Ce, and Pr) on NiMgAl catalysts for dry reforming of methane. RSC Advances. 2016; 6: 112215-25.

[84] Ruckenstein E, Hu YH. Carbon dioxide reforming of methane over nickel/alkaline earth metal oxide catalysts. Applied Catalysis A: General. 1995; 133: 149-61.
[85] Chang J-S, Park S-E, Yoo JW, Park J-N. Catalytic Behavior of Supported KNiCa Catalyst and Mechanistic Consideration for Carbon Dioxide Reforming of Methane. Journal of Catalysis. 2000; 195: 1-11.
[86] Arora S, Prasad R. An overview on dry reforming of methane: strategies to reduce carbonaceous deactivation of catalysts. RSC Advances. 2016; 6: 108668-88.
[87] Lavoie JM. Review on dry reforming of methane, a potentially more environmentally-friendly approach to the increasing natural gas exploitation. Frontiers in chemistry. 2014; 2: 81.
[88] Castro Luna AE, Iriarte ME. Carbon dioxide reforming of methane over a metal modified Ni-Al_2O_3 catalyst. Applied Catalysis A: General. 2008; 343: 10-5.
[89] Alipour Z, Rezaei M, Meshkani F. Effect of alkaline earth promoters (MgO, CaO, and BaO) on the activity and coke formation of Ni catalysts supported on nanocrystalline Al2O3 in dry reforming of methane. Journal of Industrial and Engineering Chemistry. 2014; 20: 2858-63.
[90] Liu H, Da Costa P, Hadj Taief HB, Benzina M, Gálvez ME. Ceria and zirconia modified natural clay based nickel catalysts for dry reforming of methane. International Journal of Hydrogen Energy. 2017; 42: 23508-16.
[91] Noronhaa FB, Shamsib A, Taylorb C, Fendleyc EC, Stagg-Williamsc S, Resascoc DE. Catalytic performance of Pt/ZrO_2 and Pt/Ce-ZrO_2 catalysts on CO_2 reforming of CH_4 coupled with steam reforming or under high pressure. Catalysis Letters. 2003; 90(1-2): 13-21.
[92] Damyanova S, Pawelec B, Arishtirova K, Huerta MVM, Fierro JLG. The effect of CeO_2 on the surface and catalytic properties of Pt/CeO_2–ZrO_2 catalysts for methane dry reforming. Applied Catalysis B: Environmental. 2009; 89: 149-59.
[93] Albarazi A, Gálvez ME, Da Costa P. Synthesis strategies of ceria-zirconia doped Ni/SBA-15 catalysts for methane dry reforming. Catalysis Communications. 2015; 59: 108-12.
[94] Frontera P, Macario A, Aloise A, Crea F, Antonucci PL, Nagy JB, et al. Catalytic dry-reforming on Ni-zeolite supported catalyst. Catalysis Today. 2012; 179: 52-60.
[95] Liu BS, Au CT. Carbon deposition and catalyst stability over La2NiO4/γ-Al2O3 during CO2 reforming of methane to syngas. Applied Catalysis A: General. 2003;244:181-95.

[96] Schulz LA, Kahle LCS, Delgado KH, Schunk SA, Jentys A, Deutschmann O, et al. On the coke deposition in dry reforming of methane at elevated pressures. Applied Catalysis A: General. 2015;504:599-607.
[97] Theofanidis SA, Batchu R, Galvita VV, Poelman H, Marin GB. Carbon gasification from Fe-Ni catalysts after methane dry reforming. Applied Catalysis B: Environmental. 2016;185:42-55.
[98] Kolb G. Fuel processing for fuel cells [online]. 2008 WILEY-VCH Verlag GmbH & Co. KGaA, Weinheim. ISBN: 978-3-527-31581-9.
Available on:
<https://books.google.fr/books?id=p30j25f-7kkC&pg=PA59&lpg=PA59&dq=definition+of+GHSV&source=bl&ots=zpCGty4t4r&sig=U7d8EAuOfqpo_5sO9D2c2wXNyDY&hl=zh-CN&sa=X&ved=0ahUKEwjK78-HuMnZAhUCaFAKHW-9B8E4ChDoAQgnMAA#v=onepage&q=definition%20of%20GHSV&f=false>
(accessed on 01.03.2018)
[99] Tang P, Zhu Q, Wu Z, Ma D. Methane activation: the past and future. Energy & Environmental Science. 2014; 7: 2580.
[100] Labinger JA, Bercaw JE. Understanding and exploiting C-H bond activation. Nature. 2002; 417: 507-14.
[101] Theofanidis SA, Batchu R, Galvita VV, Poelman H, Marin GB. Carbon gasification from Fe–Ni catalysts after methane dry reforming. Applied Catalysis B: Environmental. 2016; 185: 42-55.
[102] Rosen BA, Gileadi E, Eliaz N. Electrodeposited Re-promoted Ni foams as a catalyst for the dry reforming of methane. Catalysis Communications. 2016; 76: 23-8.
[103] Benrabaa R, Löfberg A, Caballero J.C., Bordes-Richard E, Rubbens A, Vannier R-N, et al. Sol-gel synthesis and characterization of silica supported nickel ferrite catalysts for dry reforming of methane. Catalysis Communications. 2015; 58: 127-31.
[104] Kehres J, Jakobsen JG, Andreasen JW, Wagner JB, Liu H, Molenbroek A, et al. Dynamical Properties of a Ru/MgAl2O4 Catalyst during Reduction and Dry Methane Reforming. The Journal of Physical Chemistry C. 2012; 116: 21407-15.
[105] Sutthiumporn K, Kawi S. Promotional effect of alkaline earth over Ni–La_2O_3 catalyst for CO2 reforming of CH4: Role of surface oxygen species on H2 production and carbon suppression. International Journal of Hydrogen Energy. 2011; 36: 14435-46.
[106] Carrara C, Múnera J, Lombardo EA, Cornaglia LM. Kinetic and Stability Studies of Ru/La_2O_3 Used in the Dry Reforming of Methane. Topics in Catalysis. 2008; 51: 98-106.

[107] Asencios YJO, Assaf EM. Combination of dry reforming and partial oxidation of methane on NiO–MgO–ZrO_2 catalyst: Effect of nickel content. Fuel Processing Technology. 2013; 106: 247-52.
[108] Y. Schuurman, C. Mirodatos, P. Ferreira-Aparicio, I. Rodriguez-Ramos and A. Guerrero-Ruiz. Bifunctional pathways in the carbon dioxide reforming of methane over MgO-promoted Ru/C catalysts. Catalysis Letters. 2000; 66: 33-7.
[109] Osawa T, Nakai Y, Mouri A, Lee IYS. Studies of the preparation method of ceria-promoted nickel catalyst for carbon dioxide reforming of methane. Applied Catalysis A: General. 2014; 474: 100-6.
[110] Daza CE, Kiennemann A, Moreno S, Molina R. Dry reforming of methane using Ni-Ce catalysts supported on a modified mineral clay. Applied Catalysis A: General. 2009; 364: 65-74.
[111] Liu D, Quek XY, Cheo WNE, Lau R, Borgna A, Yang Y. MCM-41 supported nickel-based bimetallic catalysts with superior stability during carbon dioxide reforming of methane: Effect of strong metal-support interaction. Journal of Catalysis. 2009; 266: 380-90.
[112] Bel Hadjltaief H, Da Costa P, Galvez ME, Ben Zina M. Influence of operational parameters in the heterogeneous photo-fenton discoloration of wastewaters in the presence of an iron-pillared clay. Industrial & Engineering Chemistry Research. 2013; 52: 16656-65.
[113] Akri M, Pronier S, Chafik T, Achak O, Granger P, Simon P, et al. Development of nickel supported La and Ce-natural illite clay for autothermal dry reforming of methane: Toward a better resistance to deactivation. Applied Catalysis B: Environmental. 2017; 205: 519-31.
[114] Qian L, Ma Z, Ren Y, Shi H, Yue B, Feng S, et al. Investigation of La promotion mechanism on Ni/SBA-15 catalysts in CH_4 reforming with CO_2. Fuel. 2014; 122: 47-53.
[115] Habibi N, Rezaei M, Majidian N, Andache M. CH4 reforming with CO_2 for syngas production over La_2O_3 promoted Ni catalysts supported on mesoporous nanostructured γ-Al_2O_3. Journal of Energy Chemistry. 2014; 23: 435-42.
[116] Pn I, Cp U. Overview on the Effect of Particle Size on the Performance of Wood Based Adsorbent. Journal of Chemical Engineering & Process Technology. 2016; 07.
[117] Borodzinski A, Bonarowska M. Relation between Crystallite Size and Dispersion on Supported Metal Catalysts. Langmuir. 1997; 13: 5613-20.
[118] Liu X, Toyir J, Ramírez de la Piscina P, Homs N. Hydrogen production from methanol steam reforming over Al_2O_3- and ZrO_2- modified $CuOZnOGa_2O_3$ catalysts. International Journal of Hydrogen Energy. 2017; 42: 13704-11.

[119] Yao L, Zhu J, Peng X, Tong D, Hu C. Comparative study on the promotion effect of Mn and Zr on the stability of Ni/SiO_2 catalyst for CO_2 reforming of methane. International Journal of Hydrogen Energy. 2013; 38: 7268-79.

[120] Koike M, Ishikawa C, Li D, Wang L, Nakagawa Y, Tomishige K. Catalytic performance of manganese-promoted nickel catalysts for the steam reforming of tar from biomass pyrolysis to synthesis gas. Fuel. 2013; 103: 122-9.

[121] Martinez R, Romero E, Guimon C, Bilbao R. CO_2 reforming of methane over coprecipitated Ni-Al catalysts modified with lanthanum. Applied Catalysis A: General. 2004; 274: 139-49.

[122] Tsoukalou A, Imtiaz Q, Kim SM, Abdala PM, Yoon S, Müller CR. Dry-reforming of methane over bimetallic $Ni\text{-}M/La_2O_3$ (M = Co, Fe): The effect of the rate of $La_2O_2CO_3$ formation and phase stability on the catalytic activity and stability. Journal of Catalysis. 2016; 343: 208-14.

[123] Agrell J. Production of hydrogen from methanol over Cu/ZnO catalysts promoted by ZrO_2 and Al_2O_3. Journal of Catalysis. 2003; 219: 389-403.

[124] Liu H, Yao L, Hadj Taief HB, Benzina M, Da Costa P, Gálvez ME. Natural clay-based Ni-catalysts for dry reforming of methane at moderate temperatures. Catalysis Today. 2016. http://dx.doi.org/10.1016/j.cattod.2016.12.017

[125] Kidambi PR, Cleeton JPE, Scott SA, Dennis JS, Bohn CD. Interaction of Iron Oxide with Alumina in a Composite Oxygen Carrier during the Production of Hydrogen by Chemical Looping. Energy & Fuels. 2012; 26: 603-17.

[126] Djaidja A, Messaoudi H, Kaddeche D, Barama A. Study of Ni–M/MgO and Ni–M–Mg/Al (M=Fe or Cu) catalysts in the CH_4-CO_2 and CH_4-H_2O reforming. International Journal of Hydrogen Energy. 2015; 40: 4989-95.

[127] Shi C, Zhang P. Effect of a second metal (Y, K, Ca, Mn or Cu) addition on the carbon dioxide reforming of methane over nanostructured palladium catalysts. Applied Catalysis B: Environmental. 2012; 115-116: 190-200.

[128] Granlund MZ, Jansson K, Nilsson M, Dawody J, Pettersson LJ. Evaluation of Co, La, and Mn promoted Rh catalysts for autothermal reforming of commercial diesel. Applied Catalysis B: Environmental. 2014; 154-155: 386-94.

[129] Christel L, Pierre A, Rousset Abel D. Temperature programmed reduction studies of nickel manganite spinels. Thermochimica Acta. 1997; 306: 51-9.

[130] Yu X, Wang N, Chu W, Liu M. Carbon dioxide reforming of methane for syngas production over La-promoted NiMgAl catalysts derived from hydrotalcites. Chemical Engineering Journal. 2012; 209: 623-32.
[131] Liu H, Da Costa P, Hadj Taief HB, Benzina M, Gálvez ME. Ceria and zirconia modified natural clay based nickel catalysts for dry reforming of methane. International Journal of Hydrogen Energy. 2017; 42: 23508-16.
[132] Dębek R, Galvez ME, Launay F, Motak M, Grzybek T, Da Costa P. Low temperature dry methane reforming over Ce, Zr and CeZr promoted Ni-Mg-Al hydrotalcite-derived catalysts. International Journal of Hydrogen Energy. 2016; 41: 11616-23.
[133] He S, Wu H, Yu W, Mo L, Lou H, Zheng X. Combination of CO2 reforming and partial oxidation of methane to produce syngas over Ni/SiO_2 and $Ni–Al_2O_3/SiO_2$ catalysts with different precursors. International Journal of Hydrogen Energy. 2009; 34: 839-43.
[134] Pakhare D, Spivey J. A review of dry (CO2) reforming of methane over noble metal catalysts. Chemical Society reviews. 2014; 43: 7813-37.
[135] Wu T, Li S, Yan Q. Effect of Interaction between Nickel and Alumina on Coke Deposition on Ni/Al_2O_3 Catalyst for Partial Oxidation of Methane to Syngas. Chinese Journal of Catalysis. 2001; 05: 501-4. (In Chinese)
[136] Liu H, Wierzbicki D, Debek R, Motak M, Grzybek T, Da Costa P, et al. La-promoted Ni-hydrotalcite-derived catalysts for dry reforming of methane at low temperatures. Fuel. 2016; 182: 8-16.
[137] Noronhaa FB, Shamsib A, Taylorb C, Fendleyc EC, Stagg-Williamsc S, Resascoc DE. Catalytic performance of Pt/ZrO_2 and $Pt/Ce-ZrO_2$ catalysts on CO_2 reforming of CH_4 coupled with steam reforming or under high pressure. Catalysis Letters. 2003; 90(1-2): 13-21.
[138] Seok S-H, Choi SH, Park ED, Han SH, Lee JS. Mn-Promoted Ni/Al_2O_3 Catalysts for Stable Carbon Dioxide Reforming of Methane. Journal of Catalysis. 2002; 209: 6-15.
[139] Oh G, Park SY, Seo MW, Kim YK, Ra HW, Lee J-G, et al. $Ni/Ru–Mn/Al_2O_3$ catalysts for steam reforming of toluene as model biomass tar. Renewable Energy. 2016; 86: 841-7.
[140] O. Gamba, S. Moreno, R. Molina. Catalytic performance of Ni–Pr supported on delaminated clay in the dry reforming of methane. International Journal of Hydrogen Energy. 2011; 36: 1540-50.
[141] A. Serrano-Lotina, A.J. Martin, M.A. Folgado, L. Daza. Dry reforming of methane to syngas over La-promoted hydrotalcite clay-derived catalysts. International Journal of Hydrogen Energy. 2012; 37: 12342-50.
[142] Shaobin Wang, H. Y. Zhu, and G. Q. (Max) Lu. Preparation, Characterization, and

Catalytic Properties of Clay-Based Nickel Catalysts for Methane Reforming. Journal of Colloid and Interface Science. 1998; 204: 128-134.
[143] Luo M-F, Fang P, He M, Xie Y-L. In situ XRD, Raman, and TPR studies of CuO/Al_2O_3 catalysts for CO oxidation. Journal of Molecular Catalysis A: Chemical. 2005; 239: 243-8.
[144] Li Y, Fu Q, Flytzani-Stephanopoulos M. Low-temperature water-gas shift reaction over Cu- and Ni-loaded cerium oxide catalysts. Applied Catalysis B: Environmental. 2000; 27:179-91.
[145] Mariño F, Baronetti G, Jobbagy M, Laborde M. Cu-Ni-K/γ-Al_2O_3 supported catalysts for ethanol steam reforming Formation of hydrotalcite-type compounds as a result of metal–support interaction. Applied Catalysis A: General. 2003; 238: 41-54.
[146] Chen H-Y, Sachtler WMH. Activity and durability of Fe/ZSM-5 catalysts for lean burn NOx reduction in the presence of water vapor. Catalysis Today. 1998; 42: 73-83.
[147] Wang L, Li D, Koike M, Koso S, Nakagawa Y, Xu Y, et al. Catalytic performance and characterization of Ni-Fe catalysts for the steam reforming of tar from biomass pyrolysis to synthesis gas. Applied Catalysis A: General. 2011; 392: 248-55.
[148] Djaidja A, Messaoudi H, Kaddeche D, Barama A. Study of Ni–M/MgO and Ni–M–Mg/Al (M=Fe or Cu) catalysts in the CH_4-CO_2 and CH_4-H_2O reforming. International Journal of Hydrogen Energy. 2015; 40: 4989-95.
[149] Ashok J, Kawi S. Nickel–Iron alloy supported over iron-alumina catalysts for steam reforming of biomass tar model compound. ACS Catalysis. 2013; 4: 289-301.
[150] Qi J, Sun Y, Xie Z, Collins M, Du H, Xiong T. Development of Cu foam-based Ni catalyst for solar thermal reforming of methane with carbon dioxide. Journal of Energy Chemistry. 2015; 24: 786-93.
[151] Huang T-J, Jhao S-Y. Ni-Cu/samaria-doped ceria catalysts for steam reforming of methane in the presence of carbon dioxide. Applied Catalysis A: General. 2006; 302: 325-32.
[152] Dębek R, Motak M, Duraczyska D, Launay F, Galvez ME, Grzybek T, et al. Methane dry reforming over hydrotalcite-derived Ni-Mg-Al mixed oxides: the influence of Ni content on catalytic activity, selectivity and stability. Catalysis Science & Technology. 2016; 6: 6705-15.
[153] Sepehri S, Rezaei M, Garbarino G, Busca G. Preparation and characterization of mesoporous nanocrystalline La-, Ce-, Zr-, Sr-containing Ni/Al_2O_3 methane autothermal reforming catalysts. International Journal of Hydrogen Energy. 2016; 41: 8855-62.

[154] Di Cosimo JI, Apesteguı´a CR, Ginés MJL, Iglesia E. Structural requirements and reaction pathways in condensation reactions of alcohols on Mg_yAlO_x catalysts. Journal of Catalysis. 2000; 190: 261-75.
[155] Akri M, Chafik T, Granger P, Ayrault P, Batiot-Dupeyrat C. Novel nickel promoted illite clay based catalyst for autothermal dry reforming of methane. Fuel. 2016; 178: 139-47.
[156] Carrero A, Vizcaíno AJ, Calles JA, García-Moreno L. Hydrogen production through glycerol steam reforming using Co catalysts supported on SBA-15 doped with Zr, Ce and La. Journal of Energy Chemistry. 2016.
[157] Yao L, Shi J, Xu H, Shen W, Hu C. Low-temperature CO_2 reforming of methane on Zr-promoted Ni/SiO_2 catalyst. Fuel Processing Technology. 2016; 144: 1-7.
[158] Homsi D, Aouad S, Gennequin C, Nakat JE, Aboukaïs A, Abi-Aad E. The effect of copper content on the reactivity of Cu/Co_6Al_2 solids in the catalytic steam reforming of methane reaction. Comptes Rendus Chimie. 2014; 17: 454-8.
[159] Yao L, Shi J, Hu C. The structure, carbon deposition and stability of a $ZrO_x/Ni\text{-}MnO_x/SiO_2$catalyst for the CO_2 reforming of methane. RSC Adv. 2015; 5: 90168-77.
[160] Forutan HR, Karimi E, Hafizi A, Rahimpour MR, Keshavarz P. Expert representation chemical looping reforming: A comparative study of Fe, Mn, Co and Cu as oxygen carriers supported on Al_2O_3. Journal of Industrial and Engineering Chemistry. 2015; 21: 900-11.
[161] Vaccari A. Clays and catalysis: a promising future. Applied Clay Science. 1999; 14: 161-98.
[162] Gamba O, Moreno S, Molina R. Catalytic performance of Ni-Pr supported on delaminated clay in the dry reforming of methane. International Journal of Hydrogen Energy. 2011; 36: 1540-50.
[163] Wang H, Zhu H, Lu G. Preparation, characterization, and catalytic properties of clay-based nickel catalysts for methane reforming. Journal of Colloid and Interface Science. 1998; 204: 128-34.
[164] Hao Z, Zhu HY, Lu GQ. Zr-Laponite pillared clay-based nickel catalysts for methane reforming with carbon dioxide. Applied Catalysis A: General. 2003; 242: 275-86.
[165] Li D, Li R, Lu M, Lin X, Zhan Y, Jiang L. Carbon dioxide reforming of methane over Ru catalysts supported on Mg-Al oxides: A highly dispersed and stable Ru/Mg(Al)O catalyst. Applied Catalysis B: Environmental. 2017; 200: 566-77.
[166] Singha RK, Yadav A, Agrawal A, Shukla A, Adak S, Sasaki T, et al. Synthesis of highly coke resistant Ni nanoparticles supported MgO/ZnO catalyst for reforming of methane with carbon dioxide. Applied Catalysis B: Environmental. 2016; 191: 165-78.

[167] Dieuzeide ML, Laborde M, Amadeo N, Cannilla C, Bonura G, Frusteri F. Hydrogen production by glycerol steam reforming: How Mg doping affects the catalytic behaviour of Ni/Al_2O_3 catalysts. International Journal of Hydrogen Energy. 2016; 41: 157-66.
[168] Djeffal L, Abderrahmane S, Benzina M, Fourmentin M, Siffert S, Fourmentin S. Efficient degradation of phenol using natural clay as heterogeneous Fenton-like catalyst. Environmental science and pollution research international. 2014; 21: 3331-8.
[169] Sutthiumporn K, Maneerung T, Kathiraser Y, Kawi S. CO_2 dry-reforming of methane over $La_{0.8}Sr_{0.2}Ni_{0.8}M_{0.2}O_3$ perovskite (M = Bi, Co, Cr, Cu, Fe): Roles of lattice oxygen on C–H activation and carbon suppression. International Journal of Hydrogen Energy. 2012; 37: 11195-207.
[170] Zhu Y, Zhang S, Chen B, Zhang Z, Shi C. Effect of Mg/Al ratio of NiMgAl mixed oxide catalyst derived from hydrotalcite for carbon dioxide reforming of methane. Catalysis Today. 2016; 264: 163-70.
[171] Abelló S, Bolshak E, Montané D. Ni–Fe catalysts derived from hydrotalcite-like precursors for hydrogen production by ethanol steam reforming. Applied Catalysis A: General. 2013; 450: 261-74.
[172] Bolshak E, Abelló S, Montané D. Ethanol steam reforming over Ni–Fe-based hydrotalcites: Effect of iron content and reaction temperature. International Journal of Hydrogen Energy. 2013; 38: 5594-604.
[173] Benrabaa R, Löfberg A, Rubbens A, Bordes-Richard E, Vannier RN, Barama A. Structure, reactivity and catalytic properties of nanoparticles of nickel ferrite in the dry reforming of methane. Catalysis Today. 2013; 203: 188-95.
[174] Ligthart DAJM, van Santen RA, Hensen EJM. Influence of particle size on the activity and stability in steam methane reforming of supported Rh nanoparticles. Journal of Catalysis. 2011; 280: 206-20.
[175] Wei J, Iglesia E. Isotopic and kinetic assessment of the mechanism of reactions of CH4 with CO_2 or H_2O to form synthesis gas and carbon on nickel catalysts. Journal of Catalysis. 2004; 224: 370-83.
[176] Centi G, Perathoner S. Opportunities and prospects in the chemical recycling of carbon dioxide to fuels. Catalysis Today. 2009; 148: 191-205.
[177] Edwards JH, Maitra AM. The chemistry of methane reforming with carbon dioxide and its current and potential applications. Fuel Processing Technology. 1995; 42: 269-89.
[178] Al-Fatesh AS, Naeem MA, Fakeeha AH, Abasaeed AE. CO2 Reforming of Methane to Produce Syngas over γ-Al_2O_3-Supported Ni-Sr Catalysts. Bulletin of the Chemical Society of

Japan. 2013; 86: 742-8.
[179] Bradford MCJ, Vannice MA. Catalytic reforming of methane with carbon dioxide over nickel catalysts II. Reaction kinetics. Applied Catalysis A: General. 1996; 142: 97-122.
[180] Koo KY, Lee S-h, Jung UH, Roh H-S, Yoon WL. Syngas production via combined steam and carbon dioxide reforming of methane over Ni-Ce/$MgAl_2O_4$ catalysts with enhanced coke resistance. Fuel Processing Technology. 2014; 119: 151-7.
[181] Barroso-Quiroga MM, Castro-Luna AE. Catalytic activity and effect of modifiers on Ni-based catalysts for the dry reforming of methane. International Journal of Hydrogen Energy. 2010; 35: 6052-6.
[182] Mark MF, Maier WF. CO2-Reforming of methane on supported Rh and Ir catalysts. Journal of Catalysis. 1996; 164: 122-30.
[183] Keulen ANJv, Seshan K, Hoebink JHBJ, Ross JRH. TAP Investigations of the CO_2 reforming of CH_4 over Pt/ZrO_2. Journal of Catalysis. 1997; 166: 306-14.
[184] Kroll VCH, Swaan HM, Lacombe S, Mirodatos C. Methane Reforming Reaction with Carbon Dioxide over Ni/SiO2 Catalyst II. A Mechanistic Study. Journal of Catalysis. 1997; 164: 387-98.
[185] Gao J, Hou Z, Guo J, Zhu Y, Zheng X. Catalytic conversion of methane and CO_2 to synthesis gas over a La_2O_3-modified SiO_2 supported Ni catalyst in fluidized-bed reactor. Catalysis Today. 2008; 131: 278-84.
[186] Verykios X. Catalytic dry reforming of natural gas for the production of chemicals and hydrogen. International Journal of Hydrogen Energy. 2003.
[187] Cavani F, Trifirb F, Vaccari A. Hydrotalcite-type anionic clays: preparation, properties and applications. Catalysis Today. 1991; 11: 173-301.
[188] Forano C, Costantino U, Prévot V, Gueho CT. Layered Double Hydroxides (LDH). Handbook of clay science. 2013; 5: 745-82.
[189] Debecker DP, Gaigneaux EM, Busca G. Exploring, tuning, and exploiting the basicity of hydrotalcites for applications in heterogeneous catalysis. Chemistry. 2009; 15: 3920-35.
[190] Yan H, Lu J, Wei M, Ma J, Li H, He J, et al. Theoretical study of the hexahydrated metal cations for the understanding of their template effects in the construction of layered double hydroxides. Journal of Molecular Structure: THEOCHEM. 2008; 866: 34-45.
[191] Lü Z, Duan X. Controllable Preparation of Layered Anionic Materials. Chinese Journal of Catalysis. 2008; 29: 839-56. (In Chinese)

[192] Pavel OD, Tichit D, Marcu I-C. Acido-basic and catalytic properties of transition-metal containing Mg-Al hydrotalcites and their corresponding mixed oxides. Applied Clay Science. 2012; 61: 52-8.
[193] Liu H, Wierzbicki D, Dębek R, Motak M, Grzybek T, Da Costa P, et al. La-promoted Ni-hydrotalcite-derived catalysts for dry reforming of methane at low temperatures. Fuel. 2016; 182: 8-16.
[194] Wang Q, O'Hare D. Recent advances in the synthesis and application of layered double hydroxide (LDH) nanosheets. Chemical reviews. 2012; 112: 4124-55.
[195] Theiss FL, Ayoko GA, Frost RL. Synthesis of layered double hydroxides containing Mg^{2+}, Zn^{2+}, Ca^{2+} and Al^{3+} layer cations by co-precipitation methods - A review. Applied Surface Science. 2016; 383: 200-13.
[196] Pn I, Cp U. Overview on the Effect of Particle Size on the Performance of Wood Based Adsorbent. Journal of Chemical Engineering & Process Technology. 2016; 07.
[197] Serrano-Lotina A, Rodríguez L, Muñoz G, Daza L. Biogas reforming on La-promoted NiMgAl catalysts derived from hydrotalcite-like precursors. Journal of Power Sources. 2011; 196: 4404-10.
[198] Dębek R, Radlik M, Motak M, Galvez ME, Turek W, Da Costa P, et al. Ni-containing Ce-promoted hydrotalcite derived materials as catalysts for methane reforming with carbon dioxide at low temperature - On the effect of basicity. Catalysis Today. 2015; 257: 59-65.
[199] Lucrédio AF, Assaf JM, Assaf EM. Reforming of a model sulfur-free biogas on Ni catalysts supported on Mg(Al)O derived from hydrotalcite precursors: Effect of La and Rh addition. Biomass and Bioenergy. 2014; 60: 8-17.
[200] Yu X, Wang N, Chu W, Liu M. Carbon dioxide reforming of methane for syngas production over La-promoted NiMgAl catalysts derived from hydrotalcites. Chemical Engineering Journal. 2012; 209: 623-32.
[201] Di Cosimo JI, Apesteguı,́a CR, Ginés MJL, Iglesia E. Structural Requirements and Reaction Pathways in Condensation Reactions of Alcohols on Mg_yAlO_x Catalysts. Journal of Catalysis. 2000; 190: 261-75.
[202] Liu P, Derchi M, Hensen EJM. Promotional effect of transition metal doping on the basicity and activity of calcined hydrotalcite catalysts for glycerol carbonate synthesis. Applied Catalysis B: Environmental. 2014; 144: 135-43.
[203] Dębek R, Galvez ME, Launay F, Motak M, Grzybek T, Da Costa P. Low temperature dry methane reforming over Ce, Zr and CeZr promoted Ni-Mg-Al hydrotalcite-derived catalysts. International Journal of Hydrogen Energy. 2016; 41: 11616-23.

[204] Wang L, Zhang S, Liu Y. Reverse water gas shift reaction over Co-precipitated Ni-CeO_2 catalysts. Journal of Rare Earths. 2008; 26: 66-70.
[205] Wu HC, Chang YC, Wu JH, Lin JH, Lin IK, Chen CS. Methanation of CO_2 and reverse water gas shift reactions on Ni/SiO_2 catalysts: the influence of particle size on selectivity and reaction pathway. Catalysis Science & Technology. 2015; 5: 4154-63.
[206] Usman M, Wan Daud WMA, Abbas HF. Dry reforming of methane: Influence of process parameters - A review. Renewable and Sustainable Energy Reviews. 2015; 45: 710-44.
[207] Sutthiumporn K, Kawi S. Promotional effect of alkaline earth over Ni–La_2O_3 catalyst for CO_2 reforming of CH_4: Role of surface oxygen species on H2 production and carbon suppression. International Journal of Hydrogen Energy. 2011; 36: 14435-46.
[208] Akri M, Pronier S, Chafik T, Achak O, Granger P, Simon P, et al. Development of nickel supported La and Ce-natural illite clay for autothermal dry reforming of methane: Toward a better resistance to deactivation. Applied Catalysis B: Environmental. 2017; 205: 519-31.
[209] Ashok J, Kawi S. Steam reforming of toluene as a biomass tar model compound over CeO2 promoted Ni/CaO–Al_2O_3 catalytic systems. International Journal of Hydrogen Energy. 2013; 38: 13938-49.
[210] Jing J-y, Wang S-d, Zhang X-w, Li Q, Li W-y. Influence of Ca/Al molar ratio on structure and catalytic reforming performance of Ni/CaO-Al_2O_3 catalyst. Journal of Fuel Chemistry and Technology. 2017; 45: 956-62.
[211] Yu X, Wang N, Chu W, Liu M. Carbon dioxide reforming of methane for syngas production over La-promoted NiMgAl catalysts derived from hydrotalcites. Chemical Engineering Journal. 2012; 209: 623-32.
[212] Zhu J, Peng X, Yao L, Shen J, Tong D, Hu C. The promoting effect of La, Mg, Co and Zn on the activity and stability of Ni/SiO_2 catalyst for CO_2 reforming of methane. International Journal of Hydrogen Energy. 2011; 36: 7094-104.
[213] Serrano-Lotina A, Rodríguez L, Muñoz G, Daza L. Biogas reforming on La-promoted NiMgAl catalysts derived from hydrotalcite-like precursors. Journal of Power Sources. 2011; 196: 4404-10.
[214] Serrano-Lotina A, Rodríguez L, Muñoz G, Martin AJ, Folgado MA, Daza L. Biogas reforming over La-NiMgAl catalysts derived from hydrotalcite-like structure: Influence of calcination temperature. Catalysis Communications. 2011; 12: 961-7.
[215] Lucrédio AF, Assaf JM, Assaf EM. Reforming of a model sulfur-free biogas on Ni

catalysts supported on Mg(Al)O derived from hydrotalcite precursors: Effect of La and Rh addition. Biomass and Bioenergy. 2014; 60: 8-17.
[216] Dębek R, Motak M, Duraczyska D, Launay F, Galvez ME, Grzybek T, et al. Methane dry reforming over hydrotalcite-derived Ni-Mg-Al mixed oxides: the influence of Ni content on catalytic activity, selectivity and stability. Catalysis Science & Technology. 2016; 6: 6705-15.
[217] Kima J-H, Suhb DJ, Parkb T-J, Kim K-L. Effect of metal particle size on coking during CO_2 reforming of CH_4 over Ni–alumina aerogel catalysts. Applied Catalysis A: General. 2000; 197: 191-200.
[218] Rives V. Characterisation of layered double hydroxides and their decomposition products. Materials Chemistry and Physics. 2002; 75: 19-25.
[219] Sun N, Wen X, Wang F, Peng W, Zhao N, Xiao F, et al. Catalytic performance and characterization of Ni–CaO–ZrO_2 catalysts for dry reforming of methane. Applied Surface Science. 2011; 257: 9169-76.
[220] Liu BS, Au CT. Carbon deposition and catalyst stability over La_2NiO_4/γ-Al_2O_3 during CO_2 reforming of methane to syngas. Applied Catalysis A: General. 2003; 244: 181-95.
[221] Abbas HF, Wan Daud WMA. Hydrogen production by methane decomposition: A review. International Journal of Hydrogen Energy. 2010; 35: 1160-90.
[222] Wei J, Iglesia E. Isotopic and kinetic assessment of the mechanism of reactions of CH4 with CO_2 or H_2O to form synthesis gas and carbon on nickel catalysts. Journal of Catalysis. 2004; 224: 370-83.
[223] Albarazi A, Beaunier P, Da Costa P. Hydrogen and syngas production by methane dry reforming on SBA-15 supported nickel catalysts: On the effect of promotion by $Ce_{0.75}Zr_{0.25}O_2$ mixed oxide. International Journal of Hydrogen Energy. 2013; 38: 127-39.
[224] Gálvez ME, Frei A, Albisetti G, Lunardi G, Steinfeld A. Solar hydrogen production via a two-step thermochemical process based on MgO/Mg redox reactions - Thermodynamic and kinetic analyses. International Journal of Hydrogen Energy. 2008; 33: 2880-90.
[225] Verykios X. Catalytic dry reforming of natural gas for the production of chemicals and hydrogen. International Journal of Hydrogen Energy. 2003.
[226] Gould BD, Chen X, Schwank JW. n-Dodecane reforming over nickel-based monolith catalysts: Deactivation and carbon deposition. Applied Catalysis A: General. 2008; 334: 277-90.
[227] Rode J, Le Menestrel M, Cornelissen G. Ecosystem Service Arguments Enhance Public Support for Environmental Protection - But Beware of the Numbers! Ecological Economics.

2017; 141: 213-21.

[228] Jancovici J. Energy and choice of life [online]. Revue du Palais de la Découverte. 2001; 11.

Available on:

<https://jancovici.com/en/publications-and-co/newspaper-articles-en/energy-and-choice-of-life/>

(accessed on 09.05.2018)

[229] Makri MM, Vasiliades MA, Petallidou KC, Efstathiou AM. Effect of support composition on the origin and reactivity of carbon formed during dry reforming of methane over 5wt% Ni/$Ce_{1-x}M_xO_{2-\delta}$ ($M=Zr^{4+}$, Pr^{3+}) catalysts. Catalysis Today. 2016; 259: 150-64.

[230] Usman M, Wan Daud WMA, Abbas HF. Dry reforming of methane: Influence of process parameters-A review. Renewable and Sustainable Energy Reviews. 2015; 45: 710-44.

[231] Aramouni NAK, Touma JG, Tarboush BA, Zeaiter J, Ahmad MN. Catalyst design for dry reforming of methane: Analysis review. Renewable and Sustainable Energy Reviews. 2018; 82: 2570-85.

[232] Abdullah B, Abd Ghani NA, Vo D-VN. Recent advances in dry reforming of methane over Ni-based catalysts. Journal of Cleaner Production. 2017; 162: 170-85.

[233] Trovarelli A, Zamar F, Llorca J, Leitenburg Cd, Dolcetti G, Kiss JT. Nanophase Fluorite-Structured CeO_2–ZrO_2 Catalysts Prepared by High-Energy Mechanical Milling. Journal of Catalysis. 1997; 169: 490-502.

[234] Xu F, Deng S, Xu J, Zhang W, Wu M, Wang B, et al. Highly active and stable Ni-Fe bimetal prepared by ball milling for catalytic hydrodechlorination of 4-chlorophenol. Environmental science & technology. 2012; 46: 4576-82.

[235] Meloni D, Monaci R, Cutrufello MG, Rombi E, Ferino I. Adsorption microcalorimetry characterization of K-doped MgAl mixed oxide catalysts for soybean oil transesterification synthesized by impregnation and ball milling techniques. Journal of Thermal Analysis and Calorimetry. 2014; 119: 1023-36.

[236] Barroso Quiroga MM, Barbero BP, Cadus LE. Synthesis of a catalyst of Mn-Fe-O by mechano-chemical reaction. Applied Catalysis A: General. 2014; 474: 26-33.

[237] Borodzinski A, Bonarowska M. Relation between crystallite size and dispersion on supported metal catalysts. Langmuir 1997; 13: 5613-20.

[238] Ikenyiri PN, Ukpaka CP. Overview on the effect of particle size on the performance of wood based adsorbent. Journal of Chemical Engineering & Process Technology. 2016; 07: 315.

[239] Liu H, Da Costa P, Hadj Taief HB, Benzina M, Gálvez ME. Ceria and zirconia modified natural clay based nickel catalysts for dry reforming of methane. International Journal of Hydrogen Energy. 2017; 42: 23508-16.
[240] Liu H, Wierzbicki D, Debek R, Motak M, Grzybek T, Da Costa P, et al. La-promoted Ni-hydrotalcite-derived catalysts for dry reforming of methane at low temperatures. Fuel. 2016; 182: 8-16.
[241] Mekasuwandumrong O, Wongwaranon N, Panpranot J, Praserthdam P. Effect of Ni-modified α-Al_2O_3 prepared by sol–gel and solvothermal methods on the characteristics and catalytic properties of Pd/α-Al_2O_3 catalysts. Materials Chemistry and Physics. 2008; 111: 431-7.
[242] Seo H. Recent Scientific Progress on Developing Supported Ni Catalysts for Dry (CO_2) Reforming of Methane. Catalysts. 2018; 8: 110.
[243] Christensen KO, Chen D, Lødeng R, Holmen A. Effect of supports and Ni crystal size on carbon formation and sintering during steam methane reforming. Applied Catalysis A: General. 2006; 314: 9-22.
[244] De S, Zhang J, Luque R, Yan N. Ni-based bimetallic heterogeneous catalysts for energy and environmental applications. Energy & Environmental Science. 2016; 9: 3314-47.

Table des illustrations

Table des tableaux

Annexes

Annex.1 Abbreviations and symbols

Table Annexes 1-1. List of abbreviations and explanations

Abbreviations	Explanations
BET	Brunauer–Emmett–Teller
BTL	Biomass to Liquids
CTL	Coal to Liquids
DEA	Diethanolamine
DMD	Direct Methane Decomposition
DRM	Dry Reforming of Methane
EOR	Enhanced Oil Recovery
F-T	Fischer-Tropsch Process
GHSV	Gas Hourly Space Velocity
GTL	Natural Gas into Liquids
IUPAC	International Union of Pure and Applied Chemistry
MDEA	Methyldiethanolamine
MEA	Monoethanolamine
MOFs	Metal Organic Frameworks
OTL	Bitumen from Oil Sands to Liquids
Raman	Raman Spectroscopy
RWGS	Reverse Water Gas Shift
TEM	Transmission Electron Microscope
TGA	Thermogravimetric Analysis
TOS	Time on Stream
TPD	Temperature-Programmed Desorption
TPR	Temperature-Programmed Reduction
UNFCCC	United Nations Framework Convention on Climate Change
XRD	X-ray Diffraction

Table Annexes 1-2. List of symbols and explanations

Symbols	Explanations
Cu-clay	Cu-modified Clay
d	Particle Size
D	Dispersion
d_p	Average Pore Size
Fe-clay	Fe-modified Clay
H_2/CO	H_2/CO Molar Ratio
HBa	Ni-hydro-barium derived Catalysts
HCa	Ni-hydrocalumite derived Catalysts
HCa+1%La	1wt.% La promoted Ni-hydrocalumite derived Catalysts
HCa+2%La	2wt.% La promoted Ni-hydrocalumite derived Catalysts
HCa+4%La	4wt.% La promoted Ni-hydrocalumite derived Catalysts
HSr	Ni-hydro-strontium derived Catalysts
HT/HN4/NiMgAl-HT	Ni-hydrotalcite derived Catalysts
HT+1%La/HN1	1wt.% La promoted Ni-hydrotalcite derived Catalysts
HT+2%La/HN2	1wt.% La promoted Ni-hydrotalcite derived Catalysts
HT+4%La/HN3	1wt.% La promoted Ni-hydrotalcite derived Catalysts
Ni/clay	Non-promoted natural clay supported Ni-based Catalysts
Ni/Cu-clay	Non-promoted Cu-modified clay supported Ni-based Catalysts
Ni/Fe-clay	Non-promoted Fe-modified clay supported Ni-based Catalysts
Ni-Al/Fe-clay	Al-promoted Fe-modified clay supported Ni-based Catalysts
Ni-Ce/Cu-clay	Ce-promoted Cu-modified clay supported Ni-based Catalysts
Ni-Ce/Fe-clay	Ce-promoted Fe-modified clay supported Ni-based Catalysts
Ni-La/Fe-clay	La-promoted Fe-modified clay supported Ni-based Catalysts
Ni-Mg/Cu-clay	Mg-promoted Cu-modified clay supported Ni-based Catalysts
Ni-Mg/Fe-clay	Mg-promoted Fe-modified clay supported Ni-based Catalysts
NiMgAl-BM300	Mg-Al mixed oxides supported Ni-based catalysts prepared by 300 rpm Ball Milling
NiMgAl-BM600	Mg-Al mixed oxides supported Ni-based catalysts prepared by 600 rpm Ball Milling
NiMgAl-BM900	Mg-Al mixed oxides supported Ni-based catalysts prepared by 900 rpm Ball Milling
Ni-Mn/Fe-clay	Mn-promoted Fe-modified clay supported Ni-based Catalysts
Ni-Zr/Cu-clay	Zr-promoted Cu-modified clay supported Ni-based Catalysts
Ni-Zr/Fe-clay	Zr-promoted Fe-modified clay supported Ni-based Catalysts
S_{BET}	Specific Surface Area
V_{BJH}	BJH Desorption Cumulative Pore Volume
V_p	Total Pore Volume
WC	Tungsten Carbide
X_{CH4}	Conversion of CH_4
X_{CO2}	Conversion of CO_2
ΔH^0	Standard Enthalpy of Formation